



UNIVERSITY OF
LEICESTER

**NOVEL APPROACHES FOR THE IDENTIFICATION AND
TARGETED CLEARANCE OF SENESCENT CELLS, AS A
THERAPEUTIC STRATEGY FOR SENESCENCE-RELATED AND
AGE-RELATED DISEASES**

Thesis submitted for the degree of

Doctor of Philosophy in Biochemistry

at the University of Leicester

By

Akang Eyo Ekpenyong-Akiba MSc (Cranfield)

Department of Molecular and Cell Biology

College of Life Sciences

University of Leicester, UK

August 2018

ABSTRACT

Novel approaches for the identification and targeted clearance of senescent cells, as a therapeutic strategy for senescence-related and age-related diseases.

Akang Eyo Ekpenyong-Akiba

Cellular senescence is a state of permanent cell cycle arrest in which cells remain metabolically active, adopting characteristic phenotypic changes. Although senescence is a potent tumour suppressor mechanism, the accumulation of senescent cells in tissues over time has been shown to contribute to several pathophysiological conditions, including fibrosis, diabetes, cancer, Alzheimer's disease and ageing, making the targeting of these cells a potentially relevant therapeutic strategy for fighting these pathologies. Clearing senescent cells has been reported to protect against cancer and the onset of age-related pathologies. Furthermore, preventing the accumulation of senescent cells in tissues also prolonged healthspan and lifespan in mouse models. Currently available markers of senescence, however, lack specificity and selectivity, limiting their therapeutic use. This underscores the need for senescence-specific markers that could be targeted and translated into clinical use. Here, we describe the application of molecularly imprinted polymer nanoparticles (nanoMIPs) designed to target an extracellular epitope of B2MG, a membrane protein recently characterized as a novel marker of senescence, and propose this as a novel tool for the specific detection of senescent cells both *in vitro* and *in vivo*. We further show that B2MG nanoMIPs laden with a toxic payload selectively kill senescent cells in culture. Consistent with this, we show that antibody-drug conjugates (ADCs) against B2MG selectively kill senescent cells in culture. We also demonstrate that Ibrutinib, a clinically approved chemical inhibitor of BTK, reduced the accumulation of senescent cells *in vivo*, prolonging lifespan and healthspan in a mouse model of progeria. *Zmpste24*^{-/-} mice treated with Ibrutinib showed an increase in maximum lifespan and a reduction in age-related fitness decline, evidenced by their increased physical strength, reduced anxiety and better long-term memory, with no evidence of spontaneous tumour formation. The results from this research altogether highlight new strategies for reducing the accumulation of senescent cells *in vivo*, which could find translational application in the clinical management of senescence-related and age-related ailments.

ACKNOWLEDGEMENTS

I would like to say a huge thank you to my supervisor, Dr Salvador Macip for his outstanding supervision that has led to the completion of this great piece of work. I appreciate his support, encouragement and guidance throughout my PhD. I also want to thank my supportive committee members, Dr Shaun Cowley and Dr Alessandro Rufini for their stimulating questions and ideas during the course of my PhD. I would like to also thank Dr Karl Herbert, my second supervisor for his encouragement during my programme. I most especially want to appreciate the counsel and support of my Postgraduate Tutor, Dr Sue Shackleton during my PhD. Many thanks for the advice and encouragement of Dr Jesvin Samuel, Dr Miran Rada and Dr Mohammad Althubiti, who were all finishing off their PhD in our lab when I had just started mine. Their support gave me a great start to my PhD journey. I also want to thank all members of the MoCAA Lab and Lab 3/37 who have been such a wonderful lab family. The cakes during lab meetings made the group a fun place to work in. I especially want to thank the students and staff, Marta Poblocka, Dr. Gabriella Kocsis-Fodor, Yu Shi, Dr Ana Sousa-Manso, Sam Resendez, Mireia Casulleras, Laura Vallmanya and Sandra Germano who worked hard to support this project.

My special thanks goes to Martin Coffey and the entire Doctoral College team for their support during our successful Three Minute Thesis (3MT) and Biotechnology YES competitions. These activities among others gave me a wholesome PhD experience. I want to appreciate the Tertiary Education Trust Fund (TETFund) Nigeria for the initial funding to carry out my PhD in the United Kingdom. I most especially want to thank the University of Leicester for taking up this responsibility during my time of funding challenges. I would like to appreciate Aditya, Pooyeh and Dr Kostas for their friendship which has made life during the PhD so much easier. I want to appreciate my parents, Obonn Ndanyam Eyo Otu Ekpenyong and Elder Mrs Arit E. O. Ekpenyong who have always been there for me, supported and encouraged me in my career path. I thank all my brothers and sisters for constantly being in touch and making home seem not so distant. My deepest appreciation goes to my beloved husband Leonard, who has been ever so loving and supportive throughout my PhD programme.

My profound gratitude goes to God Almighty, to whom I am beholden.

In Loving Memory of my Beloved Sister

Late Mrs Inyang Georgina C. Okere

1963 - 2016

TABLE OF CONTENTS

| | |
|--|-----|
| ABSTRACT..... | i |
| ACKNOWLEDGEMENTS..... | ii |
| LIST OF FIGURES..... | x |
| LIST OF TABLES..... | xiv |
| ABBREVIATIONS | xv |
| CHAPTER 1 INTRODUCTION..... | 1 |
| 1.1 CELLULAR SENESENCE | 1 |
| 1.2 TYPES OF SENESENCE | 2 |
| 1.2.1 REPLICATIVE SENESENCE | 4 |
| 1.2.2 STRESS INDUCED PREMATURE SENESENCE (SIPS)..... | 6 |
| 1.2.3 ONCOGENE INDUCED SENESENCE (OIS) | 9 |
| 1.2.4 DEVELOPMENTALLY PROGRAMMED SENESENCE | 14 |
| 1.3 CHARACTERISTICS OF SENESENT CELLS..... | 15 |
| 1.3.1 GROWTH ARREST, MORPHOLOGICAL AND PHYSICAL CHANGES | 16 |
| 1.3.2 SENESENCE ASSOCIATED β -GALACTOSIDASE (SA β -GAL) | 17 |
| 1.3.3 THE SENESENCE-ASSOCIATED SECRETORY PHENOTYPE (SASP) | 18 |
| 1.3.4 SENESENCE ASSOCIATED HETEROCHROMATIC FOCI (SAHF) .. | 23 |
| 1.3.5 GENE EXPRESSION CHANGES DURING SENESENCE | 25 |
| 1.3.6 THE SEARCH FOR NOVEL MARKERS OF SENESENCE | 26 |
| 1.4 PATHWAYS INVOLVED IN SENESENCE | 28 |
| 1.4.1 p16 ^{INK4A} AS A MARKER OF SENESENCE | 32 |
| 1.4.2 p53 and p21 | 34 |
| 1.5 PLEIOTROPIC EFFECTS OF SENESENCE..... | 37 |
| 1.5.1 BENEFICIAL ROLES OF SENESENCE | 39 |
| 1.5.2 DETRIMENTAL EFFECTS OF SENESENCE | 40 |
| 1.6 AGEING, CELLULAR SENESENCE AND DISEASE..... | 41 |
| 1.6.1 SENESENCE-DRIVEN FUNCTIONAL DECLINE | 42 |

| | | |
|--------------------------------------|--|----|
| 1.6.2 | OTHER DISEASES..... | 46 |
| 1.6.3 | TOOLS TO MEASURE AGEING..... | 48 |
| 1.6.4 | ANTI-AGEING INTERVENTIONS | 50 |
| 1.7 | TARGETED THERAPY..... | 53 |
| 1.7.1 | MOLECULARLY IMPRINTED POLYMERS | 54 |
| 1.7.2 | ANTIBODY-DRUG CONJUGATES..... | 55 |
| 1.8 | THERAPEUTIC CLEARANCE OF SENESCENT CELLS: THE JOURNEY SO FAR | 57 |
| 1.9 | AIMS AND OBJECTIVES..... | 59 |
| 1.9.1 | AIM OF RESEARCH:..... | 59 |
| 1.9.2 | OBJECTIVES:..... | 59 |
| CHAPTER 2 MATERIALS AND METHODS..... | | 60 |
| 2.1 | HISTOLOGY..... | 60 |
| 2.1.1 | ISOLATION AND FIXATION OF MOUSE TISSUES | 60 |
| 2.1.2 | SUBBING OF MICROSCOPE SLIDES | 60 |
| 2.1.3 | SECTIONING OF TISSUES AND MOUNTING ON SLIDES | 61 |
| 2.1.4 | HAEMATOXYLIN AND EOSIN STAINING | 61 |
| 2.1.5 | IMMUNOHISTOCHEMISTRY | 61 |
| 2.2 | CELL CULTURE | 64 |
| 2.2.1 | THAWING AND GROWING OF CELLS..... | 64 |
| 2.2.2 | PASSAGING OF CELLS..... | 65 |
| 2.2.3 | COUNTING OF CELLS..... | 66 |
| 2.2.4 | FREEZING OF CELLS..... | 66 |
| 2.3 | CELL PROLIFERATION AND VIABILITY ASSAYS | 68 |
| 2.3.1 | COLONY FORMATION ASSAY..... | 68 |
| 2.3.2 | MTS ASSAY | 68 |
| 2.4 | FLOW CYTOMETRY | 69 |
| 2.4.1 | PROPIDIUM IODIDE STAINING..... | 69 |
| 2.5 | GENETIC ANALYSES | 70 |

| | | |
|--------|--|----|
| 2.5.1 | BACTERIAL TRANSFORMATION..... | 70 |
| 2.5.2 | PLASMID TRANSFECTION..... | 71 |
| 2.5.3 | TOTAL RNA EXTRACTION FROM TISSUES..... | 72 |
| 2.5.4 | QUANTITATIVE REVERSE TRANSCRIPTION REAL TIME PCR (RT-qPCR) | 72 |
| 2.6 | PROTEIN ANALYSIS..... | 75 |
| 2.6.1 | EXTRACTION OF TOTAL PROTEIN FROM CELLS | 75 |
| 2.6.2 | EXTRACTION OF TOTAL PROTEIN FROM TISSUES..... | 75 |
| 2.6.3 | SODIUM DODECYL SULFATE – POLYACRYLAMIDE GEL ELECTROPHORESIS (SDS-PAGE). | 76 |
| 2.6.4 | WESTERN BLOT ANALYSIS..... | 77 |
| 2.7 | SENESCENCE ASSOCIATED β -GALACTOSIDASE STAINING | 80 |
| 2.8 | <i>IN VITRO</i> AND <i>IN VIVO</i> TECHNIQUES USING MOLECULARLY IMPRINTED POLYMERS (MIPs) | 82 |
| 2.8.1 | FLOW CYTOMETRIC DETECTION OF MEMBRANE SURFACE MARKERS OF SENESCENT CELLS USING FLUORESCENT MIPS..... | 82 |
| 2.8.2 | FLUORESCENCE MICROSCOPY OF LIVE CELLS..... | 83 |
| 2.8.3 | IMMUNOFLUORESCENCE MICROSCOPY OF MOLECULARLY IMPRINTED POLYMERS (MIPs) IN FIXED CELLS | 83 |
| 2.8.4 | IMMUNOFLUORESCENCE MICROSCOPY OF MOLECULARLY IMPRINTED POLYMERS (MIPs) IN FFPE TISSUES..... | 84 |
| 2.8.5 | <i>IN VIVO</i> IMAGING USING MOLECULARLY IMPRINTED POLYMERS | 85 |
| 2.8.6 | MTS ASSAY ON CELLS TREATED WITH MIP-DRUG CONJUGATES | 85 |
| 2.9 | SENOLYTIC ANTIBODY-DRUG CONJUGATES (ADCs) | 86 |
| 2.10 | ANIMAL STUDY PROCEDURES..... | 86 |
| 2.10.1 | ZMPSTE24 ^{-/-} MOUSE EAR PUNCH GENOTYPING | 87 |
| 2.10.2 | EXPERIMENTAL DESIGN..... | 89 |
| 2.10.3 | DRUG DOSING AND ADMINISTRATION..... | 92 |
| 2.10.4 | MEASURING THE MUSCLE STRENGTH OF MICE | 92 |
| 2.10.5 | CLINICAL FRAILTY SCORING..... | 95 |

| | | |
|-----------|--|-----|
| 2.10.6 | MOUSE BEHAVIOURAL STUDIES | 97 |
| 2.10.7 | SURVIVAL ANALYSIS..... | 101 |
| 2.11 | STATISTICAL ANALYSES..... | 101 |
| CHAPTER 3 | VALIDATION OF NOVEL MARKERS OF SENESENCE | 102 |
| 3.1 | IMMUNOHISTOCHEMISTRY IN TISSUES FROM AN OLD MOUSE | 105 |
| 3.2 | SCREENING OF MARKERS IN YOUNG AND OLD TISSUES | 107 |
| 3.2.1 | IMMUNOHISTOCHEMISTRY OF MARKERS IN MICE TISSUES..... | 107 |
| 3.2.2 | WESTERN BLOT ANALYSIS OF MARKERS IN MICE TISSUES..... | 110 |
| 3.2.3 | qPCR ANALYSIS OF MARKERS IN MOUSE SKIN TISSUES..... | 119 |
| 3.2.4 | SCREENING OF MARKERS IN HUMAN LUNG TISSUES | 120 |
| 3.3 | SCREENING OF MARKERS IN DISEASED TISSUES | 122 |
| 3.3.1 | SENESENCE MARKERS IN HUMAN LUNG CANCER SAMPLES .. | 122 |
| 3.3.2 | SENESENCE MARKERS IN MICE LIVER FIBROSIS SAMPLES | 125 |
| 3.4 | INVESTIGATING NOVEL MODULATORS AND EFFECTORS OF SENESENCE..... | 127 |
| 3.4.1 | THE ROLE OF BTK IN CELLULAR SENESENCE | 127 |
| 3.4.2 | THE ROLE OF DEP1 IN CELLULAR SENESENCE | 132 |
| 3.4.3 | THE ROLE OF B2MG IN CELLULAR SENESENCE | 134 |
| 3.5 | DISCUSSION..... | 136 |
| CHAPTER 4 | TARGETING SENESENCE CELLS WITH MOLECULARLY IMPRINTED POLYMERS (MIPs) AND ANTIBODY-DRUG CONJUGATES (ADCs). | 139 |
| 4.1 | MODELS OF CELLULAR SENESENCE USED FOR MIPs AND ADC TARGETING..... | 140 |
| 4.2 | OPTIMIZATION OF MIP BINDING ASSAYS..... | 143 |
| 4.3 | FLUORESCHEIN-TAGGED B2MG MIPs BIND TO SENESENCE CELLS <i>IN</i> <i>VITRO</i> AND ARE INTERNALIZED | 151 |
| 4.3.1 | FLUORESCHEIN AND CONFOCAL MICROSCOPY OF MIPs..... | 151 |
| 4.3.2 | B2MG-TARGETED MIPs BIND TO SENESENCE CELLS BY FLOW CYTOMETRY..... | 156 |

| | | |
|--|---|-----|
| 4.4 | FLUORESCHEIN-TAGGED DEP1 MIPs BIND TO SENESCENT CELLS <i>IN VITRO</i> | 158 |
| 4.5 | MIPs ARE BIOCOMPATIBLE AND NON-CYTOTOXIC | 159 |
| 4.6 | FLUORESCENTLY TAGGED B2MG MIPs DETECT SENESCENT CELLS <i>IN VIVO</i> | 164 |
| 4.7 | MIPs TARGETED DRUG DELIVERY INTO SENESCENT CELLS | 173 |
| 4.8 | ANTIBODY-DRUG CONJUGATES (ADCs) SELECTIVELY KILL SENESCENT CELLS | 177 |
| 4.9 | DISCUSSION..... | 179 |
| 4.9.1 | BETA-2 MICROGLOBULIN AS A MARKER OF SENESCENCE | 179 |
| 4.9.2 | BIO-DISTRIBUTION, CYTOTOXICITY AND BIOCOMPATIBILITY OF MIPs | 180 |
| 4.9.3 | TARGETED SENOLYTIC THERAPY USING MIPs AND ADCs..... | 181 |
| CHAPTER 5 THE EFFECT OF BTK INHIBITION ON AGEING | | 184 |
| 5.1 | CONFIRMING THE GENOTYPE OF ZMPSTE24 ^{-/-} MICE | 185 |
| 5.2 | PILOT STUDY ON THE EFFECT OF BTK INHIBITION ON AGEING IN ZMPSTE24 ^{-/-} MICE | 186 |
| 5.2.1 | ASSESSMENT OF MUSCLE STRENGTH IN THE PILOT STUDY | 186 |
| 5.2.2 | PILOT STUDY SURVIVAL ANALYSIS..... | 189 |
| 5.3 | FULL STUDY ON THE EFFECT OF BTK INHIBITION ON AGEING IN ZMPSTE24 ^{-/-} MICE | 190 |
| 5.3.1 | ASSESSMENT OF MUSCLE STRENGTH..... | 190 |
| 5.3.2 | ASSESSMENT OF CLINICAL FRAILITY IN MICE | 191 |
| 5.3.3 | EFFECT OF BTK INHIBITION ON ANXIETY-LIKE BEHAVIOUR IN ZMPSTE24 ^{-/-} MICE..... | 194 |
| 5.3.4 | EFFECT OF BTK INHIBITION ON SPATIAL MEMORY IN ZMPSTE24 ^{-/-} MICE | 196 |
| 5.3.5 | SURVIVAL ANALYSIS..... | 202 |
| 5.4 | DISCUSSION..... | 205 |
| 5.4.1 | IMPROVEMENT OF MUSCLE STRENGTH | 205 |
| 5.4.2 | PREVENTION OF LATE-LIFE CLINICAL FRAILITY | 205 |

| | | |
|--|---|-----|
| 5.4.3 | REDUCED ANXIETY-LIKE BEHAVIOUR | 206 |
| 5.4.4 | IMPROVEMENT IN COGNITIVE FUNCTION | 207 |
| 5.4.5 | INCREASED SURVIVAL..... | 207 |
| CHAPTER 6 DISCUSSION AND CONCLUSION..... | | 209 |
| 6.1 | DETECTION AND CLEARANCE OF SENESCENT CELLS USING TARGETED APPROACHES AGAINST SPECIFIC MEMBRANE MARKERS | 209 |
| 6.2 | BTK INHIBITION IMPROVES HEALTHSPAN AND LIFESPAN <i>IN VIVO</i> ... | 211 |
| 6.3 | CONCLUDING REMARKS | 212 |
| REFERENCES..... | | 213 |

LIST OF FIGURES

| | |
|---|-----|
| Figure 1-1 Types of senescence..... | 3 |
| Figure 1-2 The different pathways that lead to oncogene induced senescence. | 10 |
| Figure 1-3 Senescence-associated β -galactosidase staining of IMR-90 cells.. | 17 |
| Figure 1-4 The multifaceted program of the senescence associated secretome. | 22 |
| Figure 1-5 Senescence associated heterochromatic foci (SAHF). | 24 |
| Figure 1-6 Proteins differentially expressed on the membrane of senescent cells..... | 27 |
| Figure 1-7 Control of senescence by the p53/p21 and p16/Rb pathways. | 29 |
| Figure 1-8 Involvement of senescence in adult diseases..... | 38 |
| Figure 1-9 The hallmarks of ageing..... | 43 |
| Figure 1-10 A schematic representation of the process of molecular imprinting. | 55 |
| Figure 1-11 Key components of an antibody-drug conjugate (ADC). | 57 |
| Figure 2-1: An image of the health monitoring sheet used to check animals' welfare | 90 |
| Figure 2-2: The Kondziela's Inverted Screen and fleece bedding used | 93 |
| Figure 2-3: Various weights used for weight lifting tests | 94 |
| Figure 2-4: Clinical Frailty Indices used to assess mice..... | 96 |
| Figure 2-5 Diagram of the Barnes maze | 97 |
| Figure 2-6 The Barnes Maze set-up used for cognitive function tests. The target hole is indicated by the red arrow and visual cues on the wall are indicated by black arrows..... | 98 |
| Figure 2-7 The Elevated Plus Maze used to assess anxiety-like behaviour in mice | 100 |
| Figure 3-1 Immunohistochemistry of skin samples from mice of different ages | 107 |
| Figure 3-2 Immunohistochemistry of muscle from mice of different ages | 108 |
| Figure 3-3 Immunohistochemistry of brain tissue from mice of different ages | 109 |
| Figure 3-4 Western blot analysis of brain tissue samples from 4 mice of different ages | 111 |

| | |
|--|-----|
| Figure 3-5 Western blot of senescence markers in young and old tissues | 112 |
| Figure 3-6 Western blot analysis of skin tissues from 11 mice of different ages | 113 |
| Figure 3-7 Western blot analysis of brain tissues from 11 mice of different ages | 114 |
| Figure 3-8 Western blot of muscle tissues from 11 mice of different ages | 115 |
| Figure 3-9 Western blot analysis of liver tissues from 11 mice of different ages | 116 |
| Figure 3-10 Analysis of mice brain tissues from 7 age groups by Western blot | 117 |
| Figure 3-11 Analysis of mice skin tissues from 7 age groups by Western blot | 118 |
| Figure 3-12 qPCR analysis of mice skin tissues from 7 age groups | 120 |
| Figure 3-13 Immunohistochemistry of human lung tissues | 121 |
| Figure 3-14 Immunohistochemistry of markers in lung cancer samples 1-3 .. | 123 |
| Figure 3-15 Immunohistochemistry of markers in lung cancer samples 4-7 .. | 124 |
| Figure 3-16 Immunohistochemistry of senescence markers in fibrotic livers . | 125 |
| Figure 3-17 Growth curve of Ibrutinib treated IPF and NFC pulmonary fibroblasts..... | 128 |
| Figure 3-18 SA β -Gal staining of pulmonary fibroblasts | 129 |
| Figure 3-19 Effect of Ibrutinib on senescent cell viability..... | 131 |
| Figure 3-20 Gene silencing studies on DEP1 protein in EJp53 cells..... | 133 |
| Figure 3-21 Gene silencing studies on B2MG protein in EJp53 cells..... | 134 |
| Figure 4-1 SA β -Gal and Western blot validation of EJ senescent cell models. | 140 |
| Figure 4-2 Western blot analysis of B2MG in EJ models of senescence. | 141 |
| Figure 4-3 Western blot analysis of DEP1 protein expression in EJ cells. | 142 |
| Figure 4-4 Structure of human histocompatibility antigen HLA-A and β 2Microglobulin | 143 |
| Figure 4-5 A schematic representation of senescent cell targeting by molecularly imprinted polymers (MIPS)..... | 145 |
| Figure 4-6 Fluorescence microscope images of 20% B2MG MIPS in EJp16 cells..... | 146 |
| Figure 4-7 FACS binding assay with 20% B2MG MIPS in EJp16 cells..... | 147 |

| | |
|--|-----|
| Figure 4-8 FACS binding assay for 15% B2MG MIPs in EJp16 cells..... | 148 |
| Figure 4-9 Fluorescence microscope images of 2% and 5% MIPs in EJp21 cells..... | 149 |
| Figure 4-10 Fluorescence microscope images of MIPs in EJp21 cells after wash steps. | 150 |
| Figure 4-11 More B2MG MIPs bind to senescent EJp21 cells than proliferating cells..... | 151 |
| Figure 4-12 Confocal microscope images of B2MG-targeted MIPs in EJp21 cells..... | 152 |
| Figure 4-13 Fluorescence microscope images of 2% B2MG MIPs in EJp16 cells | 153 |
| Figure 4-14 Confocal microscope images of B2MG-targeted MIPs in EJp16 cells..... | 154 |
| Figure 4-15 Confocal microscope images of B2MG-MIPs in mouse skin tissue | 155 |
| Figure 4-16 FACS binding of 2% B2MG-targeted MIPs in EJ cells..... | 157 |
| Figure 4-17 FACS binding of 2% DEP1-targeted MIPs in EJ cells..... | 158 |
| Figure 4-18 Cell cycle analysis of EJ cells incubated with MIPs for 12 hours. | 159 |
| Figure 4-19 Cell cycle analysis of EJ cells incubated with MIPs for 24 hours | 160 |
| Figure 4-20 EJp21 cells incubated with 2% MIPs remain viable after several days | 161 |
| Figure 4-21 EJp21 cells incubated with 5% MIPs are still viable after 8 days | 162 |
| Figure 4-22 Colony Formation assays in EJ cells incubated with MIPs | 163 |
| Figure 4-23 Detection of senescent cells by topically applied fluorescein-MIPs | 164 |
| Figure 4-24 Detection of senescent cells by topically applied Alexa Fluor-MIPs | 165 |
| Figure 4-25 <i>In vivo</i> imaging of mice after topical application of MIPs..... | 166 |
| Figure 4-26 Detecting senescent cells with intravenous Alexa Fluor647-MIPs | 167 |
| Figure 4-27 Fluorescent B2MG MIPs detect senescent cells in old but not young mice..... | 168 |
| Figure 4-28 Mouse whole-body micro-CT and fluorescence imaging tomography | 169 |

| | |
|---|-----|
| Figure 4-29 <i>In vivo</i> imaging of senescent cells using DyLight™ 800-labelled MIPs..... | 170 |
| Figure 4-30 Mice <i>ex vivo</i> imaging in supine position using DyLight™ 800 MIPs | 172 |
| Figure 4-31 Screening of drug compounds for targeted delivery into cells using MIPs..... | 174 |
| Figure 4-32 MTS cell viability assay for 5µM MIP-Drug complexes in EJp16 cells..... | 175 |
| Figure 4-33 Drug delivery into senescent cells using 5µM, 10µM and 20µM MIP-Dasatinib Complex | 176 |
| Figure 4-34 Western Blot analysis of EJp53 cells transfected with B2MG cDNA | 177 |
| Figure 4-35 Antibody-drug conjugates targeting B2MG kill senescent cells... .. | 178 |
| Figure 4-36 Basal mRNA expression of B2MG and DEP1 in human tissues. | 182 |
| Figure 5-1: Sample genotyping results for ZMPSTE24 deficient mice | 185 |
| Figure 5-2: Strength score from mouse weight lifting tests | 187 |
| Figure 5-3: Strength scores from the Kondziela's inverted screen test | 188 |
| Figure 5-4: Kaplan Meier survival curve for the pilot <i>Zmpste24</i> ^{-/-} mice study. | 189 |
| Figure 5-5 Main study Kondziela's strength scores..... | 191 |
| Figure 5-6 Clinical Frailty Scoring in <i>Zmpste24</i> ^{-/-} mice | 192 |
| Figure 5-7 Behavioural effects of Ibrutinib treatment in mice using the EPM. | 195 |
| Figure 5-8 Latency and entrance time of mice into target hole during acquisition | 196 |
| Figure 5-9 Mice nose pokes into maze holes during acquisition stage | 197 |
| Figure 5-10 Accuracy of Target Hole Identification during Acquisition | 198 |
| Figure 5-11 Latency during Barnes Maze Probe Trial..... | 199 |
| Figure 5-12 Mice Nose Pokes into holes during the Probe Trial | 200 |
| Figure 5-13 Latency during the Barnes Maze Recall tests | 201 |
| Figure 5-14 Mice nose pokes into Barnes maze holes during Recall tests | 202 |
| Figure 5-15 Kaplan Meier survival curves for the <i>Zmpste24</i> ^{-/-} mice main study | 203 |
| Figure 5-16 Average lifespan for male and female study animals..... | 204 |

LIST OF TABLES

| | |
|---|-----|
| Table 2.1: Reagents used for Immunohistochemistry | 63 |
| Table 2.2: List of cells used | 66 |
| Table 2.3: Cell Culture Reagents and Supplements | 67 |
| Table 2.4: Primers used for qRT-PCR | 74 |
| Table 2.5: Composition of resolving and stacking gels for SDS-PAGE | 78 |
| Table 2.6: List of Primary Antibodies used | 79 |
| Table 2.7: Secondary Antibodies used for Western Blots | 80 |
| Table 2.8: SA β -Gal Staining Solution | 81 |
| Table 2.9: Tail Lysis Buffer Composition | 88 |
| Table 2.10: Distress scoring sheet with scoring criteria | 91 |
| Table 2.11: Scoring Criteria for Kondziela's Inverted Screen Tests | 93 |
| Table 2.12: Scoring System for Weight Lifting Experiments | 95 |
| Table 2.13: Study design for the Barnes Maze | 99 |
| Table 3.1 SUMMARY OF FINDINGS FROM SCREENING OF MARKERS IN TISSUES..... | 126 |
| Table 5.1 Variables used to measure clinical frailty in mice. Number of cases and % of cases are shown..... | 193 |

ABBREVIATIONS

| | |
|--------------------|--|
| ADC | Antibody- drug conjugate |
| ADCC | Antibody-dependent cell-mediated cytotoxicity |
| ARF | Alternate reading frame |
| ARMCX3 | Armadillo repeat-containing X-linked protein 3 |
| ATM | Ataxia telangiectasia mutated kinase |
| ATR | Ataxia telangiectasia and Rad3-related protein |
| B2MG | Beta- 2 Microglobulin |
| BBB | Blood-brain barrier |
| BrdU | 5-bromo-2'deoxyuridine |
| BSA | Bovine Serum Albumin |
| BTK | Bruton's tyrosine kinase |
| CDK | Cyclin- dependent kinase |
| CDKI | Cyclin- dependent kinase inhibitor |
| CDKN1A | Cyclin Dependent Kinase Inhibitor 1A |
| CDKN1B | Cyclin Dependent Kinase Inhibitor 1B |
| CDKN2A | Cyclin Dependent Kinase Inhibitor 2A |
| CDKN2B | Cyclin Dependent Kinase Inhibitor 2B |
| Chk1 | Checkpoint kinase1 |
| Chk2 | Checkpoint kinase2 |
| Cip1 | CDK-interacting protein 1 |
| CLL | Chronic lymphocytic leukemia |
| COPD | Chronic Obstructive Pulmonary Disease |
| CSF | Cerebrospinal fluid |
| CXCL1 | Chemokine (C-X-C motif) ligand 1 |
| CXCR2 | Chemokine (C-X-C motif) receptor 2 |
| DAPI | 4',6-diamidino-2-phenylindole |
| ddH ₂ O | Double-distilled water |
| DDR | DNA damage response |
| DEP1 | Density-enhanced phosphatase |
| DMEM | Dulbecco's Modified Eagle's medium |
| DMSO | Dimethyl sulfoxide |

| | |
|-------------------------------|---|
| DNA | Deoxyribonucleic acid |
| DPP4 | Dipeptidyl peptidase 4 |
| DTT | Dithiothreitol |
| E2F1 | E2F transcription factor 1 |
| EDTA | Ethylene diamine tetra acetic acid |
| EGTA | ethylene glycol tetra acetic acid |
| ERK | Extracellular signal-regulated kinases |
| FACS | Fluorescence Activated Cell Sorting |
| FITC | Fluorescein isothiocyanate |
| GAPDH | Glyceraldehyde 3-phosphate dehydrogenase |
| GRK | G protein-coupled receptor kinase |
| H ₂ O ₂ | Hydrogen peroxide |
| HDF | Human diploid fibroblast |
| IGF-1 | Insulin-like growth factor 1 |
| IPF | Idiopathic Pulmonary Fibrosis |
| IPTG | Isopropyl β-D-1-thiogalactopyranoside |
| MAPK | Mitogen-activated protein kinase |
| MCL | Mantle cell lymphoma |
| MEF | Murine embryonic fibroblast |
| MiDAS | Mitochondrial dysfunction associated senescence |
| MIPs | Molecularly imprinted polymers |
| MM | Multiple myeloma |
| mTOR | Mammalian target of rapamycin |
| NACWO | Named Animal Care & Welfare Officer |
| NanoMIPs | Molecularly imprinted nano-polymers |
| NBS1 | Nijmegen Breakage Syndrome-1 |
| NK | Natural killer |
| NOTCH3 | Neurogenic locus notch homolog protein-3 |
| NTAL | Non-T cell activation linker |
| NVS | Named Veterinary Surgeon |
| OD | Optical Density |
| OIS | Oncogene-induced senescence |
| OSMF | Oral Submucous Fibrosis |

| | |
|------------------|---|
| PCNA | Proliferating cell nuclear antigen |
| PD | Population Doublings |
| PI | Propidium Iodide |
| PI3K | Phosphatidylinositol 3 kinase |
| PIIPS | proteasome inhibition induced premature senescence |
| PTEN | Phosphatase and tensin homolog |
| Raf | Rapidly accelerated fibrosarcoma |
| Rb | Retinoblastoma |
| RNA | Ribonucleic acid |
| ROS | Reactive oxygen species |
| SADS | Senescence-associated distension of satellites |
| SAHF | Senescence-associated heterochromatin foci |
| SASP | Senescence associated secretory phenotype |
| SA- β -Gal | Senescence-associated β galactosidase |
| Sdi1 | Senescence derived inhibitor 1 |
| SDS | Sodium dodecyl Sulfate |
| SDS-PAGE | Sodium dodecyl Sulfate - polyacrylamide gel electrophoresis |
| shRNA | Short hairpin ribonucleic acid |
| STX4 | Syntaxin 4 |
| TAF | Telomere associated foci |
| TAp73 | Transcriptionally active p73 |
| TEMED | Tetramethyl ethylene diamine |
| Tet | Tetracycline |
| TGF- β | Transforming growth factor beta |
| TIF | Telomere dysfunction-induced foci |
| TLR | Toll like receptor |
| UV | Ultra violet |
| WAF1 | Wild-type p53-activated fragment 1. |
| WT | Wild type |
| X-gal | 5-bromo-4-chloro-3-indolyl- β -d-galactopyranoside |
| XLA | X linked agammaglobulinemia |
| ZMPSTE24 | Zinc metalloproteinase STE24 |

CHAPTER 1 INTRODUCTION

1.1 CELLULAR SENESCENCE

Senescence is derived from the Latin word *senex*, which means an old man, with the word “*senescere*” meaning to grow old. Thus, senescence has often been used to depict biological ageing. Cellular senescence can be defined as a state of permanent growth arrest of biological cells, whereby a cell stops proliferating and withdraws from the cell cycle but remains metabolically active (Dimri *et al.*, 1995; Zhang *et al.*, 2006; Chen *et al.*, 2006; d'Adda di Fagagna & Campisi, 2007; Rufini *et al.*, 2013). This arrest in the growth of cells is usually in response to triggers such as DNA damage, strong mitogenic signals or oncogenic stress due to introduction of *ras* (Serrano *et al.*, 1997) or *raf* (Zhu *et al.*, 1998) into cells, loss of telomeres, which are specialized protective caps with hexameric repetitive sequences (TTAGGG) at the ends of linear chromosomes (Shay, 1997), increased reactive oxygen species, ionizing radiation or chemotherapeutic drugs (Macip *et al.*, 2002; Collado & Serrano, 2010; Muñoz-Espín & Serrano, 2014; Kim *et al.*, 2017). In the face of oncogenic stressors, the cellular senescence mechanism is put in place to protect cells from hyperproliferation signals (Romagosa *et al.*, 2011), indicating its role in tumor suppression.

Cellular senescence was first described by the American anatomist, Leonard Hayflick, alongside his cytogeneticist colleague, Paul Moorhead, when they discovered in 1961 that normal human fibroblasts have a finite proliferative capacity *in vitro*. They referred to this phenomenon as “senescence at the cellular level” (Hayflick & Moorhead, 1961; Hayflick, 1965). They postulated that this cellular senescence may be one of the underlying causes of ageing. In line with their postulation, senescent cells have been found to accumulate in some aged tissues of human, monkey and mouse origin (Naylor *et al.*, 2013; Muñoz-Espín & Serrano, 2014). This type of senescence described by Hayflick and Moorhead is what is now understood to be replicative senescence, which is achieved after telomere shortening due to serial cell division (Campisi, 1997; Holt & Shay, 1999; Gire *et al.*, 2004).

Despite mounting evidence about the process of cellular senescence and its involvement in age-related diseases and cancer, it had previously been suggested that senescence was most likely an artefact of cell culture that does not represent an obstacle to carcinogenesis *in vivo* and also doesn't reflect any phenotype of the cells found within living tissues. (Rubin, 1998; Faragher *et al.*, 1998; Hanahan & Weinberg, 2000). Until the final decade of the 20th century, the concept of senescence was not given wide enough attention due to doubts about its credibility and relevance in tumor development and other diseases of ageing (Narita & Lowe, 2005). Since then, there has been an increasing number of studies in this field that demonstrate the role of senescence in many pathophysiological conditions, including cancer and ageing, which have done an adequate job in settling this debate (Muñoz-Espín & Serrano, 2014; Zhu *et al.*, 2014).

1.2 TYPES OF SENESCENCE

As described in the initial discovery by Hayflick, normal mammalian somatic cells are known to reach a state of irreversible growth arrest and altered functionality after a limited number of population doublings (PD) (Hayflick, 1965; Campisi, 1997; Hayflick, 1997). This phenomenon, termed replicative senescence was later found to be merely one of the ways by which cellular senescence occurs. Another phenotypically alike but much more acute and swiftly occurring event, dubbed accelerated senescence (Chang *et al.*, 1999b) or stress-induced premature senescence (SIPS), can be triggered by ionising radiation, chemotherapeutic drugs, oxidative stress and other DNA damaging agents (Chang *et al.*, 1999a; Toussaint *et al.*, 2000). Based on these findings, cellular senescence has been classified into two general categories namely: replicative senescence and stress-induced premature senescence (Figure 1-1) (Toussaint *et al.*, 2001; Wang & Bennett, 2012).

A vast array of stress signals, including oncogenes, bring about SIPS. However, Oncogene Induced Senescence (OIS) is sometimes described separately from the more general SIPS due to its own distinctive origin. Hence, Debacq-

Chainiaux and colleagues postulate that three main paths lead to and define senescence. According to them, these are: telomere-dependent replicative senescence, oncogene-induced senescence and stress-induced premature senescence (Debacq-Chainiaux *et al.*, 2016). However, the general consensus and view in most research groups including ours, is that there are two main classes of senescence – replicative senescence and SIPS.

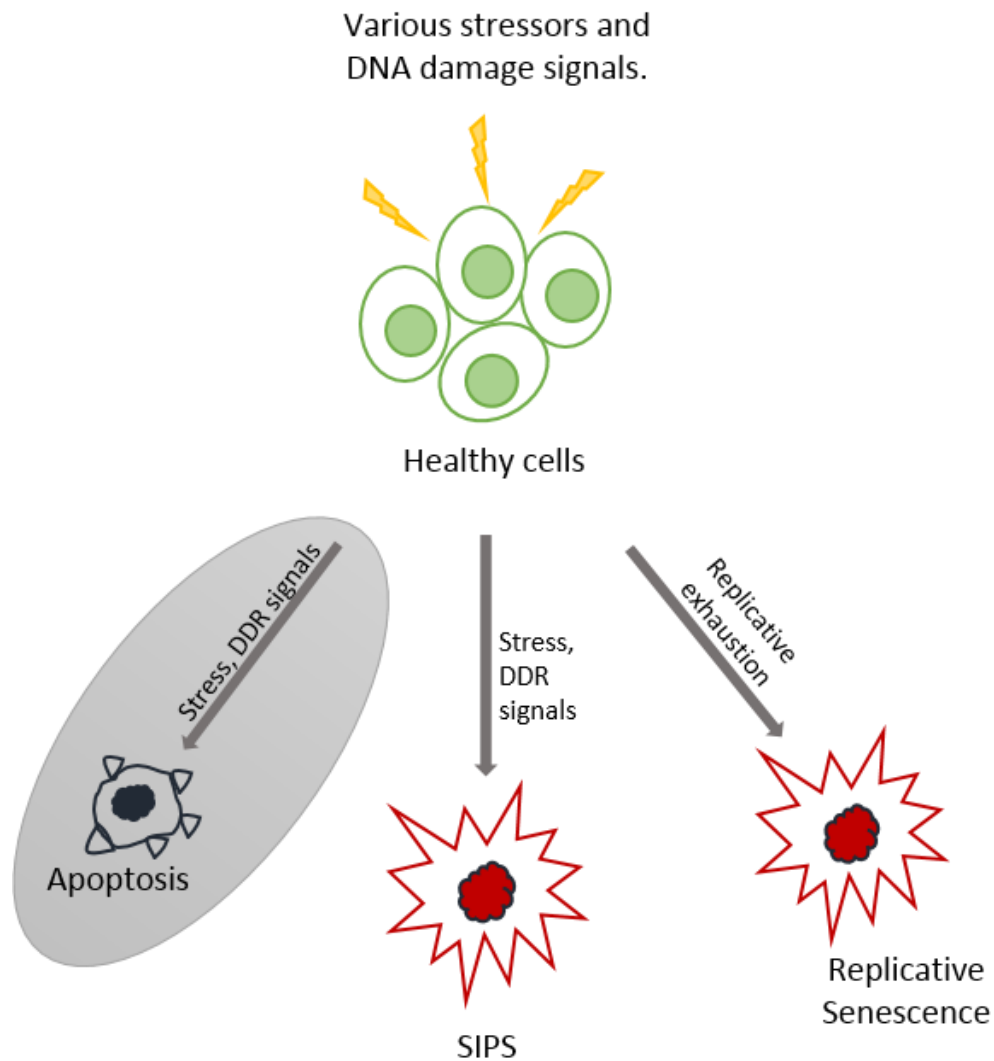


Figure 1-1 Types of senescence.

Different DNA damaging signals bring about the permanent cell cycle arrest that is characteristic of senescence. This could either be due to replicative exhaustion or stress-induced. Some stress signals result in apoptosis instead.

1.2.1 REPLICATIVE SENEESCENCE

Replicative senescence is a form of irreversible growth arrest that occurs as a result of exhaustion of the cell's replicative potential or proliferative lifespan over time, an occurrence rightly dubbed the "Hayflick Limit" (Wright & Shay, 2000b; Shawi & Autexier, 2008). All human somatic cells, with the exception of stem cells and germ line cells, have a limited proliferative capacity (Herbig & Sedivy, 2006; Aravinthan, 2015). Replicative senescence as first described by Leonard Hayflick and Paul Moorhead (Hayflick & Moorhead, 1961; Hayflick, 1965), was observed in cultured fibroblasts showing limited serial division thought to be controlled by a biological clock or "replicometer" (Hayflick, 1997).

Replicative senescence, which is also a characteristic of aging, is sometimes referred to as cellular ageing (MDuff & Turner, 2011) and is associated with shortened telomeres at the chromosomal end due to their erosion during cell division (Xu *et al.*, 2014). This loss or shortening of telomeres is interpreted by cells as damage to the DNA, triggering a DNA damage response (DDR) similar to that elicited by other DNA damaging agents. The DDR is mediated by chromatin regulators such as γ -H2A.X, mediator proteins like Nijmegen Breakage Syndrome-1 (NBS1) and 53 Binding Protein-1 (53BP1), as well as DNA damage checkpoint kinases such as ATM, ATR, CHK1 and CHK2 (d'Adda di Fagagna *et al.*, 2003; Evan & d'Adda di Fagagna, 2009; MDuff & Turner, 2011; Aravinthan, 2015). These kinases phosphorylate and activate various proteins that play a role in the cell cycle. Among these proteins are p16^{INK4a}, a cyclin dependent kinase (CDK) inhibitor and p53, which when phosphorylated activates p21^{Waf1/Cip1/Sdi1}, leading to CDK - cyclin complex inhibition (Shay & Roninson, 2004; d'Adda di Fagagna & Campisi, 2007; Rufini *et al.*, 2013; Muñoz-Espín & Serrano, 2014).

Normal cells from mouse and human origin were observed as they underwent a limited number of divisions in culture. The murine cells were found to undergo senescence more rapidly, just after a few divisions although a few cells escaped and formed permanent cultures. The human cells, on the other hand, slowly stopped dividing with little or no evidence of a permanent cell line formation (Levine, 1997). Telomeres progressively erode over time, with each cell division, eventually leading to a limit in the replicative capacity of cells. The possibility of

telomeres shortening was first proposed in 1986, when it was found that human tissues did not have the same lengths of telomeres (Cooke & Smith, 1986; Wright & Shay, 2000b). In human cells, replicative senescence is thought to set in at an average telomere length of 6 to 8 kilobase pairs (kbp) and these cells remain viable afterwards for a long time (Herbig *et al.*, 2004), although it has been argued that the exact threshold of telomere length or dysfunctional telomeres that can trigger a DDR within a cell and lead to senescence is not known (d'Adda, 2008). In various strains of HDF (human diploid fibroblasts), it was observed that the average telomere length decreased 20bp to 3 kbp at each serial cell division. Also, this telomere attrition and the Hayflick limit is determined by biological, rather than chronological age. In other words, not just by length of days but by physiological activity and other determining factors (Goldstein, 1990; Harley *et al.*, 1990; Hayflick, 1998; Wright & Shay, 2000b; Sikora *et al.*, 2011; Aravinthan, 2015).

The telomerase enzyme is a ribonucleoprotein with a reverse transcriptase (TERT) protein moiety that has a reverse transcription domain. Telomerase is responsible for adding TTAGGG repetitive sequences to telomeres at the ends of chromosomes, replacing that which is lost from erosion during replication. Telomerase is absent in adult tissues with the exception of renewable tissues which keep proliferating, such as hematopoietic and adult stem cells, cells in the intestinal crypt and basal cells of the epidermis. The enzyme is also present in embryonic cells as well as the germline cells (Wright & Shay, 2000b; Herbig & Sedivy, 2006; Shawi & Autexier, 2008). As this enzyme's activity diminishes, it results in telomere attrition as cells complete their biological clock (Hoare *et al.*, 2010).

Replicative senescent cells usually contain one or more short telomeres and marked allelic variations of telomeres have been found among replicative senescent cells of the same cell type. This observation raises the question as to whether this variation accounts for the differences in the rates at which humans age (Baird *et al.*, 2003). Other factors such as nutrition have also been proposed to contribute to telomere length, senescence and ageing (Dhillon *et al.*, 2016; Provinciali *et al.*, 2016). In primary fibroblasts, ectopic expression of the

telomerase enzyme was found to avert telomere loss-dependent replicative senescence and also extend the lifespan of these cells (Bodnar *et al.*, 1998; Shawi & Autexier, 2008).

Telomerase alone is however not always enough to keep primary cells in a state of limitless proliferative capacity. In studies with human keratinocyte and mammary epithelial cells, it was found that both telomerase and p16^{INK4A}/pRb inactivation was required for an extended proliferative capacity (Shawi & Autexier, 2008). It was also discovered that under the same experimental conditions, mouse embryonic fibroblasts (MEFs) which have longer telomeres (40–60 kb) compared to human fibroblasts (5–15 kb), entered into a state of senescence faster (after fewer PDs) than human fibroblasts. This occurrence was thought to be as a result of a higher sensitivity to oxidative stress and oxidative DNA damage rather than as a result of telomere attrition. Replicative senescence in MEFs was found to be a consequence of severe oxidative stress leading to DNA damage, while human cells were able to prevent or repair similar oxidative DNA damage. In 20% oxygen culture conditions, DNA damage limits the proliferation of MEFs, where they accumulate more damage than in 3% oxygen conditions, and more damage than human fibroblasts do in 20% oxygen. Differences in the phenotypes of senescent MEFs and human fibroblasts are thought to be due to differences in their oxygen sensitivity and it is proposed that this may account for variations in cancer incidence and the rate of ageing between mice and humans (Wright & Shay, 2000a; Campisi, 2001; Parrinello *et al.*, 2003; Chen *et al.*, 2007). Senescence in MEFs is thought to depend primarily on the p19^{ARF}/p53 tumour suppressor pathway while fibroblasts from humans can become immortal via a loss of both p53 and retinoblastoma (Rb) tumour suppressor functions (Kamijo *et al.*, 1997; Wright & Shay, 2000a).

1.2.2 STRESS INDUCED PREMATURE SENESCENCE (SIPS)

Stress induced premature senescence (SIPS) is an accelerated form of senescence that occurs without the need for exhaustive cell proliferation. It can be induced by a number of physical or chemical stress stimuli, including oxidizing agents or oxidative stress, ionizing radiation, chemotherapeutic drugs, osmotic stress, heat shocks, mitogenic stimulation and other DNA damage inducing

signals (Serrano & Blasco, 2001; Toussaint *et al.*, 2002a; Toussaint *et al.*, 2002c; Erusalimsky & Kurz, 2005; Debacq-Chainiaux *et al.*, 2016). SIPS has also been referred to as 'stress or aberrant signalling-induced senescence' (STASIS) and has been suggested to be a protective mechanism programmed within the organism against possible carcinogenic insults (Serrano *et al.*, 1997; Drayton & Peters, 2002).

Although stress induced premature senescence is similar to replicative senescence morphologically and molecularly, it is not usually characterized by shortened telomeres (d'Adda di Fagagna & Campisi, 2007; Wang & Bennett, 2012). Studies have now shown that stress accelerates telomere shortening and dysfunctional telomeres can also induce senescence without the attendant telomere shortening (Jurk *et al.*, 2014; Victorelli & Passos, 2017). It was also discovered that p16 can be induced in a telomere independent manner, stirring up speculations that there may be several senescence driving mechanisms available (Drayton & Peters, 2002). While the onset of replicative senescence is determined by the cell's replicative clock or "telomere replicometer" (Hayflick, 1997), SIPS on the other hand is triggered by external stimuli which activate the intracellular senescence cascade prematurely (Muñoz-Espín & Serrano, 2014).

Senescent cells are known to have higher levels of reactive oxygen species (ROS), which are by products of normal cellular oxidative processes, than normal cells. Also, hyperoxia or sub lethal doses of hydrogen peroxide (H₂O₂) can cause oxidative stress and lead to a senescent-like arrest in human fibroblasts (Dumont *et al.*, 2000; Toussaint *et al.*, 2002b; Macip *et al.*, 2003), implicating ROS in the induction of the senescence phenotype. Aged animals possess defective mitochondria and are able to produce higher levels of ROS than young animals. Lipids, proteins and DNA from tissues of aged individuals or aged experimental animals have been known to accumulate oxidative damage (Toussaint *et al.*, 2000). Overexpression of p53 has been shown to cause ROS accumulation, likely to be facilitated by the transcriptional activity of p53 on pro-oxidant genes (Macip *et al.*, 2003). On the other hand, the tumour suppressor TAp73, a member of the p53 family, was found to protect cells against the negative effects of

oxidative stress upon exposure to H₂O₂ (Agostini *et al.*, 2016; Agostini *et al.*, 2018).

Up-regulation of the p21^{Waf1/Cip1/Sdi1} CDK inhibitor led to increase in ROS levels in both normal cells and tumor cells, with the increase being proportional to p21^{Waf1/Cip1/Sdi1} levels (Macip *et al.*, 2002). In this experiment, the EJ cells bladder cancer cells which are known to lack functional p53 were used, showing that accumulation of ROS was as a result of a p53-independent p21^{Waf1/Cip1/Sdi1} induction. ROS is thought to function as a fail-safe mechanism for the maintenance of senescence (Macip *et al.*, 2002; Macip *et al.*, 2003). Accumulation of ROS was not a universal consequence of cell cycle arrest, since induction of growth arrest by p16^{INK4A}, another CDK inhibitor, did not increase ROS levels. Also, ROS inhibition rescued p21-induced senescence in EJ cells. Studies on oxidative stress have shown that senescence can be delayed or prevented upon treatment with antioxidants. In *Drosophila*, overexpression of antioxidant genes such as catalase or superoxide dismutase (SOD) was found to extend lifespan (Parkes *et al.*, 1999). Cell cultures maintained in a low oxygen environment also were found to have enhanced proliferation, indicating a strong link between oxidative damage, senescence and aging (Macip *et al.*, 2003; Campisi, 2013; Carrera *et al.*, 2014).

Just like in replicative senescence induced by telomere loss, persistent DNA damage foci and DDR signalling have been observed in SIPS and about half of these foci are located at telomeres regardless of telomerase activity. These persistent DNA damage foci are referred to as telomere dysfunction induced foci (TIF) when they are found at telomeres otherwise they are called DNA segments with chromatin alterations reinforcing senescence (DNA-SCARS) (Campisi, 2013; Rufini *et al.*, 2013). Radiation and chemotherapeutic agents have been reported to induce telomere dysfunction in normal fibroblasts and T cells (Li *et al.*, 2012). Live-cell imaging studies have also shown that all persistent foci are associated with telomeres. When the DNA damage foci observed were due to random double strand breaks (DSB) caused by irradiation, they were named telomere associated foci (TAF) rather than telomere-induced foci (TIF) which are usually accredited to telomere uncapping. Although the gut and liver of mice have

long telomeres and active telomerase, both tissues show an increase in the frequencies of DNA damage foci with age. Telomeres are significant targets for stress both *in vitro* and *in vivo*, and are critical to the ageing process (Hewitt *et al.*, 2012; Birch *et al.*, 2015; de Magalhães & Passos, 2017).

1.2.3 ONCOGENE INDUCED SENESCENCE (OIS)

Oncogene Induced Senescence (OIS) is an example of SIPS and is so named because it is triggered by oncogenes. It is a form of senescence that can be induced prematurely in young cells independent of replicative potential, by activation of oncogenes (Xu *et al.*, 2014) and it has been observed that many paths lead to OIS (Courtois-Cox *et al.*, 2008). OIS is a protective physiological process, a tumor-suppressing defence mechanism that must be bypassed for cancer to develop (Michaloglou *et al.*, 2005; Alexandraki *et al.*, 2012; Muñoz-Espín & Serrano, 2014). Activation of either the p53/p21^{WAF1} or the p16^{INK4A}/Rb tumor suppressor pathways is essential to implement OIS and how each pathway contributes to the phenotype depends on the senescence trigger as well as the cell type (Kiyono *et al.*, 1998; Drayton *et al.*, 2003; Barradas *et al.*, 2009; Vizioli *et al.*, 2014). Also, the DNA damage response (DDR), chromatin remodelling, and senescence-associated secretory phenotype (SASP) are important for the initiation and maintenance of OIS (Figure 1-2) (Di Micco *et al.*, 2006; Xu *et al.*, 2014). Although the tumor suppressor protein p53 plays a fundamental role in the establishment of OIS, as observed in various types of human fibroblasts and also in MEFs, it is however not the only mediator of OIS. Some cell types have been found to undergo senescence in response to deviant oncogene activation in a p53-independent manner (MDuff & Turner, 2011; Drayton *et al.*, 2003). Also, it is suggested that p16 plays the specific role of maintaining growth arrest in OIS through the activation of retinoblastoma (Rb) (MDuff & Turner, 2011).

Oncogenic *ras* induced senescence occurs via the mitogen activated protein kinase (MAPK) pathway and also involves the Rb as well as the p53 tumor suppressor pathways (Lin *et al.*, 1998; Narita & Lowe, 2005). Serrano and colleagues have shown that primary fibroblasts of mouse and human origin enter into a permanent cell cycle arrest in response to *ras* induction and that this arrest happens at the G1 phase with p53, p21, and p16 proteins being significantly

upregulated (Serrano *et al.*, 1997). Also, activation of *ras* proto-oncogenes as well as mutations that activate the Ras protein are common in human cancers.

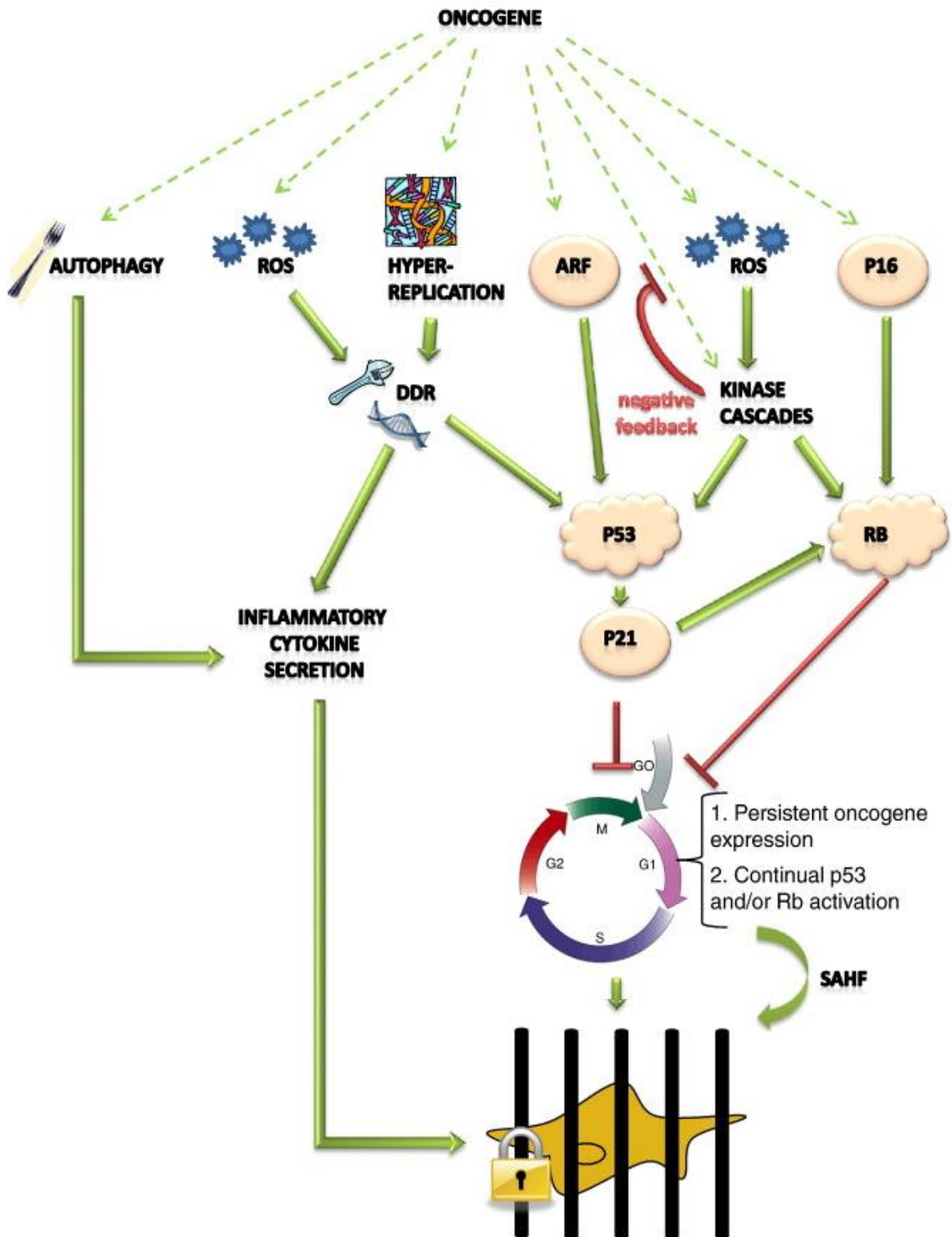


Figure 1-2 The different pathways that lead to oncogene induced senescence. Following oncogenic insult, a complex network of pathways including the ARF/p53/p21 pathway, the p16/RB pathway as well as autophagy, bring about the irreversible cell cycle arrest in oncogene induced senescence. Adapted from (MDuff & Turner, 2011).

Aberrant activation of the Ras signalling pathway leads to cancer development (Downward, 2003). Mitogen activated protein kinases triggered by cytokines, tyrosine kinases, as well as serpentine receptors, which are mostly linked to the pathway through Ras activation, play a role in proliferation signalling. Some studies have shown that activated Ras or a sustained activation of MAPK speeds up the onset of senescence in some cells and induces growth arrest in others (Lee *et al.*, 2000). Also, a negative feedback signalling network is thought to drive OIS, where mutations affecting Raf, Ras and NF1 induce a response that efficiently suppresses Ras and its effectors (Courtois-Cox *et al.*, 2006).

Different intensities of *ras* signals have been found to produce opposing cellular responses via a differential activation of the MAPK pathways mediating them. It was found that a moderate increase in *ras* expression stimulated the mitogenic MEK-ERK pathway and promoted cell proliferation, while a further increase in *ras* expression further stimulated MEK and ERK still, initially enhancing proliferation, but eventually leading to MKK3/6-p38 pathway activation and premature senescence with an induction of p53 and p16^{INK4A}, in the presence of a sustained stronger *ras* expression (Lin *et al.*, 1998; Deng *et al.*, 2004; Courtois-Cox *et al.*, 2008). A similar dose-dependent pleiotropic response is obtained with Raf, which is a downstream effector of Ras. When activated at low levels, Raf leads to cell cycle progression, but higher levels lead to cell cycle arrest with a p53-independent induction of p21. A cross talk is thought to exist between the proliferation and differentiation pathways activated by Ras/Raf/MAPK, and the growth arrest functions of tumor suppressor genes such as p53, p16, and Rb (Zhu *et al.*, 1998; Lee *et al.*, 2000).

Apart from oncogenic *ras*, OIS can also be induced by other oncogenes, such as *BRAF*^{V600E}, *AKT*, *E2F1*, *cyclin E*, *mos*, *c-Myc* and *Cdc6*, as well as by inactivation of tumor-suppressor genes such as *PTEN* and *NF1* (Courtois-Cox *et al.*, 2006; MDuff & Turner, 2011; Bianchi-Smiraglia & Nikiforov, 2012; Xu *et al.*, 2014). *BRAF* is a protein kinase and downstream effector of Ras. Human naevi (moles or benign tumours of melanocytes) usually carry a V600E oncogenic mutation (substitution of valine for glutamic acid) in *BRAF* (Davies *et al.*, 2002; Pollock *et al.*, 2002). Benign melanocytic nevi often express the *BRAF*^{V600E} oncogene and

show features of senescence, such as a high p16^{INK4a} expression and a positive senescence-associated β -galactosidase (SA- β -Gal) activity. When the senescence barrier is escaped, oncogenic stimuli leads to formation of a malignant melanoma rather than a benign naevi. (Vizioli *et al.*, 2014). Also, BRAF^{V600E} delivery by a retrovirus inhibited proliferation of normal human fibroblasts, with an increase in p16^{INK4A} expression (Michaloglou *et al.*, 2005). However, inactivation of p16^{INK4A}, on its own or in combination with p14^{ARF}, did not result in an escape from BRAF^{V600E}- induced senescence (Michaloglou *et al.*, 2005; Haferkamp *et al.*, 2009; Kuilman *et al.*, 2010).

Loss of PTEN (phosphatase and tensin homolog), a lipid phosphatase and a negative regulator of the PI3K/AKT survival pathway, triggers a p53-dependent OIS in primary murine fibroblasts (Chen *et al.*, 2005). Total depletion of PTEN, induces the expression of p19^{ARF}, an inhibitor of the murine double minute 2 (MDM2) protein, which then leads to p53 stabilization and a high expression of p21^{WAF1}, resulting in senescence. Loss of PTEN, has been shown to produce premalignant hyperplasia in prostate epithelial cells in mice, triggering a p19^{ARF}/p53/p21^{WAF} dependent senescence program to suppress cancerous growth *in vivo* (Narita & Lowe, 2005; Xu *et al.*, 2014). Studies using primary human fibroblasts demonstrate that the mammalian target of rapamycin (mTOR) is required for oncogenic *ras*-induced senescence and that this type of OIS response is p53 dependent, underscoring the importance of the PI3K/AKT/mTOR pathway in OIS (Aistle *et al.*, 2011; Kolesnichenko *et al.*, 2012).

A study by Vredeveld and fellow researchers has however questioned the role of the PI3K/AKT/mTOR pathway in OIS. They suggest that activation of this pathway blocks BRAF^{V600E}-induced senescence rather than enhance it. Using both primary human fibroblasts and primary human melanocytes transfected with shRNA against PTEN, BRAF^{V600E}-induced senescence was seen to be disrupted. Also, in a BRAF^{V600E} knock-in mouse model, introduction of a lentivirus which carried PTEN shRNA led to tumor formation in skin nevi, suggesting that depletion of PTEN allows BRAF^{V600E}- expressing nevi cells to resume proliferation (Vredeveld *et al.*, 2012).

Overexpression of the proto-oncogene *c-myc* promotes growth and proliferation but it also drives cells into senescence and apoptosis (Lin *et al.*, 1998; Guney & Sedivy, 2006; Bianchi-Smiraglia & Nikiforov, 2012). Like several other oncogenic agents, c-Myc induces an overexpression of p16^{INK4a} and a disruption of the p16^{INK4a}/Rb pathway is needed to circumvent senescence. The ability of c-Myc to bypass the p16^{INK4a}/Rb checkpoint and also up-regulate telomerase activity accounts for its capacity to immortalize human prostate epithelial cells (Gil *et al.*, 2005). Oncogenic Myc expression in Hs68 primary human foreskin fibroblasts results in a p16-dependent senescence response which can be bypassed when this tumour suppressor protein is down-regulated. Also, Leiden cells which are primary human dermal fibroblasts with a germ line mutation of p16 are resistant to senescence induced by oncogenic Myc (MDuff & Turner, 2011).

Similar to the classical oncogenes *RAS* and *MYC*, PI3K (phosphoinositide 3-kinase) is also an important regulator of malignant transformation. However, depending on the cellular context, all three can result in cell cycle arrest, senescence or cell death when excessively stimulated in normal cells. OIS is not brought about by a simple singular pathway, but rather by a complex signalling network that is more often than not context dependent. Hence, depending on the cell type and the OIS inducer, the signalling pathways mediating the activation of p53 and p16^{INK4A} may vary (Grandori *et al.*, 2003; Xu *et al.*, 2014).

Autophagy, a catabolic degradative process characterised by the formation of double lipid membrane vesicles (autophagosomes) which sequesters intracellular cytoplasmic components for lysosomal degradation, is another mechanism that is important for establishing or reinforcing OIS (Levine & Kroemer, 2008; Gorgoulis & Halazonetis, 2010; MDuff & Turner, 2011). There is an increase in autophagy in OIS, as it contributes to cell cycle arrest and production of the SASP, which are critical for inducing and establishing OIS (Kuilman *et al.*, 2010; Young *et al.*, 2013). A stable down-regulation of two vital autophagy-related genes, *ATG5* and *ATG7*, resulted in senescence bypass, confirming the underlying role of autophagy in the establishment of OIS. Also, *ATG6/beclin*, a crucial autophagy gene is found to be deleted in cancer, further demonstrating the role of autophagy in tumor suppression. Autophagy is however

also employed by cancer cells, suggesting that it could be a process engaged during stress and could promote or inhibit cancer growth depending on the cellular context (Gorgoulis & Halazonetis, 2010; MDuff & Turner, 2011).

The *ras* oncogene has also been found to induce OIS by generating and accumulating ROS which trigger DNA damage responses (Lee *et al.*, 1999). OIS is furthermore marked by chromatin remodelling and accumulation of senescence-associated heterochromatic foci (SAHF), which are believed to enforce the irreversibility of OIS (Figure 1-2) (Michaloglou *et al.*, 2005; Salama *et al.*, 2014; Xu *et al.*, 2014). A study linking mitochondrial dysfunction with OIS shows that production of reactive oxygen species (ROS) by dysfunctional mitochondria increased prior to OIS in a p53-dependent as well as pRb-dependent manner, suggesting that mitochondrial dysfunction is a trigger for senescence (Moiseeva *et al.*, 2009; Gorgoulis & Halazonetis, 2010).

Although it was previously reported that the induction of OIS was not reliant on telomerase activity or telomere length (Wei *et al.*, 1999), Suram and co-researchers have shown that oncogenes induce telomere dysfunction and telomere attrition in primary fibroblasts. They also demonstrated that OIS is stabilized by dysfunctional telomeres and is unstable in cells with a high activity of telomerase enzyme, an occurrence they called telomere dysfunction-induced cellular senescence (TDIS) (Suram *et al.*, 2012; Xu *et al.*, 2014). It is likely that OIS also depends on DNA damage signals at the telomeres (Hewitt *et al.*, 2012; Jacobs, 2013). Cells will need to escape replicative senescence and SIPS through mechanisms such as the mutation and inactivation of p53 or p16, overexpression of oncogenes (Serrano *et al.*, 1997) or the activation of telomerase (Shay, 1997) in order for neoplastic transformation to occur (Chang *et al.*, 1999b). Evasion of the senescence barrier is therefore a critical step in tumor progression *in vivo* (Hanahan & Weinberg, 2011).

1.2.4 DEVELOPMENTALLY PROGRAMMED SENESCENCE

It is proposed that depending on the cell type and conditions, the mechanisms that ultimately lead to senescence may vary. There is another type of senescence known as Developmental Senescence or developmentally programmed senescence which is so named due to the fact that it has been observed during

embryonic development, to allow for tissue remodelling (Munoz-Espin *et al.*, 2013). Developmentally programmed senescence shares some features with OIS such as expression of p21 and the senescence associated secretory phenotype (SASP). It is also thought that OIS is an adaptation of developmentally programmed senescence (Storer *et al.*, 2013). This type of senescence found in the developing embryo has some characteristic features that are distinct from damage-induced senescence, such as the absence of DNA damage markers and selective absence of proliferative arrest (Muñoz-Espín & Serrano, 2014).

1.3 CHARACTERISTICS OF SENESCENT CELLS

Certain characteristics distinguish senescent cells from normal proliferating cells. Senescent cells are growth inhibited and can no longer respond to growth factors or mitogens and they express unique characteristic features or markers that are not expressed in growing cells. These features include having morphological changes to show a flattened and enlarged shape; staining positive for β -galactosidase at pH 6.0 also known as senescence-associated β -galactosidase (SA β -Gal); increased expression of p21, p53, p16, p15, p27 and ARF; presence of senescence-associated heterochromatin foci (SAHF), enlarged and prominent nucleoli (Figure 1-3), as well as a unique profile of secretions involving inflammatory cytokines and chemokines, growth factors and matrix-remodelling proteins, known as the senescence-associated secretory phenotype (SASP) (Hayflick, 1965; Narita *et al.*, 2003; Campisi, 2011; Rodier & Campisi, 2011; Rufini *et al.*, 2013; Naylor *et al.*, 2013; Muñoz-Espín & Serrano, 2014; Pérez-Mancera *et al.*, 2014).

Senescent cells are also known to stain positive for the histochemical Sudan Black-B (SBB), which stains the lysosomal aggregate and "age-pigment", lipofuscin (Terman & Brunk, 2004; Georgakopoulou *et al.*, 2013). SBB stains senescent cells in tissues regardless of sample preparation and can be used on formalin-fixed, paraffin-embedded tissues, giving it an advantage over SA β -Gal, which requires the use of fresh cells or tissue samples (Georgakopoulou *et al.*, 2013; Muñoz-Espín & Serrano, 2014). NOTCH3, a member of the Notch family

receptors, is also used as a senescence marker as it is reported to have tumour suppressor functions and is overexpressed in senescent fibroblasts (Cui *et al.*, 2013; Althubiti *et al.*, 2014). Senescent cells also display a senescent-associated distension of satellites (SADS), a display of constitutive peri/centriomeric satellite heterochromatin decondensation, which are not exclusive to either the p53-p21 or the p16^{INK4A} pathways. These SADS occur prior to and independently of SAHF formation (Swanson *et al.*, 2013; Ogrodnik *et al.*, 2017).

1.3.1 GROWTH ARREST, MORPHOLOGICAL AND PHYSICAL CHANGES

The inability of a cell to progress through the cell cycle is the main hallmark of cellular senescence. Senescent cells lose their proliferative potential but remain metabolically active. In addition, they resist apoptosis, i.e. they do not respond to cell-death signals, and they also have an altered gene expression (Hensler & Pereira-Smith, 1995; d'Adda di Fagagna & Campisi, 2007; Demidenko *et al.*, 2010). Senescent cells are generally growth arrested in an irreversible manner at the G1 phase of the cell cycle, where they are unable to progress into the S phase (Di Leonardo *et al.*, 1994; Zhang *et al.*, 2006; d'Adda di Fagagna & Campisi, 2007). This type of arrest is different from the temporary growth arrest at G0 known as quiescence, which is reversible when the right conditions are presented (Hensler & Pereira-Smith, 1995). However, senescence has also been reported to occur as a growth arrest at the G2/M phase of the cell cycle, known as the “G2 exit program”. This notion has however failed to receive a wide enough acceptance (Levine, 1997; Zhang *et al.*, 2006; d'Adda di Fagagna & Campisi, 2007; Demidenko *et al.*, 2009; Gire & Dulic, 2015). The EJ bladder cancer cells have been shown to exhibit G1 and G2 growth arrest when p21^{Waf1/Cip1/Sdi1} was overexpressed in them. This G1 and G2/M dual arrest by p21^{Waf1/Cip1/Sdi1} differed from the G1 specific arrest mediated by other Cdk inhibitors like p27 and p16^{INK4A} (Sugrue *et al.*, 1997; Fang *et al.*, 1999; Macip *et al.*, 2002).

p53 and p21^{Waf1/Cip1/Sdi1} are thought to mediate DNA damage induced cell cycle arrest at G1 and G2/M (Levine, 1997; Chang *et al.*, 1999b). It has been observed that an upregulation of either of the growth inhibitory genes p16^{INK4A} or p21^{Waf1/Cip1/Sdi1} is enough to inhibit cell proliferation significantly and only a minor fraction of cell cultures entering senescence harbour an overexpression of both

p16 and p21 (Herbig *et al.*, 2004). In this study, using single cell detection methods, it was also found that expression of p16, p21 and SA- β -gal increased as cultured cells approached senescence, while BrdU labelling decreased (Herbig *et al.*, 2004). What distinguishes senescent cells from quiescent ones is the inability of senescent cells to proliferate even when adequate growth signals are reintroduced.

1.3.2 SENESCENCE ASSOCIATED β -GALACTOSIDASE (SA β -GAL)

Dimri and colleagues described the senescence associated β -galactosidase (SA- β -Gal) staining which stained senescent cells blue *in vitro* at a pH of 6.0 (Figure 1-3) (Dimri *et al.*, 1995). Their work provided evidence that senescent cells not only existed but persist in tissues and accumulate *in vivo* with age. They demonstrated that, several human cells express β -galactosidase upon senescence, which is detectable cytologically or histochemically in freshly fixed cells or tissues at pH 6.0 (Dimri *et al.*, 1995; Campisi, 2011; Muñoz-Espín & Serrano, 2014). They found that the SA- β -Gal marker was expressed in senescent fibroblasts and keratinocytes but not in pre-senescent ones. SA- β -Gal was also absent from terminally differentiated keratinocytes, quiescent fibroblasts as well as immortal cells. However, SA- β -Gal was induced by genetic manipulations that reversed immortality and induced senescence in cells. Furthermore, an age-dependent increase in SA- β -Gal was observed in dermal fibroblasts and epidermal keratinocytes in skin samples from human donors of different ages (Dimri *et al.*, 1995).

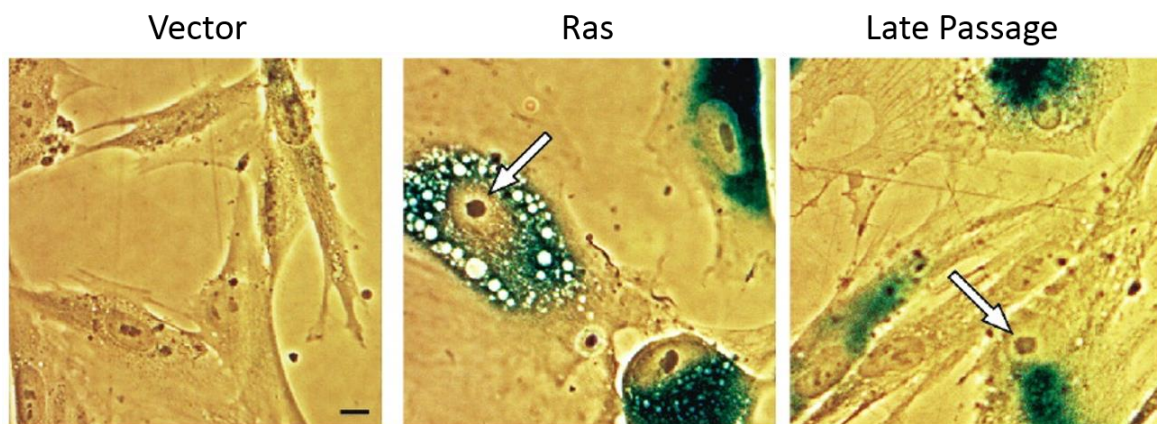


Figure 1-3 Senescence-associated β -galactosidase staining of IMR-90 cells. Oncogene-induced and replicative senescent human lung fibroblasts stain positive for SA β -Gal at pH 6. Typical flattened, enlarged morphology and large prominent nucleoli (arrows) of senescent cells are seen. Adapted from (Narita *et al.*, 2003).

Senescent cells are detected by the SA- β -Gal assay based on increased levels of lysosomal β -galactosidase activity which is thought to be as a result of increased content and mass of the lysosomes in these cells (Kurz *et al.*, 2000). SA- β -Gal activity is detected when cells are incubated with the chromogenic artificial substrate 5-bromo-4-chloro-3-indolyl- β -d-galactopyranoside (X-gal) using a citric acid/sodium phosphate buffer at pH 6.0, to yield an insoluble blue precipitate upon cleavage by β -galactosidase (Kurz *et al.*, 2000; Itahana *et al.*, 2007; Aravinthan, 2015). The assay is able to identify senescent cells in a heterogeneous population of cells and in ageing tissues. However, it is worthy of note that almost all cells express endogenous lysosomal β -galactosidase activity at pH 4.0 and certain cell types such as human epithelial cells and mouse fibroblasts stain with less intensity for SA- β -Gal at pH 6.0 but their intensity can be improved by slightly lowering the pH. Moreover, when cells are maintained at confluency for long periods, a false positive density-induced SA- β -Gal activity can be detected. Serum starvation is also known to produce false positive SA- β -gal (Itahana *et al.*, 2007; Campisi *et al.*, 2009; Evangelou *et al.*, 2017). SA- β -gal is currently considered to be one of the best senescence markers available despite its unreliability and presentation of false positives (Erusalimsky & Kurz, 2005).

1.3.3 THE SENESCENCE-ASSOCIATED SECRETORY PHENOTYPE (SASP)

Senescent cells secrete factors collectively called the senescence associated secretory phenotype (SASP), also referred to as the senescence messaging secretome (SMS). The SASP comprises inflammatory cytokines, chemokines, matrix remodelling proteins, damage-associated molecular pattern proteins (DAMPs), growth factors, such as interleukins 6, 7, and 8 (IL-6, IL-7, IL-8), Macrophage Inflammatory Protein 3 α (MIP-3 α), Growth Regulated Oncogene alpha (GRO α), Monocyte Chemoattractant Proteins 1 and 2 (MCP-1 and MCP-2), Insulin-like Growth Factor Binding Protein (IGFBP), Hepatocyte Growth Factor (HGF), etc., which are able to disrupt tissue structure and function, causing chronic age-related diseases and cancer progression (Kuilman & Peeper, 2009; Young *et al.*, 2013; Salama *et al.*, 2014; Laberge *et al.*, 2015; Maciel-Barón *et al.*, 2016; Kirkland & Tchkonja, 2017; McHugh & Gil, 2018). The

SASP varies between tissues and different senescence triggers, however, pro-inflammatory cytokines such as IL-6 and IL-8 are highly conserved aspects of the secretome and play key roles in the maintenance of the SASP response within the senescent cell and all over the affected tissue (Kuilman *et al.*, 2008; Lasry & Ben-Neriah, 2015). As senescent cells are known to accumulate with ageing (Naylor *et al.*, 2013; Muñoz-Espín & Serrano, 2014), their SASP perpetuate chronic inflammation in surrounding tissues and lead to several diseases of ageing including cancer. Hence, the quest to clear senescent cells as a therapeutic strategy for age-related diseases including cancer (Baker *et al.*, 2011; Baker *et al.*, 2016).

The senescence response is induced by various stimuli or triggers, many of which directly or indirectly lead to DNA damage and activate the DDR. Hence, SASP may be a result of severe DNA damage and not merely permanent cell cycle arrest. Persistent DDR such as that associated with DNA-SCARS helps to maintain senescence via p53 activation (Rodier *et al.*, 2009; Coppe *et al.*, 2010; Rodier *et al.*, 2011). The DDR also activates SASP formation but this happens independently of p53, as loss of p53 function increases the development of this phenotype. Thus, it is suggested that p53 restrains the development of SASP (Coppe *et al.*, 2008). Senescence induction through DDR-p53-p21^{Cip1/Waf1/Sdi1} is a rapid process, but the SASP takes several days to develop. The SASP is also regulated by microRNAs, the JAK/STAT signalling pathway, cytokine receptor for interleukin-1 (IL-1) and IL-8 chemokine receptor CXCR2 as well as transcription factors such as NF-κB (Coppe *et al.*, 2011).

The various mechanisms involved in the generation of the secretory phenotype of senescent cells are increasingly being investigated and mTOR has been linked to the secretory activity of these cells. Studies have shown that mTOR inhibition with rapamycin inhibits the SASP and reduces SA-βgal staining of senescent cells but does not affect their growth arrest. This implies that in cell senescence, the SASP and cell cycle arrest are not coupled and thus can be independently regulated. Senescence growth arrest does not always result in production of SASP and the SASP is not tied to other characteristics of senescence such as enlarged cell morphology and SA-βgal expression (Laberge *et al.*, 2015; Herranz

et al., 2015; Wang *et al.*, 2017b). Ectopic expression of p16^{INK4a} and p21^{WAF1/Cip1/Sdi1} induced senescence without production of SASP, although other features of senescence such as a stable growth arrest were seen (Coppe *et al.*, 2011). It has been suggested that the SASP is not an essential feature of senescent cells and as is the case with p53, SASP can also develop independently of p16^{INK4a} status (Coppe *et al.*, 2011). It was proposed that p16^{INK4a} neither establishes nor maintains the SASP and it is also suggested that p16^{INK4a} may not affect the SASP but might indirectly diminish cytokine secretion by restraining proliferation and its accompanying DNA damage. This can be observed in p16^{INK4a} depleted late passage cells which secreted more IL-6 than their unmodified counterparts at similar population doublings. It is possible that stress stimuli which induce p16^{INK4a} or p21^{WAF1/Cip1/Sdi1} expression without DNA damage could bring about the beneficial effects of senescence such as growth arrest of stressed cells without the deleterious effects SASP formation and attendant disruption of the tissue microenvironment (Coppe *et al.*, 2011; Malaquin *et al.*, 2016). In a recent study, inhibition of MDM2 has also been found to reduce the inflammatory secretome of senescent cells (Wiley *et al.*, 2018).

The SASP is known to exert both autocrine (cell autonomous) as well as paracrine (non-cell autonomous) effects on surrounding cells and is able to induce cell proliferation in transformed cells (see Figure 1-4). IL-6 and IL-8 for instance have cell autonomous properties which reinforce senescence in a paracrine fashion (Collado & Serrano, 2010; Campisi *et al.*, 2011; Acosta *et al.*, 2013; Hoare & Narita, 2013). It has also recently been reported that NOTCH1 plays a vital role as both a regulator of the composition SASP and a regulator of juxtacrine signalling within the context of OIS (Hoare & Narita, 2017; Ito *et al.*, 2017). Chemokines, which are part of the secretome of SASP, encourage cancer promotion, metastasis, vascularisation and angiogenesis. Several pro-inflammatory cytokines and chemokines including IL-8, IL-6, growth regulated protein α (GRO α ; CXCL1), IL-1 α , granulocyte colony stimulating factor (G-CSF) and granulocyte-macrophage colony stimulating factor (GM-CSF) which are capable of maintaining the invasive and metastatic phenotype have been implicated in thyroid carcinomas (Acosta *et al.*, 2008; Acosta & Gil, 2009). IL-8 was found to act together with its receptor CXCR2 to reinforce senescence in

thymocytes. Findings have suggested that IL-8 and GRO α signalling can reinforce senescence early during tumorigenesis, thereby preventing tumor growth. Incorporating these findings is challenging, considering that IL-8 and GRO α already have well-known tumor promoting effects (Acosta & Gil, 2009). Components of the SASP are thought to fuel malignant phenotypes in nearby tumour cells and at the same time play a role in stimulating immune cells to clear out senescent cells (Collado & Serrano, 2010). It has also been proposed that the SASP may originally had the function to help to clear senescent cells by attracting immune effector cells (Coppe *et al.*, 2010; Moreno-Blas *et al.*, 2018).

The chemokine receptor CXCR2 is upregulated during senescence and along with many of its ligands forms part of a chemokine network acting to reinforce growth arrest in a p53-dependent way (Acosta *et al.*, 2008). Mutation or downregulation of CXCR2 was found to alleviate both replicative and oncogene-induced senescence (OIS) and diminish the DNA-damage response thereby annulling its pro-senescent activity to facilitate tumour progression. Ectopic expression of CXCR2 results in premature senescence which occurs via a p53-dependent mechanism (Acosta *et al.*, 2008; Vizioli *et al.*, 2014). The role played by CXCR2 ligands in tumor progression is complex. While evidence suggests they exert a pro-senescent effect in primary cells, they may also have several pro-tumorigenic effects on tumor progression. The origin of the cellular insult, its genetic background as well as the stage and status are some of the factors that may determine what effect CXCR2 exerts. It is still unclear what switches the activity of the components of the senescence secretome from pro-senescence to pro-tumorigenic as several factors could be responsible for this (Kuilman & Peeper, 2009; Acosta & Gil, 2009; Vizioli *et al.*, 2014).

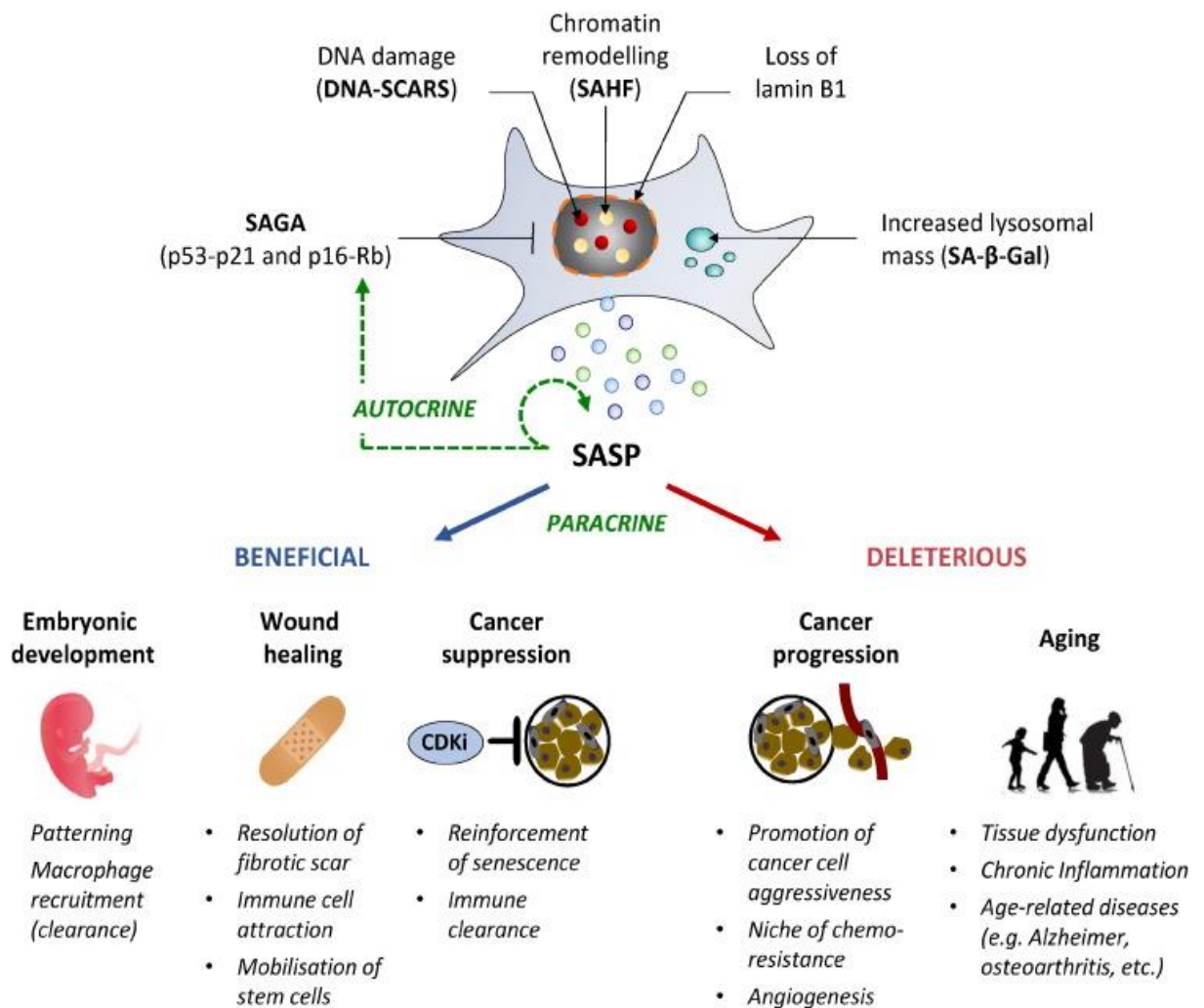


Figure 1-4 The multifaceted program of the senescence associated secretome.

A typical senescent cell displays morphological and biochemical changes including production of the SASP. This secretome exerts autocrine effects which re-inforce senescence associated growth arrest (SAGA), as well as paracrine effects which could be beneficial or deleterious. Adapted from (Malaquin *et al.*, 2016).

It has recently been discovered that the SASP composition from a senescent cell is dependent on the insult triggering the senescence and the molecular regulation of the SASP program is complex and multifaceted in space and time (Malaquin *et al.*, 2016; Wang *et al.*, 2017b). Researchers have shown that mitochondrial dysfunction can lead to a type of cellular senescence referred to as mitochondrial dysfunction associated senescence (MiDAS) (Wiley *et al.*, 2016; Gallage & Gil, 2016; Herranz & Gil, 2016; Wiley & Campisi, 2016), producing a secretory phenotype that is different from the SASP which is obtained from senescence induced by genotoxic stress (Wiley *et al.*, 2016). Also, using models of stress

induced premature senescence (SIPS), proteasome inhibition induced premature senescence (PIIPS) and replicative senescence (RS), Maciel-Barón and colleagues demonstrated that RS and SIPS induced SASP with similar composition, while the composition of SASP due to PIIPS was substantially different with significantly lower amounts of cytokines and chemokines when compared to RS and SIPS (Maciel-Barón *et al.*, 2016). Additionally, using conditioned media obtained from each of these three models of senescence (SIPS, PIIPS and RS) the researchers tested their effect on cell proliferation and found each conditioned media to have a different effect, suggesting that the SASP originating from different senescence inducers activate different pathways in neighbouring cells and lead to different responses (Maciel-Barón *et al.*, 2016; Wang *et al.*, 2017b).

1.3.4 SENESCENCE ASSOCIATED HETEROCHROMATIC FOCI (SAHF)

Cellular senescence is known to be associated with an altered chromatin assembly forming easy to visualize heterochromatin regions. Narita and colleagues described a unique heterochromatic structure that was found to accumulate in senescent human fibroblasts (Narita *et al.*, 2003; Cichowski & Hahn, 2008), which they termed the senescence associated heterochromatic foci (SAHF). These are highly condensed regions of chromatin that are characterised by a build-up of histone H3 that is tri-methylated at lysine 9 (K9M-H3; a modification catalysed by the histone methyltransferase (HMTase) Suv39h1), as well as heterochromatin proteins, such as high-mobility group A (HMGA) proteins, macroH2A and heterochromatin protein 1 (HP1) (Adams, 2007; Kuilman *et al.*, 2010; Salama *et al.*, 2014). The SAHF contain some proliferative genes and are also thought to silence certain genes, such as the E2F target genes (Campisi, 2013).

DNA dyes usually display a generally consistent staining pattern in cycling or quiescent human cells but show outstandingly different staining patterns in senescent cells (see Figure 1-5). In proliferating and quiescent cells, the euchromatin markers K9Ac-H3 (histone H3 acetylated on lysine 9) and K4M-H3 (histone H3 methylated on lysine 4) homogeneously stain the DNA, however, they are excluded from the heterochromatic DNA of senescent cells. Instead,

senescent cells richly stain for K9M-H3. Methylated lysine 9 provides a binding site for HP1 proteins, which are a family of adaptor molecules required for the assembly of heterochromatin and which are involved in epigenetic gene regulation (Lachner *et al.*, 2001; Bannister *et al.*, 2001). In normally proliferating and quiescent cells, it was observed that HP1 proteins were spread out all over the nucleoplasm but in senescent cells, they were rather focussed in regions of the DNA foci. These senescence-associated DNA foci contain heterochromatin and are thus named SAHF. These SAHF usually lack lysine 9 acetylated H3 (K9Ac-H3) and lysine 4 methylated H3 (K4M-H3) but rather are enriched in histone H3 methylated on lysine 9 (K9M-H3) (Narita *et al.*, 2003).

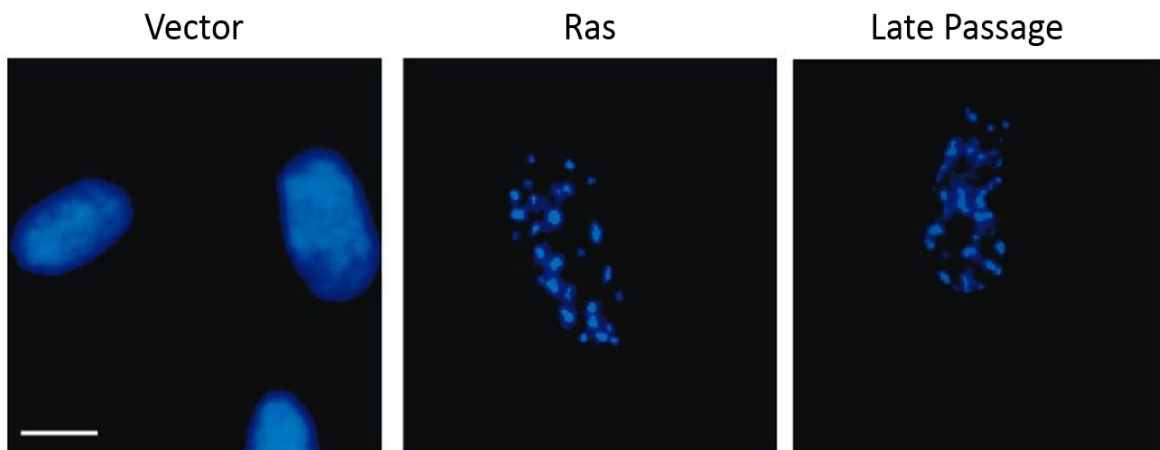


Figure 1-5 Senescence associated heterochromatin foci (SAHF).

Proliferating IMR-90 lung fibroblasts (vector) show uniform DAPI staining of the nucleus, while senescent fibroblasts display the characteristic dot-like heterochromatin assembly known as SAHF. Adapted from (Narita *et al.*, 2003).

Tampering with the expression of certain genes such as those encoding p53, interleukin-6 (IL-6) or C/EBP β , inhibits the formation of SAHF, depending on the experimental system, and this is linked to suppression of senescence. The p16^{INK4A} /Rb pathway is thought to be vital for the formation of SAHF as SAHF formation can be prevented by interfering with the signalling of this pathway, which correlates with senescence bypass (Narita *et al.*, 2003; Cichowski & Hahn, 2008; Kuilman *et al.*, 2010). Senescent cells often exhibit binding of heterochromatin-associated proteins to the promoters of some E2F target genes. SAHF prevent the E2F transcription factor from accessing its target genes, thus

blocking the transcription of genes that lead to S phase and ultimately leading to cell-cycle arrest. It is possible that SAHF contribute to the collective changes in gene expression observed in senescent cells, due to their influence on gene expression (MDuff & Turner, 2011; Young *et al.*, 2013). It has also been shown that the SAHF restrains the DDR, suggesting that the role of SAHF may not be limited to gene expression (Di Micco *et al.*, 2011; Salama *et al.*, 2014). Importantly, the SAHF are not consistently expressed in all senescent cell types. They are not found in any senescent mouse cells, neither are they found in every senescent human cell, even though SAHF are common. Of note also, cells from Hutchinson Gilford progeria syndrome (HGPS) patients and cells from aged individuals showed loss of visible heterochromatin blocks and accompanying marks (Narita *et al.*, 2003; Swanson *et al.*, 2013).

1.3.5 GENE EXPRESSION CHANGES DURING SENESCENCE

Senescent cells display various changes in gene expression, the most significant being increase in expression of several secreted proteins (Coppe *et al.*, 2011). The changes in gene expression patterns of senescent cells also affect cell cycle regulatory genes, extra-cellular matrix (ECM) remodelling genes, as well as genes involved in cytokine signalling and inflammation (MDuff & Turner, 2011). During cellular senescence, the cell's epigenetic maintenance system is altered. For instance, during replicative senescence of human fibroblasts, there is a marked reduction in the levels and modification status of the histone deacetylases (HDAC) HDAC1 and HDAC2. Histone acetylation has been linked to senescence as a short exposure of cells to HDAC inhibitors was found to accelerate senescence in human fibroblasts (Serrano & Blasco, 2001). In cellular senescence, START RNAs, which are a family of antisense RNAs, are produced and they inhibit the expression of their corresponding sense RNAs (Muniz *et al.*, 2017). Also, one of the key pathways of the lysosomal-autophagy proteolytic system, chaperone-mediated autophagy (CMA), which regulates various cellular processes by selectively degrading cytosolic proteins, is impaired in cellular senescence and it is thought that the decline in CMA activity contributes to aging by inducing cellular senescence (Moreno-Blas *et al.*, 2018). These various senescence-associated gene expression changes are specific to and conserved within individual cell types (Coppe *et al.*, 2010).

A mass spectrometry screening of the membrane fraction of senescent cell lysates revealed 107 proteins that were preferentially expressed in senescent cell membranes over non-senescent ones (Althubiti *et al.*, 2014). Furthermore, gene expression profiling analysis of G protein-coupled receptor kinase (GRK) 4 – induced senescent HEK293 cells showed differential expression of 17 senescence-related genes in GRK4 positive cells compared to control cells (Xiao *et al.*, 2017). Ontologic and gene expression analysis of skin from Caucasian females between the ages of 20 years and 70 years revealed changes in the expression of thousands of genes with age. (Kimball *et al.*, 2018). Studies have shown that the expression of cellular damage related genes such as inflammatory or stress response genes increase with age while biosynthetic and metabolic genes expression decrease with age (Edwards *et al.*, 2007; Kimball *et al.*, 2018). In order to facilitate research on the mechanisms of gene regulation in cellular senescence, a database of senescence associated genes is greatly needed. To this end, Dong and colleagues have established the Human Cellular Senescence Gene Database (HCSGD) using a combination of data from published literature sources, gene expression profiling as well as protein-protein interaction networks (Dong *et al.*, 2017).

1.3.6 THE SEARCH FOR NOVEL MARKERS OF SENESCENCE

To date, several markers have been used to detect senescent cells *in vitro* and *in vivo*. The fact that none of the currently available markers of senescence are exclusive to the senescent state and lack specificity (Rodier & Campisi, 2011; Sikora *et al.*, 2011; Muñoz-Espín & Serrano, 2014) necessitates the search for novel and more reliable markers which could be used either alone or in combination with other markers. The senescence program harbours transcriptional heterogeneity with a dynamic phenotype which changes at variable intervals (Sharpless & Sherr, 2015; Hernandez-Segura *et al.*, 2017). Also, the expression of thousands of genes is significantly altered in cellular senescence and these changes are by and large conserved within individual cell types and are specific to these cells only (Coppe *et al.*, 2010). Of all the remarkable changes in gene expression observed during senescence, very few

of them are senescence specific and of great enough magnitude to be declared markers of senescence, (Wang *et al.*, 2009; Sharpless & Sherr, 2015) making it necessary to clearly define markers for the senescent state.

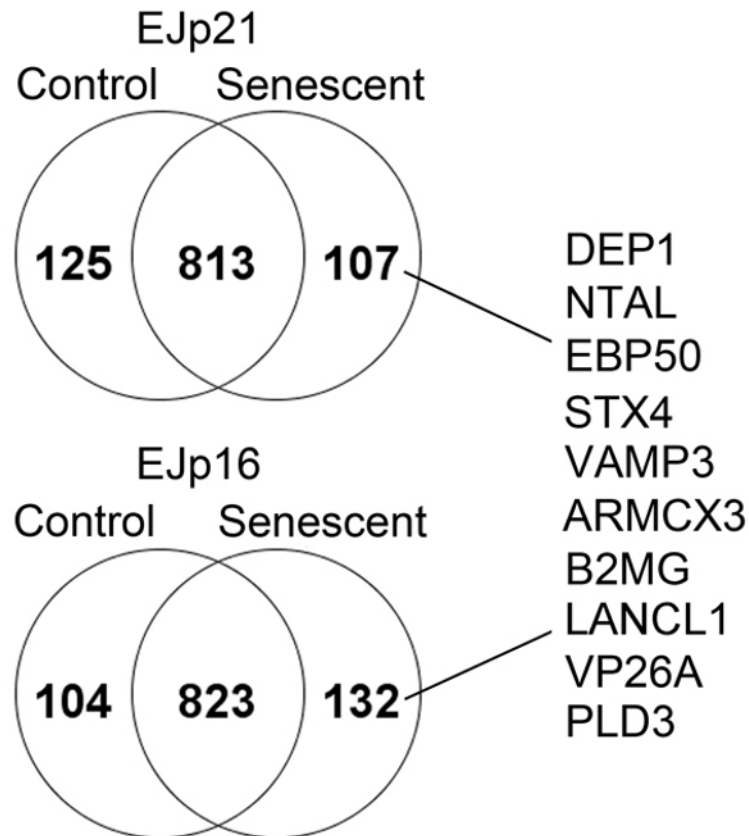


Figure 1-6 Proteins differentially expressed on the membrane of senescent cells. Novel markers of senescence were identified through a mass spectrometry screening of the membrane fraction of senescent cell lysates. These proteins were preferentially expressed on the surface of senescent EJp21 and EJp16 cells over non-senescent control cells. Adapted from (Althubiti *et al.*, 2014).

Novel markers of senescence with potential in cancer prognosis and therapy (see Figure 1-6) have been identified in our laboratory (Althubiti *et al.*, 2014). These are proteins present in the isolated membrane fraction of senescent cell lysates that have extracellular epitopes, and had not been previously linked with senescence. These proteins include: Density Enhanced Phosphatase-1 (DEP-1), Non-T cell Activation Linker (NTAL), Syntaxin4 (STX4), β -2 Microglobulin (B2MG), Armadillo repeat-containing X-linked protein 3 (ARMCX3), among

others. Considering the fact that currently known senescent markers are not sufficient on their own as exclusive markers of senescence (Yang & Hu, 2005; Deursen, J M A van, 2014), there is the need to identify and characterise better markers. These protein markers characterised in our laboratory, could also be useful targets for the identification and possible clearance of accumulated senescent cells from the body.

1.4 PATHWAYS INVOLVED IN SENESCENCE

More than one effector pathway is involved in the senescence program. Cellular senescence can be signalled through various paths, many of which activate p53 (encoded by the human TP53 and mice Trp53 genes) as well as the cyclin dependent kinase (CDK) inhibitors p16 (known as INK4A and encoded by *CDKN2A*), p15 (known as INK4B and encoded by *CDKN2B*), p21 (known as WAF1/Cip1/Sdi1 and encoded by *CDKN1A*) and p27 (encoded by *CDKN1B*), resulting in proliferative arrest (Campisi, 2005; Muñoz-Espín & Serrano, 2014). Although it has been half a century since Leonard Hayflick and his colleague first described senescence (Hayflick & Moorhead, 1961), the molecular pathways involved in senescence are yet to be fully understood (Althubiti *et al.*, 2014; Salama *et al.*, 2014).

Two key and well-studied senescence pathways are the p53/p21 and the p16/Rb tumor suppressor pathways mediated by the cell cycle inhibitors p53 and p16 respectively (Campisi *et al.*, 2011). The retinoblastoma (Rb) tumor suppressor gene product, pRb, is an important gatekeeper during cell cycle progression through the G1 phase and its activity is tightly controlled by several post-translational modifications, such as phosphorylation, acetylation and ubiquitination (Campisi, 2005; Takahashi *et al.*, 2007). The activity of cyclin dependent protein kinases which phosphorylate and inactivate the retinoblastoma protein (Rb), is inhibited by both p21^{Cip1/Waf1/Sdi1} (CDK2) and p16^{INK4A} (CDK4, CDK6), leading to accumulation of an active, hypo-phosphorylated form of Rb, which prevents the transcription factor E2F from transcribing genes needed for cell cycle progression, thereby mediating cell cycle arrest and other senescence phenotypes (see Figure 1-7) (Herbig *et al.*, 2004; d'Adda di Fagagna & Campisi, 2007; Xu *et al.*, 2014).

Products of the *INK4a/ARF* locus activate p53 and Rb in various settings, to bring about senescence. The two products of this locus, p16^{Ink4a} and p19^{Arf} (p14^{ARF} in humans) are key tumor suppressors which regulate the activities of the p53 transcription factor and the Rb protein, and are expressed from partly overlapping nucleotide sequences read in alternative reading frames (Lowe & Sherr, 2003). Both p16^{INK4a} and p19^{ARF} have been found to accumulate in senescent cells and their overexpression also promotes senescence (Lundberg *et al.*, 2000).

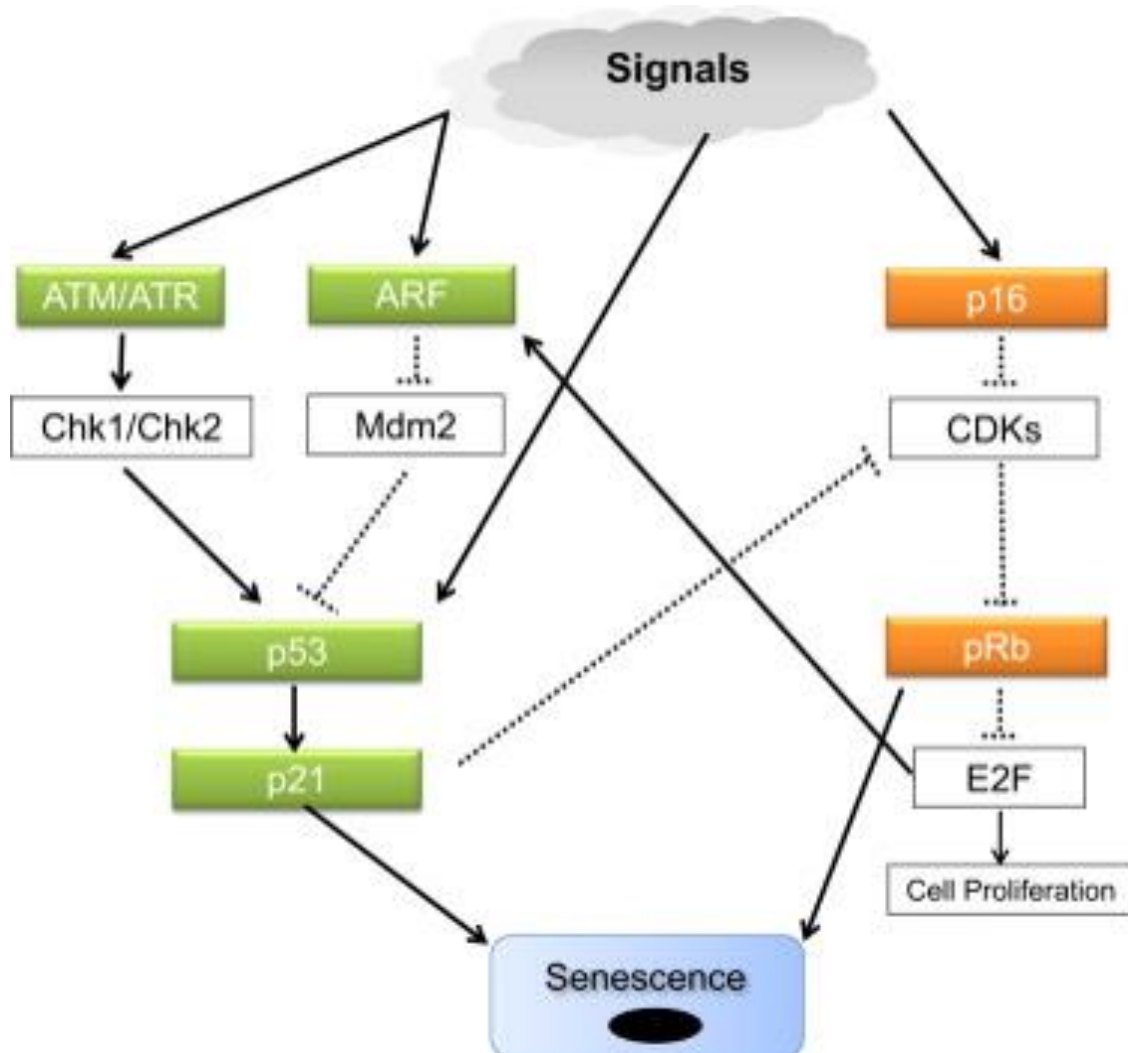


Figure 1-7 Control of senescence by the p53/p21 and p16/Rb pathways.

Various stress signals lead to the upregulation of ATM/ATR, ARF, p53 and p16. Upregulation of p53, triggers overexpression of p21, resulting in cellular senescence. Also, p21 and p16 prevent the phosphorylation and activation of Rb by cyclin dependent kinases, resulting in an accumulation of the hypo-phosphorylated active form of Rb, which in turn hinders E2F from transcribing genes for cell proliferation, ultimately leading to senescence. ATM/ATR induces p53-p21 via the checkpoint kinases (Chk1/Chk2), leading also to senescence. ARF inhibits Mdm2, the negative regulator of p53, resulting in an abundance of p53. The E2F transcription factor is also able to induce ARF expression. Adapted from (Park & Sin, 2014).

For the Rb pathway activation, p16^{INK4a} functions to inhibit cyclin D dependent kinases, preventing them from phosphorylating and subsequently inactivating Rb. p14^{ARF} on the other hand increases the growth inhibitory functions of p53 by sequestering its negative regulator, Mdm2 (mouse double minute 2). These proteins, p16^{INK4a} and p14^{ARF} (p19^{Arf} in mouse), form part of an important signalling network that is disrupted in many cancers. The *Ink4a-Arf* locus responds to stress signals and restrict cell proliferation. Mutations affecting INK4a or ARF can compromise senescence on various levels depending on the cell type and specie (Lowe & Sherr, 2003; Narita *et al.*, 2003; Park & Sin, 2014).

p53 is an important tumour-suppressor protein involved in senescence and is a mediator of the DDR, such as that triggered by dysfunctional telomeres, reactive oxygen species (ROS), oncogenes etc., which comprises the senescence response (Muñoz-Espín & Serrano, 2014). The type of senescence arrest facilitated by the p53 pathway is supposedly reversed by inactivation of p53. This reversal of senescence is possible in some cells but not in others. When the senescence response is mediated by the p16 pathway, which is also induced by oncogenes and other stressors, p53 inactivation fails to reverse senescence suggesting that the p16/RB pathway engages an irreversible barrier to cell growth (Beausejour *et al.*, 2003; Campisi, 2005; Chen *et al.*, 2005; d'Adda di Fagagna & Campisi, 2007). Fibroblasts are able to escape from replicative senescence, also referred to as 'mortality stage 1' (M1) as a result of inactivation of the p53 and Rb pathways. They can undergo several PDs before arriving at a second barrier, known as 'mortality stage 2' (M2) or 'crisis', which is essentially a stage of cell death rather than growth arrest (Shay & Wright, 2005; d'Adda di Fagagna & Campisi, 2007; Georgakopoulou *et al.*, 2016). It has been reported that the function of p53 and p21 are not absolutely required for the maintenance of senescence (Chang *et al.*, 1999b) even though they are induced during senescence-like proliferation arrest.

The decision of a cell to go into either quiescence, senescence or apoptosis upon induction of p53 or p16 may be dependent on the threshold levels of the stress triggering the induction. For instance, the form and severity of cellular effects such as the type and extent of DNA damage imposed by stressors, are critical

parameters for determining whether a fibroblast or epithelial cell will respond by way of senescence or apoptosis. Senescence is thought to be a response to less severe damage and apoptosis a response in the face of overwhelming damage (Childs *et al.*, 2014; Georgakopoulou *et al.*, 2016). In a study by Demidenko and colleagues, they showed that the accumulative loss in proliferative capacity of cells is affected by the duration of the cell cycle arrest that drives it. The longer the timeline of arrest in cell cycle, the deeper the cells senesce (Demidenko *et al.*, 2009). Studies have shown that not every kind of cell is able to senesce when faced with a similar stress stimuli as the events that come together to induce senescence are both cell type and tissue specific (Romagosa *et al.*, 2011).

There appears to be a variation in response to senescence related stimuli between cells of the same type but of different species *in vitro*. For instance, under the same experimental conditions, MEFs enter into a senescent state quicker than human fibroblasts (Chen *et al.*, 2007). Also, whereas epithelial cells have a high-turnover in situ, fibroblasts stay in a quiescent state, displaying structural features, and proliferate only in response to certain stimuli such as trauma (Lemons *et al.*, 2010). It is proposed that, upon stress insults, human fibroblasts largely respond via senescence, while epithelial cells undergo apoptosis instead. Therefore, considering the whole tissue epithelium and stroma would be of advantage when carrying out research into new therapies for chronic diseases and cancer (Georgakopoulou *et al.*, 2016). A model integrating the intensity of hyperproliferation or stress signals, the microenvironment conditions and the cell type could help explain better the decision of a cell to either proliferate, senesce or go into apoptosis (Narita & Lowe, 2005).

It has been observed that mTOR activation is necessary for cellular senescence to take place as mTOR enables transition from cell cycle arrest and quiescence to senescence (geroconversion). Factors that activate the mTOR pathway (gerogens) accelerate geroconversion (Blagosklonny, 2014; Leontieva & Blagosklonny, 2017). Using various cell models of senescence, rapamycin (an inhibitor of the nutrient-sensing mTOR pathway) was found to slow down cellular senescence and prevent the accompanying irreversible loss of proliferative capacity (Demidenko *et al.*, 2010; Xu *et al.*, 2014). A study has revealed that

growth stimulation by serum addition promoted cellular senescence in the presence of the p21^{Waf1/Cip1/Sdi1} cell cycle inhibitor. However, when serum was absent, cell cycle inhibition rather led to quiescence, which either advanced to senescence upon addition of serum or was upturned when the cell cycle inhibition induced by p21 was stopped (Demidenko & Blagosklonny, 2008). There is a school of thought that proposes that basal levels of p53 may suppress cellular senescence in a paradoxical manner (Demidenko *et al.*, 2010). The study by Demidenko and co-researchers show that the presence of p53 in physiological levels inhibits the mTOR pathway thereby suppressing cellular senescence. Cells affected through this mechanism instead go into a state of reversible arrest or quiescence.

Many markers including SA-βgal activity, expression of CDK inhibitors, constitutive DDR signalling, reduced expression of LaminB1 nuclear lamina protein, presence of SAHF, DNA-SCARS, as well as the SASP, can be used to identify senescent cells both in culture and *in vivo*, yet none of them are exclusive to the senescent state (Yang & Hu, 2005; d'Adda di Fagagna & Campisi, 2007; Deursen, J M A van, 2014; Loaiza & Demaria, 2016). Some of these markers, modulators and effectors of senescence are discussed here.

1.4.1 p16^{INK4A} AS A MARKER OF SENESCENCE

p16^{INK4A} is a cell cycle regulator which inhibits the progression from G1 to S phase of the cell cycle. It is an anti-proliferative protein and a member of the INK4 family of CDK inhibitors, inhibiting CDK4 and CDK6 complex formation with cyclin D. The INK4 family of CDK inhibitors include p15^{Ink4b}, p18^{Ink4c} and p19^{Ink4d} (Hirai *et al.*, 1995; Luh *et al.*, 1997; Sharpless & DePinho, 1999; Taniguchi *et al.*, 1999; Romagosa *et al.*, 2011; de Jesus & Blasco, 2012). Currently, p16^{INK4A} is considered a leading marker for indicating the presence of senescent cells (Naylor *et al.*, 2013). Most senescent cells express p16^{INK4A} and, as seen in replicative senescent cells as well as some terminally differentiated cells, its expression is increased in the final stage of population doubling. Hence, it is often referred to as a senescence gene (Taniguchi *et al.*, 1999; Campisi, 2011; Simboeck & Di Croce, 2013). The levels of p16^{INK4A} have been used as a biomarker of ageing in humans as it is seen to increase with ageing – up to 7 fold

in some human tissues and up to 30 fold in most mouse tissues (Krishnamurthy *et al.*, 2004; Collado *et al.*, 2007; Wang *et al.*, 2009; Romagosa *et al.*, 2011; Sherr, 2012).

Deletions and mutations of the p16^{INK4A} gene are frequent in human malignancies (Taniguchi *et al.*, 1999). p16^{INK4A} is a tumour suppressor protein and its expression is downregulated in a large number of cancers and malignant tumours, whereas it is overexpressed in benign and pre-malignant lesions (e.g. nevi and adenomas), where it functions to prevent the emergence of transformed cells. Thus, it plays its role in establishing oncogene induced senescence (OIS). It is widely accepted that the ability to bypass senescence is a critical molecular mechanism that enables the progression from pre-malignant to malignant cells, hence the overexpression of p16 in benign and pre-malignant lesions and its absence in malignant cells (Collado *et al.*, 2005; Collado *et al.*, 2007; Romagosa *et al.*, 2011).

Immunostaining of benign tumours show a positive p16^{INK4A} expression and a negative or very low Ki67 (a marker of proliferation) index, while malignant tumours often stain positive for Ki67 but negative for p16^{INK4A} (Collado *et al.*, 2005; Romagosa *et al.*, 2011). However, in high grade malignant tumours, where there are alterations in the p16^{INK4A}-Rb pathway, a high p16^{INK4A} as well as a high Ki67 immunostaining has been observed. In human tumours, the overexpression of p16 could either be as a result of OIS, as seen in benign or pre-malignant lesions, or as a result of the Rb pathway failure, as seen in some malignant lesions. Hence, p16^{INK4A} is often used as a prognostic marker for several cancers in order to grade or distinguish between benign and malignant lesions. It is also often used as a diagnostic marker of cervical cancer (Romagosa *et al.*, 2011).

In its role as a cell cycle regulator, p16^{INK4A} appears to be preferentially expressed in the nucleus, while in other cases such as in breast cancer, it is also seen in the cytoplasm and is used to ascertain tumour progression and prognosis (Romagosa *et al.*, 2011). In certain conditions, p16^{INK4A} is expressed in both the nucleus and cytoplasm. The subcellular location of p16^{INK4A} in a cell might be dependent on its function in that cell, which could anchor on its complex formation ability with other proteins or on post-translational modifications. However, it is

important to note that this supposed differential localization of p16 might simply be influenced by the antibody used for its detection, depending on the immunogen or epitope being recognised. Practically, staining for p16 *in vivo* using antibodies has been quite unreliable and requires robust positive and negative controls. Upregulation of p16 by a tetracycline regulated promoter, was found to induce growth arrest in both tumour cells and normal cells. This growth arrest was reversible upon repression of p16, allowing more than 60% of the cell population to proliferate and form colonies five days later (Macip *et al.*, 2002). This observation was supported by a subsequent study which demonstrated that p16 expression was needed as a second barrier to cell proliferation during senescence and ensured irreversibility of the senescence arrest (Beausejour *et al.*, 2003). However, the cyclin dependent kinase inhibitor p16 does not seem to be a key regulator of development as it is not expressed during embryogenesis (Guney & Sedivy, 2006) even though senescence is known to play a role during embryonic development.

1.4.2 p53 and p21

The p53 gene has long been established as a cell cycle regulator and guardian of the genome. Tumor cells were found to undergo growth arrest or apoptosis when wild-type p53 was overexpressed in them. Early studies using normal fibroblasts also showed a link between p53 and cellular senescence. The activity of p53 as well as levels of its downstream effector p21^{Waf1/Cip1/Sdi1} increase during late passage of cells, leading to a slowdown in proliferation (Kastan *et al.*, 1991; Lane, 1992; Levine, 1997). p53 was found to delay functional decline in skeletal muscle and in fat depots of *BubR1* progeroid mice in a p21-dependent manner via inhibition of p16^{lnk4a}-mediated senescence of progenitor cells. p53 also prevented the formation of cataracts in lenses but interestingly, this antiaging effect was in a p21-independent fashion as p21 was found to promote senescence of lens epithelial cells and the formation of cataract (Baker *et al.*, 2008; Baker *et al.*, 2013). It was also observed that senescence induced by p53 was more readily reversible than senescence induced by p21 (Fang *et al.*, 1999).

As a cell protective machinery, p53 induction after genotoxic stress and DNA damage can lead to either DNA repair, transient cell cycle arrest, senescence or

apoptosis, depending on various signalling factors (Sionov & Haupt, 1999; Macip *et al.*, 2002; Bieging *et al.*, 2014). Overexpression of wild type p53 using an inducible tetracycline-off expression system in EJ human bladder cancer cells without a functional p53 was shown to elicit growth arrest at G1 and G2/M in these cells. The growth arrest was irreversible by 48 – 72 hours after p53 induction, with cells showing ultra-structural and biochemical markers as well as morphological changes consistent with the senescence phenotype. This growth arrest was also accompanied by an up-regulation of p21^{Waf1/Cip1/Sdi1}, and repression of cdc2 as well as cyclin A and cyclin B (Sugrue *et al.*, 1997). Cells obtained from a p53 nullizygous mouse were found to easily escape senescence and produce immortalized cell lines. Furthermore, the introduction of *raf* or *c-myc* cDNA clones led to a higher rate of immortalization in p53-deficient cells than in cells which possessed the wild-type p53 gene. (Levine, 1997).

The Bruton's tyrosine kinase (BTK) has recently been reported by our laboratory to be a part of the p53 family where it phosphorylates p53, modulating its apoptotic and senescence related responses (Althubiti *et al.*, 2016). BTK was found to be expressed in response to damage and induces phosphorylation of p53 at serine 15 at the N-terminus, increasing its protein levels and activity. In addition, it was found that BTK binds to and phosphorylates MDM2, facilitating its loss of ubiquitination activity and further stabilising p53 (Rada *et al.*, 2017). Inhibition of BTK was found to reduce the expression of p53 and interfered with the upregulation of p53 target genes, leading to an impairment in the induction of p53-mediated cell fates such as senescence (Althubiti *et al.*, 2016). A mass spectrometry screening of the membrane fraction of senescent cell lysates carried out in our laboratory (Althubiti *et al.*, 2014) identified BTK as one of the markers overexpressed on senescent cells. BTK is mainly located at the cell membrane but it can also be found in the nucleus (Gustafsson *et al.*, 2012).

BTK is a dual-specificity non-receptor tyrosine kinase belonging to the Tec family and is vital for B cell maturation (Mohamed *et al.*, 2009). It's mutation in humans leads to X-linked agammaglobulinemia (Vetrie *et al.*, 1993). In B cells, BTK is activated when an antigen binds to the B cell receptor (BCR), which then leads to its phosphorylation at tyrosine 551 by the Src family kinases (SFKs), and its

auto-phosphorylation at tyrosine 223 (Rawlings *et al.*, 1996). BTK has been shown to be up-regulated in B cell malignancies such as mantle cell lymphoma, chronic lymphocytic leukaemia and multiple myeloma (Herman *et al.*, 2011; Kuehl & Bergsagel, 2012; Chang *et al.*, 2013). Several BTK inhibitors are currently in the market, including Ibrutinib (PCI-32765), which has been approved for mantle cell lymphoma and chronic lymphocytic leukaemia (CLL) therapy (Hendriks *et al.*, 2014; Hutchinson & Dyer, 2014).

p21^{Waf1/Cip1/Sdi1} is an important cyclin-dependent kinase inhibitor whose expression is directly induced by p53. It is a well characterised transcriptional target of p53 and links the p53 pathway to the Rb pathway to enhance tumor suppression (Takahashi *et al.*, 2007). p21^{Waf1/Cip1/Sdi1} belongs to the Cip/Kip family of CDK inhibitors that includes p27^{Kip1} and p57^{Kip2} (Deng *et al.*, 1995; Fang *et al.*, 1999; Taniguchi *et al.*, 1999). p21^{Waf1/Cip1/Sdi1} is a dual inhibitor of proliferating cell nuclear antigen (PCNA) and cyclin dependent kinases, which are both crucial in the cell cycle. The p21 gene has been self-sufficiently and concomitantly identified as a gene which inhibited cyclin and cyclin-dependent kinase complexes (CIP1), is activated by p53 (WAF1), and is significantly overexpressed during cellular senescence (SDI1) (el-Deiry *et al.*, 1993; Waldman *et al.*, 1995; Brugarolas *et al.*, 1995). p21^{Waf1/Cip1/Sdi1} is an effector of p53 functions and a crucial mediator of the p53-induced cell cycle arrest. In late passage human diploid fibroblasts, an increase in p21^{Waf1/Cip1/Sdi1} expression was observed and targeting the deregulation of p21^{Waf1/Cip1/Sdi1} in these cells increased their lifespan. In p21-null mice, p53 is unable to cause G1 cell cycle arrest upon DNA damage and this was observed in p21^{-/-} MEFs whose ability to undergo G1 arrest following DNA damage was impaired. It is also noteworthy that no p21 mutations have been found in human malignancies (Shiohara *et al.*, 1994; Abbas & Dutta, 2009; Romanov & Rudolph, 2016).

p21^{Waf1/Cip1/Sdi1} has been shown to be involved in the control of cell proliferation, cell differentiation and cell death both in a p53-dependent and p53-independent manner (Karimian *et al.*, 2016; Georgakilas *et al.*, 2017). In EJ bladder carcinoma cells which lack a functional p53 gene, a tetracycline (tet) regulated p21 expression system was employed. Overexpression of p21 in these EJ cells

triggered senescence with characteristic morphological changes such as a flattened shape, increased cell size and enlarged nuclei. Biochemical and ultrastructural markers depicting the senescent phenotype were also observed. Induction of p21^{Waf1/Cip1/Sdi1} also led to a reduction in Cdk2 kinase activity as well as cell cycle arrest in both G1 and G2/M which was irreversible. The dual arrest at both G1 and G2/M triggered by p21 is unlike the G1 specific arrest seen with other Cdk inhibitors like p16 and p27 (Fang *et al.*, 1999). Immortal Li - Fraumeni fibroblasts were also found to undergo senescence when p21^{Waf1/Cip1/Sdi1} expression was induced by retroviral vectors (Vogt *et al.*, 1998). p21 can also play a role in DNA repair via its interaction with PCNA, which binds to the p21/cyclin/CDK complex through the C-terminal of p21 (Karimian *et al.*, 2016).

There are indications that p21 might also function as an anti-apoptotic agent, suggesting that it could also be oncogenic although the mechanism by which this happens remains unclear. Expression of p21 has been found to induce senescence and also apoptosis in the same cell line and this is thought to be mediated by reactive oxygen species (Masgras *et al.*, 2012). This newly identified function of p21 could be of relevance for future therapeutic interventions. Also, it has recently been found that chronic overexpression of p21 in a p53-null environment encouraged the escape of a subpopulation of cells from a senescence-like state and promoted replication stress owing to constant re-replication. Complex genomic and phenotypic analyses using p21-inducible, p53-null, malignant as well as near-normal cellular models has shown that a subpopulation of proliferating cells emerged after an initial senescence-like phase. These cells expressed p21 and exhibited increased genomic instability, aggressiveness and resistance to chemotherapeutic agents but there were also atypical cancer cells, co-expressing p21 and Ki67 (Galanos *et al.*, 2016; Georgakilas *et al.*, 2017).

1.5 PLEIOTROPIC EFFECTS OF SENESCENCE

The senescence mechanism is said to be antagonistically pleiotropic, having health benefits for the younger individuals but promoting chronic diseases in the elderly (d'Adda di Fagagna & Campisi, 2007; Campisi, 2011).

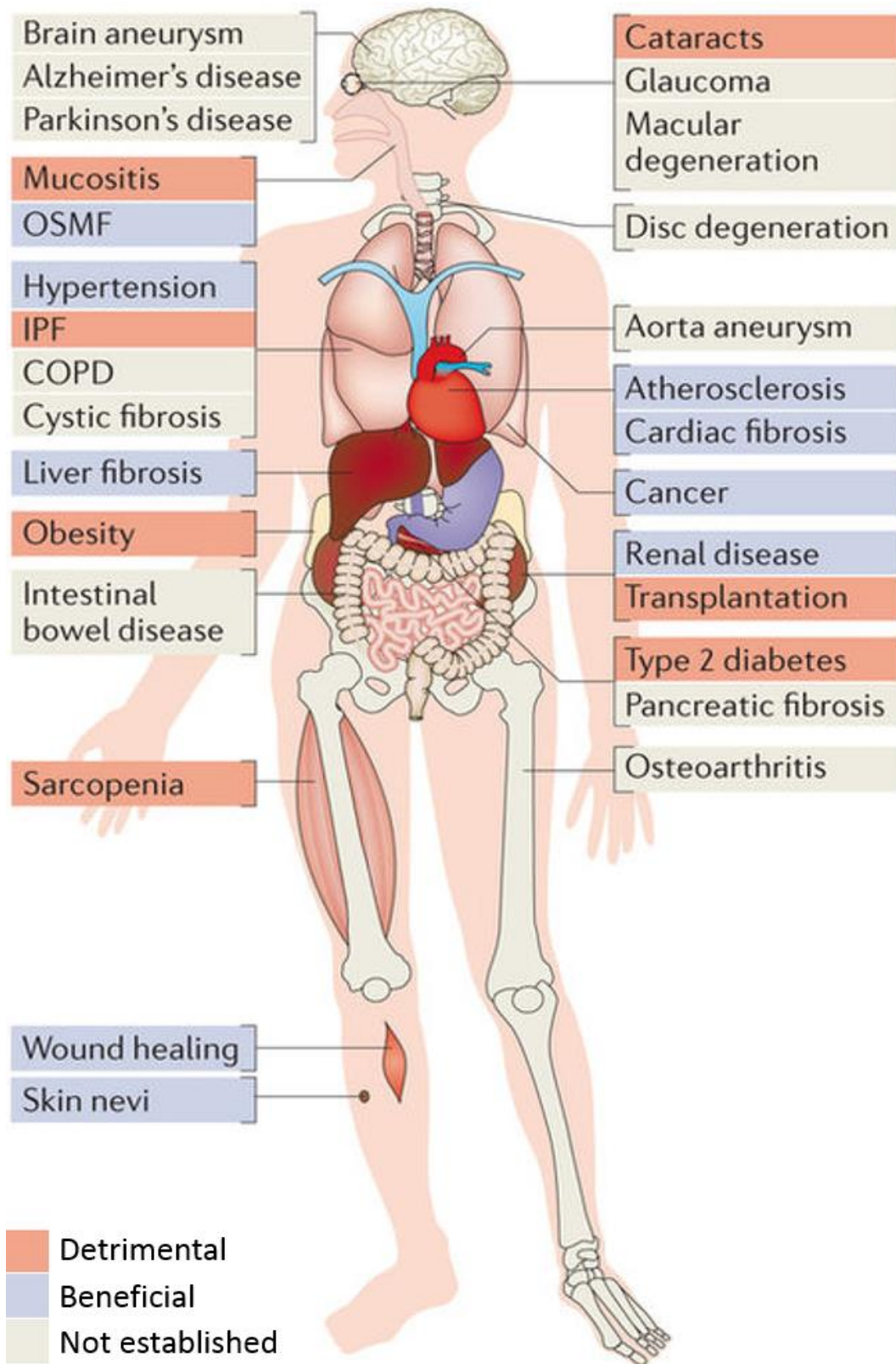


Figure 1-8 Involvement of senescence in adult diseases.

A number of diseases where senescence either plays known beneficial (blue boxes) or detrimental roles (red boxes), or a role that is yet to be established (beige boxes).

Adapted from (Muñoz-Espín & Serrano, 2014).

1.5.1 BENEFICIAL ROLES OF SENESENCE

Senescence can be both beneficial and detrimental. The growth and survival of an organism depends on cell division. However, when there is an oncogenic insult or damage to a cell, it triggers either a programmed cell death (apoptosis) or growth arrest (senescence) to halt cell division and stop the propagation of the damage. This is often mediated by tumor suppressor proteins such as p53. In this context, senescence plays a beneficial role by bringing about tumour growth arrest. Thus one of the ways in which our bodies fight against cancer is by activating cellular senescence - a tumour suppression mechanism that is put in place to prevent the emergence of cancerous or transformed cells. Cellular senescence will have to be bypassed for malignant transformation to take place (Campisi, 2001; Campisi *et al.*, 2011; Rodier & Campisi, 2011; Muñoz-Espín & Serrano, 2014). Then again senescent cells are also involved in several non-pathological physiological processes both during embryonic development and in adulthood. Unexpectedly, senescence has been observed in embryos and it is understood to be a preserved feature in vertebrate embryonic development. These senescent cells play a role in morphogenesis in embryos (Munoz-Espin *et al.*, 2013; Storer *et al.*, 2013).

Additionally, cellular senescence plays a role in the pathology of wound healing and restricts fibrosis, limiting tissue damage. In this instance, senescence is necessary for organ and tissue development, remodelling and regeneration (Muñoz-Espín & Serrano, 2014; Burton & Krizhanovsky, 2014). In conditions such as atherosclerosis, pulmonary hypertension, renal fibrosis, liver fibrosis, oral submucous fibrosis, wound healing, prevention of cancer and in the regulation of cardiac fibrosis, senescence is found to exert beneficial effects, while in other conditions like idiopathic pulmonary fibrosis, sarcopenia, cataracts, obesity, type 2 diabetes, chronic kidney disease, oral mucositis and even cancer progression, senescence has been found to have detrimental effects (Jimenez *et al.*, 2005; Tchkonja *et al.*, 2013; Kim *et al.*, 2013; Muñoz-Espín & Serrano, 2014; Biran *et al.*, 2015; He & Sharpless, 2017).

1.5.2 DETRIMENTAL EFFECTS OF SENESENCE

While cellular senescence has been found to be an important tumour-suppressor mechanism, it is also proposed to be the underlying cause of ageing and aggravates as well as triggers accompanying diseases of aging, including cancer. Persistent accumulation of senescent cells in tissues results in secretion and infiltration of cytokines, chemokines, natural killer cells, growth factors and metalloproteinases (SASP) into their microenvironment or surroundings. Consequently, this results in tissue damage, thereby promoting different pathological conditions (Collado & Serrano, 2010; Campisi *et al.*, 2011; Naylor *et al.*, 2013; Biran *et al.*, 2015).

As a result of all these, senescence demonstrates antagonistic pleiotropy (Austad & Kirkwood, 2000; d'Adda di Fagagna & Campisi, 2007; Campisi, 2011) as it tends to have beneficial tumour-suppression in the young but promotes chronic degenerative diseases in the old. According to Rodier and Campisi (2011), cellular senescence has four faces: tumour suppression, tissue repair, ageing and tumour promotion – four complex activities, some of them with contrasting effects. Paradoxically, the first two activities are beneficial to the organism while the last two are detrimental (Rodier & Campisi, 2011; Campisi, 2011). This has opened up new fields of research whereby senescent cells are being targeted as a therapeutic strategy for cancer and several aging-associated diseases (Campisi *et al.*, 2011; Naylor *et al.*, 2013). A fifth face or activity – development and *in vivo* reprogramming has recently been assigned to senescence and there is already growing research around this topic (Mosteiro *et al.*, 2016; Chiche *et al.*, 2017; Ritschka *et al.*, 2017; Davaapil *et al.*, 2017; Mosteiro *et al.*, 2018; Senís *et al.*, 2018).

Cellular senescence can be induced by chemotherapeutic drugs and this is termed therapy-induced senescence (TIS). Although TIS is beneficial in preventing malignant transformation (Childs *et al.*, 2015), the role of TIS in cancer is double-edged as prolonged chemotherapy can enable the cancer promoting effects SASPs, thereby outweighing the benefits of TIS (Lasry & Ben-Neriah, 2015; Ruhland *et al.*, 2016; Demaria *et al.*, 2017). It could therefore be more beneficial to combine senescence-inducing chemotherapy with drugs that

suppress the deleterious effects of the SASP which could arise as a result of prolonged therapy (Lasry & Ben-Neriah, 2015; Soto-Gamez & Demaria, 2017).

1.6 AGEING, CELLULAR SENESENCE AND DISEASE

Ageing, which is often defined as a progressive loss of tissue and organ function over time (Austad & Kirkwood, 2000; Childs *et al.*, 2015), is the greatest risk factor for the development of many diseases. It increases the susceptibility to various degenerative pathological conditions, which are mostly chronic, leading to high morbidity and mortality rates (Campisi *et al.*, 2011; Tchkonja *et al.*, 2013; McHugh & Gil, 2018). The incidence of many diseases such as atherosclerosis, osteoporosis, arthritis, cataracts, hypertension, type 2 diabetes, Alzheimer's disease as well as cancer increases rapidly with age (Muñoz-Espín & Serrano, 2014). The incidence of cancer also rises exponentially with age (Campisi, 2003; Campisi *et al.*, 2011; Naylor *et al.*, 2013). According to Cancer Research UK, in 2012, there were 14.1 million new cases and 8.2 million deaths from cancer worldwide and over one third of cancer cases in the UK are diagnosed in patients aged 75 years and above (Cancer Research UK, 2015). In the United States, cancer has been the second leading cause of death since 1938 (Centre for Disease Control and Prevention, 2015). This increasing link between ageing and debilitating ailments has fuelled the search for anti-ageing interventions over the years (Austad & Kirkwood, 2000; Tchkonja *et al.*, 2013; de Cabo *et al.*, 2014).

Accumulation of senescent cells over time without efficient clearance of these cells is detrimental, as they secrete factors which promote inflammation, tumor growth and tissue damage, resulting in several diseases (see Figure 1-8) which are often age-related (Jeyapalan & Sedivy, 2008; He & Sharpless, 2017). Evidence has shown that accumulated senescent cells in tissues leads to age-related progressive loss of tissue function (Baker *et al.*, 2011; Baker *et al.*, 2016). In line with this, senescent cells have been found at sites of chronic diseases of ageing and have been implicated as a causative factor in the development of pulmonary fibrosis, bronchiectasis, osteoarthritis (OA), liver steatosis (Muñoz-Espín & Serrano, 2014; Birch *et al.*, 2016; Schafer *et al.*, 2017; Jeon *et al.*, 2017;

Ogrodnik *et al.*, 2017) and atherosclerosis (Wang & Bennett, 2012; Childs *et al.*, 2016), even though senescence has also been reported to be beneficial in atherosclerosis (Gonzalez-Navarro *et al.*, 2010; Muñoz-Espín & Serrano, 2014).

Key senescence signalling molecules such as p16^{Ink4a}, p21^{Waf1/Cip1/Sdi1} and p53 play important roles in the maintenance of stem cells as they prevent their premature exhaustion. These components reprogram cancer cells to self-renew, promoting their stem cell functions otherwise known as “stemness” (Milanovic *et al.*, 2017). Senescent cells can normally be eliminated from the body via immune-mediated mechanisms. However, the fact that they have been found to accumulate with aging suggests that the efficiency of the mechanism by which these cells are cleared from the body also diminishes with time (d'Adda di Fagagna & Campisi, 2007; Muñoz-Espín & Serrano, 2014) as the immune system function equally declines (Hensler & Pereira-Smith, 1995; Badiola *et al.*, 2015). Being a hallmark of ageing (see Figure 1-9) (López-Otín *et al.*, 2013), accumulated senescent cells in aged tissues may indicate an increased rate of generation and/or a decreased rate of clearance of these cells from the body (d'Adda di Fagagna & Campisi, 2007; Muñoz-Espín & Serrano, 2014).

1.6.1 SENESCENCE-DRIVEN FUNCTIONAL DECLINE

Cellular senescence is frequently being implicated in aging and has been listed as one of the hallmarks of ageing (López-Otín *et al.*, 2013). It has been proposed that cellular senescence could be responsible for ageing phenotypes which may arise due to a loss of cell proliferative and tissue regenerative capacity, because of the inability of senescent cells to self-renew. *In vivo* accumulation of dysfunctional senescent cells and their SASP also disrupt the tissue microenvironment and cause loss of tissue integrity and function (Campisi, 2003; Itahana & Dimri, 2017), leading to a senescence-driven functional decline or aging. Ageing has been defined as a functional waning that is accompanied by decreased fertility and increased mortality (Austad & Kirkwood, 2000), agreeing with Weismann's theory of wear and tear and natural selection (Weismann & August, 1891). However, senescence has been shown to occur not just as a result of wear and tear but also due to stress, insults and various DNA damage triggers on the cell, and also exhibits antagonistic pleiotropy (Rodier & Campisi,

2011; Campisi, 2011). Ageing therefore can be driven by these stressors, and pleiotropy also plays a role in the manifestations of ageing phenotypes.



Figure 1-9 The hallmarks of ageing.

The nine hallmarks representing common denominators of ageing in mammals and several other organisms. Adapted from (López-Otín *et al.*, 2013).

1.6.1.1 COGNITIVE DECLINE

Ageing is the main risk factor for Parkinson's disease and Alzheimer's disease and it has been proposed that senescent astrocytes contribute to these ailments (Esiri, 2007; Bitto *et al.*, 2010; Bhat *et al.*, 2012; Chinta *et al.*, 2013). Astrocytes cultured from the brains of ageing rats showed a positive staining for SA β -gal and their ability to maintain the survival of co-cultured neurons decreased.

Astrocytes also develop a senescent phenotype, overexpressing p53, p21, p16 and SAHF in response to telomere shortening and oxidative stress. Also, astrocytic glial acidic fibrillary protein (GFAP)-positive cells presented age-related synaptic impairment, as well as a flat morphology *in vivo*. Additionally, chronic microglial activation has been implicated in the neuronal death associated with Alzheimer's disease and Parkinson's disease. The ageing brain is beset with subtle chronic inflammation and senescence has been associated with human brain aneurysms (Bitto *et al.*, 2010; Hewitt *et al.*, 2012; Chinta *et al.*, 2013; Muñoz-Espín & Serrano, 2014; Zhu *et al.*, 2014). More recently, an age-related decline in the *BubR1* mitotic checkpoint kinase has been found to impair neurogenesis in adult hippocampus, making *BubR1* a potential target for age-related cognitive impairment (Yang *et al.*, 2017).

1.6.1.2 LOSS OF MUSCLE FUNCTION

Loss of muscle mass and function (sarcopenia) is a common age-related event and senescence of muscle satellite cells are thought to play a key role in the pathogenesis of sarcopenia (Muñoz-Espín & Serrano, 2014). It is also known that muscle satellite cells are required for regeneration of skeletal muscle and are considered myogenic stem cells (Relaix & Zammit, 2012). Aged muscles display the presence of senescent cells as they stain positive for SA β -Gal, accumulate p16 and harbour raised levels of pro-inflammatory cytokines. Muscle satellite cells from diseased human and mice also displayed shortened telomeres. Genetic inactivation of p16 was found to rejuvenate aged satellite cells and encourage muscle regeneration after injury. Also, genetic elimination of satellite cells expressing p16 in a mouse model of progeria ameliorated sarcopenia, further stressing the negative role senescent satellite cells play in muscle function (Cai *et al.*, 2004; Baker *et al.*, 2011; Cosgrove *et al.*, 2014; Sousa-Victor *et al.*, 2014; Tichy *et al.*, 2017). Furthermore, p53 was found to delay the functional waning of skeletal muscle and fat in a p21-dependent manner via inhibition of the p16-mediated progenitor cell senescence (Baker *et al.*, 2013).

1.6.1.3 LUNG DISEASES

Idiopathic pulmonary fibrosis (IPF) and chronic obstructive pulmonary disease (COPD) and are typical examples of senescence-associated respiratory diseases that progress with age (Tsuji *et al.*, 2006; Amsellem *et al.*, 2011; Birch

et al., 2015; Schafer *et al.*, 2017). IPF and COPD usually occur late in life and advance pathophysiologically with ageing (Faner *et al.*, 2012), showing predominance in males (Chilosi *et al.*, 2012). Several characteristics of cellular senescence have been identified in the lungs of IPF and COPD patients (Birch *et al.*, 2017). For instance, persistent inflammatory cytokines including TNF α , IL-6, IL-8, CRP and CCL2 have been observed in IPF and COPD (Faner *et al.*, 2012). IPF and COPD also increase the risk of pneumonia, which is thought to be aggravated in the elderly by the presence of accumulated senescent cells (Yanagi *et al.*, 2017). Senescence has also been implicated in the pathology of non-cystic fibrosis bronchiectasis (Birch *et al.*, 2016), an inflammatory lung disease characterized by irreversible bronchial dilation.

IPF is a progressive and deadly lung disease characterised by interstitial fibrosis which leads to scarring of the lung parenchyma (Birch *et al.*, 2017). Cellular senescence has been implicated in the pathogenesis of IPF (Yanai *et al.*, 2015; Kuwano *et al.*, 2016) and cells of the bronchial epithelium of IPF patients showed an increase in p21 levels and SA β -Gal activity (Minagawa *et al.*, 2011). It has also been demonstrated that not only are senescence markers elevated in IPF, but that the expression of p16 increases with severity of the disease and the secretome of senescent fibroblasts is fibrogenic. Furthermore, a senolytic cocktail of dasatinib plus quercetin (DQ) was found to selectively kill senescent fibroblasts (Birch *et al.*, 2017; Schafer *et al.*, 2017). A study using mouse models of IPF also showed that telomere dysfunction and short telomeres induced pulmonary fibrosis in mice (Povedano *et al.*, 2015), and short telomeres are a risk factor as well as a predisposing factor for poor survival in patients with IPF (Alder *et al.*, 2008; Calado, 2014; Dai *et al.*, 2015). Telomere dysfunction and activation of senescence linked pathways have also been reported in the airways of patients with bronchiectasis (Birch *et al.*, 2016). Large airway epithelial cells from these patients harboured a considerable increase in the percentage of TAF as well as elevated p21 levels.

COPD, a lung disease that affects the peripheral airways and lung parenchyma, causing structural changes such as alveolar airspaces destruction and peri-airway fibrosis, is characterised by imbalances in inflammatory and repair

processes, displaying a pro-inflammatory phenotype and impaired cellular regeneration (Birch *et al.*, 2017; Barnes, 2017). COPD is leading cause of morbidity, financial cost and mortality globally (Mannino & Buist, 2007). Apart from cigarette smoke, ageing is the greatest risk factor for the development of COPD (Naylor *et al.*, 2013). As COPD progresses, there is observed decline in lung function resembling that which takes place during normal lung ageing, although at a more advanced rate (Ito & Barnes, 2009). Senescence markers including p16, p21, SA β -Gal activity as well as dysfunctional telomeres have been reported in pulmonary vascular endothelial cells, airway epithelial cells and alveolar type II cells cultured *in vitro* from the lung tissue of COPD patients (Tsuji *et al.*, 2006; Amsellem *et al.*, 2011; Nouredine *et al.*, 2011; Park & Sin, 2014; Birch *et al.*, 2015; Birch *et al.*, 2016). A significantly higher amount of DNA damage foci have also been found in airway epithelial cells, endothelial cells as well as in type I and type II alveolar epithelial cells of the lungs of COPD patients (Aoshiba *et al.*, 2012; Birch *et al.*, 2015). PI3K-mTOR signalling, impaired autophagy, stem cell exhaustion and mitochondrial dysfunction have also been reported in COPD (Barnes, 2017). Moreover, lung fibroblasts obtained from COPD patients with emphysema showed reduced rate of proliferation and markers of senescence *in vitro* (Holz *et al.*, 2004; Muller *et al.*, 2006).

1.6.2 OTHER DISEASES

Cellular senescence has been implicated in the pathology of chronic liver diseases, where increasing age also correlates with poor disease outcomes (Hoare *et al.*, 2010; Aravinthan & Alexander, 2016) A recent study has shown that cellular senescence drives hepatic steatosis in patients with non-alcoholic fatty liver disease (NAFLD) (Ogrodnik *et al.*, 2017), a disease which is prevalent in older populations and whose incidence increases with age (Hardy *et al.*, 2016). The frequency of markers of hepatocyte senescence such as p21, SADS and TAF were found to increase significantly with age and their expression also correlated with the severity of NAFLD. A suicide gene-mediated ablation of p16^{Ink4a}-expressing senescent cells using the small molecule AP20187 in *INK-ATTAC* (INK-linked apoptosis through targeted activation of caspase) mice or treatment with a combination of the senolytic drugs dasatinib and quercetin (D+Q) was found to reduce overall hepatic steatosis (Ogrodnik *et al.*, 2017).

Osteoarthritis, a chronic degenerative disease of the articular cartilage and joint tissues, is also thought to be caused by senescence as accumulation of senescent articular chondrocytes as well as their SASP are found in dysfunctional cartilage cells (Zhu *et al.*, 2014). A recent study has also demonstrated that selective removal of senescent cells diminished the development of post-traumatic osteoarthritis, decreased pain and increased the development of cartilage. Chondrocytes were isolated from patients with osteoarthritis who had knee replacement therapy (Jeon *et al.*, 2017) and *in vitro* cultures of these cells were treated with a new senolytic drug and the selective elimination of senescent cells was found to decrease the expression of senescence and inflammatory markers and also increase expression of cartilage tissue extracellular matrix proteins.

Cellular senescence has also been implicated in renal ageing and disease. In a mouse model of allograft nephropathy, old donor kidneys exhibited a reduced growth of tubular epithelial cells post transplantation, an increase in p16 levels, and a higher tendency to develop transplantation related stress when compared to young donor kidneys. There was also an observed increase in renal senescent cell numbers in response to injury, marked by elevated p16, p21, p53 and SA β -gal in animal models as well as in human renal disease (Sturmlechner *et al.*, 2017; Valentijn *et al.*, 2017).

Ageing is a major risk factor for the development of cardiovascular diseases, and senescent vascular endothelial cells as well as vascular smooth muscle cells have been found to accumulate with age in arteries and atherosclerotic plaques (Zhu *et al.*, 2014; Sikora *et al.*, 2014). Activation of the *CDKN2A* locus has been found to prevent the formation of atherosclerotic plaque. Conversely, clearance of p16^{INK4a}-expressing macrophages from atherosclerotic lesions in murine models decreased plaque size, showing that the growth inhibitory aspect of senescence was beneficial while the secretory aspect was detrimental with regards to atherogenesis (Childs *et al.*, 2016; He & Sharpless, 2017).

Senescent cells have been found to accumulate with age in skin and they overexpress p16^{INK4a} (Ressler *et al.*, 2006; Jeyapalan *et al.*, 2007; Dellambra & Dimri, 2009; Tigges *et al.*, 2014). Also, in a recent study by Kimball and

colleagues, the senescence gene *CDKN2A* or p16^{INK4a} increased significantly with age in the photo-exposed arm and facial skin of Caucasian females, highlighting age-induced and photo-induced senescence in these skin areas. However, the different cell types of the skin enter into senescence differently, producing a mosaic of skin ageing (Tchkonina *et al.*, 2013; Toutfaire *et al.*, 2017; Kimball *et al.*, 2018).

Type 2 diabetes mellitus (T2DM) is a common chronic disease of ageing. Senescence is thought to influence predisposition to T2DM by its effect on pancreatic β cells and on tissue insulin resistance (Zhu *et al.*, 2014; Helman *et al.*, 2016; He & Sharpless, 2017). Resistance to insulin as a result of obesity is usually compensated for by an initial insulin overproduction by, as well as expansion of the β -cells. However, this chronic burden on the cells ultimately leads to proliferative exhaustion and loss of β -cell mass (Sharpless & DePinho, 2007; Donath *et al.*, 2013; Muñoz-Espín & Serrano, 2014; Childs *et al.*, 2015). Senescent pre-adipocytes and endothelial cells have been found to accumulate in adipose tissue from diabetic, obese individuals (Zhu *et al.*, 2014). Age is also the greatest risk factor for the development of various cancers and it has been shown that senescent cells contribute to cancer progression through their SASP (Parrinello *et al.*, 2005; Campisi, 2013; Pérez-Mancera *et al.*, 2014) and promote cancer relapse (Demaria *et al.*, 2017). Also, an assessment of middle-aged adults who were survivors of childhood cancer showed a striking prevalence of adverse health outcomes and age-related pathologies including new cancers that were not related to their childhood cancers (Hudson *et al.*, 2013; Neves *et al.*, 2015; Yang *et al.*, 2016). This may be due to accumulated senescent cells over time which were possibly induced by chemotherapy (TIS).

1.6.3 TOOLS TO MEASURE AGEING

In order to measure ageing, it is important to identify specific criteria and biomarkers that are associated with ageing, which when assessed alone or in combination with other factors, can adequately define the ageing process. Telomere length, which is the principal factor implicated in replicative senescence, has been proposed as a marker of ageing, although studies also show that it is not sufficient on its own to predict ageing and therefore should be

combined with other parameters (Martin-Ruiz *et al.*, 2005; von Zglinicki & Martin-Ruiz, 2005). The SASP has been linked with local inflammation which bring about cellular transformation, altering the tissue microenvironment and structure, and eventually leading to neurodegenerative diseases and cancer (Campisi *et al.*, 2011; Maciel-Barón *et al.*, 2016). There is known to be an elevation in circulating levels of TNF α and IL-1 in human ageing, and many reports have shown that pro-inflammatory cytokines promote extracellular matrix degradation (Toussaint *et al.*, 2002a; Toussaint *et al.*, 2002c). The aforementioned parameters such as skin wrinkling (Kimball *et al.*, 2018), muscle strength (Cosgrove *et al.*, 2014), cognitive function (Esiri, 2007; Bhat *et al.*, 2012), overexpression of biomarkers like p16 (Baker *et al.*, 2008), and also clinical frailty indices (Ullman-Cullere & Foltz, 1999; Whitehead *et al.*, 2014) are commonly used as tools to measure ageing.

There is thought to be a gradual reduction in the ability of organisms to handle stressors as they age. Chronic inflammation, also referred to as inflammaging, is one end result of the perpetual stream of antigenic load and stress. Markers of inflammation such as interleukin 6 (IL-6) and C-reactive protein (CRP) have been associated with several ageing phenotypes (Franceschi *et al.*, 2000; Franceschi & Campisi, 2014). Chronic inflammation has been demonstrated to be a good biomarker of ageing. In a study which measured the inflammatory biomarkers IL-6 and CRP in human cohorts over time, it was discovered that these markers predicted the risk of age-related diseases and mortality/lifespan successfully (Jenny *et al.*, 2012; Osorio *et al.*, 2016). Another study involving a large cohort with a wide age range from 45 to 115 years has also shown inflammation to be an important driver of ageing and suggests that suppressing chronic inflammation is a key determinant of effective longevity. In the study, several inflammatory indicators including nuclear factor- κ B (NF- κ B) - driven inflammation were assessed as biomarkers of ageing. However, it was noted that some proposed markers of immunosenescence and ageing (cytomegalovirus (CMV) titre, CD4, CD28 and telomere length) were limited in their ability to successfully predict healthspan and lifespan (Arai *et al.*, 2015; Osorio *et al.*, 2016). Additionally, using a modified SILAC (stable isotope labelling by amino acids in cell culture) technique in whole animals, as well as high resolution mass spectrophotometry, Walther and Mann demonstrated that there are only minor changes in the

proteome composition across several tissues during ageing (Walther & Mann, 2011). This supports the need for the combination of more than one parameter or indicator when attempting to measure ageing.

1.6.4 ANTI-AGEING INTERVENTIONS

In a bid to slow down ageing and its accompanying morbidities, several measures have been adopted ranging from diet changes to metabolic pathways targeting, and more researches on anti-ageing strategies are still ongoing (de Cabo *et al.*, 2014; Longo *et al.*, 2015; López-Otín *et al.*, 2016). The ultimate goal of anti-ageing interventions is to improve health and quality of life during ageing, with little or no adverse effects (López-Otín *et al.*, 2013).

1.6.4.1 NUTRITION

Nutrition, fasting and the reduction of calorie intake without malnutrition (caloric restriction) have been shown to extend longevity in several species ranging from yeast to flies, worms, rodents, non-human primates as well as humans (de Cabo *et al.*, 2014; Madeo *et al.*, 2015; Dhillon *et al.*, 2016; Provinciali *et al.*, 2016; López-Otín *et al.*, 2016). Longevity as a result of caloric restriction is thought to be regulated by nutrient signalling pathways such as the TOR/S6K and insulin pathways which when inhibited, through caloric restriction, confer resistance to stress and promote survival in ageing (Fontana *et al.*, 2010). It also has been reported that caloric restriction slows down the age dependent upregulation of p16 (Ganey & Sedivy, 2006). The impact of caloric restriction in humans was quite unpersuasive until recently, where research has shown improved health and survival in rhesus monkeys (Mattison *et al.*, 2017) as well as improved health indices in human subjects on a fasting-mimicking diet (Wei *et al.*, 2017). These results were further backed by additional data on specific biomarkers using mice studies (Miller *et al.*, 2017; Barger *et al.*, 2017).

Exercise or physical fitness is also viewed as a determining factor for longevity as regular exercise has been shown to reduce morbidity and mortality in humans and obesity is a known accelerator of ageing (de Cabo *et al.*, 2014; López-Otín *et al.*, 2016) It is proposed that anti-ageing intervention should be focussed more on preventive measures, using parameters that can be easily controlled such as diet changes, exercise, lifestyle changes and pollution control (Badiola *et al.*,

2015). However, where this is not entirely possible, it is expedient to employ therapeutic measures that can slow down or halt the ageing process and its attendant morbidities.

1.6.4.2 mTOR INHIBITION

Previous studies have shown that inhibiting the nutrient-sensing mTOR pathway can avert both cellular and organismal aging, extending lifespan in a variety of species (Robida-Stubbs *et al.*, 2012; Leontieva & Blagosklonny, 2016). Rapamycin inhibition of the TOR pathway extended lifespan across different species such as in both inbred and genetically heterogeneous mice (Harrison *et al.*, 2009; Anisimov *et al.*, 2011), in the fruit fly *Drosophila melanogaster* (Bjedov *et al.*, 2010; Danilov *et al.*, 2013) and in yeast (Powers *et al.*, 2005; Blagosklonny, 2008). Rapamycin and its analogs (rapalogs) can prevent ageing-associated diseases, such as neurodegeneration, atherosclerosis, retinopathy, obesity and cancer. Also, they can potentially rejuvenate stem cells, metabolism and immunity (Blagosklonny, 2012; Leontieva & Blagosklonny, 2016; Blagosklonny, 2017). In order to ascertain whether inhibiting the target of rapamycin complex 1 (TORC1) was able to reverse established senescence and the accompanying cellular changes, rapamycin was added to late passage senescent cells and also to control cells prior to staining for SA- β gal. Rapamycin treatment did not have any effect on proliferation or cell morphology or on SA- β gal-staining in cells that were already senescent (Kolesnichenko *et al.*, 2012), suggesting that interventions to avert senescence and ageing are better approached early as preventive rather than reversal therapy. It has been proposed that combining rapamycin with other drugs and inhibitors could provide a better anti-ageing formula (Blagosklonny, 2017). However, rapamycin being an immunosuppressor already discredits its use clinically as an anti-ageing drug to a great extent.

1.6.4.3 NF- κ B INHIBITION

Telomere-dependent cell senescence (replicative senescence) and inflammation are able to drive each other to speed up the ageing process. Accordingly, interventions to combat inflammation have been shown to rescue premature ageing in mice (Jurk *et al.*, 2014). Several data have indicated that NF- κ B signalling pathway is the major pathway which stimulates the production of SASP (Salminen *et al.*, 2012). Pharmacological or genetic intervention via the NF- κ B

signalling pathway has the potential to slow down the physiological ageing process. Inhibition of NF- κ B has been shown to extend longevity in wild-type *Drosophila melanogaster* and in various mouse models of ageing and disease. Moreover, NF- κ B blockade was also found to ameliorate aging-associated physiological changes seen in skin, muscle, bone as well as in metabolism. Interestingly, many of the roles NF- κ B plays in ageing also have an effect on stem cell function and by extension tissue homeostasis (Cai *et al.*, 2004; Rando & Chang, 2012; Freije & López-Otín, 2012; Chen *et al.*, 2013; Leung *et al.*, 2013; Studer *et al.*, 2015; Osorio *et al.*, 2016; Loaiza & Demaria, 2016).

1.6.4.4 OTHER MEASURES

Cellular reprogramming by transient expression of *Oct4*, *Sox2*, *Klf4*, and *c-Myc* (OSKM), also known as the Yamanaka factors (Takahashi & Yamanaka, 2006), was recently reported to ameliorate symptoms of ageing and extend lifespan in progeroid mice, ameliorate cellular ageing phenotypes in mouse and human cells, and also improve pancreatic and muscle tissue homeostasis in physiologically aged mice (Ocampo *et al.*, 2016). Another approach toward anti-ageing intervention is directed at telomerase activation either pharmacologically or through gene therapy (Bernardes de Jesus *et al.*, 2011; Bernardes *et al.*, 2012; Victorelli & Passos, 2017). Studies have shown also that non-steroidal anti-inflammatory drugs (NSAIDs) such as aspirin, ibuprofen and sulindac can be used to alleviate the senescence-associated inflammation that occurs during ageing. NSAIDs have also been reported to be anti-tumorigenic, preventing tumours that are not necessarily preceded by inflammation (Herfs *et al.*, 2009; Rothwell *et al.*, 2011; Lasry & Ben-Neriah, 2015).

It has been shown that cancer-related target genes (oncotargets) such as NF- κ B, mTOR, Ras, PI3K, FOXO (forkhead box O), S6K (p70 S6 kinase), IGF-1 (Insulin-like growth factor 1), MEK and AMPK are also involved in ageing. Some genes like AMPK (adenosine monophosphate-activated protein kinase), TSC1/2 (tuberous sclerosis 1/2), sirtuins, PTEN and p53, though tumor suppressors, act as gerosuppressors (suppressors of the ageing process) and inactivation of PI3K, TOR, S6K and Ras pathways have been found to prolong lifespan (Guarente & Kenyon, 2000; Pinkston *et al.*, 2006; Blagosklonny, 2013; Danilov

et al., 2013). Based on these observations, selective anti-cancer drugs have been proposed for use as anti-ageing therapeutics (Blagosklonny, 2013).

López-Otín and his fellow researchers have suggested that metabolism controls ageing and have described how all the nine hallmarks of ageing are connected to undesirable changes in metabolism (López-Otín *et al.*, 2013; López-Otín *et al.*, 2016). Wiley and Campisi have also highlighted in their review, various metabolic pathways that are connected to cellular senescence. For instance, there is increased glycolysis and an increase in fatty acid oxidation (FAO) during senescence, and the malate-aspartate shuttle reportedly antagonises senescence while a low NAD⁺/NADH ratio stimulates senescence (Wiley & Campisi, 2016).

Ageing and its associated diseases have many debilitating consequences to mankind and pose worldwide economic and social challenges. In order to effectively tackle age-related morbidities and improve the quality of life of a population, it is necessary to create a database of ageing associated genes and resources (Tacutu *et al.*, 2013; Huhne *et al.*, 2014), as well as drug compounds that target ageing and age-related ailments (Moskalev *et al.*, 2016; Barardo *et al.*, 2017) thereby facilitating the translation of anti-ageing interventions to the clinic.

1.7 TARGETED THERAPY

Targeted therapies have been developed for the management of various cancers and they have proven over the years to be more specific and more effective than the traditional cytotoxic chemotherapy. Unlike cytotoxic chemotherapy, which generally blocks DNA replication and cell division, targeted therapies can inhibit specific molecular targets of interests without acting in a non-specific cytotoxic manner. Although not without their adverse effects, targeted therapies are often better tolerated and generally more efficient than cytotoxic chemotherapies (Walter & Ahmed, 2017; Ke & Shen, 2017).

Although targeted therapies have been mainly developed for cancers with majority of patients being elderly (≥ 65 years), the principle can be applied to several other ailments (Florence & Lee, 2011; Daste *et al.*, 2016; Pauliah *et al.*, 2018). Targeted therapies have been tailored to individual patients' ailments with new approaches towards disease assessment and dosing. The three main categories of targeted therapies available are small molecule inhibitors, immunotherapies and monoclonal antibodies (Walter & Ahmed, 2017).

1.7.1 MOLECULARLY IMPRINTED POLYMERS

One of these novel strategies uses Molecular Imprinting Technology (MIT), a technique used to design artificial receptors, to produce Molecularly Imprinted Polymers (MIPs), which are synthetic receptors made from nanoparticles and have the advantage of high stability, long shelf life, cost effectiveness, ease of preparation and adaptation over their bio-analogues such as antibodies or biological receptors (Sellergren & Allender, 2005; Piletsky *et al.*, 2006; Vasapollo *et al.*, 2011; Canfarotta *et al.*, 2016a; Canfarotta *et al.*, 2016b).

MIPs are synthesized from methacrylic or acrylic monomers polymerized by creating a matrix around a template target molecule, which is later removed, leaving behind cavities complementary to its shape and functional groups (see Figure 1-10). The produced MIPs are thereafter able to selectively re-bind to their target molecule (Poma *et al.*, 2010; Canfarotta *et al.*, 2016a). The use of MIPs to selectively detect and quantify biological targets can be applied to a wide range of fields including *in vitro* and clinical diagnostics, therapeutic monitoring, controlled/sustained drug delivery, separation techniques, control of bioreactors as well as the detection of biological entities and toxins, including agents of bio-terrorism. MIPs can also be used as the recognition element in biosensors (Soper *et al.*, 2006; Piletsky *et al.*, 2006; Whitcombe *et al.*, 2011; Puoci *et al.*, 2011).

Molecularly imprinted polymer nanoparticles (nanoMIPs) made by solid phase synthesis, where the template molecule is immobilised on a solid support of glass beads, have been used for *in vivo* applications and have been found to be specific, selective and biocompatible (Canfarotta *et al.*, 2016a; Canfarotta *et al.*, 2016b; Cecchini *et al.*, 2017). NanoMIPs have also been used in ELISA (enzyme-linked immunosorbent assay) -type assays to detect analytes, with a

performance that is comparable to or better than commercially available antibodies (Chianella *et al.*, 2013; Caceres *et al.*, 2016; Smolinska-Kempisty *et al.*, 2016; Piletska *et al.*, 2017). MIPs have equally been used in microtiter plate type assays that are potentially relevant clinically (Piletska *et al.*, 2012; Piletsky *et al.*, 2017).

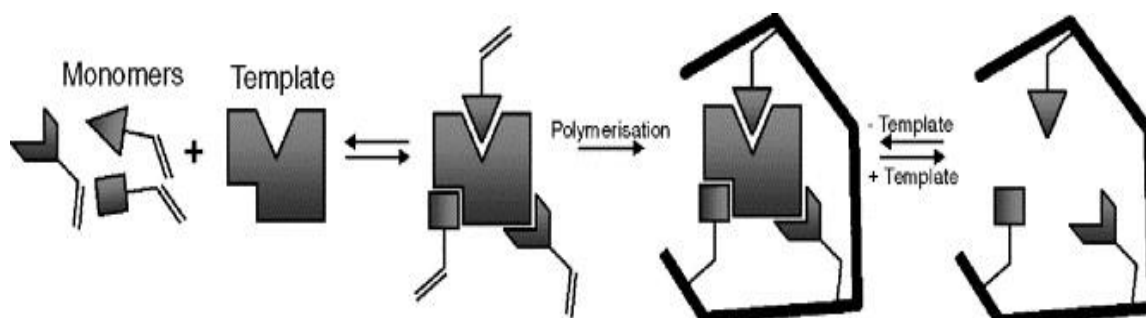


Figure 1-10 A schematic representation of the process of molecular imprinting. Functional monomers are polymerized in the presence of a template molecule. The template is later removed, leaving behind cavities with binding sites for the template molecule. Adapted from (Sellergren & Allender, 2005).

Furthermore, MIPs can potentially be used in point-of-care detection systems for medical diagnostics for cancer and a wide range of ailments (Soper *et al.*, 2006). True to this, MIPs have recently found application in the detection of different cancers (Sengupta & Sasisekharan, 2007; Voigt *et al.*, 2014; Tyagi *et al.*, 2016; Cecchini *et al.*, 2017), in sustained drug release and drug delivery systems using small molecules (Sellergren & Allender, 2005; Cunliffe *et al.*, 2005; Puoci *et al.*, 2011; Tieppo *et al.*, 2012; Kempe *et al.*, 2015; Luliński, 2017), and also for transport across an *in vitro* model of the blood-brain barrier (Dadparvar *et al.*, 2011). More recently, attempts have been made at the use of nanoparticles and two-photon probes to detect senescent cells by targeting the lysosomal β -galactosidase enzyme (Lozano-Torres *et al.*, 2017; Muñoz-Espín *et al.*, 2018).

1.7.2 ANTIBODY-DRUG CONJUGATES

The lack of selectivity and specificity of conventional chemotherapeutics often leads to non-specific toxicities to healthy tissues and poor therapeutic indices (Casi & Neri, 2012), necessitating the design of more effective therapeutic

compounds. Antibody-drug conjugates (ADCs) are monoclonal antibodies to which cytotoxic drugs are bound through a chemical linker. ADCs are an innovative therapeutic approach that combines the specificity of monoclonal antibodies with the cytotoxic activity of drugs, thereby reducing systemic toxicity and increasing the therapeutic benefit for patients (Strohl & Strohl, 2012; Casi & Neri, 2012; Perez *et al.*, 2014; Gébleux & Casi, 2016; Kumar *et al.*, 2017). The concept of ADCs was first introduced over a century ago by Paul Ehrlich, a German physician and scientist, who proposed the use of a targeting agent to selectively deliver a cytotoxic drug to a tumor. He proposed that the agent would act as a "magic bullet", which in recent times is being described as the "warhead" or "payload" (Ehrlich, 1906; Perez *et al.*, 2014).

From the introduction of the idea by Ehrlich to date, advances have been made in the development of ADCs for cancer therapy (Trail *et al.*, 1993; Sievers & Senter, 2013; Sau *et al.*, 2017; Donnell *et al.*, 2017). Several ADCs have entered into clinical trials that have been developed to target breast cancer (Trail *et al.*, 1993; Kolodych *et al.*, 2017; Trail *et al.*, 2018), ovarian cancer (Jiang *et al.*, 2016), lung and colon cancers (Trail *et al.*, 1993), hematologic malignancies (Sievers & Senter, 2013), among others. The US Food and Drug Administration (FDA) has so far approved of three ADCs namely, Mylotarg[®] and Adcetris[®] for the treatment of haematological cancers, and Kadcyła[®] for the treatment of HER2 (Human epithelial growth factor receptor 2) positive breast cancer, although Mylotarg[®] was withdrawn from the market a decade after its approval due to poor overall survival of patients (Perez *et al.*, 2014; Gébleux & Casi, 2016; Sau *et al.*, 2017).

An ADC typically consists of three parts namely, an antibody, a linker and a cytotoxic drug or "payload" (see Figure 1-11) (Thomas *et al.*, 2016; Kumar *et al.*, 2017). In the design of ADCs, the antibody's specificity, stability of the linker, potency of the cytotoxic payload, the drug to antibody ratio (DAR) as well as rate of internalization are important determinants of the ADC's efficacy (Sievers & Senter, 2013; Perez *et al.*, 2014; Gébleux & Casi, 2016; Kolodych *et al.*, 2017; Trail *et al.*, 2018). ADCs are eventually cleared from circulation either via the renal or hepatobiliary route. Studies are being carried out to evaluate the toxicity,

higher-than-normal tissue exposure and improve the localization and clearance of ADCs from the body (Casi & Neri, 2012; Sievers & Senter, 2013).

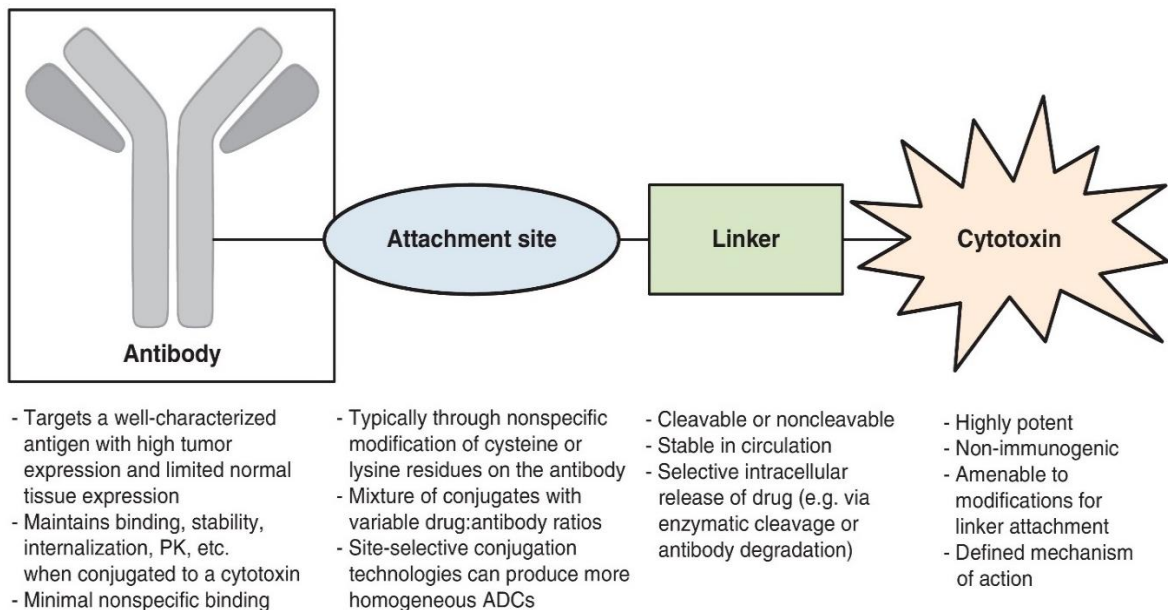


Figure 1-11 Key components of an antibody-drug conjugate (ADC).

A schematic diagram showing an antibody attached to a linker carrying a cytotoxic drug molecule. Adapted from (Ehrlich, 1906; Perez *et al.*, 2014).

1.8 THERAPEUTIC CLEARANCE OF SENESCENT CELLS: THE JOURNEY SO FAR

Therapeutic clearance of senescent cells in the elderly could prevent comorbidities and prolong life (Naylor *et al.*, 2013; de Magalhães & Passos, 2017; Demaria, 2017) as the presence of senescent cells *in vivo* plays an active role in ageing and healthspan (Deursen, J M A van, 2014; de Keizer, 2016). Genetic or chemical interventions to remove accumulated senescent cells have been shown to improve organismal health in several instances (Kirkland & Tchkonja, 2015; Moreno-Blas *et al.*, 2018). Baker and colleagues first demonstrated that the removal of p16^{Ink4a}-positive senescent cells from muscle, fat and the lens of a *BubR1^{H/H}* progeroid mouse model promotes normal functioning of tissue, delays the onset of age-related diseases, slows down the progression of already established age-related disorders when the drug was administered later in life and also extends lifespan (Baker *et al.*, 2011). Their research team also

demonstrated that clearance of p16 positive cells from naturally aged mice ameliorated age-related pathologies and improved lifespan (Baker *et al.*, 2016).

Using a pharmacological approach with drugs that inhibit Bcl-2 and activate caspase 3/7 to selectively eliminate senescent cells *in vivo*, Zhu and colleagues have also shown that partial removal of senescent cells decreased age-related phenotypes in wild type C57BL/6 mice and prolongs lifespan (Zhu *et al.*, 2015; Zhu *et al.*, 2016). These drugs that selectively kill senescent cells are collectively known as 'senolytics', and new senolytic compounds are being developed (Fuhrmann-Stroissnigg *et al.*, 2017). Clearance of senescent cells by the senolytic drug ABT263 was found to rejuvenate haematopoietic and muscle stem cells, and also improve healthspan in mice (Chang *et al.*, 2016). Additionally, using a suicide gene as well as senolytic compounds, senescent cells' clearance was found to prevent ageing-associated bone loss in mice (Farr *et al.*, 2017). Senolytic drugs have recently been shown to clear senescent type II pneumocytes and alveolar epithelial cells, indicating their usefulness in the treatment of IPF (Lehmann *et al.*, 2017; Pan *et al.*, 2017). Also, clearance of p19^{ARF}-expressing cells from mice using a toxin receptor-mediated cell knockout system ameliorated age related decline in lung function (Hashimoto *et al.*, 2016).

New approaches are being adopted for the elimination of senescent cells, such as the antibody-dependent cell-mediated cytotoxicity (ADCC) assay, which guides natural killer (NK) cells to selectively destroy anti-dipeptidyl peptidase 4 (DPP4) antibody-labelled cells (Kim *et al.*, 2017) and engineering cells to attract SASP molecules such as IL-6 (Qudrat *et al.*, 2017). Interfering with FOXO4 signalling induced a targeted apoptosis of senescent cells and improved fitness, renal function as well as fur density in normally aged and fast ageing mice (Baar *et al.*, 2017). Advances have also been made towards targeting the RB senescence pathway in cancer therapy (Shay & Roninson, 2004; Knudsen & Jean Y. J. Wang, 2010). Moreover, the elimination of senescent cells by suicide gene-mediated ablation of p16^{Ink4a}-expressing senescent cells in *INK-ATTAC* mice or by treatment with a combination of the senolytic drugs dasatinib and quercetin (D+Q) reduces overall hepatic steatosis (Ogrodnik *et al.*, 2017). Capped mesoporous silica nanoparticles (MSN) have also been used to deliver

cytotoxic drugs to senescent cells (Agostini *et al.*, 2012) through the targeting of β -galactosidase in these cells. The therapeutic clearance of senescent cells is a promising new field that could potentially be translated into clinical use if all the questions regarding safety and adverse effects are properly answered (Kirkland & Tchkonja, 2017).

1.9 AIMS AND OBJECTIVES

1.9.1 AIM OF RESEARCH:

The aim of my research is to:

- A. Validate characterised novel markers of senescence and
- B. Eliminate senescent cells by targeting these markers.

1.9.2 OBJECTIVES:

- A. To test for the presence of these novel markers in different models of senescence such as cells, aged and diseased tissues.
- B. To prevent the accumulation of senescent cells by targeting these identified markers using different tools.
 - i. Use molecular imprinted polymers (MIPs) as a proof of concept method to target and eliminate senescent cells.
 - ii. Use antibody-drug conjugates (ADCs) to deliver drugs to target cells.
 - iii. Inhibit BTK, a novel marker of senescence, to prevent the emergence of senescent cells and ameliorate symptoms of ageing *in vivo*.

CHAPTER 2 MATERIALS AND METHODS

2.1 HISTOLOGY

2.1.1 ISOLATION AND FIXATION OF MOUSE TISSUES

Brain, liver, skin and muscle tissues were isolated from mice that were culled humanely at the Preclinical Research Facility (PRF), Division of Biomedical Sciences (DBS), University of Leicester. Individual tissues were immediately placed into specimen collection tubes (Sterlin, No. 25052B) containing 10% Neutral Buffered Formalin (Sigma-Aldrich) and fixed for 24 – 48 hours. Tissues were removed from formalin and placed in 70% Ethanol before being sent to the histology facility at the university's Centre for Core Biotechnology Services (CBS) for processing into paraffin embedded tissue blocks. Old and young mouse skin, eyes, brain, liver and muscle tissues were also obtained from the Shared Ageing Research Models (ShARM) biorepository run by the University of Sheffield, for use in this project.

2.1.2 SUBBING OF MICROSCOPE SLIDES

In order to increase adherence of tissue sections onto glass slides and prevent tissue loss during histological procedures, slides were coated by submerging ("subbing") them in a solution of adhesive. The slides were coated with a solution of 3-aminopropyltriethoxysilane (APES) using an adaptation of the Maddox and Jenkins standard protocol (Maddox & Jenkins, 1987). At physiological pH, tissue sections possess a net negative charge hence their adhesiveness can be improved by making the slide surface positively charged. Coating the slides with APES leaves covalently bound amino groups on the slides and confers on them net positive charges which enhance tissue adhesion.

Plain microscope slides were placed in racks and soaked in hot water containing 5% Decon 90 overnight, after which they were washed with running hot water for 30 minutes. They were thereafter washed three times in distilled water and dried in the oven at 60°C for about 1 hour. Subbing solution was prepared by adding 8ml of 3-aminopropyltriethoxysilane (APES) into 400ml of acetone (2% 3-aminopropyltriethoxysilane in acetone).

Five jars/tanks were set up in a fume hood as follows:

Tank 1: Subbing solution

Tank 2: Acetone

Tank 3: Acetone

Tank 4: Distilled water

Tank 5: Distilled water

The racks of slides were submerged in each tank and agitated for two minutes, after which they were dried in the oven at 60°C before being replaced into their boxes, ready for use. Subbed slides can be stored for several months and years.

2.1.3 SECTIONING OF TISSUES AND MOUNTING ON SLIDES

Formalin-fixed paraffin-embedded (FFPE) tissues were cut into 5 µm sections using a microtome (LEICA RM2235). Sections were then placed on a 34°C tissue floatation bath (RA Lamb) to straighten out before being mounted on coated/subbed slides. Slides were either air-dried overnight or dried in the oven at 37°C for one hour before being used for further histological procedures.

2.1.4 HAEMATOXYLIN AND EOSIN STAINING

Tissue sections mounted on subbed slides were placed into racks and soaked in two changes of Xylene for 10 minutes each. Next, they were immersed in two changes of 100% ethanol for 10 minutes each, then in 90% ethanol for 10 minutes and lastly in 70% ethanol for 10 minutes. Slides were then rinsed in running tap water for 3 minutes before being immersed in Haematoxylin solution (Sigma-Aldrich) for 5 minutes. Slides were rinsed again in tap water for about 3 minutes before being immersed in 1% acid alcohol (1% HCL in 70% ethanol) for 10 seconds. The slides were quickly rinsed in tap water and immersed in 1% Aqueous Eosin solution (Raymond A Lamb) for 1 minute. They were washed again in tap water quickly and immersed in 70% ethanol for 30 seconds, after which they were submerged in two changes of 100% ethanol for 5 minutes each, followed by two changes of xylene for 5 minutes each. Coverslips were mounted onto the slides using DPX mountant for histology (Sigma-Aldrich).

2.1.5 IMMUNOHISTOCHEMISTRY

Slides of FFPE tissue sections were placed in racks and dewaxed in two changes of xylene for 10 minutes each. They were then dehydrated in two changes of

100% ethanol for 10 minutes each, after which the slides were soaked in 400ml of methanol containing 2.4ml of 30% hydrogen peroxide for 10 minutes to block endogenous peroxidase. At the same time, Citrate Buffer (2.94g Tri-sodium citrate in 1L distilled water) at pH 5.98–6.00 was heated in the microwave at 900W for 10 minutes. The slides were thereafter microwaved for 15 minutes in citrate buffer in a pressure cooker for heat-mediated antigen retrieval and then washed with 1x phosphate buffered saline (PBS). The edges of the slides were dried and a pap pen was used to mark around the tissue. Slides were incubated with about 100µl of 5% serum for 1 hour, after which the serum was drained and slides were then incubated with primary antibody overnight at 4°C. If using mouse primary antibody on mouse tissue, the M.O.M. (mouse on mouse) kit was utilised and the steps followed accordingly.

The next day, slides were washed in PBS and the edges dried before being incubated for 30 min to 1 hour with Biotinylated Secondary antibody (Dako), diluted 1:200 in 5% serum. Slides were thereafter washed in PBS and the edges dried before incubating for 30 minutes with Streptavidin-Peroxidase. They were again washed with PBS and incubated with DAB (3,3'-Diaminobenzidine) peroxidase for 5 minutes maximum (see Table 2.1 for full list of reagents). Slides were washed with water and counterstained with haematoxylin (or eosin) for 10–15 seconds. They were again washed with water to clear the haematoxylin, then dehydrated in 70%, 90% and 100% ethanol for 10 minutes each before being cleared in Xylene. The slides were mounted with DPX and allowed to air dry in a fume cupboard (S+B UK Ltd.) overnight. Images were taken using an inverted light microscope (Leica Microsystems). The intensity of DAB staining in each image was quantified using ImmunoRatio software available online (<http://153.1.200.58:8080/immunoratio/>). Values were plotted as graphs using the GraphPad Prism 7.0 software.

Table 2.1: Reagents used for Immunohistochemistry

| Name | Supplier | Product No. |
|---|-----------------|----------------------------|
| Goat Serum (Normal) | Dako | Ref X0907, Lot 20011859 |
| Swine Serum (Normal) | Dako | Ref X0901, Lot 20009962 |
| Polyclonal Goat Anti-Mouse IgG / Biotinylated | Dako | Ref E0433, Lot 20010754 |
| Polyclonal Swine Anti-Rabbit IgG / Biotinylated | Dako | Ref E0353, Lot 20010746 |
| Hydrogen Peroxide Solution 30% (w/w) in H ₂ O | Sigma Aldrich | H1009, Lot SZBB0390V |
| R.T.U. Horseradish Peroxidase Streptavidin | Vector Labs | Cat SA-5704, Lot ZA0421 |
| DAB Substrate Kit for Peroxidase | Vector Labs | Cat SK-4100 |
| M.O.M. Immunodetection Kit (Basic) | Vector Labs | Cat BMK-2202 |
| Haematoxylin | Sigma Aldrich | GHS132-1L |
| Eosin 1% aqueous | Raymond Lamb | LAMB/100-D, Lot 15193 |
| DPX Mountant | Sigma Aldrich | 06522, Lot BCBH4393V |

2.2 CELL CULTURE

Various cell lines (Table 2.2) were used in the course of this project. All cells were cultured in Dulbecco's Modified Eagle's Medium (DMEM) supplemented with 10% Foetal Bovine Serum (FBS) and 1% penicillin/streptomycin (100 IU/ml penicillin, 100 µg/ml streptomycin). Cells were cultured in a 37°C humidified incubator with 5% CO₂. The inducible senescence models used in the course of this research include the EJ bladder cancer cell lines EJp16 (Macip *et al.*, 2002), EJp21 (Fang *et al.*, 1999) and EJp53 (Sugrue *et al.*, 1997), all with a tetracycline off gene expression system, which enables them to overexpress p16, p21 and p53 respectively in the absence of tetracycline. These cells become senescent 3-4 days after tetracycline removal, which makes them a handy model of chemically induced senescence. Another model of cell senescence used is the HT1080p21-9 cells, a derivative of the HT1080 fibrosarcoma cell line (Chang *et al.*, 1999a; Demidenko & Blagosklonny, 2008) which overexpress p21 and become senescent after 3-4 days in the presence of Isopropyl β-D-1-thiogalactopyranoside (IPTG).

Primary fibroblast cells from Idiopathic Pulmonary Fibrosis (IPF) patients and non-fibrotic control (NFC) individuals were also used in the course of this project. These cells were obtained from the Leicester Respiratory Biomedical Research Unit (BRU). These fibroblasts were also cultured in DMEM supplemented with 10% FBS, 100 IU/ml penicillin, 100 µg/ml streptomycin and grown in a 37°C humidified incubator with 5% CO₂. Another cell line used was the HCT116 colorectal cancer cells. These cells have a wild type p53 gene and were also cultured in DMEM that was supplemented with 10% FBS, 100 IU/ml penicillin, 100 µg/ml streptomycin, maintained in a 37°C humidified incubator with 5% CO₂.

2.2.1 THAWING AND GROWING OF CELLS

Cryovials of frozen cells were thawed quickly by placing them in a 45°C bead bath and contents were gently re-suspended in Dulbecco's Modified Eagle's Medium (DMEM) in a 15ml Falcon tube and centrifuged at 1,100 rpm for 3 minutes to remove old freezing media and dimethyl sulfoxide (DMSO). The supernatant was discarded and cell pellets were re-suspended in complete culture media, which is DMEM supplemented with 10% FBS, 100 IU/ml penicillin

and 100 µg/ml streptomycin. Cells were seeded into 60 mm or 100 mm culture dishes and incubated at 37°C in a humidified incubator with 5% CO₂.

To keep the EJ cells proliferating, 1µM tetracycline was added to the culture media and this was replaced every three days. EJ p16 cells were maintained in complete culture media supplemented with 100 µg/ml hygromycin and 2 µg/ml puromycin, while EJ p21 and EJ p53 cells were maintained in complete media supplemented with 100 µg/ml hygromycin and 750 µg/ml geneticin (See Table 2.3). To induce senescence in the EJ cells model via removal of tetracycline, cells were trypsinized and washed three times with 1x PBS by centrifuging at 1,100 rpm for 3 minutes. To initiate p21 – induced senescence in HT1080p21-9 cells, 100µM IPTG was added to the media and the cells were allowed to senesce for up to five days. IPTG and fresh media was replaced after three days. EJp53 cells were also transfected with shRNA for B2MG and DEP1 (Santa Cruz Biotechnology) in the course of this project and these cells were selected with 4 µg/ml puromycin to create stably transfected EJp53 shB2MG and EJp53 shDEP1 cell lines. All cell culture work was carried out in a microbiological safety cabinet (BioMAT).

2.2.2 PASSAGING OF CELLS

When the cells reached 80% confluency, they were passaged by splitting into new culture dishes. To split cells, old media was discarded and cells were washed with 1x Dulbecco's Phosphate Buffered Saline (DPBS; GIBCO) before adding 0.5ml of 0.25% Trypsin–EDTA (GIBCO) to the cells. They were incubated at 37°C for 3 minutes, after which they were collected into 15ml Falcon tubes by washing out with DMEM and afterwards were centrifuged at 1,100rpm for 3 minutes. The supernatant was discarded and pellets re-suspended in DMEM in new culture dishes according to desired seeding density.

Table 2.2: List of cells used

| NAME | SOURCE | CHARACTERISTICS |
|--------------------|---|--------------------------------|
| EJp53 | Bladder Carcinoma | Tet – off p53 inducible system |
| EJp21 | Bladder Carcinoma | Tet – off p21 inducible system |
| EJp16 | Bladder Carcinoma | Tet – off p16 inducible system |
| HT1080p21-9 | Fibrosarcoma | IPTG – on p21 inducible system |
| HCT116 | Colorectal Carcinoma | |
| IPF | Idiopathic Pulmonary Fibrosis Fibroblasts | Primary Cells |
| NFC | Non-Fibrotic Control Lung Fibroblasts | Primary Cells |

2.2.3 COUNTING OF CELLS

Cells were counted by mixing 10µl of cell suspension with 10µl of 0.4% Trypan Blue Solution (Gibco). 10µl of this mixture was added to cell counting slides (Bio-Rad) and counted using the T 20 automated cell counter (Bio-Rad). Cell count was obtained as number of cells per ml. In some cases, such as when passaging cells to maintain a culture, cells were also counted without the need for trypan blue exclusion, where all the cells were considered viable.

2.2.4 FREEZING OF CELLS

Cells were washed with 1X DPBS and trypsinized. They were then incubated at 37°C for 3 minutes after which they were washed into 15ml Falcon tubes with DMEM and centrifuged at 1,100rpm for 5 minutes. Supernatant was discarded and pellet suspended in Freezing Media (10% DMSO in DMEM supplemented with 10% FBS and 1% penicillin/streptomycin) at a concentration of 1×10^6

cells/ml – 2×10^6 cells/ml. 1ml of cell suspension were pipetted into Cryovials and immediately placed into an isopropanol freezing container (Mr Frosty; NALGENE) for slow freezing (about 1°C per minute) in -80°C for 24–48 hours. Cryovials were thereafter removed from the freezing chambers and stored at -80°C or in liquid nitrogen storage cylinders.

Table 2.3: Cell Culture Reagents and Supplements

| Reagent / Supplement | Supplier | Product No. |
|--|---------------|-------------|
| Dulbecco's Modified Eagle's medium (DMEM) | Gibco | 61965026 |
| Foetal Bovine Serum (FBS) | Gibco | 10500064 |
| Penicillin-streptomycin | Gibco | 15140122 |
| Dulbecco's Phosphate Buffered Saline (PBS) | Gibco | 20012019 |
| Trypsin-EDTA (0.25% Phenol red) | Gibco | 25200056 |
| Hygromycin B (50mg/mL) | Gibco | 10687010 |
| Geneticin™ Selective Antibiotic (G418 Sulfate) (50mg/mL) | Gibco | 10131035 |
| Puromycin dihydrochloride | Sigma-Aldrich | P8833-10MG |
| Tetracycline hydrochloride | Sigma-Aldrich | T8032-20MG |
| Isopropyl β-D-1-thiogalactopyranoside (IPTG) | Sigma-Aldrich | I5502-1G |
| Dimethyl Sulfoxide (DMSO) | Sigma-Aldrich | D8418-100ML |

2.3 CELL PROLIFERATION AND VIABILITY ASSAYS

2.3.1 COLONY FORMATION ASSAY

Colony formation assay (CFA) or clonogenic assay is an *in vitro* cell survival assay that is used to test the ability of a single cell to produce a colony (Franken *et al.*, 2006). It can be used to assess the effect of a drug or chemical compound on cell proliferation and also the effect of a specific gene on cell proliferation. In this technique, cell colonies are washed, fixed and stained with Giemsa stain modified solution (Fluka). To carry out the assay, 200 or 500 cells were seeded in 60mm cell culture dishes in replicates. Plates were incubated at 37°C for 14 days and fresh media with drugs was replaced every 3 days. To perform the Giemsa staining, media was aspirated and plates washed with 1X PBS. Cells were then fixed with 3ml of 10% Neutral Buffered Formalin for 30 minutes at room temperature. Plates were afterwards washed twice with 1x PBS and allowed to air dry completely with the lids uncovered. 5ml of fresh staining reagent was added to each plate and left to incubate for 5 hours at room temperature. After 5 hours, the staining solution was removed and plates were washed gently with distilled water. The plates were allowed to air dry before colonies were counted and images taken.

Giemsa Staining Reagent: 6.4ml of PO₄ buffer (67mM), 89.6ml of dH₂O, 4ml Giemsa stain.

1M PO₄ buffer: 1M Sodium Phosphate monobasic and 1M Sodium Phosphate dibasic mixed in a 1:2 ratio. Bring the pH to 7.0 by slowly adding more monobasic or use Sodium Hydroxide (NaOH).

2.3.2 MTS ASSAY

The MTS (3-(4,5-dimethylthiazol-2-yl)-5-(3-carboxymethoxyphenyl)-2-(4-sulfophenyl)-2H-tetrazolium) assay is a cell viability assay that uses colorimetric means to determine the number of metabolically active cells. The MTS reagent used was CellTiter 96[®] AQueous One Solution Cell Proliferation Assay (Promega). Prior to performing the assay, adherent cells were plated out according to the experiment's design, in 60mm or 6-well plates and treated with drug compounds accordingly. After the required duration of treatment, growth media from the plates were collected into 15ml Falcon tubes and cells were

trypsinized, incubated at 37°C for 3 – 5 mins and then rinsed out with media into the 15ml Falcon tubes and centrifuged at 1,100rpm for 3 minutes. Cell pellets were re-suspended in 500µl of media and 100µl of the suspension was seeded per well, in triplicates in a 96 well flat bottom plate. 20µl of MTS reagent was added to the cell suspension in each well while some wells had media and MTS only as blank.

The plates were read at an absorbance of 492nm using the Infinite F50 absorbance plate reader (Tecan) and data recorded with the Magellan for F50 data analysis software. Using Microsoft Excel 2013, cell viability was calculated by the formula:

$$\% Viability = \frac{OD Sample}{OD Control} \times 100$$

Where OD is the Optical Density (absorbance). Graphs and charts were plotted using GraphPad Prism 7.0 software.

2.4 FLOW CYTOMETRY

Flow cytometry is an analytical technique frequently used in cell biology for cell counting, biomarker detection and cell sorting. The technique relies on the detection of fluorescence of single cells in a fluidics system.

2.4.1 PROPIDIUM IODIDE STAINING

Propidium Iodide (PI) is a red fluorescent DNA intercalating dye that is impermeant to live cell membrane. It is therefore excluded by viable cells and is used to separate dead cells from live cells in a population. To assess cell viability by flow cytometry using Propidium Iodide staining, cells were seeded in 60mm plates and allowed to attach overnight. Cells were then treated with various drug concentrations and incubated at 37°C for 24 – 48 hours. After the required duration of treatment, media from each plate was collected into labelled 15 ml falcon tubes. Cells were washed with 2 ml of PBS and this was collected into the same falcon tube with media. 0.5 ml of 0.25% Trypsin was added to each plate and incubated for 3 minutes at 37°C. Cells were washed out from the plates into their respective falcon tubes with media and centrifuged at 1100 rpm for 3

minutes. Supernatant were discarded and pellets re-suspended in 2 ml of PBS and washed once by centrifuging. The supernatants were again discarded and pellets re-suspended in 1 ml of ice cold 70% ethanol to fix the cells.

The sample tubes were kept at -20°C for at least 1 hour before PI staining (samples can be fixed for weeks before staining procedure). To carry out propidium iodide staining, samples were centrifuged at 1,500rpm for 5 minutes to remove ethanol. Pellets were washed with 2 ml of PBS and centrifuged again for 5 minutes at 1,500rpm. The staining solution was prepared with 50 µg/ml PI and 40 µg/ml RNase A in 1x PBS and stored in the dark. Cell pellets were re-suspended in 300 µl of staining solution and transferred to 5 ml polystyrene round – bottom FACS tubes (Falcon). Tubes were incubated in the dark for 30 minutes at 37°C before reading samples using the BD FACSCanto II (Becton Dickenson Biosciences). Data acquisition and cell cycle analysis were done using the FACS Diva™ version 6.1.3 software (BD Biosciences) and graphs plotted using the GraphPad Prism 7.0 software.

2.5 GENETIC ANALYSES

2.5.1 BACTERIAL TRANSFORMATION

Plasmids were inserted into bacteria in order to replicate or make several copies for future experiments. This was carried out using competent Top 10 (T10) or DH5-α or Bronze α-select bacteria cells. The cells were thawed on ice and mixed by gently flicking the tube. 2µl of plasmid was added to 50µl of cells and flicked to mix. The mixture of cells and plasmid was incubated on ice for 20 minutes after which they were heat shocked for 1 minute at 42°C. The cells were again incubated on ice for 2 minutes and 950µl of LB (lysogeny broth) was added using aseptic technique. This was transferred to a 50 ml Falcon tube and incubated at 37°C with shaking for 1 hour. The tubes were centrifuged for 1 minute at maximum speed (7,500 rcf) and pellets were re-suspended in 100µl of SOC (Super Optimal broth with Catabolite repression) medium (Invitrogen). The re-suspended bacteria was plated out as streaks on an agar plate containing appropriate antibiotic to which the plasmids have resistance (Ampicillin or Kanamycin or Spectinomycin) using ColiRollers™ plating beads (Novagen), in 10% and 90% dilutions and incubated at 37°C overnight.

A single colony was picked the following day and placed into 5 ml of LB containing appropriate antibiotics and incubated at 37°C overnight with shaking. This was used for plasmid isolation with the plasmid DNA isolation/ purification mini kit (QIAGEN). Before carrying out the miniprep purification step, 500µl of the bacterial culture was mixed with 500µl of 50% glycerol (1:1 mixture of glycerol and distilled water). This was stored in -80°C as a glycerol stock of the plasmid. To carry out a midiprep purification from glycerol stock, 100µl of LB along with the appropriate antibiotic was prepared in an Erlenmeyer flask and a pipette tip was used to scrape the top of the glycerol stock and the tip was added to the flask of LB. This was incubated overnight at 37°C with shaking. Midiprep was done the following day using the QIAGEN Midi kit and following its protocol.

2.5.2 PLASMID TRANSFECTION

In order to transfect B2MG cDNA (OriGene) into EJp53 or EJp16 cells for gene overexpression, 500,000 cells were seeded per well of a 6-well plate with 2ml of DMEM growth media supplemented with 10% FBS, 100 IU/ml penicillin and 100 µg/ml streptomycin. 1µg/ml of tetracycline was added to the cells to prevent them from expressing p53 or p16 and cells were incubated at 37°C overnight. Transfection was carried out the next day using cDNA plasmid and Lipofectamine™ 2000 reagent (Invitrogen) in a 1 µg: 2.5 µl ratio, diluted in DMEM only without serum and antibiotics. 4µg of plasmid was added to 1ml of DMEM in one Falcon tube and 10µl of Lipofectamine™ 2000 was added to 1ml of DMEM in another Falcon tube. Both tubes were allowed to stand at room temperature for 5 minutes after which the contents of the two tubes were mixed together and incubated again at room temperature for 20 minutes to form complexes.

After 20 minutes, growth media was aspirated from cells and 1ml of the transfection complexes was added to each well of cells. Cells were incubated at 37°C for 6 hours after which the growth media was changed to complete DMEM with serum, antibiotics and tetracycline. Cells were used for experiments 1 – 6 days after transfection and were collected for analysis afterwards. The volumes were either scaled up or down for different sizes of cell culture dishes. For shRNA transfection to silence gene expression, the same protocol was followed but using a 1 µg: 10 µl ratio of shRNA (Santa Cruz) to Lipofectamine reagent. 4µg/ml of puromycin was added to the cells' media in order to generate stably

transfected cells and this was replaced each time the media was changed; every two to three days. Cells were selected in this manner for several weeks after transfection.

2.5.3 TOTAL RNA EXTRACTION FROM TISSUES

Total RNA was extracted from formalin fixed paraffin embedded mouse tissues using the ReliaPrep™ FFPE Total RNA Miniprep System Kit (Promega) and following the protocol on the manufacturers' manual. The concentration of extracted RNA was measured using a NanoPhotometer® P300 (Implen) and samples were either immediately used for cDNA synthesis by Reverse Transcription or stored at -80°C until needed for further analysis.

2.5.4 QUANTITATIVE REVERSE TRANSCRIPTION REAL TIME PCR (RT-qPCR)

In order to study gene expression in tissues obtained from study animals, RNA was extracted as previously described and the complementary DNA (cDNA) was synthesized by reverse transcription. Quantitative Real Time PCR was then carried out using the cDNA obtained and results analysed.

2.5.4.1 FIRST STRAND cDNA SYNTHESIS (REVERSE TRANSCRIPTION)

cDNA was synthesized from RNA using the Superscript™ III First Strand Synthesis System for RT-PCR (Invitrogen). Equal concentrations of RNA, in a range within 10pg - 5µg, from all samples were used for the reaction. For each sample, Nuclease Free Water was added to the RNA in a 0.2ml PCR tube (VWR) to bring the volume to 11µl. 1µl Random Primers and 1µl dNTPs were added to the mixture, bringing the volume in the PCR tube to 13µl. The samples were centrifuged briefly using a Micro centrifuge (Starlab) to ensure all the reagents were contained in the tube. Tubes were placed into a Thermal Cycler and samples were heated at 65°C for 5 minutes. Sample tubes were afterwards incubated on ice for at least one minute. 7µl of a master mix containing 4µl of 5X First-Strand Buffer, 1µl of 0.1M DTT, 1µl of Superscript™ III Reverse Transcriptase and 1µl of 40 U/µl RNaseOUT™ Recombinant RNase Inhibitor (Invitrogen) was added to each sample tube, bringing the total reaction volume to 20µl. Samples were returned to the Thermal Cycler and incubated first at 25°C for 10 minutes, then at 50°C for 50 minutes and the reaction was heat inactivated

at 70°C for 15 minutes. The cDNA produced was ready for use as a template for PCR. If not used immediately, it was stored in -20°C until needed for PCR.

2.5.4.2 QUANTITATIVE REAL TIME PCR (qPCR)

In order to quantify the relative gene expression, gene specific primers were designed (Table 2.4) and GAPDH was used as an internal control reference gene (housekeeping gene) to normalize the expression of the target genes. All primers were supplied by Eurofins Scientific. The PCR reaction mix was prepared by making a master mix for each gene that was to be amplified, using 10µl of 2x SensiMix SYBR No-Rox (Bioline), 4.6µl of Nuclease Free water (Applied Biosystems), 0.2µl of reconstituted forward primer and 0.2µl of reconstituted reverse primer. 15µl of the master mix was added to each well of a white LightCycler® 480 Multiwell Plate 96 (Roche), in triplicates. 5µl of diluted cDNA (or nuclease free water for control) were added to each well, bringing the reaction volume to 20µl.

The plate was sealed with a Thermal Seal RT™ Sealing Film (Alpha Laboratories) and centrifuged briefly for 1 minute, to contain liquid contents within the wells. The qPCR reactions were run on a LightCycler® 480 system (Roche) using the following conditions: 10 minutes of enzyme activation “hold” at 95°C, 50 cycles of denaturation for 15 seconds at 95°C, annealing and elongation for 60 seconds at 60°C, and data was captured with the LightCycler® 480 Software release 1.5.0 SP3. A melting curve was used to prove the specificity of the primers at the end of the PCR run. The amplification plots were viewed and the baseline and threshold values were set in order to analyse the data. Relative quantification analysis was done and a relative expression value was obtained based on the comparative Ct calculations as shown below:

$$\Delta C_t \text{ sample} = C_t \text{ sample} - C_t \text{ GAPDH}$$

$$\Delta\Delta C_t = \Delta C_t \text{ sample} - \Delta C_t \text{ reference control}$$

Results were analysed on Microsoft Excel and graphs plotted using GraphPad Prism 7.0 Software.

Table 2.4: Primers used for qRT-PCR

| GENE | PRIMER SEQUENCE (5' – 3') | REFERENCE | SUPPLIER |
|--------------|----------------------------------|----------------------------------|-----------------|
| B2MG | Fwd: GCTATCCAGAAAACCCCTCAA | | Eurofins |
| | Rev: CATGTCTCGATCCCAGTAGACGGT | (Banchio <i>et al.</i> , 2007) | Scientific |
| DEP1 | Fwd: GCAGTGTTTGGATGTATCTTTGGT | | Eurofins |
| | Rev: CTCATTATTCTTGGCATCTGTCCTT | (Hackbusch <i>et al.</i> , 2013) | Scientific |
| p16 | Fwd: CCCAACGCCCCGAACT | | Eurofins |
| | Rev: GCAGAAGAGCTGCTACGTGAA | (Edwards <i>et al.</i> , 2007) | Scientific |
| p53 | Fwd: CACAGCGTGGTGGTACCTTA | | Eurofins |
| | Rev: TCTTCTGTACGGCGGTCTCT | (Alwahaibi <i>et al.</i> , 2011) | Scientific |
| GAPDH | Fwd: GTTGTCTCCTGCGACTTCA | | Eurofins |
| | Rev: GGTGGTCCAGGGTTTCTTA | (Xiang <i>et al.</i> , 2012) | Scientific |

2.6 PROTEIN ANALYSIS

2.6.1 EXTRACTION OF TOTAL PROTEIN FROM CELLS

2.6.1.1 SAMPLE COLLECTION

To collect adherent cells for Western blot analysis, old media was discarded from the cell culture plate and cells were washed once with 1x DPBS. For a 100 mm plate, 1ml of 0.25% trypsin was added to cells and incubated at 37°C for 3 minutes. Cells were rinsed out with 5ml of 1x PBS into a falcon tube and centrifuged at 1,100rpm for 3 minutes to remove the trypsin. The supernatant was discarded and the cell pellets were either lysed immediately for whole cell protein extraction or frozen in -80°C until when needed.

2.6.1.2 PREPARATION OF WHOLE CELL LYSATES

RIPA (radio immunoprecipitation assay) lysis buffer was prepared beforehand using 150mM NaCl, 50mM Tris HCl pH 8.0, 1% NP40, 0.1% SDS and 0.5% sodium deoxycholate diluted in distilled water (dH₂O) and stored at 4°C. Cell pellets in Falcon tubes were placed on ice and 100µl of RIPA lysis buffer containing 1:100 dilution of protease inhibitor cocktail (Sigma-Aldrich) and 1:100 dilution of phosphatase inhibitor cocktail (Sigma-Aldrich) was added to the cell pellets. The volume of lysis buffer was adjusted according to the size of cell pellet for each sample. The pellets were incubated on ice for 20 minutes after which they were mechanically sheared by passing through a 0.8 x 40mm needle (BD Microlance 3) up to 20 times.

Samples were transferred into 1.5ml Eppendorf tubes on ice and centrifuged at 14,000rpm for 15 minutes at 4°C. The supernatant were transferred into new Eppendorf tubes and the pellets discarded. Protein concentration was determined by the Bradford assay, after which 4x Laemmli buffer (40% glycerol, 240mM Tris HCl pH 6.8, 8% SDS, 0.04% bromophenol blue, 20% β-mercaptoethanol in dH₂O) was added to the samples and heated at 100°C for 5 minutes. Samples were allowed to cool before either being used for Western blot or stored at -20°C until needed.

2.6.2 EXTRACTION OF TOTAL PROTEIN FROM TISSUES

Various tissues were isolated from humanely culled study animals and placed into 7 ml bijoux tubes (Starlab) containing 1x PBS on ice. Afterwards, tissues were either fixed in formalin for paraffin embedding or cut into small pieces and

mashed through a 40 µm cell strainer (Corning) using the piston of a syringe plunger (Terumo). The tissue homogenate was rinsed out using FBS with 10% DMSO, aliquoted into Cryovials and stored at -80°C for future use. To extract protein from frozen tissue homogenates, 300µl of sample was taken from each cryovial into 15 ml Falcon tubes and washed twice with 2 ml of 1x PBS by centrifuging at 2500 rpm for 5 minutes. Supernatants were discarded and pellets re-suspended in RIPA buffer containing protease and phosphatase inhibitor cocktails.

Samples were incubated on ice for 30 minutes, after which they were thoroughly lysed by passing through a syringe and 0.8 x 40mm needle at least 20 times. Samples were then centrifuged and protein concentration determined before heating as previously described. Total protein was also extracted from formalin-fixed paraffin-embedded (FFPE) mouse tissue samples using the Qproteome FFPE Tissue Kit (QIAGEN) and following its protocol. 4x Laemmli buffer was added to the protein extracts in a ratio of 1:4 and the samples were boiled at 100°C for 5 minutes. Samples were allowed to cool and then stored at -20°C until when needed for Western blot analysis.

2.6.3 SODIUM DODECYL SULFATE – POLYACRYLAMIDE GEL ELECTROPHORESIS (SDS-PAGE).

Polyacrylamide gels were hand casted using a Mini-PROTEAN Tetra Cell Casting Module (Bio-Rad). Various percentages of polyacrylamide were used, depending on the size of protein being detected (Table 2.5). Smaller molecular weight proteins required a gel with a higher percentage of Bis Acrylamide and gels with lower percentage of Bis Acrylamide were used for larger molecular weight sized proteins. The polyacrylamide gel was made up of two parts: a resolving/separating (lower) gel and a stacking (upper) gel. The components of the gels were mixed together with the exception of APS (Sigma-Aldrich) and TEMED (Sigma-Aldrich) which were added last, just before pouring onto the plates to initiate polymerization. To cast the gel, Mini-PROTEAN® Spacer Plates with 1.5 mm Integrated Spacers, comprising of an outer glass and an inner glass were cleaned and assembled onto a casting frame and stand. The spacer plates were loaded with the appropriate resolving gel (see Table 2.5) up to a level 1cm below the mark of the comb's teeth. The poured gel was overlaid with 70%

ethanol and left to polymerize for about 45 minutes at room temperature. The ethanol was poured out and the excess dried off using a Whatman filter paper. The stacking gel was gently poured on top of the resolving gel, and a 1.5 mm, 15-well, Mini-PROTEAN® Comb was immediately inserted into the glass plates containing the gel. This was left to polymerise for about 30 minutes at room temperature. After the gel had set, it was inserted into a Mini-PROTEAN Tetra cell electrophoresis module (Bio-Rad). A buffer dam was used as a seal to contain the running buffer when only one gel was being run.

The Bradford protein assay, with absorbance read at OD 600 as previously described was used to determine the protein concentration of the samples prior to loading onto the gel. Protein lysates were mixed with 4x Laemmli buffer, heated at 100°C for 5 minutes on a heating block (Stuart Equipment) and allowed to cool before being loaded onto the gel in a concentration of 20µg – 40µg of protein in each well of the gel. 4µl of PageRuler™ Plus Prestained protein ladder (Thermo Scientific) was also loaded onto the gel and the tank filled with 1X Running Buffer. Electrophoresis was carried out using a Bio-Rad PowerPac 300 Electrophoresis Power Supply and was first run slowly at 60V for 30 minutes to run samples through the stacking gel, before the voltage was increased to 100V and run for about 1 hour until samples which were monitored by the dye front, were completely separated on the resolving gel.

10X Running Buffer (1L): 30.3g Tris Base (Fisher Scientific), 144g Glycine (Fisher Scientific), 10g SDS (Fisher Scientific).

1X Running Buffer (1L): 100ml 10X Running Buffer, 900ml ddH₂O.

2.6.4 WESTERN BLOT ANALYSIS

Protein transfer from the polyacrylamide gel onto Nitrocellulose Membrane (Amersham; GE) was done using a Bio-Rad Mini Trans-Blot® Cell. Nitrocellulose Membrane and Whatman Filter Paper (Amersham; GE) were cut into the size of the polyacrylamide gel and arranged onto the Western blot cassette assembly as follows: Black side → Foam Pad → Filter Paper → Gel → Membrane → Filter Paper → Foam Pad → White side. The cassette assembly was fitted into a core module and placed into a transfer tank along with a Bio-Ice cooling unit (Bio-Rad). The tank was filled with 1X Transfer Buffer, covered and plugged into a

PowerPac 300 Electrophoresis Power Supply. Proteins were transferred at 350Amps constant current for 90 minutes, after which the cassette was opened and the membrane incubated in blocking buffer made up of 5% Bovine Serum Albumin (Sigma-Aldrich) in 1x PBS with 0.1% v/v Tween 20 (Thermo Scientific), for 1 hour at room temperature with constant agitation.

Table 2.5: Composition of resolving and stacking gels for SDS-PAGE

| Resolving/ Separating/ Lower Gel | 7% | 10% | 12% | 15% | Stacking/ Upper Gel | 5% |
|---|-----------|------------|------------|------------|---------------------------------|-----------|
| Bis Acrylamide (40%) | 4.2ml | 6ml | 7.2ml | 9ml | Bis Acrylamide (40%) | 875µl |
| 1.5M Tris (pH 8.8) | 6ml | | | | 0.5M Tris (pH 6.8) | 1.75ml |
| 10% SDS | 240µl | | | | 10% SDS | 70µl |
| 10% APS | 120µl | | | | 10% APS | 70µl |
| TEMED | 12µl | | | | TEMED | 7µl |
| ddH₂O | 13.3ml | 11.5ml | 10.3ml | 8.5ml | ddH₂O | 4.325ml |

After the blocking step, the nitrocellulose membrane was incubated with the appropriate primary antibody at 4°C overnight with constant agitation (See list of primary antibodies used in Table 2.6). The primary antibody was decanted the following day and the membrane washed three times with washing buffer (1x PBS-Tween) for 10 minutes each before being incubated with secondary antibody (see Table 2.7) for 1 hour at room temperature. After 1 hour, the secondary antibody solution was decanted and the membrane washed three times for 10 minutes each – the first two times with 1x PBS-Tween and the third time with 1x PBS only. The membrane was imaged on the Odyssey Imager (LICOR) and protein bands analysed by densitometry using Image Studio Lite software version 5.2 (LICOR).

Table 2.6: List of Primary Antibodies used

| Name | Source | Clonality | Application | Dilution | Mol. Weight | Supplier / Product No. |
|----------------|---------------|------------------|--------------------|-----------------|--------------------|--------------------------------------|
| β-actin | Rabbit | Polyclonal | WB | 1:5,000 | 42 kDa | Abcam, Ab8227 |
| Btk | Rabbit | Monoclonal | WB, IHC | 1:500, 1:100 | 77 kDa | Cell Signaling, (D3H5) #8547S |
| STX4 | Mouse | Monoclonal | WB, IHC | 1:500, 1:100 | 33 kDa | Abcam, Ab77037 |
| p16 | Mouse | Monoclonal | WB, IHC | 1:500 | 16 kDa | Abcam, Ab54210 |
| p21 | Mouse | Monoclonal | WB | 1:200 | 21 kDa | Santa Cruz, (SX118) sc-53870 |
| p53 | Mouse | Monoclonal | WB | 1:500 | 53 kDa | Santa Cruz, (DO-1) sc-126 |
| p53 | Rabbit | Polyclonal | WB, IHC | 1:500, 1:100 | 53 kDa | Santa Cruz, (FL-393) sc-6243 |
| DEP1 | Rabbit | Polyclonal | WB, IHC | 1:500, 1:100 | 220 kDa | Bioss, bs-2567R |
| NTAL | Mouse | Monoclonal | WB | 1:1000 | 33 kDa | Abcam, Ab3992 |
| EBP50 | Rabbit | Polyclonal | WB | 1:500 | 50 kDa | Abcam, Ab3452 |
| ARMCX3 | Rabbit | Polyclonal | WB | 1:500 | 43 kDa | Abcam, Ab98938 |
| ARMCX3 | Mouse | Monoclonal | WB | 1:500 | 43 kDa | Abnova, H00051566-M01 |
| B2M | Rabbit | Polyclonal | WB, IHC | 1:500, 1:100 | 13 kDa | Abcam, Ab87483 |
| B2M | Mouse | Monoclonal | WB | 1:500 | 13 kDa | LifeSpan BioSciences, LS-B2200 |

Table 2.7: Secondary Antibodies used for Western Blots

| Name | Conjugation | Dilution | Supplier / Product No. |
|------------|--------------|----------|------------------------|
| Mouse IgG | IR Dye-800CW | 1:10,000 | Li-COR #926-32210 |
| Rabbit IgG | IR Dye-680RD | 1:10,000 | Li-COR #926-68071 |

10X Transfer Buffer (1L): 30.3g Tris Base, 144g Glycine.

1X Transfer Buffer (1L): 100ml 10X Transfer Buffer, 200ml Methanol (Fisher Scientific), 700ml ddH₂O.

Washing Buffer (1L): 100ml 10X PBS, 900ml ddH₂O, 1ml Tween 20.

Blocking Buffer (5% BSA in PBS-Tween): 5g BSA, 100ml 1x PBS-Tween.

2.7 SENESCENCE ASSOCIATED β -GALACTOSIDASE STAINING

Senescence associated β -Galactosidase (SA β -Gal) staining was done using the protocol adapted from Judith Campisi's Lab (Itahana *et al.*, 2007). Adherent cells were washed with 1x PBS and fixed with 10% neutral buffered formalin at room temperature. They were washed again with 1x PBS after which 2 - 3ml of Staining Solution (1mg/ml X-gal in dimethylformamide (DMF), 40mM Citric Acid/Na Phosphate Buffer, 5mM Potassium Ferrocyanide, 5mM Potassium Ferricyanide, 150mM Sodium Chloride, 2mM Magnesium Chloride in distilled water) was added to the cells (Table 2.8). The culture dishes were incubated at 37°C in a non-CO₂ incubator and observed under the microscope after 12 to 16 hours to detect the blue coloured β -Gal staining.

Table 2.8: SA β -Gal Staining Solution

| Component | Stock Concentration | Volume | Final Concentration |
|--|----------------------------|---------------|----------------------------|
| X-gal in DMF | 20mg/ml | 1ml | 1mg/ml |
| Citric Acid /Na Phosphate Buffer pH 6.0 | 0.2M | 4ml | 40mM |
| Potassium Ferrocyanide | 100mM | 1ml | 5mM |
| Potassium Ferricyanide | 100mM | 1ml | 5mM |
| Sodium Chloride | 5M | 0.6ml | 150mM |
| Magnesium Chloride | 1M | 40 μ l | 2mM |
| Distilled Water | - | 12.36ml | 20ml Total Volume |

0.2M Citric Acid /Na Phosphate Buffer (100ml): 36.85ml 0.1M Citric Acid Solution, 63.15ml 0.2M Sodium Phosphate Dibasic Solution (pH 6.0).

0.1M Citric Acid Solution: 2.1g /100ml Citric Acid Monohydrate ($C_6H_8O_7 \cdot H_2O$).

0.2M Sodium Phosphate (Dibasic) Solution: 2.84g /100ml Sodium Phosphate Dibasic (Na_2HPO_4) or 3.56g /100ml Sodium Phosphate Dibasic Dihydrate ($Na_2HPO_4 \cdot 2H_2O$).

2.8 IN VITRO AND IN VIVO TECHNIQUES USING MOLECULARLY IMPRINTED POLYMERS (MIPs)

Molecularly imprinted polymer nanoparticles (nanoMIPs) are nanostructured polymeric particles which contain a binding site for their target molecule and are capable of selectively recognising the said target. The nanoMIPs are produced using a solid-phase synthesis approach (Canfarotta *et al.*, 2016a) which relies on the covalent immobilisation of the template molecule on a solid support such as glass beads having an average diameter of about 75–90 μm . This glass bead support which bears the immobilized template is placed in contact with the monomer mixture and polymerisation is initiated under conditions that promote the formation of polymer nanoparticles. Upon polymerisation, the solid support acts as an affinity medium to isolate the high-affinity nanoMIPs from the remaining non-reactive monomers, oligomers and low-affinity polymers, which are removed by washing the beads under conditions that allow those nanoparticles with high affinity remain attached.

2.8.1 FLOW CYTOMETRIC DETECTION OF MEMBRANE SURFACE MARKERS OF SENESCENT CELLS USING FLUORESCENT MIPs

In order to detect novel cell surface markers of senescence, fluorescein – tagged molecularly imprinted polymers (MIPs) were designed by MIP Diagnostics Ltd., Leicester and imprinted with the extracellular epitope of the novel markers, B2MG and DEP1 proteins. A modified antibody binding assay protocol was used to detect MIPs binding to cells by flow cytometry. Proliferating and senescent EJ bladder cancer cells with a tetracycline off system of overexpression of p16, p21 and p53 were used as models of cellular senescence in this assay. Cells were detached either by using trypsin or by scraping with ice cold PBS. Cells were counted as previously described, using a Bio-Rad cell counter.

After counting to determine the number, cells were collected into 15 ml falcon tubes, washed with 5 ml of PBS and centrifuged at 1100 rpm for 3 minutes. Supernatant were discarded and pellets re-suspended in ice cold FACS buffer (2% FBS in 1x PBS) to obtain at least 1×10^6 cells/ml or about 2×10^5 cells in 200 μl . Samples were transferred to round bottom polystyrene tubes (Falcon) on ice and fluorescent MIPs were added to the cells either in a 1:50 (2%), a 1:20 (5%) or 1:5 (20%) dilution and incubated in the dark for 10 minutes. Samples

were immediately read on the BD FACS Canto II using the FITC fluorochrome channel. Unstained controls were used to gate the positive populations. Acquisition and analysis of data was done using the FACS Diva™ version 6.1.3 software (BD Biosciences) while charts of the mean fluorescent intensity (MFI) were plotted using GraphPad Prism 7.0 software.

2.8.2 FLUORESCENCE MICROSCOPY OF LIVE CELLS

Fluorescence imaging technique was employed in order to visualise the binding of B2MG MIPs to the surface of senescent cells. Proliferating and 4 days senescent EJ bladder cancer cells were seeded in 6 – well plates at a density of 3×10^5 cells per well and allowed to attach for 24 hours. 0.38mg/ml fluorescein–tagged MIPs were sonicated for 5 minutes with 30 seconds on-off intervals, using a Diagenode Bioruptor 2000 standard sonicator (Diagenode), before being added to the cells in concentrations ranging between 1:10, 1:20 and 1:50 dilutions in the growth media. Cells were incubated at 37°C and images taken after 10 minutes, 30 minutes and after 4 hours, using the Nikon Eclipse TS100 inverted routine microscope (Nikon) with an Epi-fluorescence attachment. Images were acquired using the imaging software NIS-Elements F version 3.0. Old media was aspirated off and cells were washed twice with media to remove unbound MIPs and images were again taken immediately. The cells were then detached using trypsin, washed with media and centrifuged at 1,100 rpm for 3 minutes to remove the trypsin and any unbound or lightly bound MIPs. Cells were seeded back into plates and incubated overnight to allow them attach well to plates. Images were again taken 24 hours, 48 hours, 94 hours and 192 hours after MIPs application. Proliferating cells incubated with MIPs were also frozen down, thawed after several days and cultured again to assess the effect of MIPs on cell viability. Image J software (version 1.51) was used to quantify the fluorescent nanoMIPs particles.

2.8.3 IMMUNOFLUORESCENCE MICROSCOPY OF MOLECULARLY IMPRINTED POLYMERS (MIPs) IN FIXED CELLS

In order to visualise the B2MG imprinted fluorescein – tagged nano MIPs either bound to the membrane or internalised inside senescent cells, a modified immunofluorescence protocol was used. Cells used were either previously incubated with MIPs for several days to assess viability or were incubated with

MIPs on the day of the experiment. Both proliferating and senescent EJ cells were grown on sterile 22 mm x 22 mm cover slips (Thermo Fisher) in 6 – well plates. 3×10^5 cells were seeded per well, incubated at 37°C and allowed to attach overnight. Where the cells were not previously incubated with MIPs, a 1:50 dilution (2%) of sonicated MIPs was added to the media in each well of cells i.e. 40µl MIPs in 1,960µl DMEM media in a 6-well plate and incubated at 37°C for 24 hours.

The following day, the media was removed and cells were washed twice in 1x PBS and fixed with 10% neutral buffered formalin for 10 minutes. The formalin was removed after 10 minutes and cells washed three times with 1x PBS. Cells were then incubated with 1µg/ml DAPI diluted in 1x PBS in the dark for 10 minutes. Samples were washed four times, first three times with PBS and lastly with distilled water. Anti-fade mounting medium was dropped on a microscope slide and the cover slip with fixed cells was gently laid on the slide. The edges were sealed with nail varnish. Slides were protected from light and imaged using the Leica TCS SP5 confocal laser scanning microscope (Leica Microsystems), and their internalised intracellular location around the nuclear membrane was observed.

2.8.4 IMMUNOFLUORESCENCE MICROSCOPY OF MOLECULARLY IMPRINTED POLYMERS (MIPs) IN FFPE TISSUES

A modified immunofluorescence technique on formalin fixed paraffin embedded (FFPE) tissues was also carried out using MIPs. Slides with 5 µm sections of FFPE tissues were dewaxed in two changes of xylene for 10 minutes each and afterwards dehydrated in two changes of 100% ethanol for 10 minutes each. Slides were microwaved in citrate buffer for 10 minutes and allowed to cool before being washed twice in 1x PBS. Slide edges were dried and the tissue area marked with a pap pen. The slides were placed in a humidified chamber and tissue sections were incubated with blocking buffer made with 5% bovine serum albumin (BSA) in 1x PBS for 1 hour. Molecularly imprinted polymers designed to target β -2-Microglobulin (B2MG) were sonicated as previously described. Next, slides were drained and the tissue sections incubated for 2 hours in the dark with the B2MG MIPs, diluted 1:20 in the blocking buffer. Slides were washed in 1x PBS three times, for 5 minutes each. The edges were dried

and tissue sections incubated with DAPI (4', 6-Diamidine-2'-phenylindole dihydrochloride) (Thermo Fisher) for 20 minutes in the dark. Slides were again washed once with 1x PBS and then with water. Coverslips were mounted onto the slides with ProLong™ Gold anti-fade mounting medium (Invitrogen) and edges sealed with nail varnish. The slides were thereafter protected from light and imaged using the Leica TCS SP5 confocal laser scanning microscope (Leica Microsystems). The fluorescent nanoMIPs particles were quantified using Image J software version 1.51.

2.8.5 *IN VIVO* IMAGING USING MOLECULARLY IMPRINTED POLYMERS

Old and young wild type C57BL/6J mice were used for Preclinical in-vivo imaging experiments using fluorescently tagged molecularly imprinted polymer nanoparticles (Nano-MIPs) which were designed to target an epitope of β -2 Microglobulin (B2MG). The mice were either painted topically on an area of shaved skin, with 0.5 ml of a 1:2 dilution of 0.38mg/ml concentration of fluorescent nano-MIPs in distilled water and imaged after 24 hours or they were given an intravenous injection of the 0.38mg/ml concentration of fluorescent nano-MIPs (5ml/kg body weight) and imaged after 2 hours. The IVIS® Spectrum CT *In Vivo* Imaging System (PerkinElmer Inc.) and the Quantum-FX X-Ray micro computed tomography (μ CT) scanner (PerkinElmer Inc.) were used for imaging. Images were analysed using the Living Image® advanced *in vivo* imaging software version 4.0 (Caliper Life Sciences Inc.).

2.8.6 MTS ASSAY ON CELLS TREATED WITH MIP-DRUG CONJUGATES

The MTS assay previously described in section 2.3.2 was also used to assess the viability of senescent and proliferating cells treated with Molecularly Imprinted Polymer (MIP)–Drug conjugates. In this case, the experiment and reagents were scaled up for use in a 24-well plate format, where there was no need to trypsinize the cells. Thus, 100,000 cells were seeded per well in a 24 well plate and allowed to attach overnight. The media was replaced with 500 μ l of fresh media and cells were treated with drugs or MIP-Drug conjugates and incubated for 1 hour. After 1 hour, cells in the plates were washed gently with warm media to remove unbound MIPs and excess drug. Plates were returned to the incubator for another 6 – 48 hours depending on the treatment duration. At the end of the desired duration of treatment, 100 μ l of MTS reagent was added to each well of the 24-

well plate, with some wells containing media and MTS only as blank. The 24-well plate assays were read using the Hidex Sense Microplate Reader and data recorded with the plate reader software version 0.5.11.2. All graphs and charts were plotted using the GraphPad Prism 7.0 software.

2.9 SENOLYTIC ANTIBODY-DRUG CONJUGATES (ADCs)

ThioBridge[®] antibody-drug conjugates (ADCs) specific for B2MG and conjugated with the toxic drug Duocarmycin, an irreversible DNA alkylating agent, were generated to target and kill senescent cells. The ADCs were produced by ABZENA through conjugation of reagents to a monoclonal (mAb) IgG1 B2M Antibody (LifeSpan BioSciences) and IgG1 Isotype (non-binding) mAb. The result was a B2MG ADC with a final concentration of 1.16 mg/ml, a 96% purity and an average drug-antibody rate (DAR) of 2.02. EJp16 cells were then incubated with the B2MG ADCs for 48 hours. After treatment of cells with ADCs, cell viability assays were carried out in 96-well plates, using the CellTiter-Glo[®] Luminescent Cell Viability Assay reagent. The viability assays and data analyses were performed by Dr. Ana Sousa Manso of the Leicester Drug Discovery and Diagnostics (LD3).

2.10 ANIMAL STUDY PROCEDURES

In vivo animal studies were carried out using the Zinc metalloproteinase STE24 (*ZMPSTE24*) deficient mouse model of Hutchinson-Gilford Progeria Syndrome (Leung *et al.*, 2001; Bergo *et al.*, 2002). The endoprotease Zmpste24 or FACE-1 is a metalloproteinase responsible for the conversion of prelamin A to mature lamin A, an essential structural component of the nuclear envelope. Its deficiency results in laminopathies due to accumulation of prelamin A (Fong *et al.*, 2004; Gonzalo *et al.*, 2017). This mouse model was used to assess whether the Bruton's Tyrosine Kinase (BTK) inhibitor Ibrutinib could effectively prevent the accumulation of senescent cells and ameliorate the symptoms associated with ageing. All research done using animals were conducted in adherence to the UK Home Office Animals (Scientific Procedures) Act 1986. The Project Licence number for this work is PPL 70/8484.

Cryo-preserved spermatozoa was purchased from the Mutant Mouse Resource & Research Centre (MMRRC) at University of California, Davis, which is supported by the National Institutes of Health (NIH). The *ZMPSTE24^{-/-}* sperm was implanted into recipient female wild type C57BL/6J mice to produce litters that were either homozygous, heterozygous or wild type without the *ZMPSTE24^{-/-}* genetic modification. Heterozygous offspring of the founder lines were further bred to create genetically altered strains deficient in the *ZMPSTE24* gene.

2.10.1 ZMPSTE24^{-/-} MOUSE EAR PUNCH GENOTYPING

DNA was extracted from mouse ear punches or ear snips in order to determine the genotype of zinc metalloproteinase STE24 deficient mouse (*Zmpste24^{-/-}*) colonies. Polymerase Chain Reaction (PCR) was carried out using *Zmpste24* forward and reverse primers (Eurofins Genomics) and the PCR product was ran on an agarose gel electrophoresis to view the DNA bands of interest.

2.10.1.1 DNA EXTRACTION FROM MOUSE EAR SNIPS

Ear snip samples were taken from 14 days old mice into Eppendorf tubes and stored in -20 °C until when needed. Tail Lysis Buffer (TLB) was prepared using 100mM Tris HCl pH 8.0, 5mM Ethylene diamine tetra acetic acid (EDTA), 0.2% (w/v) SDS and 200mM NaCl diluted in distilled water (Table 2.9). For each ear snip sample, 2 µl of 10mg/ml Proteinase K and 198 µl of TLB was added to the tube. Samples were incubated on a heating block (Stuart Equipment) at 37°C overnight. Tubes were flicked by hand until all tissues dissolved completely and they were incubated for an additional 1 hour at 55°C. Samples were centrifuged at 14,000g for 2 minutes. Supernatants were transferred into new labelled Eppendorf tubes containing 200 µl of 100% Isopropanol (Fisher Scientific) and flicked by hand to precipitate the DNA. Samples were centrifuged again at 14,000g for 2 minutes. Supernatants were aspirated off and pellets washed with 70% ethanol. Tubes were centrifuged again at 14,000g for 2 minutes to remove the ethanol, then the supernatants were aspirated off and the tubes left on the bench for the pellets to air dry. Pellets were afterwards re-suspended in 60 µl of sterile distilled water (dH₂O) and left to incubate for 20 minutes at room temperature. DNA concentrations were measured using the NanoPhotometer® P300 and 2µl (about 0.1µg) of DNA was used as the template for PCR while the remaining DNA was stored at -20 °C.

Table 2.9: Tail Lysis Buffer Composition

| Component | Stock Concentration | Dilution in water | Working Concentration |
|------------------------|----------------------------|--------------------------|------------------------------|
| Tris HCL pH 8.0 | 1M | 1:10 | 100mM |
| EDTA | 0.5M | 1:100 | 5mM |
| SDS | 10% | 1:50 | 0.2% (w/v) |
| NaCl | 5M | 1:25 | 200mM |

2.10.1.2 POLYMERASE CHAIN REACTION (PCR)

Polymerase Chain Reaction (PCR) was used to amplify the region of interest in the extracted DNA samples using Zmpste24 forward and reverse primers. Each reaction tube contained 10µl of 2x My Taq Red Mix (Bioline), 1µl Zmpste24 forward primer (Eurofins Scientific), 1µl Zmpste24 reverse primer (Eurofins Scientific), 2µl DNA sample and 6µl of Nuclease Free Water (Applied Biosystems). A master mix was made using the My Taq Red Mix, primers and nuclease – free water. 18 µl master mix was added to each reaction tube and 2 µl DNA samples was added to it to. Negative control sample tubes contained master mix and 2 µl nuclease – free water. PCR was run on a Techne® Prime Thermal Cycler (Cole–Parmer) using a PCR protocol developed by Mutant Mouse Resource and Research Centre (MMRRC), University of California, Davis. Samples were incubated at an initiation temperature of 95°C for 5 minutes, then denatured for another 1 minute; annealing of primers was done at 60°C for 2 minutes; elongation took place at 72°C for 3 minutes and the DNA was amplified for another 10 minutes before the reaction ended and samples were held at 4°C. The PCR products were separated by agarose gel electrophoresis to detect the band of interest.

2.10.1.3 AGAROSE GEL ELECTROPHORESIS

A 1.5% agarose gel was prepared by dissolving 0.6g of agarose (Fisher Scientific) in 40 ml of 1x Tris-Borate-EDTA (TBE) in a graduated glass bottle. The mixture was heated in a microwave oven in 30 seconds intervals until well dissolved. The mixture was topped up to 40 ml again with 1x TBE and 0.8µl of 1% Ethidium Bromide (VWR Chemicals) was added to the bottle in a fume hood.

The gel was poured into a gel tank in a fume hood, a comb was inserted and the gel allowed to set for about 30 minutes. The solidified gel was then transferred to an electrophoresis tank where the comb was removed and 1x TBE was poured on the gel to remove bubbles. 4 µl of PCR Ranger 100bp DNA Ladder (Norgen Biotek) was loaded onto a well and 4 µl of the PCR products were also loaded onto other wells. The tank was filled to the maximum fill level with 1X TBE and electrophoresis run at 100V for 40 minutes. To visualise DNA bands, the gel was imaged using a Molecular Imager® Gel Doc™ XR System (Bio Rad) and captured with Image Lab software version 4.1.

2.10.2 EXPERIMENTAL DESIGN

All animals needed to reach 8 weeks of age before they could be entered into any study. *ZMPSTE24*^{-/-} mice were placed into two groups, A and B. Animals in group A were treated with Ibrutinib, while animals in group B were given water with DMSO. Group A and B animals were paired in cages, matched by sex and age. No two animals from the same experimental group were placed into the same cage to avoid this counting as $n = 1$. Where there was an odd number of animals remaining, a wild type or heterozygous cage mate or “Buddy” was assigned to the unpaired animal.

Being models of progeria, these fast-ageing mice have an average lifespan of 6 months (Bergo *et al.*, 2002; de la Rosa *et al.*, 2013) and the Home Office allowed us to keep them for a maximum age of 8 months. Clinical and pathophysical humane end points (HEP), health checks (Figure 2-1), distress scoring (Table 2.10) and clinical frailty indices were used to monitor and evaluate the animals' welfare to minimise their suffering and ensure that death was not an endpoint.

In vivo imaging was also carried out on old and young wild type C57BL/6J mice without the *ZMPSTE24* deficiency, using fluorescent tagged molecularly imprinted polymers nanoparticle (nanoMIPs) designed to target β-2 Microglobulin (B2MG). Details of the mice imaging procedures have been previously described (see section 2.8.5). In these imaging experiments, animals were either painted topically with fluorescent nanoMIPs on an area of shaved skin or they were given an intravenous injection of fluorescent nanoMIPs.

Table 2.10: Distress scoring sheet with scoring criteria

| Distress Scoring Sheet | | Animal ID: | Weight: |
|---|--|-------------------------|----------------|
| This Scoring Sheet will be used as a tool for monitoring progression of clinical signs, not to define Humane End Points (except in the case of tumours, as stated below). | | | |
| Parameters | | Score | Date/Time/By |
| Appearance | - Normal - Slight piloerection - Marked piloerection - Changes from normal to signs of deterioration of coat and skin | 0 1.5 3 4-6 | |
| Natural behaviour | - Normal - Minor changes - Less mobile and isolated - Restless or very still | 0 1 2 3-6 | |
| Food and water intake | - Normal - Body weight loss <5% - Body weight loss <10% - < 20% | 0 3 4-6 | |
| Hydration status | - Normal - Abnormal skin pinch test - Very Abnormal skin pinch test | 0 2.5 2.5-6 | |
| Body changes | - Normal - Backbones visible - Backbones very visible - Tachypnoea (fast breathing) - Dyspnoea (difficult breathing) | 0 3 6 3 6 | |
| Locomotion | - Slightly abnormal gait/posture - Markedly abnormal gait/posture | 0-1.5 3-6 | |
| Muscle tone | - Muscle groups have normal tone or mass - Muscle mass slightly soft - Muscle mass less firm, abdomen slightly soft - Muscle mass very thin, soft, undefined - Muscle mass has no tone or definition | 0 2 3 4 5-6 | |
| Procedure Specific Indicators | - Tumour size >1.0cm ³ HEP - Tumour impeding movement | HEP HEP | |
| <p>Score: 0 = normal 3 = monitor carefully (including regularity of health checks), inform PIL and consider intervention, if necessary consult NACWO and/or NVS – provide intervention pain relief/fluids etc. as appropriate/advised. ≥6 = terminate using schedule 1 method HEP = Humane end-point</p> | | | |

2.10.3 DRUG DOSING AND ADMINISTRATION

In the pilot study, animals were administered 20mg of Ibrutinib (PCI-32765, Selleck) per kilogram body weight, twice weekly by oral gavage, using a 1ml syringe (Terumo) and a 20ga x 38mm plastic feeding tube (Instech Laboratories). The oral doses were prepared and administered to each animal in a volume not exceeding 10ml per kilogram of their body weight. In subsequent studies, the dosage was reduced to 10mg of Ibrutinib per kilogram body weight, given twice weekly and also prepared to be delivered in 10ml per kilogram of the animal's body weight.

To prepare Ibrutinib doses of 10mg/kg body weight of an animal, 140 mg of Ibrutinib was first weighed into a Fisherbrand™ Type III Soda Lime Glass Specimen Vial (Fisher Scientific), 560 µl of 100% DMSO was then added to it and vortexed until completely dissolved. 10 µl aliquots of the dissolved drug were put into 56 glass tubes and stored at -80°C until when needed. To prepare working oral doses, 2,490µl of ddH₂O was added to the 10ul drug aliquot and vortexed until completely dissolved. Drug volumes were administered according to animals' body weights (e.g. a 20g mouse was dosed with 200µl of drug preparation and a 25g mouse received 250µl of drug preparation). Animals in the control (vehicle) groups received distilled water with a similar volume of DMSO as the treatment group (i.e. 2,490µl ddH₂O + 10µl DMSO), according to their body weights.

2.10.4 MEASURING THE MUSCLE STRENGTH OF MICE

In order to assess the effect of Ibrutinib on muscle strength in fast ageing mice, the Kondziela's inverted screen test and weights lifting tests were carried out (KONDZIELLA, 1964; Deacon, 2013). An inverted screen was fabricated at the Department of Genetics and Genome Biology Workshop, University of Leicester as described by Deacon, (2013) and used to test how long an animal could support its own body weight when suspended upside down. A soft fleece bedding material was placed on the animal transfer/work station (ATS) to prevent the animals from getting injured if they could not hold on for long and fell down (Figure 2-2).

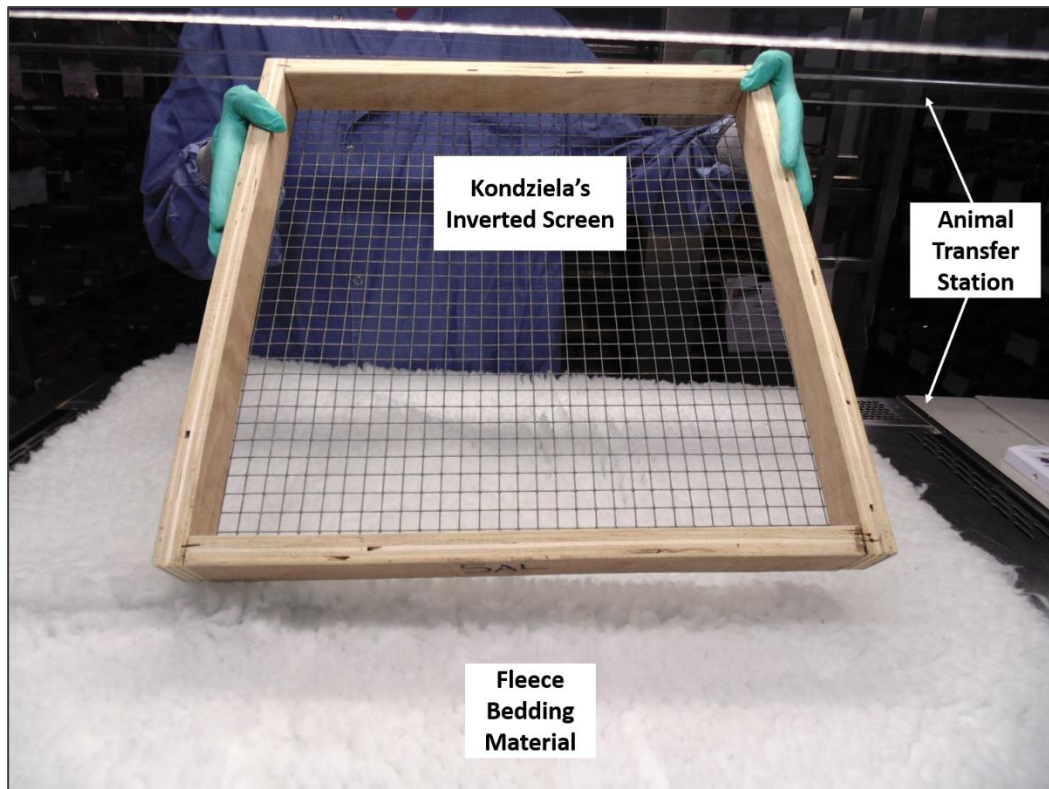


Figure 2-2: The Kondziela's Inverted Screen and fleece bedding used

The test was carried out once weekly for 13 weeks and animals were assigned a score of 1 – 4 depending on how long they were able to hold on to the inverted screen (Table 2.11).

Table 2.11: Scoring Criteria for Kondziela's Inverted Screen Tests

| Duration on the Screen | Score |
|-------------------------------|--------------|
| 1 – 10 seconds | 1 |
| 11 – 25 seconds | 2 |
| 26 – 60 seconds | 3 |
| Over 60 seconds | 4 |



Figure 2-3: Various weights used for weight lifting tests

For the weights lifting tests, plastic mesh pot scourers were used to attach the weights (Figure 2-3) instead of the tangled stainless steel sponge (scale collector) previously described (Deacon, 2013), because these fast ageing mice are smaller than their wild type counterparts and could be prone to injury from the stainless steel sponge. Seven different steel blocks weighing 20g, 33g, 46g, 59g, 72g, 85g and 98g were produced at the University of Leicester's Department of Genetics and Genome Biology Workshop. The steel blocks were assigned numbers from 1 to 7 in increasing order of weights to aid scoring (Table 2.12). Mice were tested by weight lifting once bi-weekly for 10 weeks.

Scores were generated by multiplying the weight's number by the number of seconds the mouse held on to the weight. For example, if a mouse held on to the 46g weight for five seconds, its score would be: $3 \times 5 = 15$. All data were recorded and analysed using Microsoft Excel and Graph Pad Prism 7.0 software.

Table 2.12: Scoring System for Weight Lifting Experiments

| Weight of Steel Block (g) | Assigned Number |
|----------------------------------|------------------------|
| 20g | 1 |
| 33g | 2 |
| 46g | 3 |
| 59g | 4 |
| 72g | 5 |
| 85g | 6 |
| 98g | 7 |

2.10.5 CLINICAL FRAILTY SCORING

A mouse frailty assessment form (Whitehead *et al.*, 2014) was used to score study animals' based on several clinical frailty indices (Figure 2-4). Animals were assessed mainly by physical examination. Hearing loss for instance was assessed using a clicker pen, forelimb grip strength was assessed by placing the mouse on its cage grid and gently tugging at its tail, while vision was assessed by lifting the mouse and placing them down on the palm of the hand, fore limbs first, to see if they could put down their paws to support themselves. Several parameters were assessed and rated based on the severity as follows: 0 = Absent, 0.5 = Mild and 1 = Severe (Figure 2-4). The results were analysed on Microsoft Excel and GraphPad Prism 7.0.

Table 2. Mouse Frailty Assessment Form^o

| | | | | Date: _____ |
|--|--------------------------------------|--------|---|-------------|
| Mouse #: _____ | Date of Birth: _____ | Sex: F | M | |
| Body weight (g): _____ | Body surface temperature (°C): _____ | | | |
| Rating: 0 = absent 0.5 = mild 1 = severe | | | | |
| ➤ Integument: | | | | NOTES: |
| ❖ Alopecia | 0 | 0.5 | 1 | _____ |
| ❖ Loss of fur colour | 0 | 0.5 | 1 | _____ |
| ❖ Dermatitis | 0 | 0.5 | 1 | _____ |
| ❖ Loss of whiskers | 0 | 0.5 | 1 | _____ |
| ❖ Coat condition | 0 | 0.5 | 1 | _____ |
| ➤ Physical/Musculoskeletal: | | | | |
| ❖ Tumours | 0 | 0.5 | 1 | _____ |
| ❖ Distended abdomen | 0 | 0.5 | 1 | _____ |
| ❖ Kyphosis | 0 | 0.5 | 1 | _____ |
| ❖ Tail stiffening | 0 | 0.5 | 1 | _____ |
| ❖ Gait disorders | 0 | 0.5 | 1 | _____ |
| ❖ Tremor | 0 | 0.5 | 1 | _____ |
| ❖ Forelimb grip strength | 0 | 0.5 | 1 | _____ |
| ❖ Body condition score | 0 | 0.5 | 1 | _____ |
| ➤ Vestibulocochlear/Auditory: | | | | |
| ❖ Vestibular disturbance | 0 | 0.5 | 1 | _____ |
| ❖ Hearing loss | 0 | 0.5 | 1 | _____ |
| ➤ Ocular/Nasal: | | | | |
| ❖ Cataracts | 0 | 0.5 | 1 | _____ |
| ❖ Corneal opacity | 0 | 0.5 | 1 | _____ |
| ❖ Eye discharge/swelling | 0 | 0.5 | 1 | _____ |
| ❖ Microphthalmia | 0 | 0.5 | 1 | _____ |
| ❖ Vision loss | 0 | 0.5 | 1 | _____ |
| ❖ Menace reflex | 0 | 0.5 | 1 | _____ |
| ❖ Nasal discharge | 0 | 0.5 | 1 | _____ |
| ➤ Digestive/Urogenital: | | | | |
| ❖ Malocclusions | 0 | 0.5 | 1 | _____ |
| ❖ Rectal prolapse | 0 | 0.5 | 1 | _____ |
| ❖ Vaginal/uterine/penile prolapse | 0 | 0.5 | 1 | _____ |
| ❖ Diarrhoea | 0 | 0.5 | 1 | _____ |
| ➤ Respiratory system: | | | | |
| ❖ Breathing rate/depth | 0 | 0.5 | 1 | _____ |
| ➤ Discomfort: | | | | |
| ❖ Mouse Grimace Scale | 0 | 0.5 | 1 | _____ |
| ❖ Piloerection | 0 | 0.5 | 1 | _____ |
| ❖ Temperature score: _____ | | | | |
| ❖ Body weight score: _____ | | | | |
| Total Score/ Max Score: _____ | | | | |

© Susan E. Howlett, 2013

Figure 2-4: Clinical Frailty Indices used to assess mice. Adapted from (Whitehead *et al.*, 2014)

2.10.6 MOUSE BEHAVIOURAL STUDIES

Cognitive function tests were carried out to assess the effect of Ibrutinib on spatial memory, using the Barnes Maze (Barnes, 1979; Barnes *et al.*, 1980; Capilla-Gonzalez *et al.*, 2012). Tests to study the effect of Ibrutinib on generating anxiety-like behaviour was also carried out using the Elevated Plus Maze (Pellow *et al.*, 1985; Lister, 1987; Komada *et al.*, 2008; Loxton & Canales, 2017).

2.10.6.1 BARNES MAZE

The design of the Barnes Maze consisted of an elevated white circular platform raised 1 metre above the ground and having 20 equidistant holes around its edges (Figure 2-5). One of the holes (target hole) had a black escape box fitted underneath it while the other 19 holes were sealed with black plastic and rubber tape, to give them a similar appearance as the target hole. The target hole was labelled “T”, the hole opposite it was labelled “O” and the other holes were numbered +1 to +9 to the right hand side (positive) and -1 to -9 to the left hand side (negative) of the target hole.

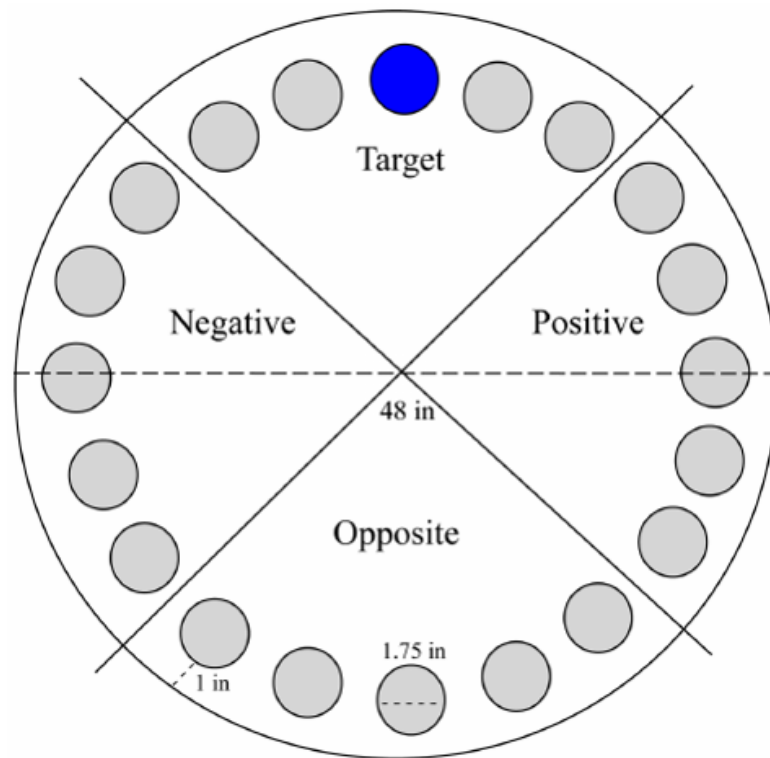


Figure 2-5 Diagram of the Barnes maze. Adapted from (Attar *et al.*, 2013).

The study was carried out in the mouse behaviour room of the Pre-Clinical Facility (PRF) at the University of Leicester. The room housed a sound booth with a sound source or loud speaker system, a desktop computer with video camera attached to the ceiling, visual cues (coloured shapes on the wall) and a source of bright light (Figure 2-6). The experiment was carried out over 14 days and consisted of four stages namely: Habituation, Acquisition, Probe Trial and Recall (Table 2.13).

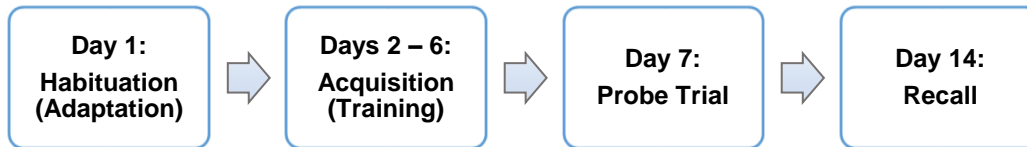


Figure 2-6 The Barnes Maze set-up used for cognitive function tests. The target hole is indicated by the red arrow and visual cues on the wall are indicated by black arrows.

The first day was for habituation or adaptation, where the mice were allowed to get familiar with the environment of the maze, the escape box, sound from the speakers (white noise), bright lights and visual cues on the wall. During habituation, white noise and bright lights were turned on to create mildly aversive stimuli, and mice were placed on the maze and gently guided into the escape box. The white noise was switched off as soon as the mouse entered into the escape box. Mice were left inside the box for 30 seconds to get comfortable with the safe space. Visual cues were left at a constant position on the wall and the position of the target hole was also kept constant for the mice throughout the

study. The maze was cleaned with 70% industrial methylated spirit (IMS) after each animal.

Table 2.13: Study design for the Barnes Maze



The next five days were for acquisition or training, where mice were given 3 minutes to locate the escape box and enter inside it. White noise generated from the computer and bright lights acted as stimuli to motivate the mice to escape into the box. The training ended once the mouse entered into the escape box or when the 3 minutes had elapsed in the event of mice not finding the box. If after 3 minutes, a mouse failed to enter the escape box, it was guided in gently. This training was carried out in three rounds for all mice with 20 minutes intervals between trainings. Again, the maze was thoroughly cleaned with 70% IMS in between animals to eliminate any scent trails. The number of errors made and the latency, which is the time it takes the animal to first reach the escape box were calculated.

On day 7 of the study, 24 hours after the 5th training day, the escape box was taken out and the hole sealed like all the others. The mice were placed on the maze and allowed to locate the target hole as before, only this time without the escape box. This was the Probe trial, and the latency as well as the number of nose pokes or errors were calculated for each animal. Seven days after the probe trial, on day 14 of the study, the Recall was conducted in the same manner as the probe trial, to test the spatial memory of the mice. The latency and number of errors were also calculated here. All trainings, probe trials and the recalls were recorded using the Microsoft LifeCam HD-3000 webcam and the SharpCap 2.9 video software. Two blind observers manually analysed the data that was obtained through video recording.

2.10.6.2 ELEVATED PLUS MAZE

A four-armed plus maze known as the Elevated Plus Maze (EPM) was used to assess anxiety-like behaviours in mice. The plus maze consisted of two opposite open arms and two opposite closed arms (Figure 2-7). Like the Barnes maze, the EPM was elevated 1 metre above the ground. Each mouse was placed in the centre of the maze and allowed to explore it for 5 minutes. The mouse's entries into the open and closed arms, as well as the time spent in each pair of arms were recorded with the LifeCam HD-3000 webcam and its SharpCap 2.9 video software.

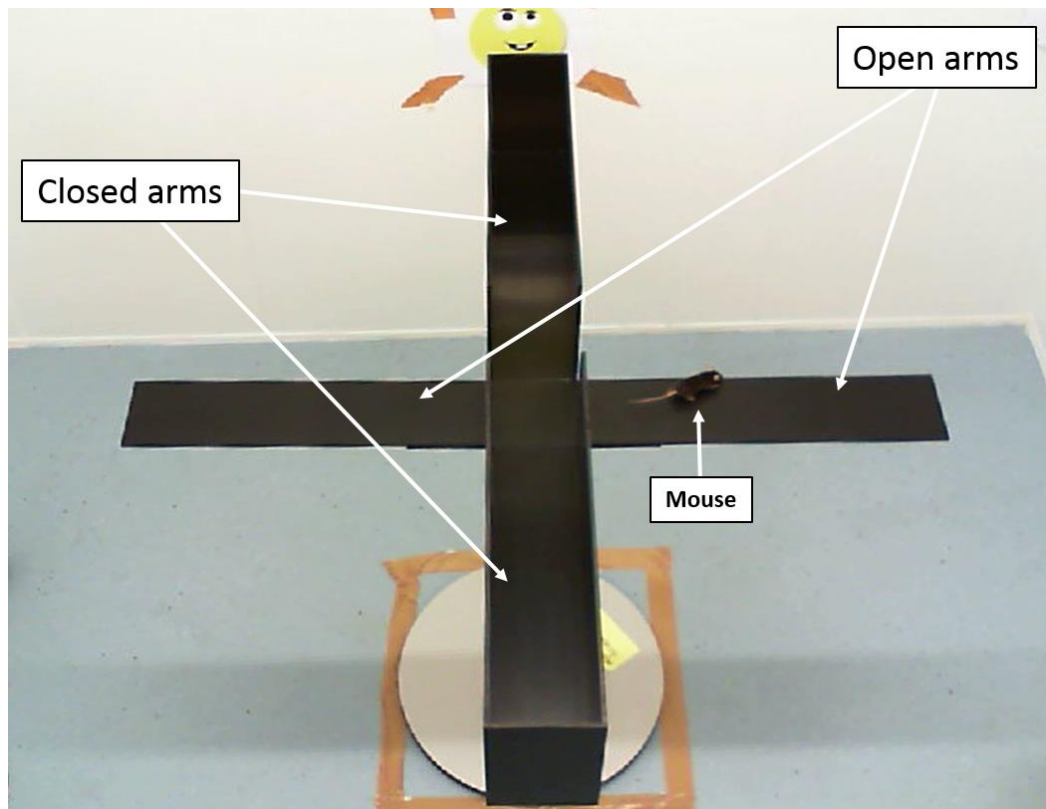


Figure 2-7 The Elevated Plus Maze used to assess anxiety-like behaviour in mice

Tests were made and recorded at base-line (basal) as well as 4 weeks and 3 months after commencement of either Ibrutinib or vehicle treatment. Wild-type and heterozygous cage-mates (buddies) were also included in the EPM tests for comparison. The results were manually analysed by a blind observer.

2.10.7 SURVIVAL ANALYSIS

In order to assess the effect of Ibrutinib on lifespan, doses were administered orally, twice a week to male and female fast ageing ZMPSTE24^{-/-} mice. The mice were kept in the study for as long as possible, usually less than 8 months, depending on their welfare. Mice were culled humanely when they reached the humane end point (HEP) criteria, such as, losing $\geq 20\%$ of their maximum body weight. Hence, survival in this case was not measured by when the mice died spontaneously but was rather measured by when their welfare was of serious concern. The difference in lifespan between treated and untreated animals was assessed by plotting the Kaplan Meier survival curve using GraphPad Prism. 7.0.

2.11 STATISTICAL ANALYSES

All results are presented as mean \pm standard deviation (SD) except in studies involving groups of animals, where they are expressed as mean \pm standard error of the mean (SEM). Statistical analyses were carried out using GraphPad Prism version 7.0 and two-tailed student's *t*-tests or other suitable tests were used to determine the significance of the experimental data. When presenting data, *p* values less than or equal to (\leq) 0.05 were considered significant and the degree of significance based on the *p* value was indicated on each graph using the asterisks (*) symbol.

CHAPTER 3 VALIDATION OF NOVEL MARKERS OF SENESCENCE

Currently used markers of senescence are not specific, as they are also present in other biochemical and physiological states (Rodier & Campisi, 2011; Deursen, J M A van, 2014; Muñoz-Espín & Serrano, 2014). These markers are often used in combination to define senescence *in vitro* and *in vivo*, and they include irreversible growth arrest, expression of CDK inhibitors, SA- β gal activity, presence of SAHF, the SASP, as well as a negative ki67 expression (Yang & Hu, 2005; d'Adda di Fagagna & Campisi, 2007; Deursen, J M A van, 2014). This lack of specificity has fuelled the search for more reliable and novel markers of senescence as it has become necessary to clearly define markers for the senescent state.

In recent years, senescent cell clearance has been increasingly investigated as a therapeutic strategy for the management of age-related diseases including cancer (Baker *et al.*, 2011; Deursen, J M A van, 2014; Baker *et al.*, 2016; Chang *et al.*, 2016; Demaria *et al.*, 2017; Baar *et al.*, 2017). Accumulation of senescent cells is being linked to many diseases, making the targeting of these cells an important strategy for fighting of cancer, fibrosis and other age-related pathologies. However, available markers of senescence are not exclusive to the senescent state and lack specificity (Deursen, J M A van, 2014), necessitating the search for novel and more efficient markers which could be used either alone or in combination with others to identify the cells that need to be cleared. Consequently, a series of novel markers of senescence – proteins preferentially expressed on the surface of senescent cells, have been identified in our laboratory through mass spectrometric screening of the membrane fraction of senescent cell lysates (Althubiti *et al.*, 2014).

None of the published proteins have previously been linked to senescence prior to the screening done in our lab. These novel markers could potentially be used to target and eliminate senescent cells from tissues or whole organisms. Using the TMHMM Server v. 2.0, a tool for the prediction of transmembrane helices in proteins (<http://www.cbs.dtu.dk/services/TMHMM-2.0/>), they were all predicted to

be located on the plasma membrane (Althubiti *et al.*, 2014). This is important when considering their use for the design of diagnostic and therapeutic tools such as antibody-drug conjugates (ADCs) or molecularly imprinted polymers (MIPs). Seven of these proteins namely EBP50, NTAL, ARM CX3, STX4, DEP1, B2MG and BTK were assessed in the course of this project and are described here.

The Ezrin-Radixin-Moesin-binding Phosphoprotein 50 (EBP50) also known as NHERF1 (Na⁺/H⁺ Exchanger Regulatory Factor 1) is a 50kDa scaffolding protein that plays important roles in regulating transmembrane signal transduction, reorganizing of cytoskeleton, phosphoinositide metabolism as well as receptor trafficking (Leslie *et al.*, 2013; Oh *et al.*, 2017). Several studies on human cancers have found EBP50 to exert tumor-suppressing effects on pancreatic cancer (Ji *et al.*, 2014), oesophageal squamous cell carcinoma (Wang *et al.*, 2014), extrahepatic bile duct carcinoma (Feng *et al.*, 2017), and breast cancer (Wang *et al.*, 2017a; Liu *et al.*, 2017).

NTAL, the Non-T cell activation linker, also known as linker for activation of B cells (LAB) and linker for activation of T cells 2 (LAT2) is a transmembrane adaptor protein, 25 to 30 kDa in size and is mainly expressed in spleen and hematopoietic cells such as B lymphocytes, mast cells, NK cells, macrophages and basophils but not resting T cells. NTAL is associated with glycolipid-enriched membrane fractions in these cells and upon engagement with immune-receptors, is phosphorylated and recruits signaling molecules into receptor-signaling complexes (Wang *et al.*, 2005; Iwaki *et al.*, 2007; Arbulo-Echevarria *et al.*, 2016).

The armadillo repeat-containing X-linked protein 3 (ARM CX3) is a 42 kDa mitochondrial outer membrane protein that is found mainly in the nervous system. ARM CX3 also known as ALEX3 plays an important role in mitochondrial distribution and trafficking in neurons, and regulates vital processes of spinal cord development (Lopez-Domenech *et al.*, 2012; Mirra *et al.*, 2016). It interacts with the transcription factor Sox10, increasing its localization in the mitochondrial outer membrane (Mou *et al.*, 2009).

Syntaxin4 (STX4) is a soluble membrane N-ethylmaleimide-sensitive factor attachment protein receptor (SNARE) protein. It is involved in inflammatory

responses as the interaction between target membrane (t-SNARE) proteins like STX4, promote membrane fusion in mucosal mast cells, which function in allergic inflammation (Liu *et al.*, 2012). STX4 is also known to promote tumour cell invasion (Brasher *et al.*, 2017) and play a role in keratinocyte differentiation (Kadono *et al.*, 2012).

Density-enhanced phosphatase 1 (DEP-1) also known as Protein-tyrosine phosphatase receptor type J (PTPRJ) or PTP- η or CD148 is a receptor-like protein tyrosine phosphatase (PTP) of about 180 to 220 kDa expressed in several cell types, including endothelial, epithelial as well as hematopoietic cells (Ostman *et al.*, 1994; Chabot *et al.*, 2009; Barr *et al.*, 2009; Spring *et al.*, 2012). DEP-1 expression was first found to be enhanced with increase in cell density, suggesting its role in contact inhibition of cell growth (Ostman *et al.*, 1994). DEP1 has been found to promote cancer cell invasion and metastasis (Spring *et al.*, 2012; Spring *et al.*, 2015) and is reported to be mutated or deleted in human breast (Xiang *et al.*, 2012; Spring *et al.*, 2015), thyroid (Iuliano *et al.*, 2004), meningioma (Petermann *et al.*, 2015) lung, and colon cancers (Ruivenkamp *et al.*, 2003; Östman *et al.*, 2006; Scott *et al.*, 2010) as well as in non-Hodgkin's lymphoma (Aya-Bonilla *et al.*, 2013). DEP1 also plays a role in cerebral arteriogenesis (Hackbusch *et al.*, 2013).

One important subunit of the major histocompatibility complex (MHC) class I proteins is beta 2 Microglobulin (β 2M or B2MG) and it is present on the surface of all nucleated cells, especially monocytes and lymphocytes (Staats *et al.*, 2013; Prizment *et al.*, 2016). Increased serum concentrations of B2MG have been observed in various pathological conditions such as renal disease, autoimmune diseases and immunodeficiency (Prizment *et al.*, 2016). B2MG has recently been found to be involved in acquired immunosurveillance escape of tumor cells and is mutated or altered in lung cancer and several other malignancies (Sun *et al.*, 2016; Pereira *et al.*, 2017). It has also been reported as a pro-ageing factor that impairs neurogenesis and promotes cognitive dysfunction in mice (Smith *et al.*, 2015). In amyotrophic lateral sclerosis (ALS), B2MG is upregulated by motor neurons in the spinal cord and its removal shortens the disease duration (Staats *et al.*, 2013).

The Bruton's tyrosine kinase (BTK) is a non-receptor tyrosine kinase and a member of the Tec family of kinases that is expressed in myeloid and lymphoid cells but not T cells (Vetrie *et al.*, 1993; Althubiti *et al.*, 2016). BTK is mutated in X-linked agammaglobulinemia, an inherited immunodeficiency disease, it plays a vital role in B-cell receptor (BCR) signaling (BRUTON, 1952; Vetrie *et al.*, 1993; Hutchinson & Dyer, 2014) and is expressed in B cell malignancies (Hendriks *et al.*, 2014).

In order to further characterise and validate these identified novel markers of senescence, we went on to screen various aged and diseased tissues – models of senescence other than the ones previously tested, for the expression of these markers, using p16 and p53 as positive controls. Small molecule inhibitor for BTK as well as shRNA for DEP1 and B2MG were also used to assess the effect that the inhibition of these markers would have on cellular senescence.

3.1 IMMUNOHISTOCHEMISTRY IN TISSUES FROM AN OLD MOUSE

The animals used in this experiment and in subsequent ones are of the C57/BL6 wild type background and are from a mixed gender population unless otherwise mentioned, as it was not possible to obtain information about the gender for some of them. The ImmunoRatio image analysis software (<http://153.1.200.58:8080/immunoratio/>) was used to quantify the percentage of DAB staining in all tissue sections assessed by immunohistochemistry. Haematoxylin and eosin staining (H&E) was also done to show the tissue morphology. Data was analysed using GraphPad Prism 7.0 software.

In order to characterize the *in vivo* expression of our novel markers in replicative senescence, skin tissue samples from an 80 week old mouse were first stained for the presence of p16^{INK4A}, as a positive control for the presence of senescent cells, and Syntaxin4 (STX4) by immunohistochemistry. The tissue stained positive for both p16^{INK4A} and STX4 when compared to the negative control without a primary antibody (data not shown). This result suggested that STX4 could be a good marker of *in vivo* skin ageing. After this, liver, muscle and brain tissues from the same animal were also stained for the senescence markers p16

and STX4. The aged liver also stained positive for both p16 and STX4, with more than a five-fold increase in p16 and more than two-fold for STX4 when normalised against the negative control. The overexpression of p16 and STX4 observed in the aged liver could also be suggestive of the presence of senescent cells in this tissue. Muscle tissue from the 80 week old animal also stained positive for both p16 and STX4 by immunohistochemistry. There was more than a two-fold increase in DAB staining for p16, while that for STX4 was less than two-folds. Additionally, brain tissue from the same 80 week old animal was also stained by immunohistochemistry for p16 and STX4 like the other tissues. The tissue was positive for p16, with about a four-fold increase in expression as measured by the percentage of DAB staining, while STX4 was much less positive with less than a two-fold increase (data not shown).

These experiments only showed that the antibodies stained positive in these tissues but could not offer concrete conclusion as there were no control samples used. A negative control sample from the same tissue and the same animal, which had no primary antibody on, could barely provide an indication that STX4 could differentiate between young and old tissues. Therefore, in order to address this problem, tissues from both old and younger animals were next screened to be able to make a comparison (Figure 3-1 to Figure 3-12). Sample size has also been a limitation of this study as it was not possible to obtain many replicates of same aged animals for use in the study in order to give a good statistical significance. It is also acknowledged that the appropriate internal controls for these samples should have been an isotype-matched control antibody rather than just a tissue sample with no primary antibody. Also, the issue of antibody specificity and variation between the epitope recognised and overall protein expressed should not be overlooked when interpreting these results. Hence, these immunohistochemistry results are still preliminary but a good indication of the expression of these markers in different tissues and disease conditions.

3.2 SCREENING OF MARKERS IN YOUNG AND OLD TISSUES

3.2.1 IMMUNOHISTOCHEMISTRY OF MARKERS IN MICE TISSUES

To further assess the expression of our novel markers of senescence in young and old animals and across different tissues, immunohistochemistry was carried out using tissue samples from four mice aged 3 weeks, 26 weeks, 70½ weeks and 87 weeks. Tissues were stained for the senescence markers p16^{INK4A}, B2MG and STX4 as well as the cell proliferation marker Ki67, which was used as a negative control. Results were presented as percentage of DAB staining after image analysis by ImmunoRatio.

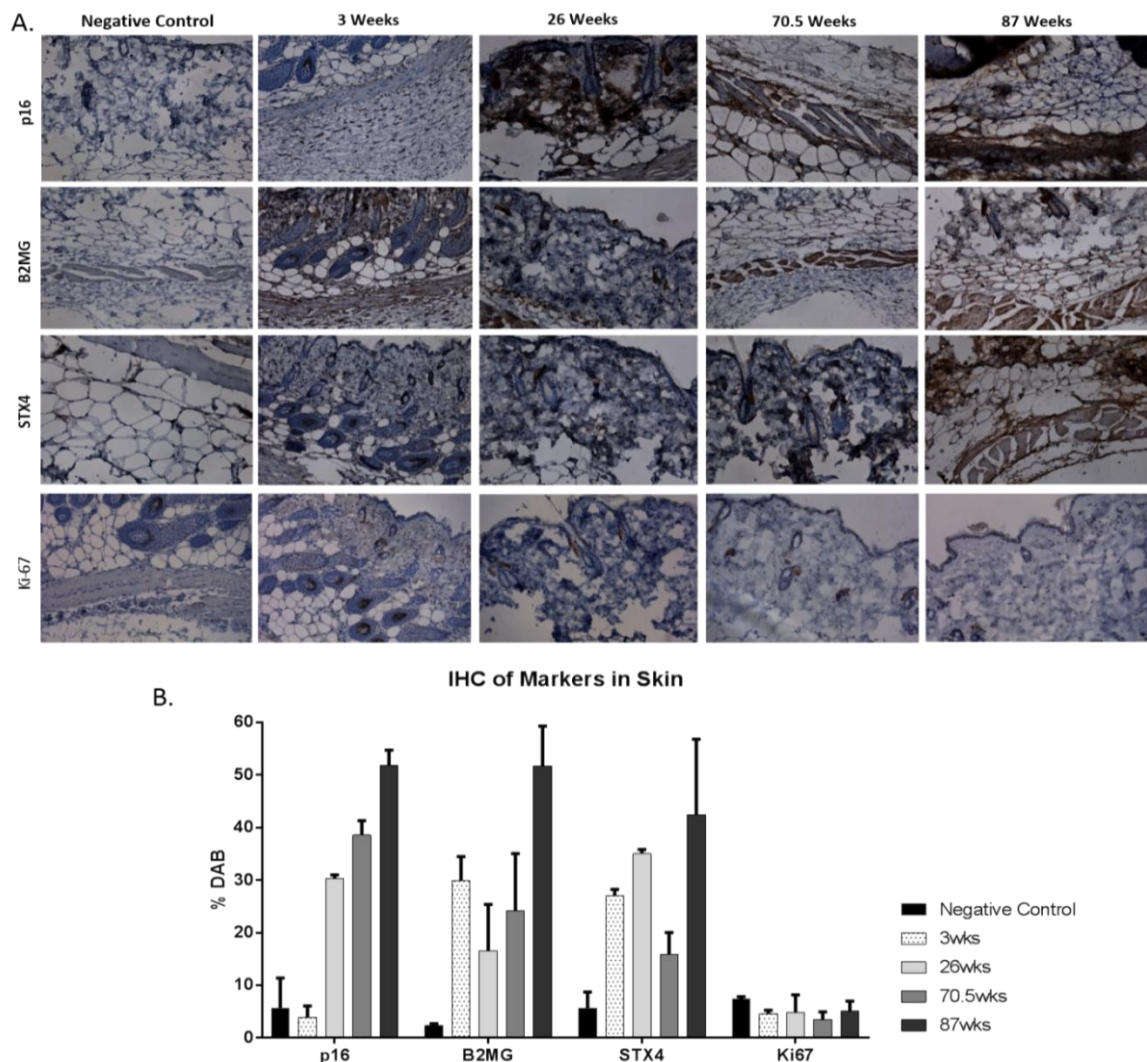


Figure 3-1 Immunohistochemistry of skin samples from mice of different ages
Skin samples from mice of different ages were stained for senescence markers p16, B2MG and STX4 while Ki67 was used as a negative control (A). ImmunoRatio software was used to quantify the percentage of DAB staining in the images and results were plotted using GraphPad Prism (B). The values presented here are averages from 3 to 5 different images.

Mouse skin tissues were stained with p16^{INK4A}, B2MG, STX4 and Ki67. Although most of the tissues were damaged during the process of antigen retrieval, fixing and staining, it can still be observed that older skin stained for our senescence markers more than younger ones and all samples were negative for Ki67 except in bulge stem cell areas (Figure 3-1).

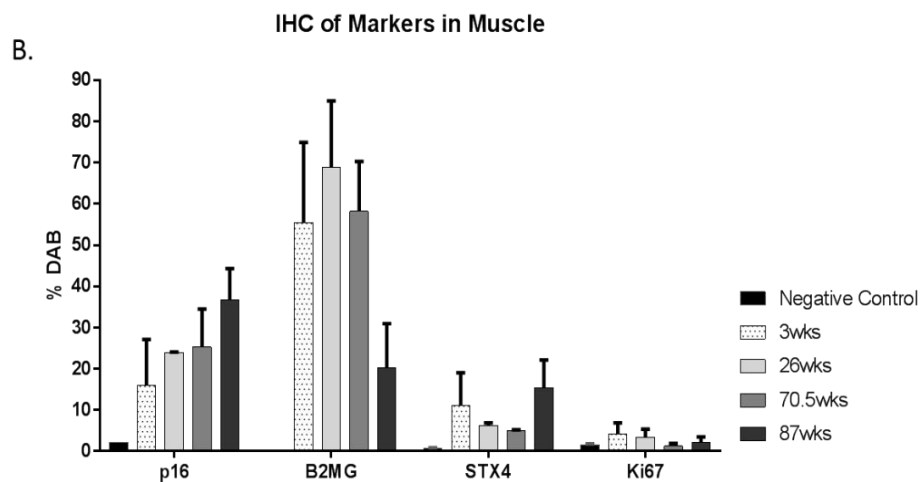
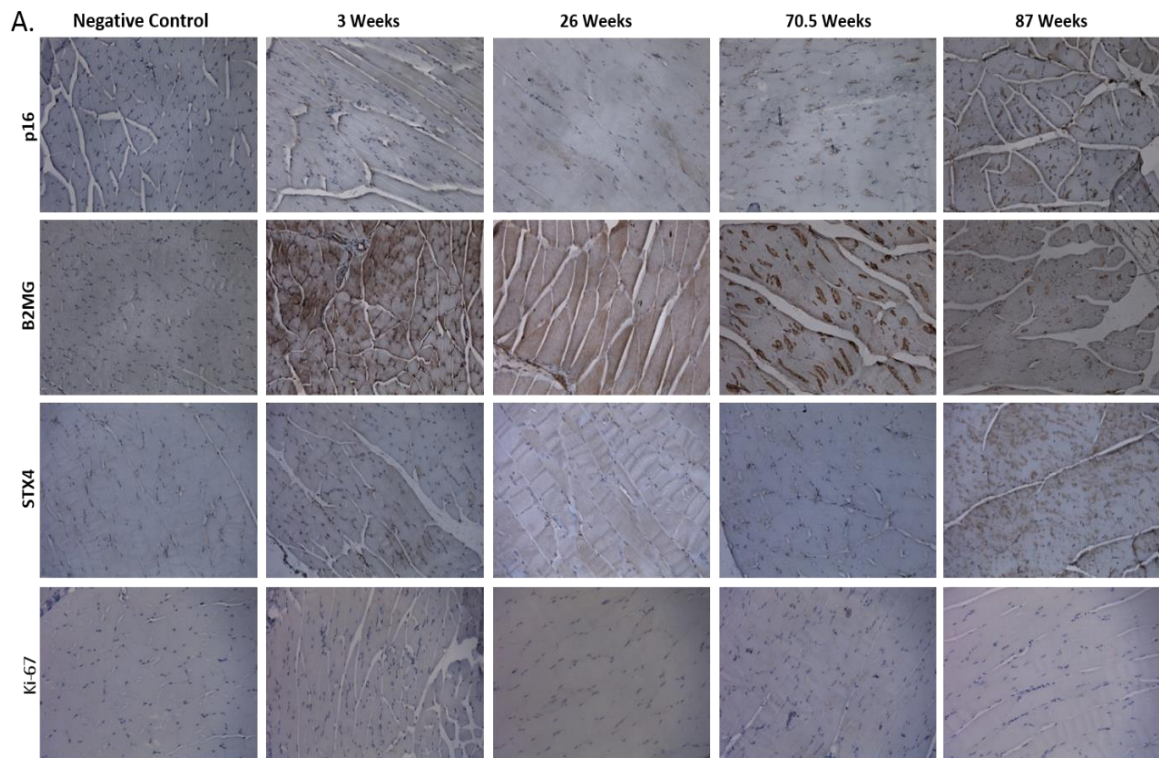


Figure 3-2 Immunohistochemistry of muscle from mice of different ages
 Muscle tissues from mice aged 3 weeks, 26 weeks, 70½ weeks and 87 weeks were stained for p16, B2MG, STX4 and Ki67 (A). ImmunoRatio software was used to quantify the percentage of DAB staining in the images. GraphPad Prism was used to analyse the results (B). The values presented here are averages from 3 to 5 different images.

Next, the novel markers B2MG and STX4 were again screened alongside p16^{INK4A} and Ki67 in muscle tissues obtained from the hind limb of these same mice aged 3 weeks, 26 weeks, 70½ weeks and 87 weeks (Figure 3-2). Ki67 was negative in all samples and p16 staining increased with age while STX4 and B2MG stained variably in the tissues.

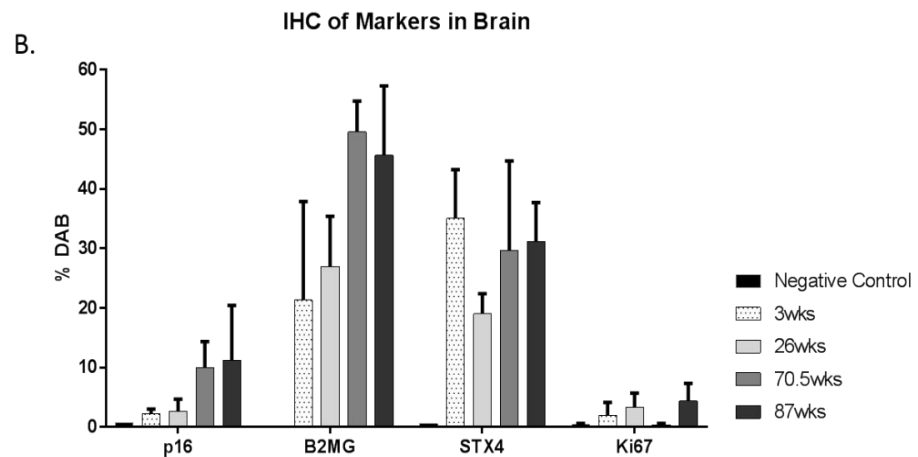
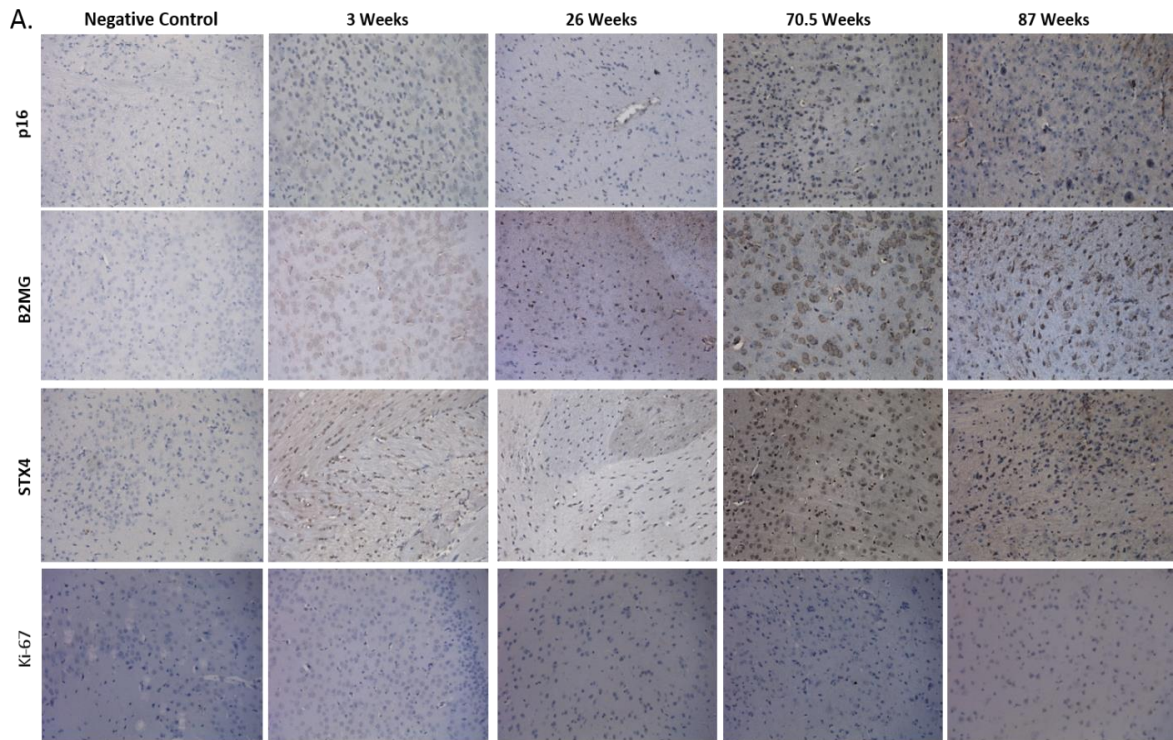


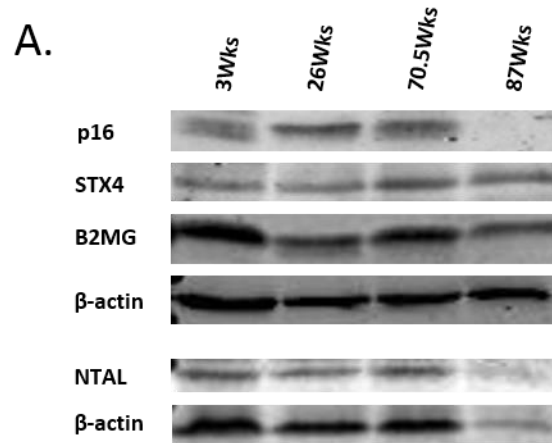
Figure 3-3 Immunohistochemistry of brain tissue from mice of different ages Brain samples from mice aged 3 weeks, 26 weeks, 70½ weeks and 87 weeks were stained for p16, B2MG, STX4 and Ki67 (A). The percentage of DAB staining in the images was quantified using ImmunoRatio software and results were analysed and presented on GraphPad Prism (B). Values presented here are averages from 3-5 different images.

Finally, brain tissue samples from these same four mice were stained for p16^{INK4A}, B2MG, STX4 and Ki67. (Figure 3-3). The older tissues stained more for senescence markers p16 and B2MG compared to the tissues from younger animals. The staining for STX4 was quite variable as it was higher in the youngest animal but increased with age in the other samples. All of the tissues stained negative for ki67. This suggests that B2MG and STX4 are not markers of proliferation but instead could be used to identify senescent or ageing cells, although it is not fully understood why their expression is higher in the younger animals in comparison to p16 expression.

3.2.2 WESTERN BLOT ANALYSIS OF MARKERS IN MICE TISSUES

To confirm the results obtained by immunohistochemistry, we used Western blots to detect the expression of these protein markers in tissues. Total protein was extracted from formalin-fixed, paraffin-embedded brain tissue samples from mice of different ages. SDS-PAGE and Western blot were carried out and the resulting bands quantified by densitometry using Image Studio Lite software version 5.2.5 from LI-COR. The fold change was calculated after signals were normalised with the loading control (β -actin) and graphs of the fold change relative to the youngest sample were plotted with GraphPad Prism version 7.0.

First, protein was extracted from brain tissues from mice aged 3 weeks, 26 weeks, 70½ weeks and 87 weeks (the same animal tissues that were previously used for immunohistochemistry). Western blot was carried out for p16^{INK4A}, B2MG, STX4 and another marker, NTAL (Non-T cell activation linker). The results show a steady increase in p16, STX4 and NTAL levels with age, although considering the low protein band for NTAL in the 87 week old animal, its quantitation may not be fully trusted. B2MG levels on the other hand were inconsistent (Figure 3-4). The 87 week old sample also did not express any p16 and it is unclear why. The Western blot data for p16 and STX4 in mouse brain confirmed immunohistochemistry results for the same tissue samples. B2MG results on the other hand were inconsistent.



B. Western Blot Analysis of Markers in Mouse Brain

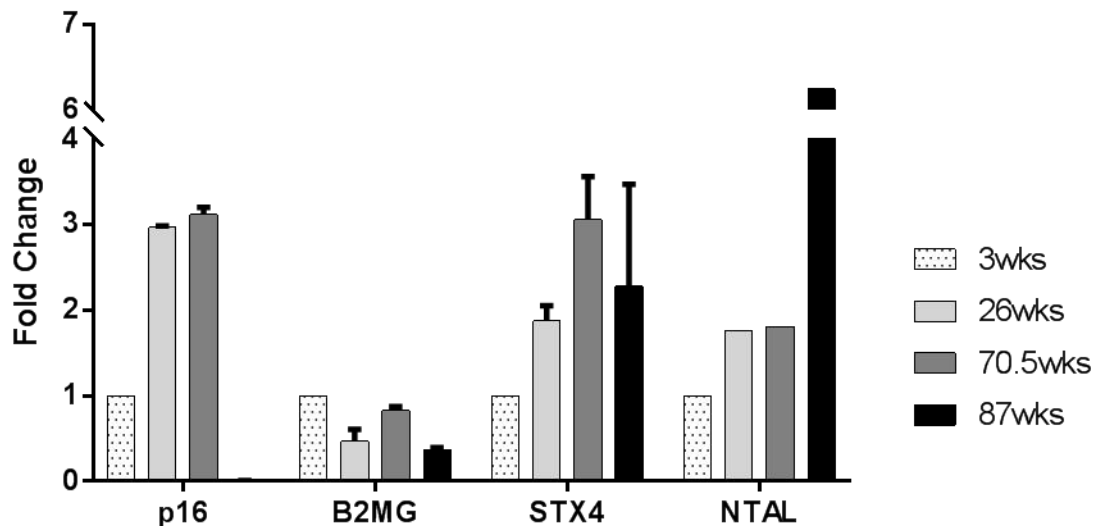


Figure 3-4 Western blot analysis of brain tissue samples from 4 mice of different ages

Brain tissues from mice aged 3 weeks, 26 weeks, 70½ weeks and 87 weeks were analysed by Western blot for expression of p16, B2MG, STX4 and NTAL (A). The protein bands were quantified using Image Studio Lite software and results plotted on GraphPad Prism (B). The graph for p16 shows results from two independent experiments. STX4 and B2MG graphs show results from three independent experiments while the NTAL data were obtained from one experiment. Results are presented as mean \pm SD except for NTAL.

Next, eyes, skin, brain, liver and muscle tissues from old and young mice obtained from the Shared Ageing Research Models (ShARM) biorepository of the University of Sheffield, UK were used to assess the expression of senescence markers between very old animals and young ones. Western blot analysis of

these tissues revealed an over expression of some of our novel senescence markers in the tissues from aged animals (Figure 3-5). The markers assessed include Syntaxin-4 (STX4), Beta-2 Microglobulin (B2MG), the Ezrin/radixin/moesin-binding phosphoprotein (EBP50), the Armadillo repeat-containing X-linked protein 3 (ARMCX3) also known as ALEX3, along with p16, a well characterized marker for ageing which was used as a positive control.

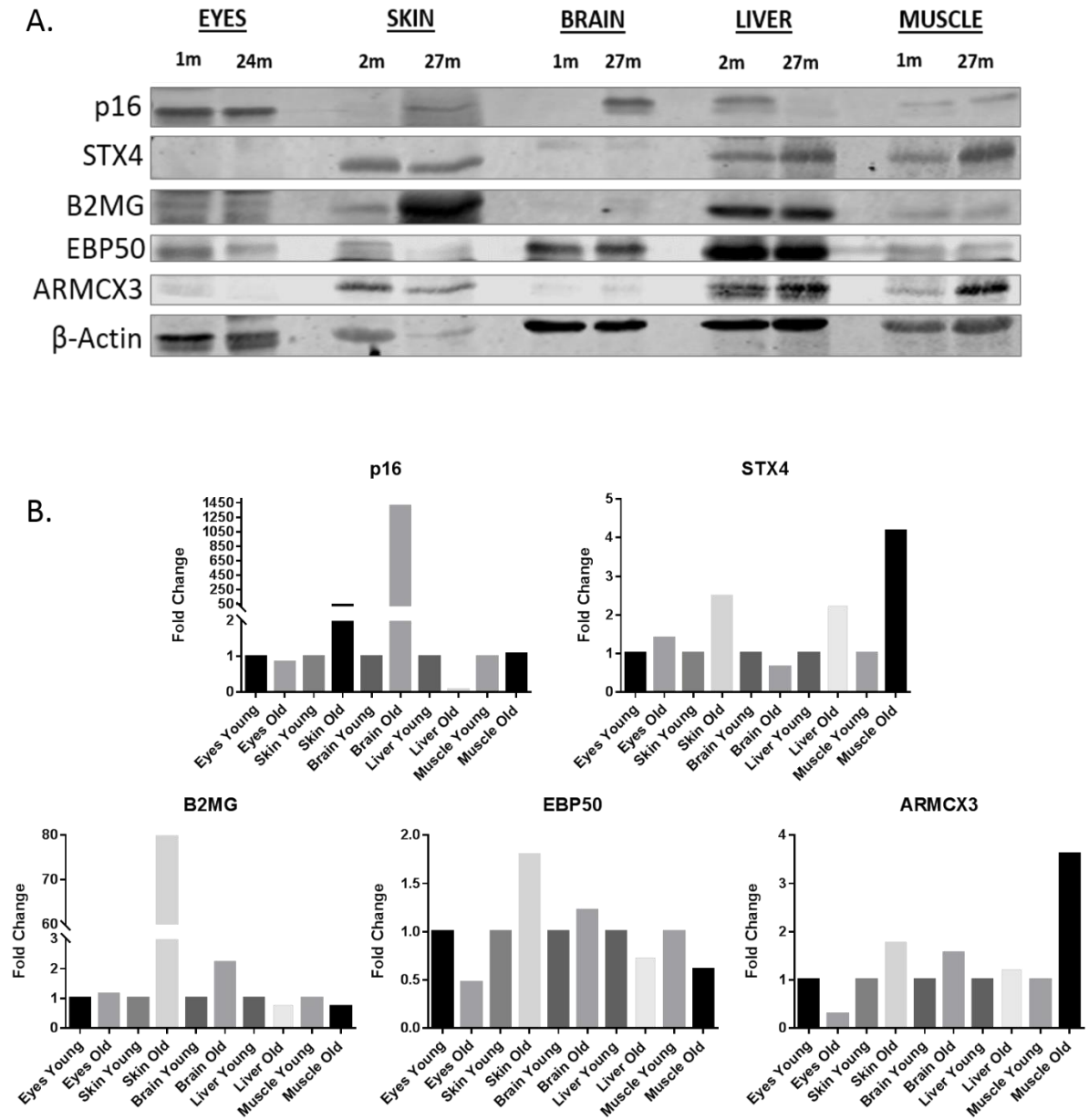


Figure 3-5 Western blot of senescence markers in young and old tissues
 The eyes, skin, brain, liver and muscle tissue from old and young mice were analysed by Western blot for the expression of senescence markers (A). Protein bands were quantified with the Image Studio Lite software and results presented using GraphPad Prism (B). These results are from a single experiment.

Levels of STX4, B2MG, EBP50 and ARMCX3 were higher in aged skin compared to younger skin, in agreement with p16 expression levels. In the aged brain, B2MG levels were also higher than what was observed in the young brain, showing more than a two-fold increase. This was still in line with p16 levels though not by similar proportions. In the aged muscle, only ARMCX3 and STX4 levels were found to be higher when compared to the young muscle as p16 expression was not significantly high. The expression levels of p16, B2MG and EBP50 in the liver were lower in the older animal while STX4 and ARMCX3 levels were higher in the older liver tissue than in the young one. The very low p16 expression in this old liver tissue was unexpected and could be due to a technical error. Protein expression levels in the eyes were generally low for all markers tested except for small increases in STX4 and B2MG levels.

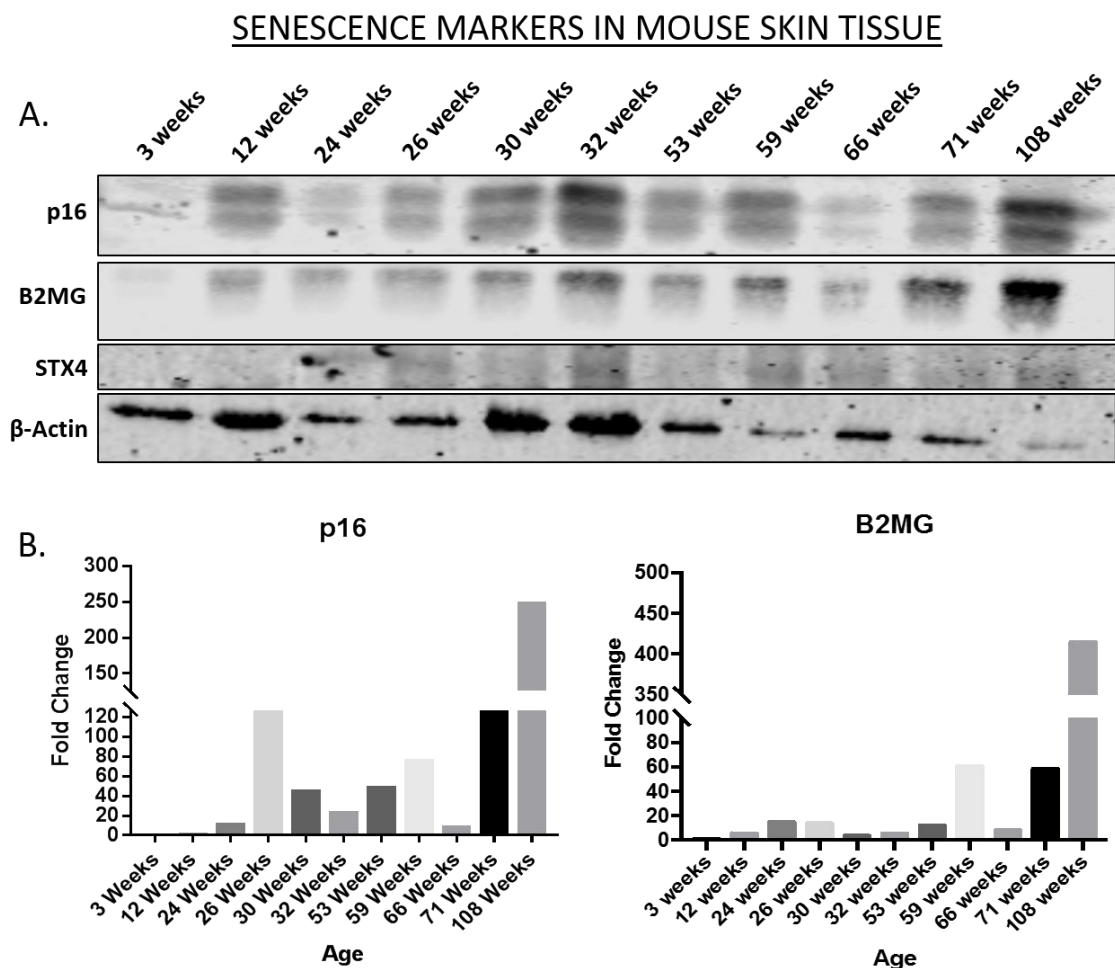


Figure 3-6 Western blot analysis of skin tissues from 11 mice of different ages Western blot was carried out on skin tissues from 11 mice, for p16, B2MG and STX4 (A). The resulting bands were quantified with the Image Studio Lite software and the data plotted using GraphPad Prism (B). Results presented here are from a single experiment.

The results obtained from the shARM tissues gave us a good glance and snapshot of the expression of these proteins in aged tissues. In order to further validate and confirm these initial results, the age range of animals was expanded and skin, brain, muscle and liver tissues were obtained from 11 wild type C57/BL6 mice of varying ages. The tissues were analysed by Western blot for expression of p16, B2MG and STX4, in order to determine the expression of these markers across a wider age range. β -actin was used as the loading control. The information about the sex of these mice was not obtainable.

Consistent with previous results, the expression of p16 and B2MG were markedly higher in the skin of older animals when compared to the younger ones (Figure 3-6).

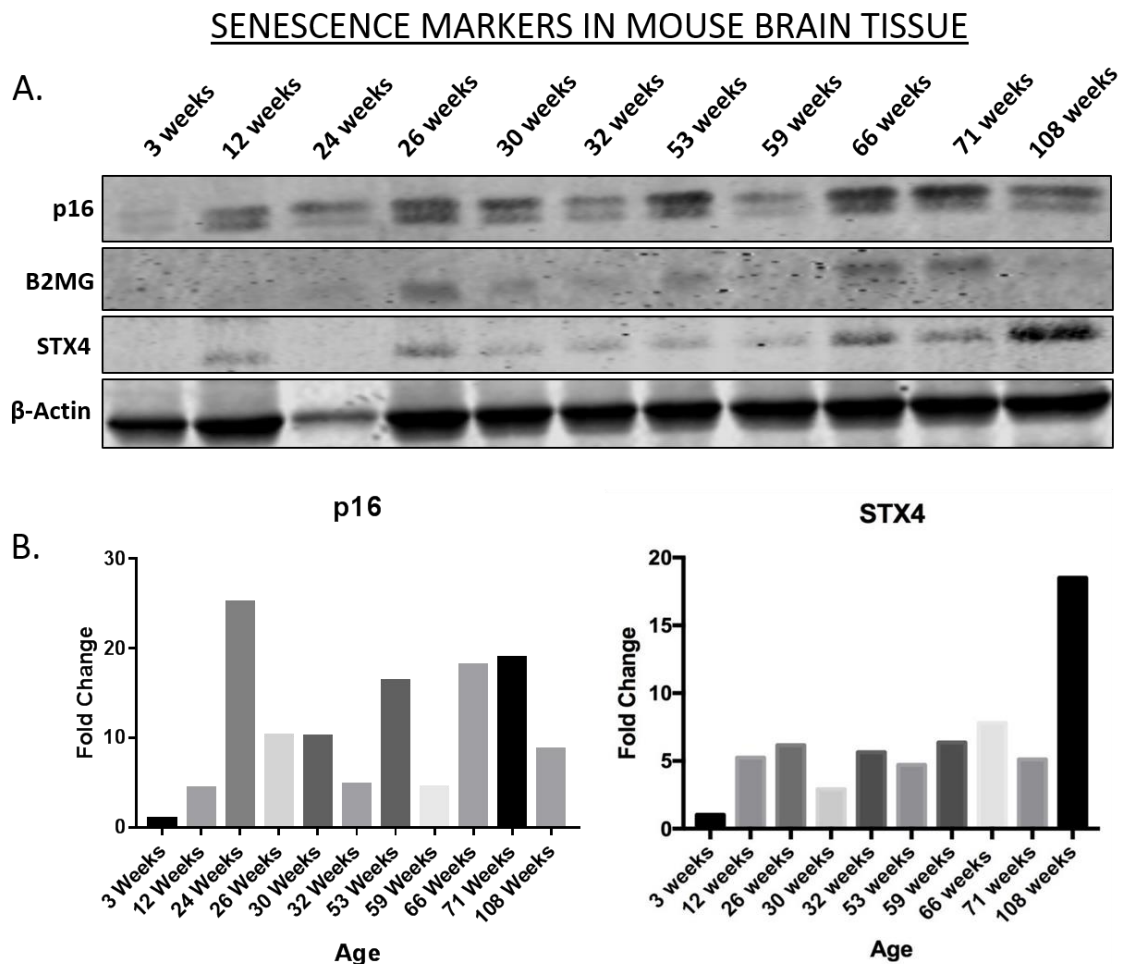


Figure 3-7 Western blot analysis of brain tissues from 11 mice of different ages Brain tissue samples from 11 mice, for p16, B2MG and STX4 (A). The resulting bands were quantified with the Image Studio Lite software and the data plotted using GraphPad Prism (B). Results presented here are from a single experiment.

In the brain tissue, p16 increased with age although not consistently. STX4 was also higher in the older animal but the levels were not significantly different among the other ages except for the youngest animal which expressed the protein in very low levels (Figure 3-7). B2MG expression levels were inconsistent and varied greatly across the age range hence the bands were not quantified.

SENESCENCE MARKERS IN MOUSE MUSCLE TISSUE

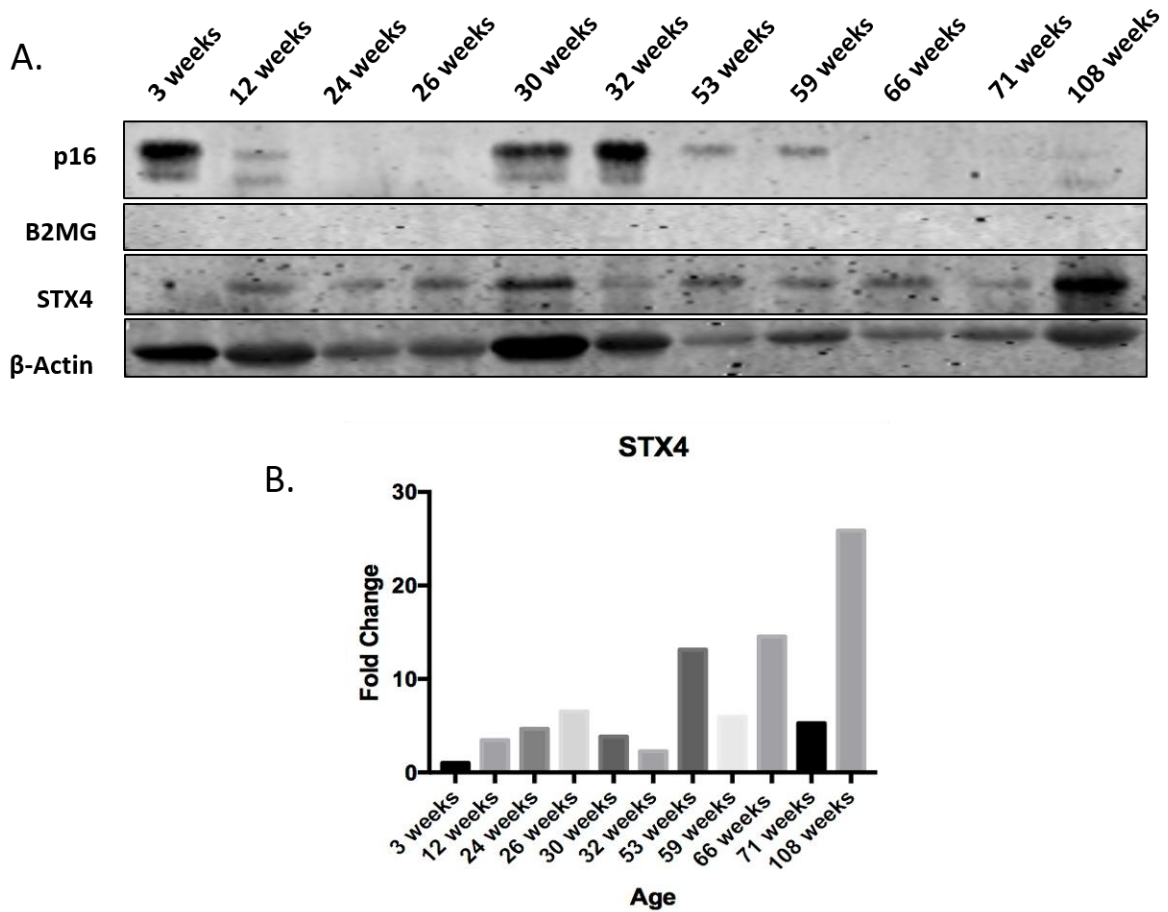


Figure 3-8 Western blot of muscle tissues from 11 mice of different ages

Western blot was carried out using muscle tissue obtained from the hind legs of 11 mice and the expression of p16, B2MG and STX4 were assessed (A). The resulting bands for STX4 were quantified using Image Studio Lite software and analysed on GraphPad Prism (B). Results shown are from a single experiment.

In the muscle tissue on the other hand, p16 did not consistently increase with age. However, STX4 expression was seen to consistently increase with age, while B2MG was undetectable in these tissues (Figure 3-8).

The expression of p16 protein in the liver was variable and did not correlate with age. STX4 levels on the other hand correlated with data from the shARM tissues as there was a higher expression in the oldest animal compared to the youngest, although its expression levels were variable and did not consistently increase with age. B2MG was undetectable in these tissues (Figure 3-9).

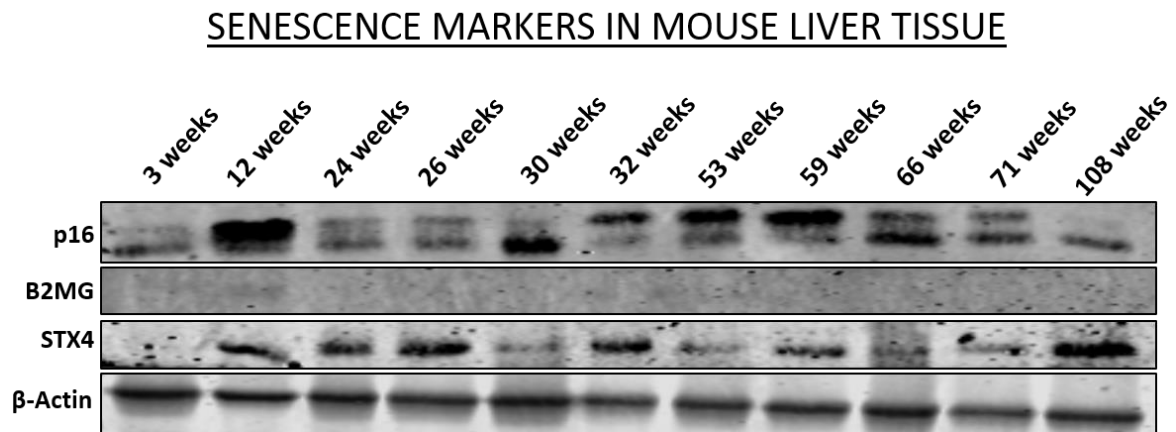


Figure 3-9 Western blot analysis of liver tissues from 11 mice of different ages
Expression of senescence markers in liver as assessed by Western blot. The protein levels are variable and do not show correlation with age.

Having observed an increase in p16, B2MG and STX4 with age in skin and brain tissues, these tissues were again obtained from a total of 17 mice ranging in age from 2 months to 24 months, in order to further verify the expression of these markers by age, using Western blot and qPCR. The mice were divided into 7 age groups namely, 2 months, 3 months, 6 months, 8 months, 13 months, 17 months and 24 months old, with 2 or 3 animals per group. The 2 months and 24 months old groups had 3 animals each while the remaining groups had 2 animals each. The mice were all males with the exception of 2 female mice in the 24 month old group. Another known marker of senescence, p53, was also included in this screening. The protein bands were quantified and the results normalised as fold change against the 2 month old group. The data was presented as mean \pm SEM.

Expression of Senescence Markers in Mice Brain

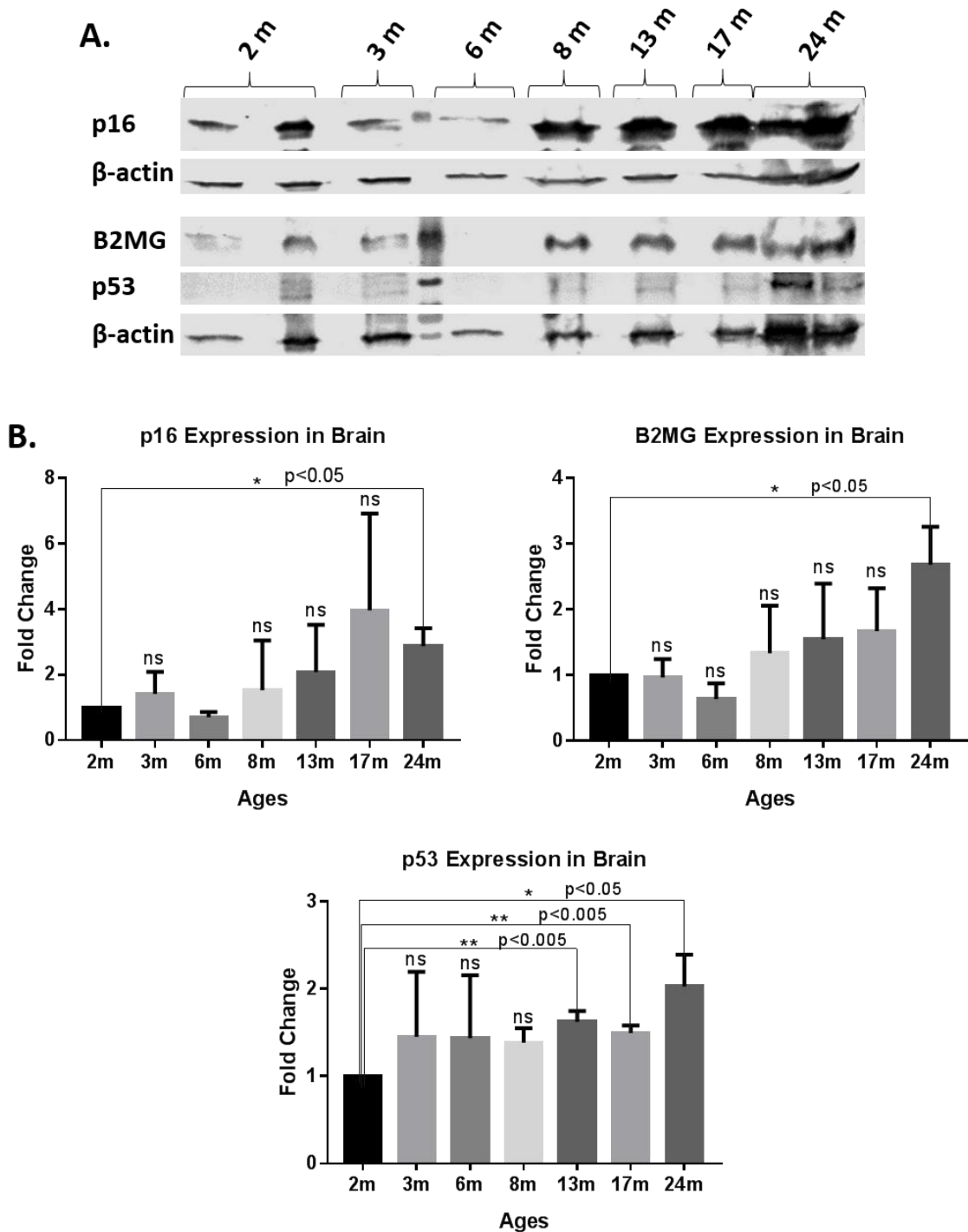


Figure 3-10 Analysis of mice brain tissues from 7 age groups by Western blot
 Western blot analysis of the expression of p16, B2MG and p53 in mice brain samples (A). Quantification of the bands show an increase in all markers with age and unpaired t tests were used to determine statistical significance (B). Results are presented as mean \pm SEM.

Expression of Senescence Markers in Mice Skin

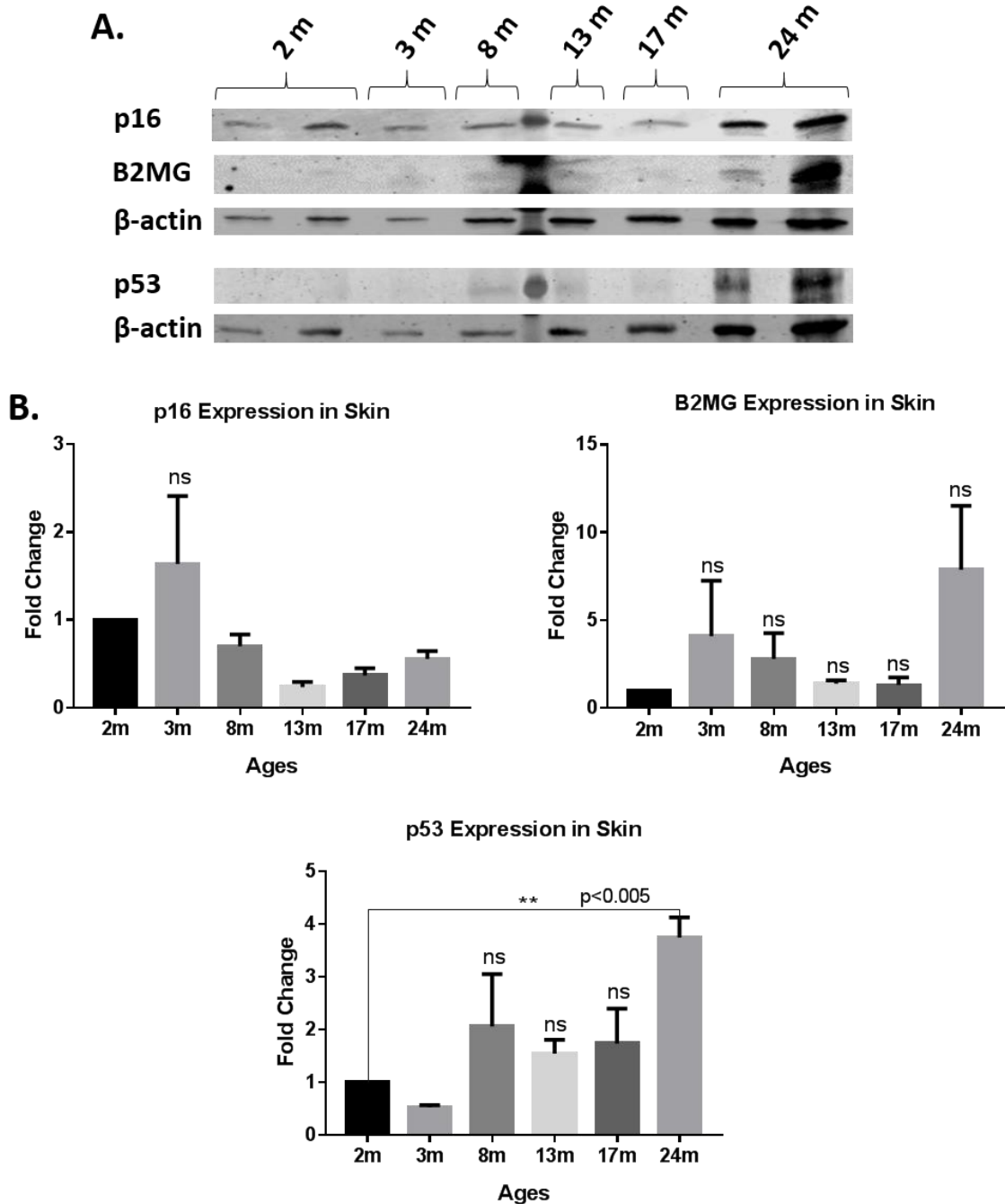


Figure 3-11 Analysis of mice skin tissues from 7 age groups by Western blot

Western blot expression of p16, B2MG and p53 in mice skin samples (A).

Quantification of the bands, show that p16 did not consistently increase with age, B2MG expression increased in the 3 month group but was highest in the 24 month old age group and p53 also increased in the older age groups although not consistently with age (B). Data is presented as mean \pm SEM. An unpaired t test was used to show statistical significance at $p < 0.005$.

The protein expression levels of all three markers tested were found to increase with age in the brain tissues although B2MG and p16 levels showed statistical significance at $p < 0.05$ only in the 24 month old group, with mean p16 levels decreasing from the 17 month group to the 24 month group. The levels of p53 on the other hand were found to increase in the older age groups compared to the young 2 month old control group, with statistical significance in the 13 month, 17 month and 24 month old groups (Figure 3-10).

In the skin samples, p16 expression was not found to be consistent with age as it increased in the 3 month old group but decreased in all other age groups when compared with the 2 months group. B2MG levels were also variable but higher in the 24 month old group than in the other age groups. The levels of p53 increased with age though higher than expected in the 8 month old group, and showed statistical significance in the 24 months group (Figure 3-11).

3.2.3 qPCR ANALYSIS OF MARKERS IN MOUSE SKIN TISSUES

In order to check the expression of these markers at the mRNA level, total RNA was extracted from the skin tissues of mice from 7 different age groups, as previously grouped for Western blot analysis. cDNA was generated and qPCR run using primers for p16, B2MG, p53, DEP1 and GAPDH was used as the internal reference control gene. Gene expression was calculated using the $\Delta\Delta C_t$ method and the final values shown as $2^{-\Delta\Delta C_t}$. Contrary to the p16 protein expression levels for these tissues, its mRNA expression was found to increase with age. B2MG mRNA expression also increased with age, agreeing in part with the protein levels although its protein expression levels were not consistent with age in this tissue. The mRNA expression for p53 increased with age also, corresponding with the protein expression levels (Figure 3-12).

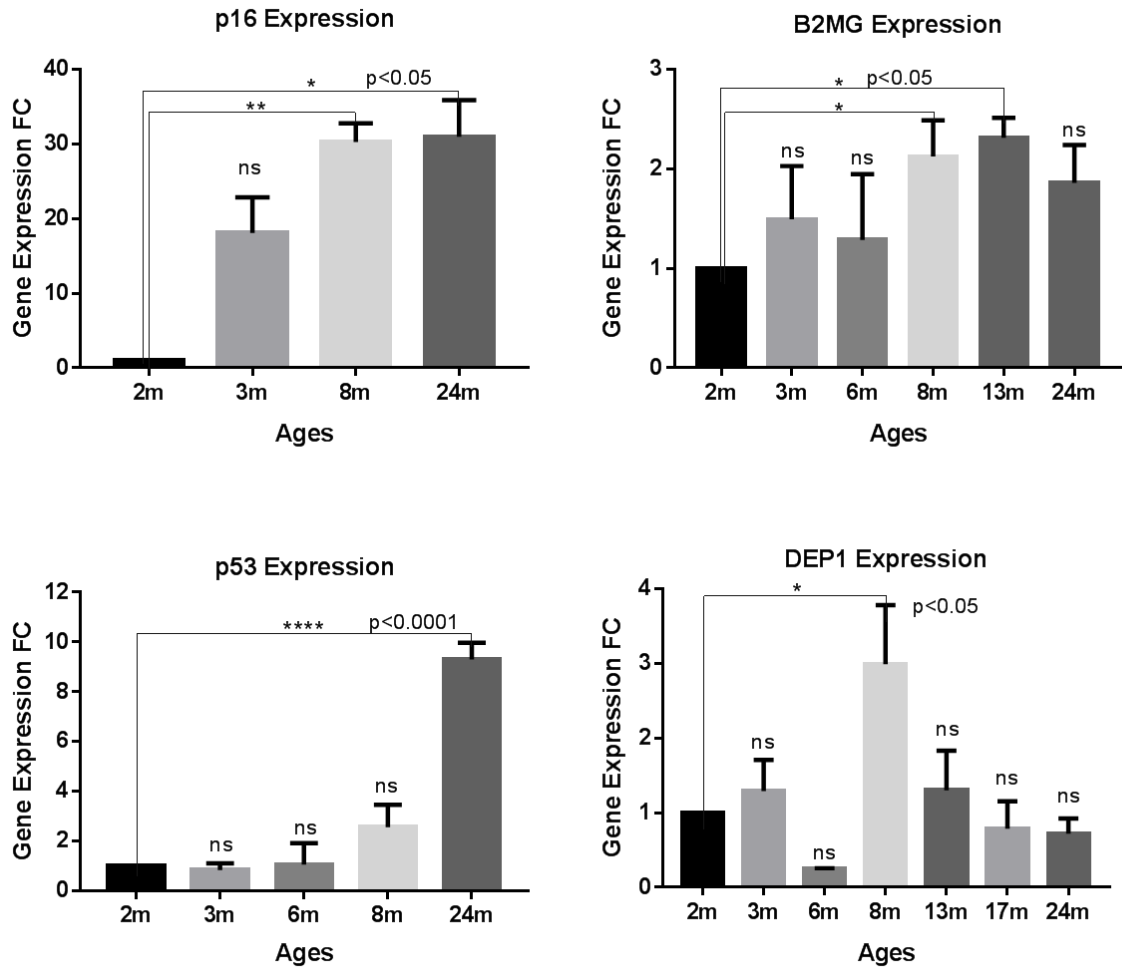


Figure 3-12 qPCR analysis of mice skin tissues from 7 age groups

Graphs showing mRNA expression levels for p16, B2MG, p53 and DEP1. The levels of p16, p53 and B2MG increased with age although B2MG expression in the 24 months old group was lower than in the 13 month old group. DEP1 expression varied across the age groups. Data was analysed with GraphPad Prism software and presented as mean \pm SEM.

3.2.4 SCREENING OF MARKERS IN HUMAN LUNG TISSUES

In order to validate the expression of these markers in aged human tissues, biopsies from healthy lung tissues of a 70 year old woman and a 42 year old man were screened by immunohistochemistry for the presence of senescence markers, in order to also establish the expression of these markers in aged human tissue.

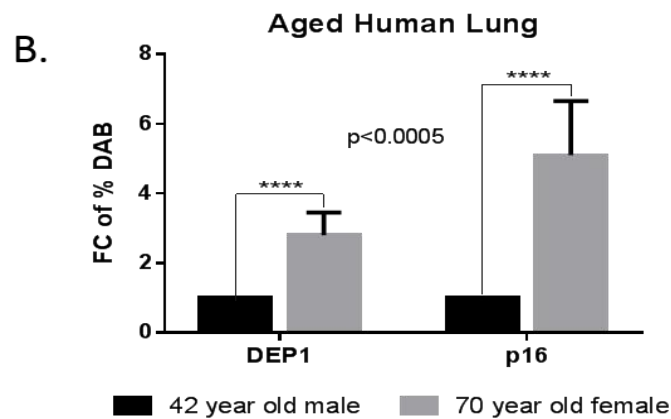
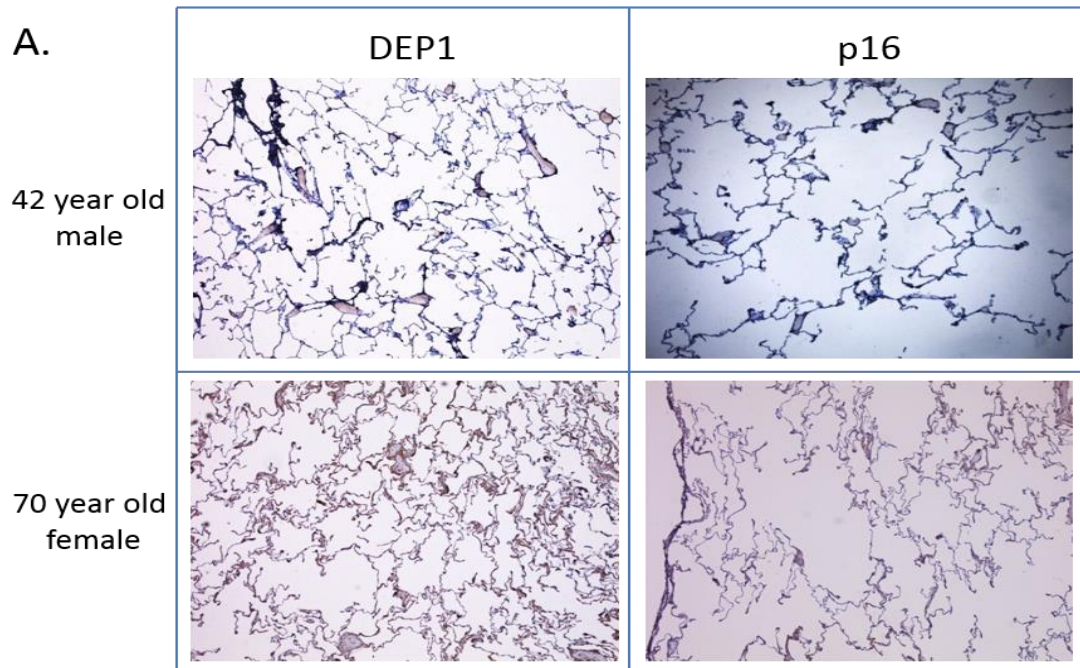


Figure 3-13 Immunohistochemistry of human lung tissues

Lung tissues from a 70 year old woman overexpressed p16 and DEP1 when screened by immunohistochemistry (A). The percentage of DAB staining in the tissue was quantified using ImmunoRatio software. The fold changes were calculated relative to the younger (42 year old) tissue. GraphPad Prism software was used to analyse the data and a two-tailed unpaired t test used to determine statistical significance (B).

Values presented here are averages from 6 images.

DEP1 and p16 were upregulated in the 70 year old woman's tissue compared to tissue from the 42 year old man (Figure 3-13). There was a five-fold increase in p16 expression and more than a two-fold increase in DEP1 expression in the older (70 year old) tissue compared to the 42 year old tissue. These results suggest that DEP1 could be used as a marker of ageing in human lung tissue, along with p16. The tissue samples used here were obtained and stained by our collaborators from the LD3.

3.3 SCREENING OF MARKERS IN DISEASED TISSUES

Apart from ageing, senescent cells have been shown to increase in pathologies such as fibrosis and are also thought to promote the progression of cancer (Muñoz-Espín & Serrano, 2014; He & Sharpless, 2017). In the previous sections, we assessed the expression of currently known as well as novel markers of senescence in human and mouse aged tissues, in order to verify the latter as potential markers of senescence and ageing. In the current section, we assess the expression of these markers in diseased tissues in order to verify if our identified markers can be used in diseases where senescence has a known involvement.

3.3.1 SENESCENCE MARKERS IN HUMAN LUNG CANCER SAMPLES

We first explored the use of these novel markers to detect senescent cells in cancerous lung tissue. Lung tissue biopsies from seven lung cancer patients were tested by immunohistochemistry for the presence of the markers STX4, BTK, DEP1 as well as p16^{INK4A}. Unfortunately, we could not obtain information about the patients' treatment history. All of the patient samples stained negative for p16^{INK4A} but were positive for STX4, BTK and DEP1 (Figure 3-14 and Figure 3-15). Haematoxylin and eosin staining was done to show the tissue morphology and the negative control slides had no primary antibody. The p16 marker, which was used as a positive control marker of senescence in aged tissue samples, was negative in the lung cancer samples. This raises the question as to whether the novel markers which stained positive in these tissues depict the presence of senescent cells or other elements or trails of senescence. Further studies would be needed to confirm that these markers are truly identifying senescent cells or elements of senescence in these tissues.

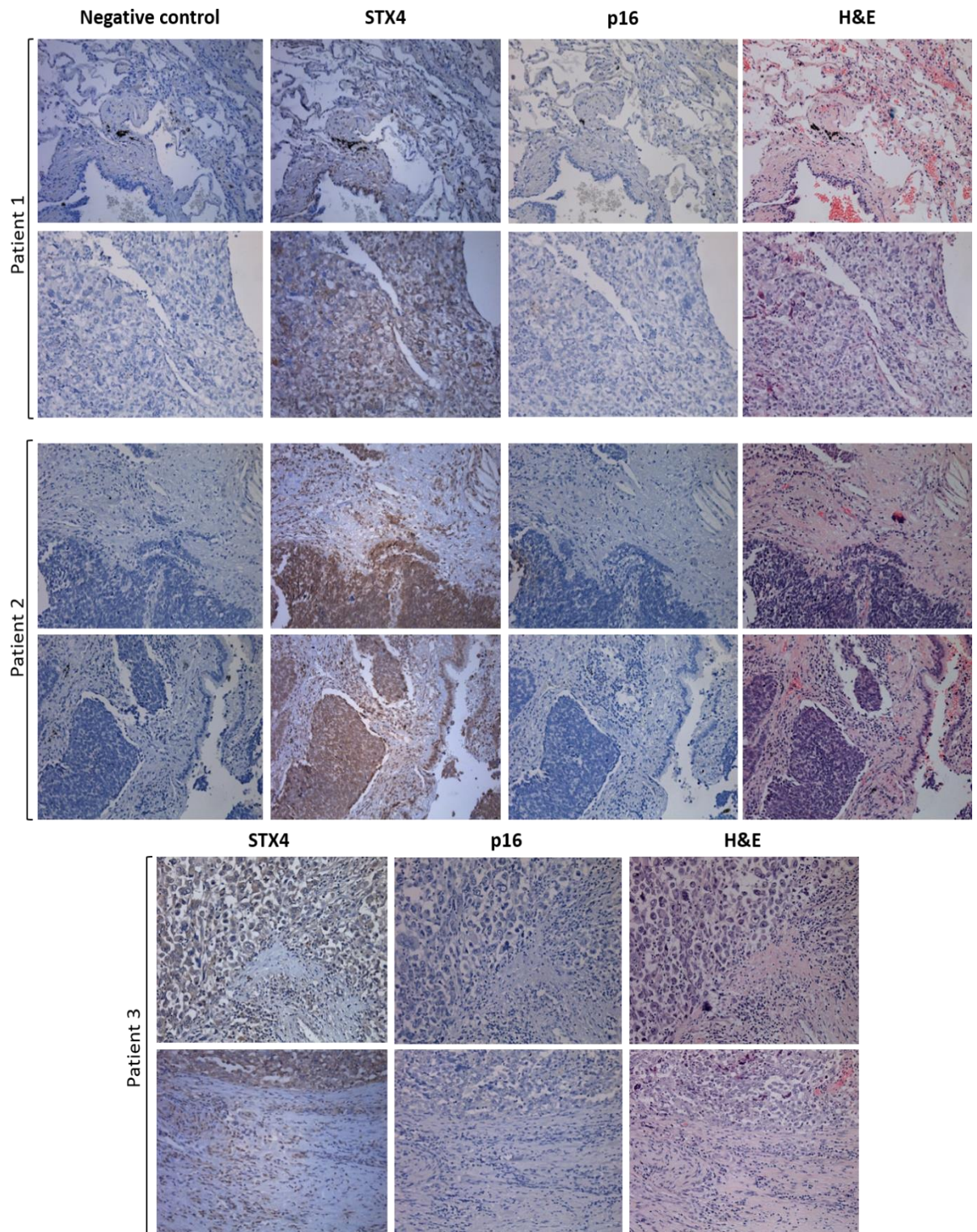


Figure 3-14 Immunohistochemistry of markers in lung cancer samples 1-3
Tissue biopsies from a total of 7 lung cancer patients were stained with senescence markers to assess the involvement of senescence in the pathology of the disease. Here, samples from 3 patients were tested for p16 and STX4. All samples overexpressed STX4 but were negative for p16. The negative control samples were treated with similar conditions as all the other samples but contain no primary antibody. H&E = Haematoxylin and eosin.

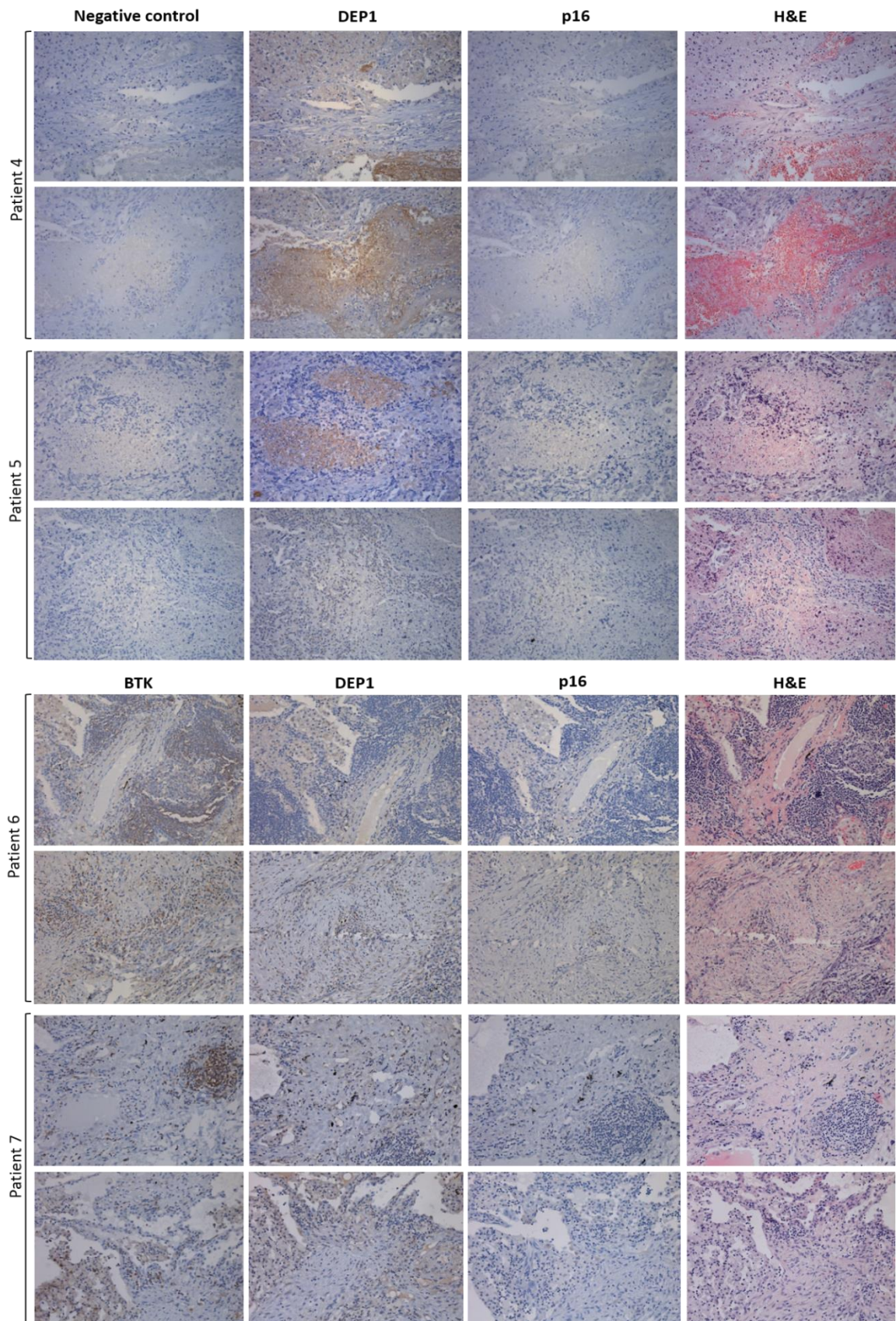


Figure 3-15 Immunohistochemistry of markers in lung cancer samples 4-7
 Lung cancer samples from 4 patients were tested for p16, DEP1 and BTK. Samples were negative for p16 but expressed BTK and DEP1. H&E = Haematoxylin and eosin.

3.3.2 SENESCENCE MARKERS IN MICE LIVER FIBROSIS SAMPLES

To test whether our markers could detect the presence of senescent cells in fibrotic lesions, liver fibrosis tissue samples from mouse models were screened by immunohistochemistry for the presence of senescence markers.

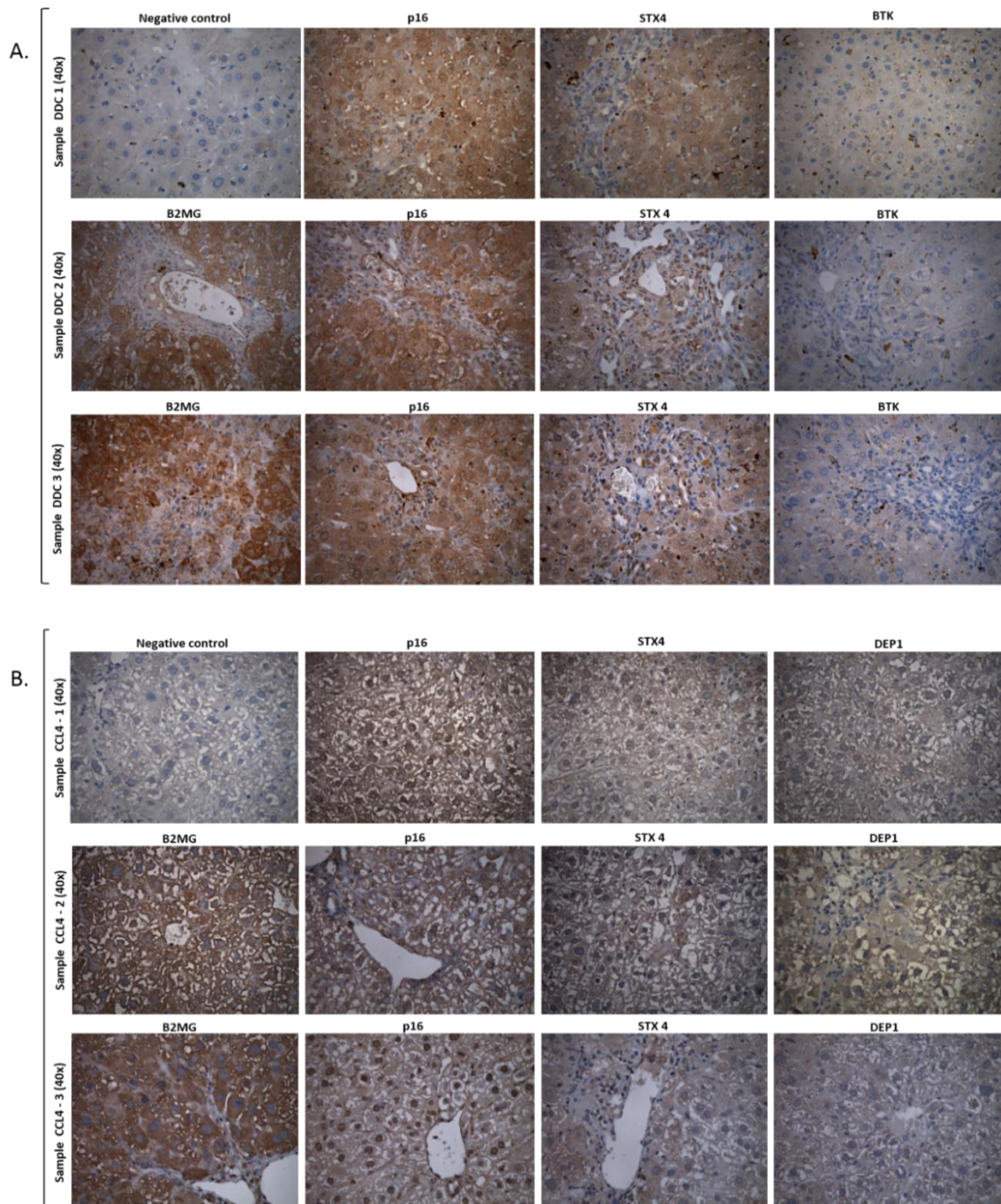


Figure 3-16 Immunohistochemistry of senescence markers in fibrotic livers
Liver fibrosis samples from mice treated with 3,5-diethoxycarbonyl 1,4-dihydrocollidine (DDC) or carbon tetrachloride (CCL4) were stained by immunohistochemistry. The fibrotic tissues stained positive for all of the markers tested. One slide was used as a negative control for each treatment group.

Liver damage was induced in mice either by using 3,5-diethoxycarbonyl 1,4-dihydrocollidine (DDC) or carbon tetrachloride (CCL₄) and there were three mice in each group. The markers p16, B2MG, STX4, DEP1 and the Bruton's Tyrosine Kinase (BTK) were assessed in these tissue samples by immunohistochemistry. The samples stained positive for all the markers when compared with the negative control, which had no primary antibody (Figure 3-16). These results suggest that these four novel markers could be used as prognostic or diagnostic tools for liver fibrosis disease. This could be further explored in the future. All of the mouse work and induction of fibrosis for these samples were done by our collaborators at the University of Barcelona, Spain.

The findings from the screening of novel potential senescence markers in different tissues from old as well as diseased mouse and human, using immunohistochemistry, Western blot and qPCR, are summarised in Table 3.1 below. Although some of these results are preliminary, they give an indication of the pathways that could be involved in senescence and present a good starting point for further investigations.

Table 3.1 SUMMARY OF FINDINGS FROM SCREENING OF MARKERS IN TISSUES (+ = positive; - = negative; NT = not tested).

| MARKER \ TISSUE | B2MG | STX4 | DEP1 | NTAL | EBP50 | ARMCX3 | BTK | p16 | P53 |
|-----------------------------|------|------|------|------|-------|--------|-----|-----|-----|
| Aged Mouse Brain | + | + | NT | + | + | + | NT | + | + |
| Aged Mouse Skin | + | + | NT | NT | + | + | NT | + | + |
| Aged Mouse Muscle | - | + | NT | NT | - | + | NT | + | NT |
| Aged Mouse Liver | - | + | NT | NT | - | + | NT | + | NT |
| Aged Mouse Eyes | + | + | NT | NT | - | - | NT | - | NT |
| Aged Human Lung | NT | NT | + | NT | NT | NT | NT | + | NT |
| Human Lung Cancer | NT | + | + | NT | NT | NT | + | - | NT |
| Mouse Liver Fibrosis | + | + | + | NT | NT | NT | + | + | NT |

3.4 INVESTIGATING NOVEL MODULATORS AND EFFECTORS OF SENESENCE.

3.4.1 THE ROLE OF BTK IN CELLULAR SENESENCE

Most of the novel markers of senescence previously identified in our laboratory (Althubiti *et al.*, 2014) do not currently have inhibitor drugs available. However, the Bruton's Tyrosine Kinase (BTK) presently has a few inhibitors in the market that are used to target the protein for the treatment of B-cell malignancies. One of these clinically approved BTK inhibitors is Ibrutinib, also known as PCI-32765, which is used to treat patients with mantle cell lymphoma (MCL) and chronic lymphocytic leukaemia (CLL) (Hendriks *et al.*, 2014; Masso-Valles *et al.*, 2015).

3.4.1.1 EFFECT OF BTK INHIBITION ON SENESENCE OF HUMAN LUNG FIBROBLASTS

Since senescence is known to play a role in the pathogenesis of idiopathic Pulmonary Fibrosis (IPF) (Yanai *et al.*, 2015; Kuwano *et al.*, 2016), and BTK has been found to block senescence (Althubiti *et al.*, 2016), we decided to test the therapeutic potential of Ibrutinib, a small molecule inhibitor of BTK in fibrotic diseases. To this end, we obtained primary samples of lung fibroblasts from a patient with Idiopathic Pulmonary Fibrosis (IPF) and non-fibrotic control (NFC) fibroblasts from the Leicester Respiratory Biomedical Research Unit (BRU). We used these cultures to assess the effect of BTK inhibition on the growth rate and senescence of these cells. This experiment was carried out to see if lung fibrosis condition can be delayed or reversed by inhibiting BTK and follows a previous study from the lab that identified BTK not only as a marker but also as a crucial component of the senescence pathway (Althubiti *et al.*, 2016).

First, the IPF and NFC lung fibroblasts were cultured in 60mm dishes and treated with 0.3 μ M Ibrutinib to study the effect of the drug on fibroblast senescence, while cells in the control group received DMSO. Cells were passaged when they reached about 70% confluence and cell counts were used to create growth curves (Figure 3-17). The goal was to see whether the lifespan of fibrotic cells, which potentially would more readily go into senescence, would be prolonged by BTK inhibition. The growth of Ibrutinib-treated IPF cells increased sharply after day 22, but the cell number was reduced to half by day 48, after which the cells

were stained with β -galactosidase. The cells in the DMSO control group also tripled in number between day 22 and day 35 but did not significantly differ from the Ibrutinib treated group. However, it is not known why the IPF fibroblasts proliferated more than the NFC ones in our experiment.

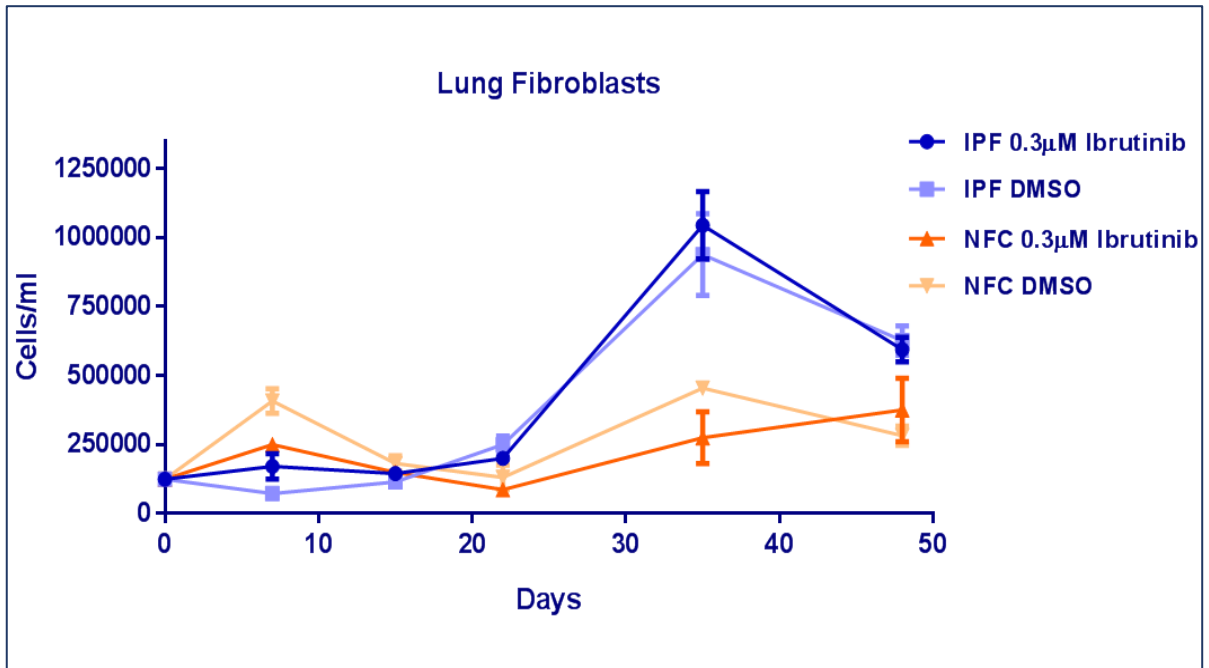


Figure 3-17 Growth curve of Ibrutinib treated IPF and NFC pulmonary fibroblasts
 Idiopathic Pulmonary Fibrosis (IPF) and non-fibrotic control (NFC) fibroblasts either treated with 0.3µM Ibrutinib or DMSO were maintained in culture for 7 weeks. The cells were counted using the T20 automated cell counter, first every 7 days for the first 3 weeks, and then every 14 days for the last 4 weeks, in order to determine their growth curve. From the results, Ibrutinib did not exert any effect on the proliferation of either IPF or NFC fibroblasts.

The fact that the growth curve for both groups of IPF cells did not differ much from one another suggests that Ibrutinib might not have an effect on preventing senescence of pulmonary fibrosis fibroblasts. Results for the NFC cells revealed an irregular and inconsistent growth curve for both the Ibrutinib treated and the DMSO control groups. This may have been due to technical or other errors. From this result, it is inconclusive the effect of Ibrutinib in normal lung fibroblasts although it appears to have no effect on their proliferation as there is no significant difference in growth between the treated and untreated groups (Figure 3-17). It

is acknowledged that control samples other than the DMSO treated IPF or NFC cells should have been used in this experiment. For example, cells previously shown to have escaped senescence upon treatment with Ibrutinib (Althubiti *et al.*, 2016) could have been used as a positive control. Also, it is important to note that tissue specificity as well as variation between donor samples could also account for differences in drug response. All experiments were carried out using triplicate samples A, B and C.

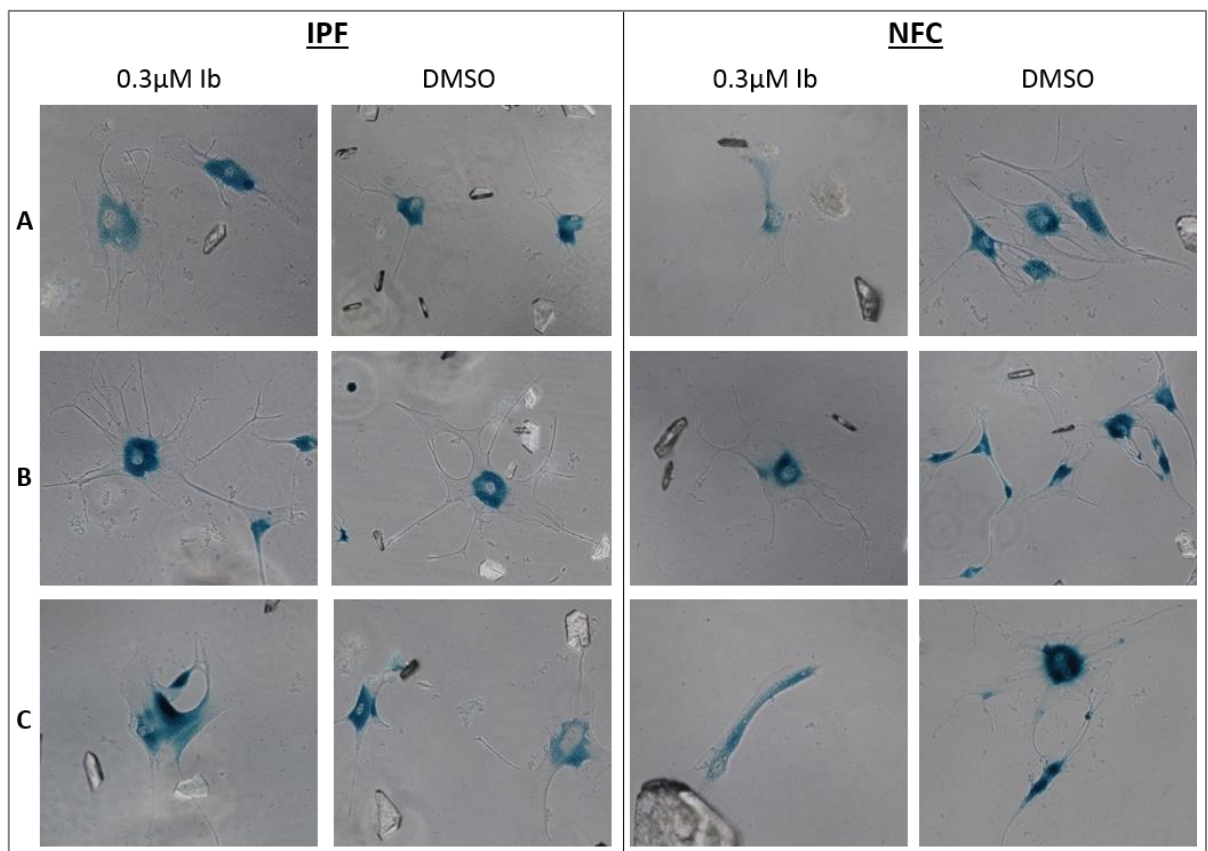


Figure 3-18 SA β -Gal staining of pulmonary fibroblasts

Senescence associated β -galactosidase (SA β -Gal) staining of pulmonary fibroblasts that had either been treated with Ibrutinib or DMSO for 52 days. Cells were stained for 16 hours with β -galactosidase at pH 6.0. All cells were clearly senescent as seen by their positive SA β -Gal staining and flattened out morphology. Samples were in triplicates, A, B and C.

On day 52 of the cell culture, IPF and NFC cells were stained with β -galactosidase at pH 6.0 (Senescence associated β -galactosidase) in order to assess the effect of BTK inhibition on senescence in these cells. The cells all

showed signs of senescence as evidenced by their flattened and enlarged shape, as well as positive staining for β -galactosidase at pH 6.0 (Figure 3-18). There was no distinction between the different experimental groups and their controls in their SA β -gal staining and senescence. From this result, we also concluded that BTK inhibition had no differential effect on the establishment of senescence in fibrotic fibroblasts and that fibroblasts from normal and IPF patients senesced at similar rates.

Cell pellets were also collected from different population doublings of these Ibrutinib treated IPF or NFC cells, and were used for Western blot analysis. The Western blot data (not shown) indicated that Ibrutinib did not have an effect on the senescence of these cells, as there was no differential expression of senescence markers between treated and untreated cells, further agreeing with the cell count and SA β -Gal data previously obtained. B2MG could be detected in the samples but only at minimal levels, while p16 and p53 could not be detected. The protein concentration from these samples were however very low and it was difficult to accurately load the samples and quantify the bands from the Western blot.

3.4.1.2 BTK INHIBITION AND SENOLYTIC ACTIVITY

Recent studies by our lab have identified an interaction between BTK and p53 in senescence and apoptotic responses (Althubiti *et al.*, 2016; Rada *et al.*, 2017). Furthermore, other studies have recently shown that senescent cells can be selectively killed using drugs that target the Bcl-2 family of anti-apoptotic proteins (Chang *et al.*, 2016; Zhu *et al.*, 2016; Zhu *et al.*, 2017) and these drug compounds have been collectively called “senolytics”.

Since Ibrutinib inhibits BTK, which has been shown to modulate the apoptotic and senescence responses of p53 (Althubiti *et al.*, 2016), we tested this inhibitor alongside a novel senolytic drug (ABT-263 or Navitoclax) to see if Ibrutinib could interfere with the effect of the senolytic drugs. When senescent and proliferating cells from different cell models were treated with the BTK inhibitor Ibrutinib and

ABT-263, a proposed senolytic drug, Ibrutinib on its own was not found to be senolytic and when combined with ABT263, the differences though statistically significant, as in the case of EJp16 and shDEP1 cells, were minimal and do not show biological relevance (Figure 3-19).

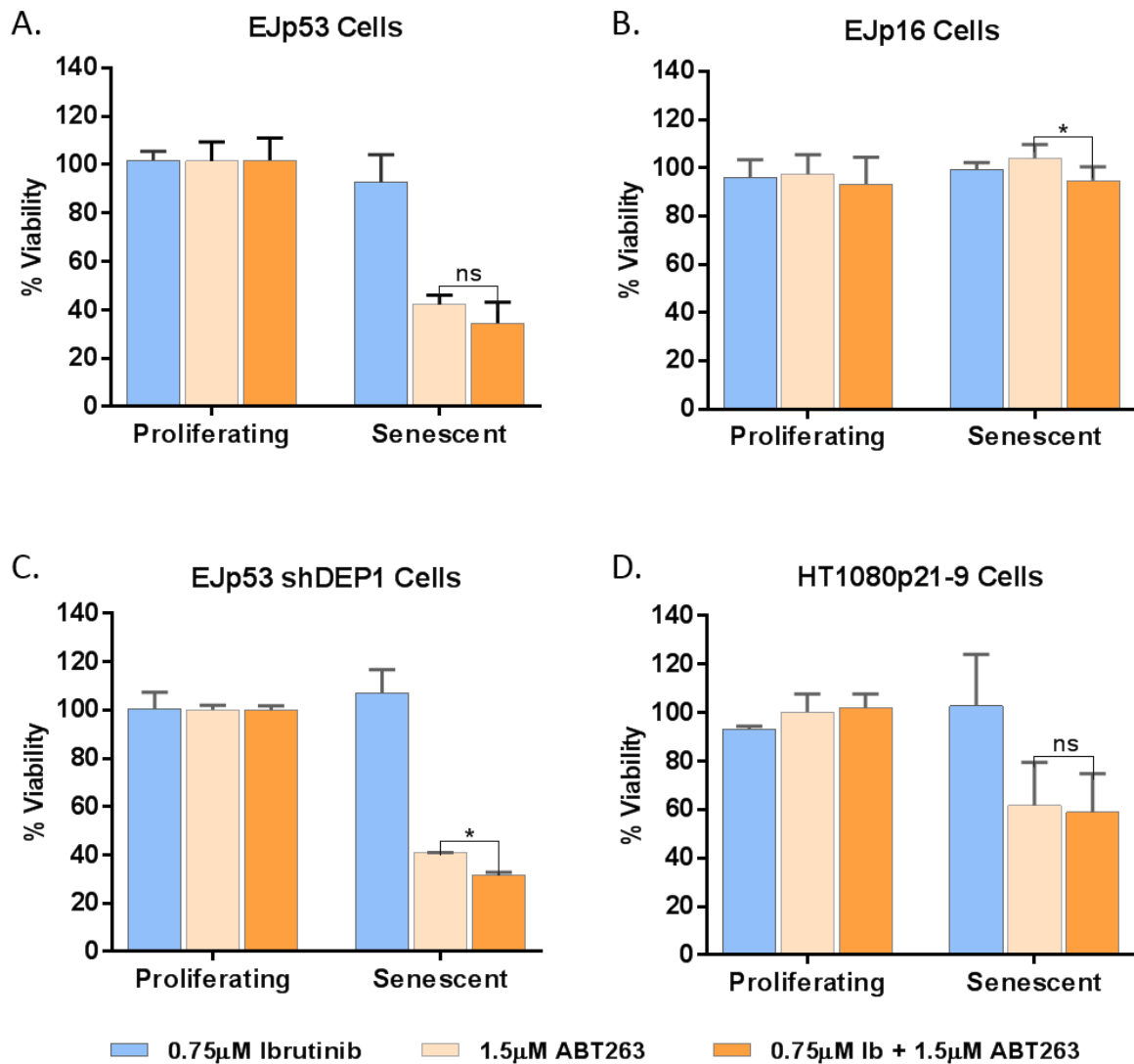


Figure 3-19 Effect of Ibrutinib on senescent cell viability

Proliferating and senescent EJp53 (A), EJp16 (B), EJp53shDEP1 (C) and HT1080p21-9 (D) cells were treated with ABT263 and Ibrutinib for 24 hours, after which MTS assay was performed. Percentage cell viability was calculated and presented using GraphPad Prism 7.0 software and paired t tests were used to determine statistical significance. Ibrutinib alone was not senolytic but in combination with ABT-263, led to more senescent cell death although not enough to be considered synergistic.

3.4.2 THE ROLE OF DEP1 IN CELLULAR SENESCENCE

Investigation of some of the potential novel markers of senescence identified in our lab, using immunohistochemistry, Western blot and qPCR as reported in previous sections have shown an overexpression of some of these proteins in aged and diseased tissues. In order to further characterize the role of the DEP1 protein, one these novel markers, in cellular senescence, gene silencing studies were carried out. shRNA for DEP1 was stably transfected into EJp53 cells and this was confirmed by Western blot (Figure 3-20 B). Tetracycline was washed off these EJp53 shDEP1 cells along with EJp53 control cells, in order to induce senescence. Proliferating and senescent cells were cultured in 6cm² plates and counted for two weeks using the T20 automated cell counter (Figure 3-20 A). DEP1 inhibition increased cell proliferation in control EJp53 cells but had no effect on the onset or maintenance of senescence in these cells as seen by the cell count. A colony formation assay also showed an increase in the ability of the proliferating EJp53shDEP1 cells to form colonies, with more than three times the number of colonies in the control EJp53 cells (Figure 3-20 C and D), also agreeing with data from the cell counts. These results indicate that although DEP1 plays a role in the proliferation of normal cells, it does not have any significant effect on the senescence growth arrest.

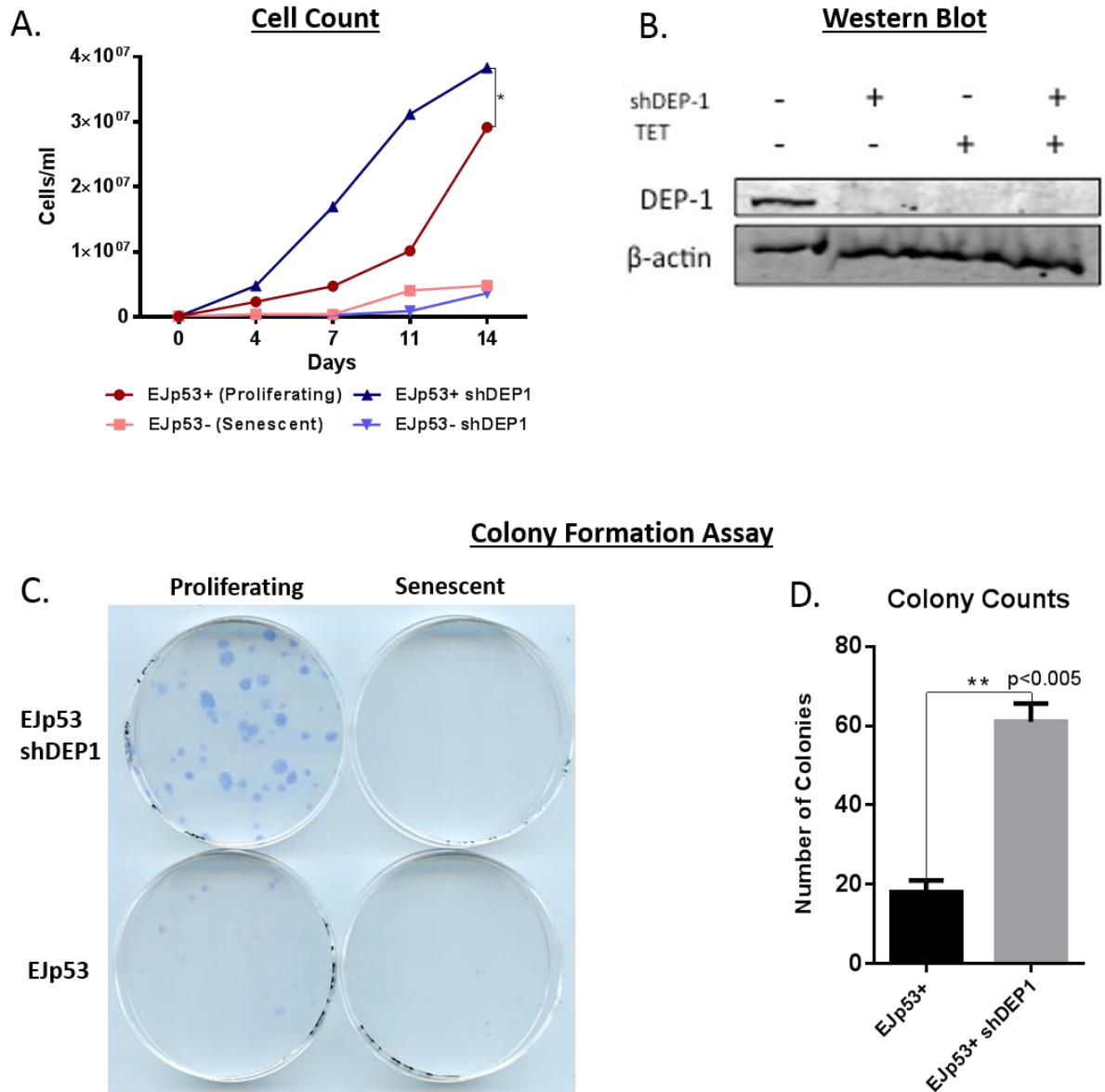


Figure 3-20 Gene silencing studies on DEP1 protein in EJp53 cells

shRNA for DEP1 was transfected into EJp53 cells and cells were selected with puromycin to generate stably transfected cell lines. shDEP1 cells were counted along with the control EJp53 cells for 14 days (A) and Western blot was used to confirm the silencing of DEP1 in these cells (B). Proliferating EJp53 shDEP1 cells increased in proliferation compared to the control EJp53 cells while the senescent cells showed no significant change in growth. A Ratio paired t test was used to show statistical significance in the cell count at $p < 0.05$. The shDEP1 cells also formed up to three times more colonies than the non-transfected control cells (C and D). The colony formation assay was done in triplicates and a two-tailed unpaired t test showed statistical significance. GraphPad Prism 7.0 was used to analyse the data.

3.4.3 THE ROLE OF B2MG IN CELLULAR SENESCENCE

Beta 2-Microglobulin (B2MG) was found to be overexpressed in aged skin and brain as well as in fibrotic liver tissues, further validating it as a potential marker of senescence. We decided to further investigate its involvement in cellular senescence.

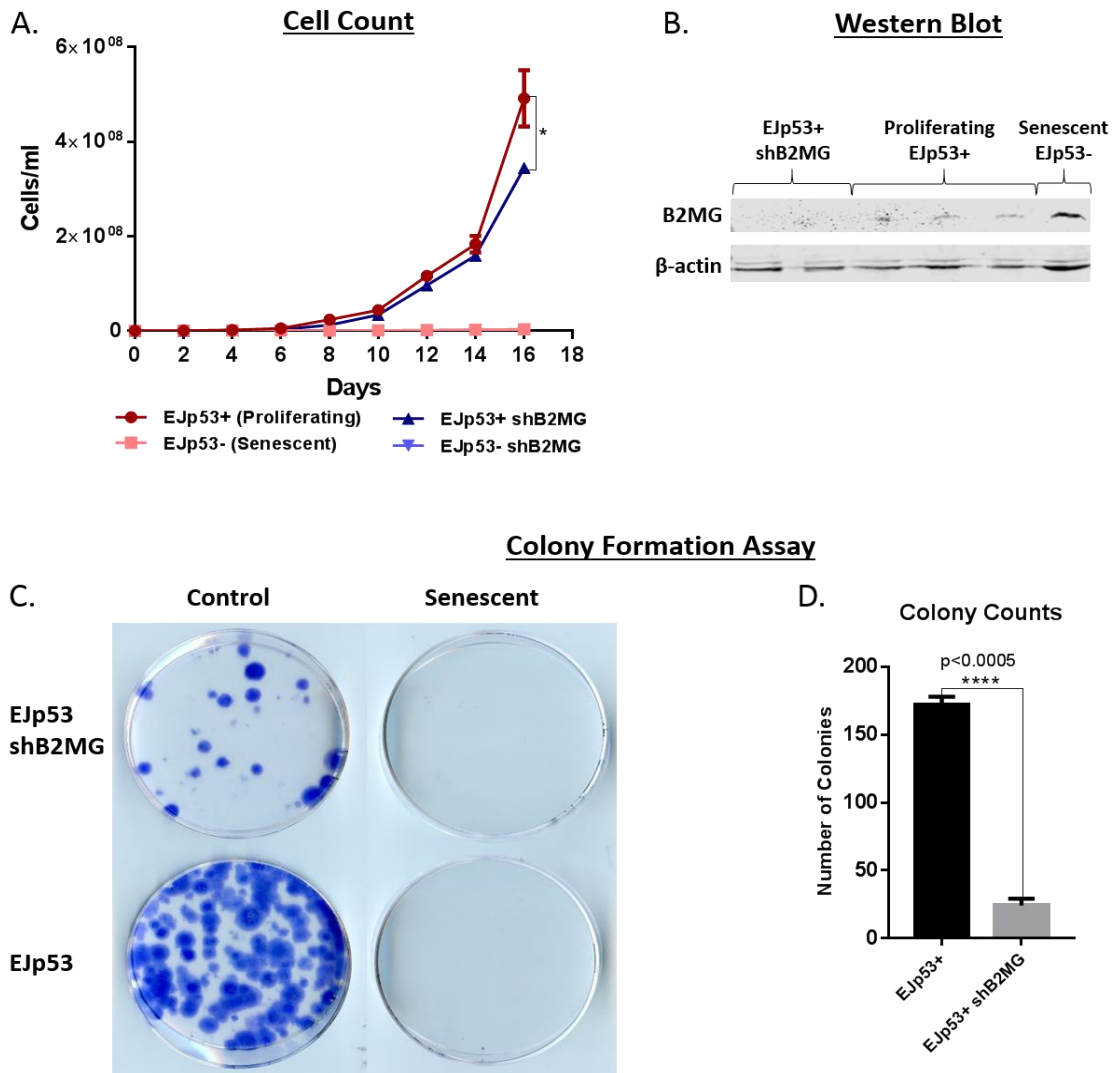


Figure 3-21 Gene silencing studies on B2MG protein in EJp53 cells

EJp53 cells were transfected with shRNA for B2MG and the cells were selected with puromycin to generate stably transfected shB2MG cells. shB2MG cells were counted along with control EJp53 cells for 14 days (A) while Western blot was used to confirm the silencing of B2MG in these cells (B). Proliferating control EJp53 cells showed increase in growth compared to the EJp53 shB2MG cells while the senescent cells showed no sign of proliferation. A Ratio paired t test was used to show statistical significance in the cell count at p<0.05. Control EJp53 cells also formed up to seven times more colonies than the shB2MG cells (C and D). The colony formation assay was done in triplicates and a two-tailed unpaired t test showed statistical significance. Data analysis was done using GraphPad Prism 7.0.

In order to understand better the role B2MG in senescence, shRNA for this gene was transfected into EJp53 cells and the cells were selected using 4 μ g/ml of puromycin for 2 weeks in order to generate a stably transfected cell line. Knockdown of B2MG was confirmed by Western blot (Figure 3-21 B). The proliferating shB2MG cells and EJp53 control cells were counted for 16 days along with their senescent counterparts (Figure 3-21 A). This was done to assess the involvement of B2MG in the attainment, maintenance or reversal of the permanent arrest seen in senescence. Silencing B2MG did not have any effect on the senescence of these EJp53 cells as the proliferating cells continued to double in number up to day 16 and did not senesce, although the control EJp53 cells grew at a higher rate than the shB2MG cells. The senescent cells showed no signs of proliferation nor reversal of senescence and remained growth inhibited for the entire 16 days. Colony formation assay showed that shB2MG cells were unable to form as many colonies as the control EJp53 cells, having about five times less number of colonies (Figure 3-21 C and D). This result agreed with data from the cell count and suggests that silencing B2MG decreased cell proliferation in growing cells but did not contribute to the senescence cell cycle arrest. It is not known why this is the case and further research will need to be carried out to fully understand this occurrence.

3.5 DISCUSSION

Novel markers of senescence preferentially expressed on the surface of senescent cells over non-senescent ones were identified in our lab using proteomic screening, and further confirmed by Western blot analysis of the membrane fraction of senescent cell lysates (Althubiti *et al.*, 2014). This was done in response to the lack of specificity of currently available senescence markers. Here we further validate and characterise these novel markers by defining in which specific senescence-related condition each of these markers is best expressed. The information obtained here will offer guidance on the use of these markers as diagnostic tools for senescent cell detection and also on therapeutic strategies for the elimination of senescent cells through the targeting of these novel markers.

Results from our findings are summarised in Table 3.1 and show that seven of these novel senescence markers namely B2MG, STX4, DEP1, NTAL, EBP50, ARMCX3 and BTK are overexpressed in either aged or diseased tissues from mice or human. Their expression however, may be both tissue and disease specific. Our data suggests, for instance, that B2MG, STX4, DEP1 and BTK are highly induced in fibrotic lesions and thus could be prognostic markers or therapeutic targets for fibrotic disease. Also, B2MG is overexpressed in aged brain and skin tissues but not in aged muscle and liver tissues, showing that its expression is tissue specific and could serve as a marker for ageing in some but not all tissues. EBP50 on the other hand was upregulated in aged skin and brain but downregulated in liver, muscle and the eyes. It could be that EBP50 levels decrease with age in some of these tissues. Also, B2MG was downregulated in aged muscle and aged liver, while ARMCX3 and p16 were downregulated in the aged eyes. In the lung cancer samples however, p16 was negative for all 7 patients.

Overall, the data obtained from the screening of these tissues suggests that some of the novel markers could serve as markers of ageing in certain tissues but are not universal markers for ageing. Nevertheless, owing to the overexpression of these novel markers in senescent cells and the involvement of senescence in ageing, fibrosis and cancer, the upregulation of some of these

markers in ageing and disease might be indicative of cellular senescence in the pathology of these conditions. It is interesting to see that the CDK inhibitor p16 was downregulated in lung cancer, while all other markers tested were upregulated. Altered p16 expression has been reported in non-small cell lung cancers and correlates with poor patient outcomes (Vos *et al.*, 1995; Gazzeri *et al.*, 1998; Huang *et al.*, 1999; Groeger *et al.*, 1999; Tam *et al.*, 2013). Since we did not have a record of the patients' treatment history, it is not known if the tissues could have undergone therapy induced senescence. Also, as it is a well postulated notion that the senescence barrier has to be overcome for malignancy to occur (Hanahan & Weinberg, 2011), it could mean that senescence growth arrest was indeed overcome in the lung cancer but other elements of senescence such as the SASP still linger and are being detected by these novel markers which are not necessarily cell cycle inhibitors. It would therefore be useful to study the relationship between the senescence secretome and markers like STX4, DEP1 and BTK.

Bruton's Tyrosine Kinase (BTK), one of the markers identified which already has inhibitors in the market for the treatment of B-Cell malignancies (Hendriks *et al.*, 2014; Hutchinson & Dyer, 2014), was found to have no differential effect on the senescence of pulmonary fibroblasts from IPF patients and normal subjects. The growth rate of fibroblasts from the Ibrutinib treated groups did not differ from those treated with only DMSO (Figure 3-17) and the cells all senesced by day 52 regardless of disease or treatment, as evidenced by the positive SA β -Gal staining (Figure 3-18). The BTK inhibitor Ibrutinib was also not found to be senolytic in the cells tested and although it contributed to more senescent cell death when used in combination with ABT-263, this was not biologically significant. It is however likely that BTK inhibition could find applications in other senescence-related diseases other than lung fibrosis. Inhibiting BTK could therefore interfere with the senescence response and prevent the accumulation of senescent cells. Further studies will be needed to adequately characterise all of these novel markers of senescence across more tissues and diseases.

Silencing of DEP1 and B2MG in EJp53 cells using shRNA revealed that these two markers did not prevent or reverse the permanent cell cycle arrest in these

cells but instead had opposite effects on cell proliferation (Figure 3-20 and Figure 3-21). While shDEP1 caused increased proliferation in growing EJp53 cells, shB2MG reduced the rate of proliferation in these cells but neither shRNA had an effect on the senescent cells. It is however noted that these results are still considered preliminary due to the fact that the appropriate control shRNA was not used in these experiments. The non-transfected EJp53 cells were used as the controls instead of shLuciferase cells. This was due to unavailability of this shRNA at the time of carrying out these experiments. It also would have been best to check that B2MG and DEP1 were knocked down not only at the protein level but also at the mRNA level. In the future, these points should be taken into account when designing gene silencing experiments.

Biomarker discovery is an important and yet challenging field in biomedical science research (de Jesus & Blasco, 2012), and more so the discovery of markers of senescence, owing to the erratic gene expression changes observed in senescent cells (Coppe *et al.*, 2010; Young *et al.*, 2013; Sharpless & Sherr, 2015). Available senescence markers are non-specific and therefore not reliable. Our newly characterized markers of senescence are expressed varyingly but consistently across different tissues and diseases. They could therefore be used either alone or in combination with other markers as tissue specific and disease specific markers of senescence and ageing. A universal senescence marker will need to be very robust and exclusive to the senescent state (Lawless *et al.*, 2010; Matjusaitis *et al.*, 2016). A suitable biomarker should be able to distinguish between senescent and non-senescent cells *in vitro* and *in vivo*. Its expression should be detectable regardless of sample preparation. The novel markers tested in this study have been detected both in fresh cells or tissues, as well as in FFPE samples, giving them an advantage over a marker like the SA- β -Gal which relies on enzymatic activity in fresh or frozen samples. The expression of a senescence marker if at all in non-senescence states should be very minimal and easy to exclude in assays. B2MG for instance is overexpressed in other conditions such as renal disease, therefore its use as a senescence marker may need to be accompanied by tests to exclude renal disease. Nonetheless, a reliable and consistent combination of markers such as the ones identified in our laboratory and listed in this study, would be valuable to research on senescence and ageing.

CHAPTER 4 TARGETING SENESCENT CELLS WITH MOLECULARLY IMPRINTED POLYMERS (MIPs) AND ANTIBODY-DRUG CONJUGATES (ADCs).

The elimination of senescent cells is increasingly being explored as a therapeutic strategy towards healthspan improvement and for the management of several age-related diseases, including cancer. The deleterious effect of the senescence secretome arising from long term accumulation of senescent cells has been linked to many diseases, making the targeting of these cells a crucial and novel strategy for fighting cancer, fibrosis and various age-related pathologies (Baker *et al.*, 2011; Naylor *et al.*, 2013; Baker *et al.*, 2016; Chang *et al.*, 2016; Demaria *et al.*, 2017; Baar *et al.*, 2017; de Magalhães & Passos, 2017).

This study aims to use Molecularly Imprinted Polymers (MIPs) (Canfarotta *et al.*, 2016a; Smolinska-Kempisty *et al.*, 2016) and Antibody-Drug Conjugates (ADCs) (Casi & Neri, 2012) to target senescent cells, thereby defining novel detection and therapeutic strategies for age-related diseases and cancer. These nanoparticle sized MIPs are also referred to as nanoMIPs.

Proteins preferentially expressed on the surface of senescent cells were previously identified (Althubiti *et al.*, 2014) through proteomic analysis of the membrane fraction of senescent cell lysates. Some of these proteins can potentially be targeted for drug delivery into senescent cells, owing to the extracellular positioning of their epitopes. The work presented here combines the specificity and selectivity of MIPs and ADCs for senescent cell membrane-bound targets and the potency of cytotoxic drugs to bring about senescent cells detection and clearance.

Having seen an overexpression of Beta 2 Microglobulin (β 2M or B2MG) in senescent cells and in older tissues (Althubiti *et al.*, 2014), and also due to the external positioning of its epitope, MIPs and ADCs were generated to target the extracellular portion of this protein for the purpose of detection as well as drug delivery into senescent cells.

4.1 MODELS OF CELLULAR SENESCENCE USED FOR MIPs AND ADC TARGETING

Models of cellular senescence used for the MIPs and ADC experiments were the EJp16 (Macip *et al.*, 2002), EJp21 (Fang *et al.*, 1999) and EJp53 (Sugrue *et al.*, 1997) bladder cancer cells, which have a tetracycline on/off system that enables them senesce upon overexpression of p16, p21 or p53 respectively (Figure 4-1). These cells are a handy model of premature senescence since they can become senescent and display the characteristic features 3-4 days after tetracycline removal.

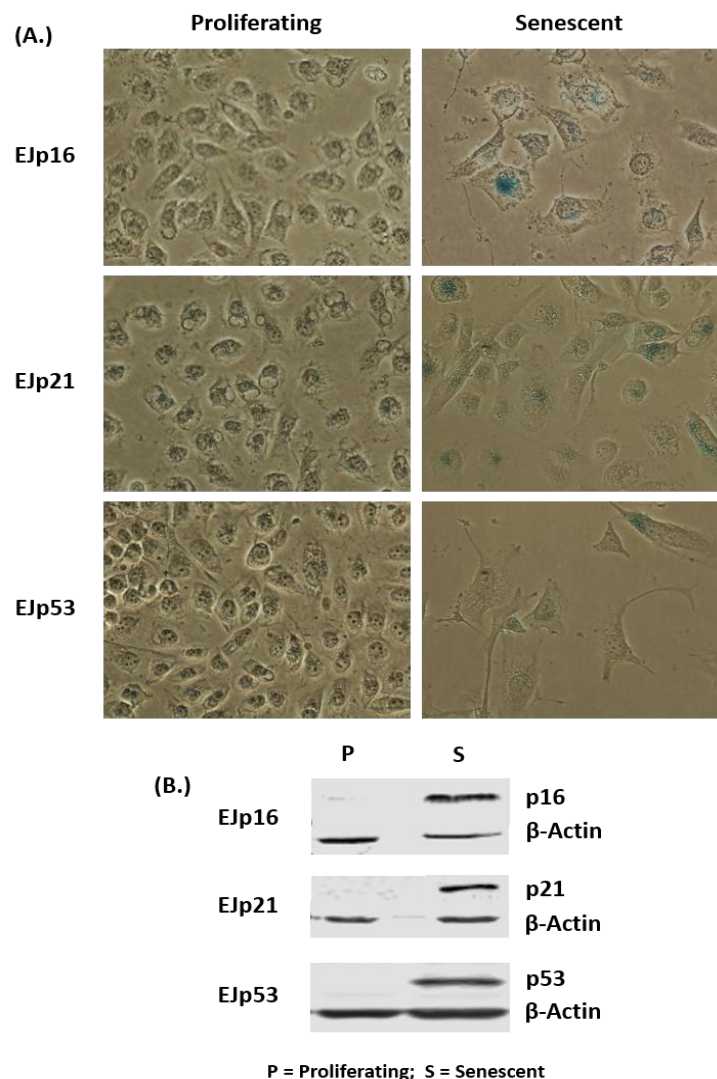


Figure 4-1 SA β -Gal and Western blot validation of EJ senescent cell models.

Senescent EJp16, EJp21 and EJp53 bladder cancer cells display growth arrest, a flattened, enlarged morphology and stain positive for the senescence associated β -galactosidase (SA β -Gal) compared to their proliferating counterparts (A). They also overexpress p16, p21 and p53 respectively as observed by Western blotting (B). β -actin is used as loading control.

Western blot analysis of the EJp16, EJp21 and EJp53 bladder cancer cells, showed a higher expression of B2MG and DEP1 proteins in senescent cells than in proliferating ones (Figure 4-2 and Figure 4-3), confirming the first observation by Althubiti and colleagues (Althubiti *et al.*, 2014). The expression of these proteins was found to be greater in the EJp16 model than in the EJp21 or EJp53 cellular models, although the latter two models displayed a more distinct typical senescence morphology in culture than the EJp16 cells. Because of this, EJp16 were chosen as the main model of senescence for this study.

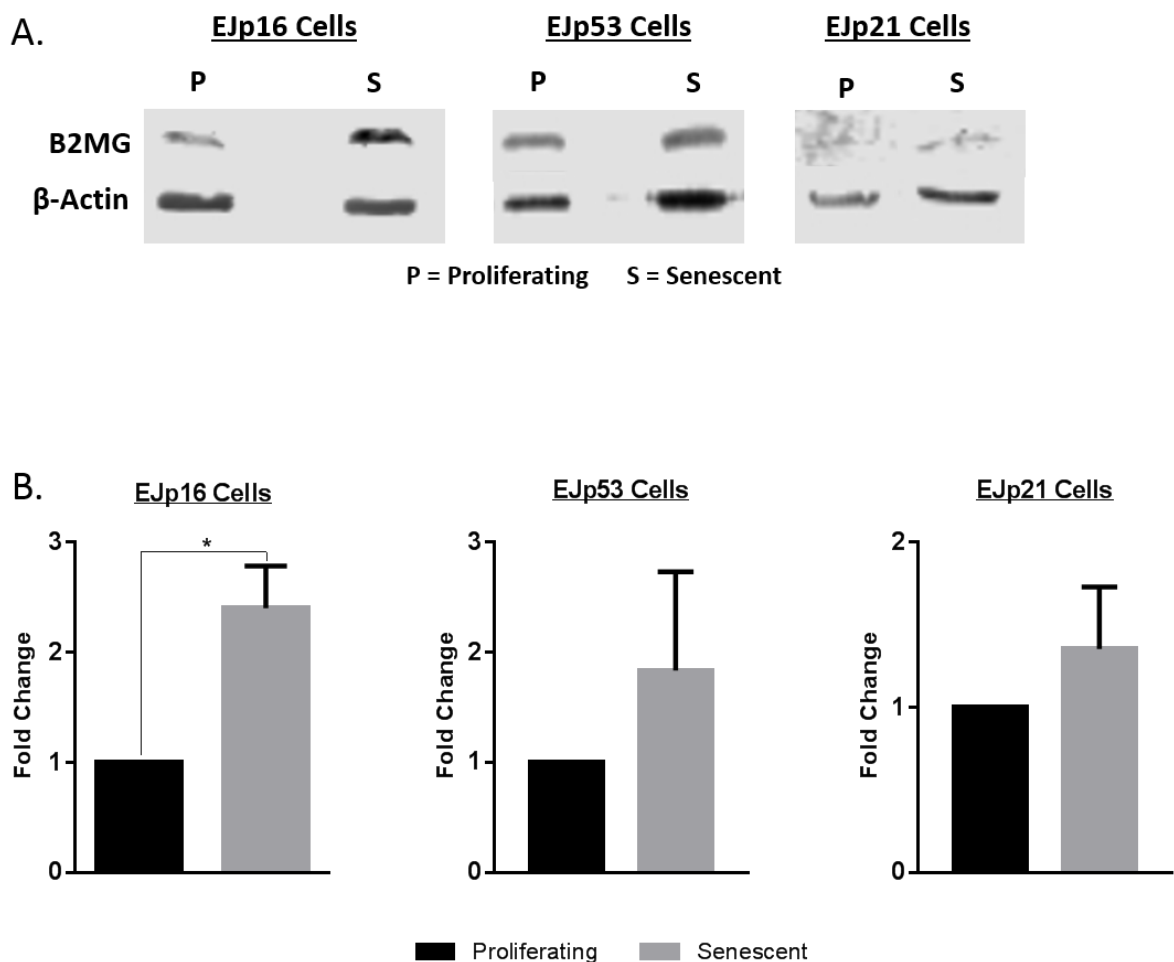


Figure 4-2 Western blot analysis of B2MG in EJ models of senescence.

Western blot bands showing B2MG protein expression in EJp16, EJp21 and EJp53 cells with β -actin used as a loading control (A). Senescence was induced by culturing cells without tetracycline for 4 days. The corresponding fold change of the quantified protein bands are also shown (B). Results are from three independent experiments and are presented as mean \pm SD. Unpaired two-tailed student's t test analysis indicates statistical significance in B2MG expression for EJp16 cells at $p < 0.05$.

More than a two-fold increase in the expression of B2MG was observed in senescent EJp16 cells and this was statistically significant, while B2MG expression in EJp53 and EJp21 cells did not reach statistical significance at $p < 0.05$ (see Figure 4-2). DEP1 expression was also higher than two-folds in the senescent EJp16 cells, about two-folds in EJp53 cells, and only a little more than a fold increase in EJp21 cells. None of these was however statistically significant at $p > 0.05$ (see Figure 4-3).

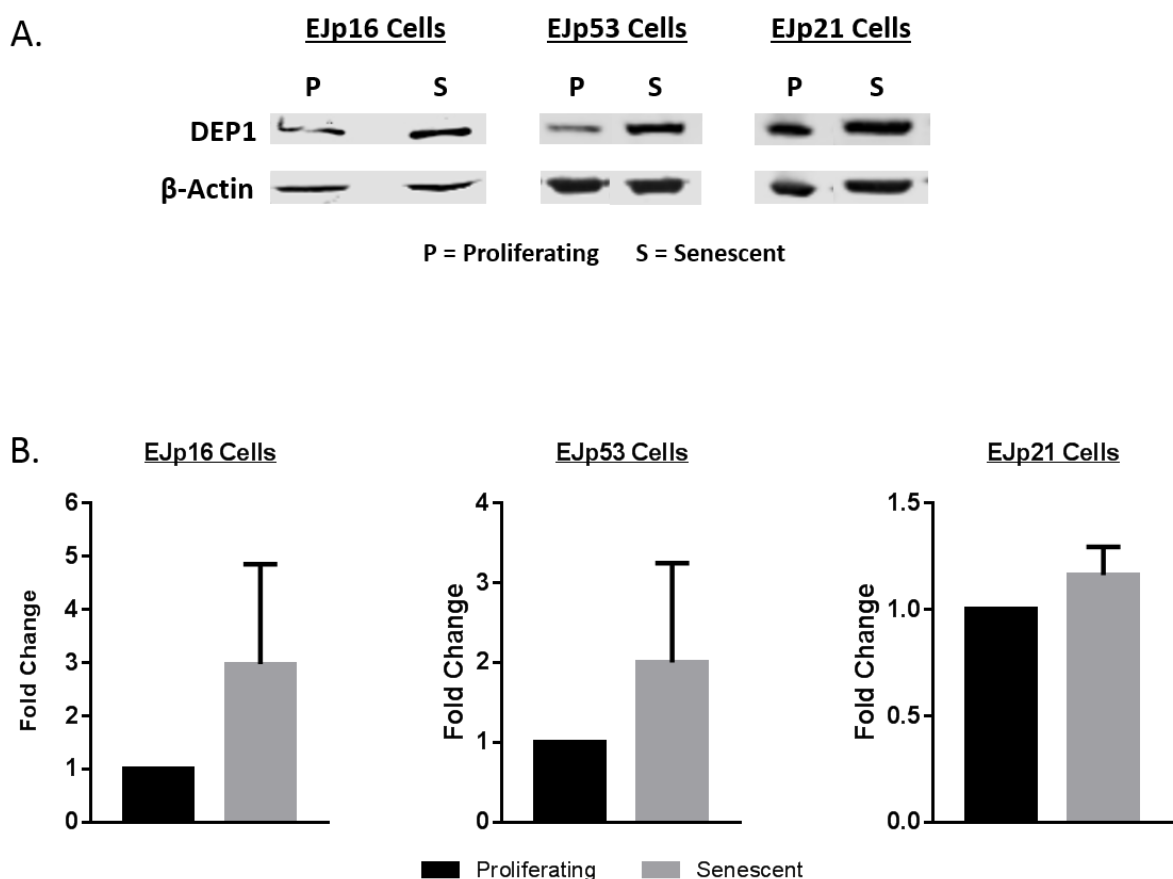


Figure 4-3 Western blot analysis of DEP1 protein expression in EJ cells.

Expression of DEP1 protein in proliferating and senescent EJp16, EJp21 and EJp53 cells by Western blot, using β -actin as loading control (A). Senescence was induced by growing cells without tetracycline for 4 days. Corresponding quantification of the protein bands are shown as fold change (B) although with no statistical significance at $p < 0.05$ using student's t test. Results are from three independent experiments and are presented as mean \pm SD.

4.2 OPTIMIZATION OF MIP BINDING ASSAYS

Proliferating and senescent EJp16 cells were incubated with Fluorescein-tagged MIPs that were designed to target an extracellular epitope of the B2MG protein. Beta-2 Microglobulin (B2MG) is a low molecular weight protein with 99 amino acid residues in length and has sequence homology to immunoglobulins, with seven strands of β sheets (Bernier, 1980; Trinh *et al.*, 2002) (see Figure 4-4).

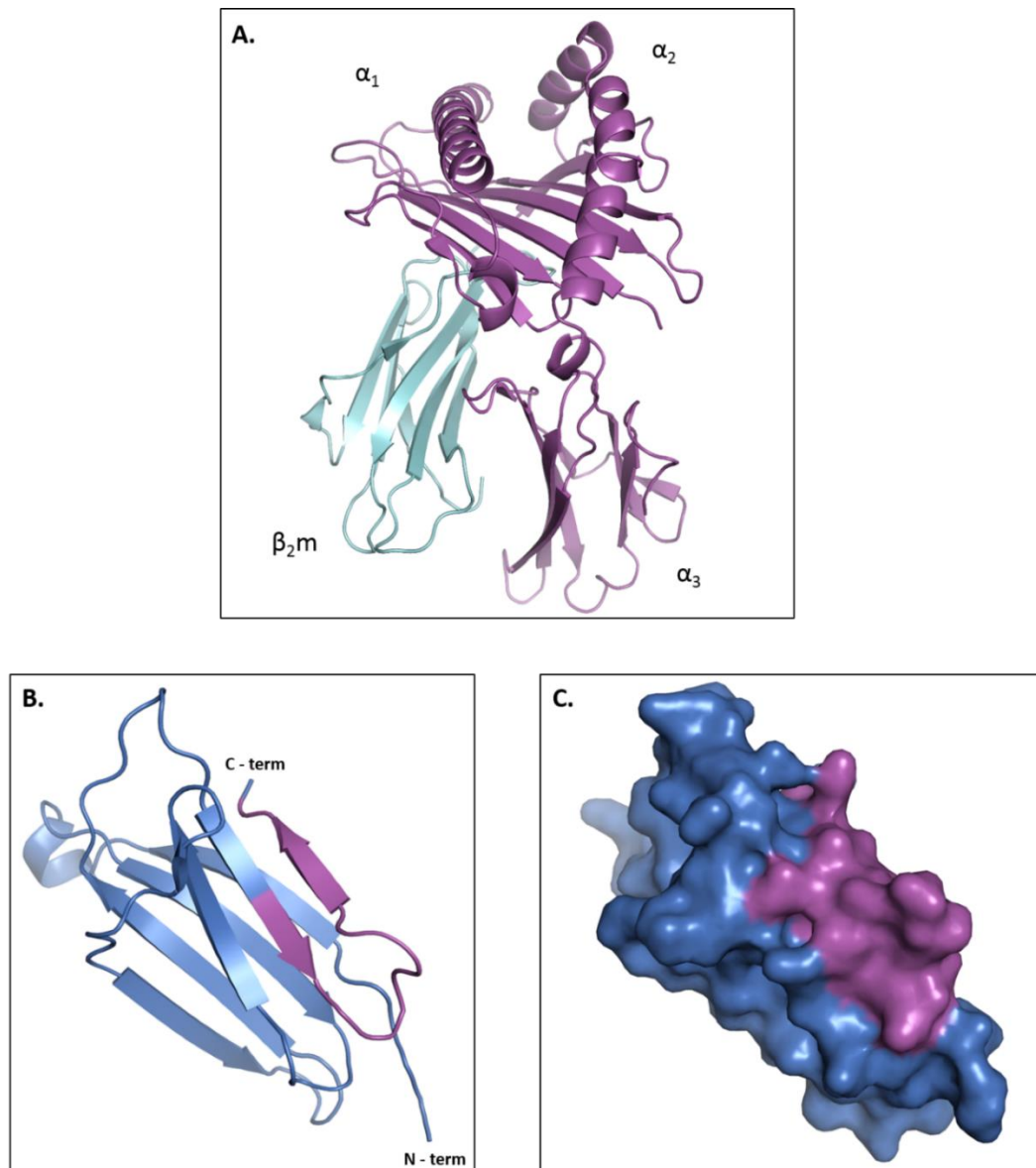


Figure 4-4 Structure of human histocompatibility antigen HLA-A and β_2 Microglobulin

Schematic representation of the structure of HLA-A2 showing the positions of the α_1 , α_2 , α_3 and β_2M domains (A). The crystal structure (B) and surface presentation (C) of β_2M are also shown, with the epitope used for MIPs design indicated in magenta near the C-terminal (B and C). Structure adapted from (Bjorkman *et al.*, 1987), using PyMOL 1.0.

B2MG is a component of the major histocompatibility complex class I (MHC I) molecules of the immune system and participates in the presentation of peptide antigens to immune cells (Smith *et al.*, 2015; Filiano & Kipnis, 2015; Zhang *et al.*, 2016). B2MG makes up the non-covalently bound light chain of the class I human leukocyte antigen (HLA class I) complex and is an important cell surface structure (Bernier, 1980; Trinh *et al.*, 2002). MIPs were generated to target an epitope at the C terminal of B2MG, representing amino acids 101 – 115, with sequence **RVNHVTL SQPKIVKW**, highlighted in magenta in Figure 4-4 B and C.

Different experiments were performed in order to ascertain the optimal conditions for efficient and reproducible MIP binding assays. Similarly to antibodies, the concentration, wash steps, as well as incubation time was found to affect the sensitivity and fluorescence signal obtained from Fluorescein-tagged B2MG MIPs, as observed by fluorescence microscopy (see Figure 4-6, Figure 4-9, Figure 4-10 and Figure 4-20) and FACS binding assays (see Figure 4-7, Figure 4-8 and Figure 4-16).

A 1:5 dilution (20%) of B2MG-targeted MIPs (0.38mg/ml stock), tagged with fluorescein molecules, was made using culture medium, and added to cells grown and well attached in 6-well plates. The MIP particles were seen to bind indiscriminately to cells at this high concentration (see Figure 4-6). Also, the fluorescence intensity observed in images taken 6 hours later was reduced in comparison to images taken after 30 minutes and after 1 hour. However these images did not reveal sufficient information about the specificity of the MIPs as the 20% concentration was too high and the particles were seen floating around in a non-specific manner within the culture media. To curb this problem, it was decided that the MIPs' final assay concentration and the incubation times would have to be adjusted. Wash steps were also included in the protocol where necessary to remove unbound MIPs.

In addition to Beta 2 Microglobulin (B2MG), MIPs were equally designed to target the extracellular epitope of the density enhanced phosphatase (DEP1) which was also found to be overexpressed on the surface of senescent cells. A schema for the application of MIPs in the detection and elimination of senescent cells is proposed by the model in Figure 4-5.

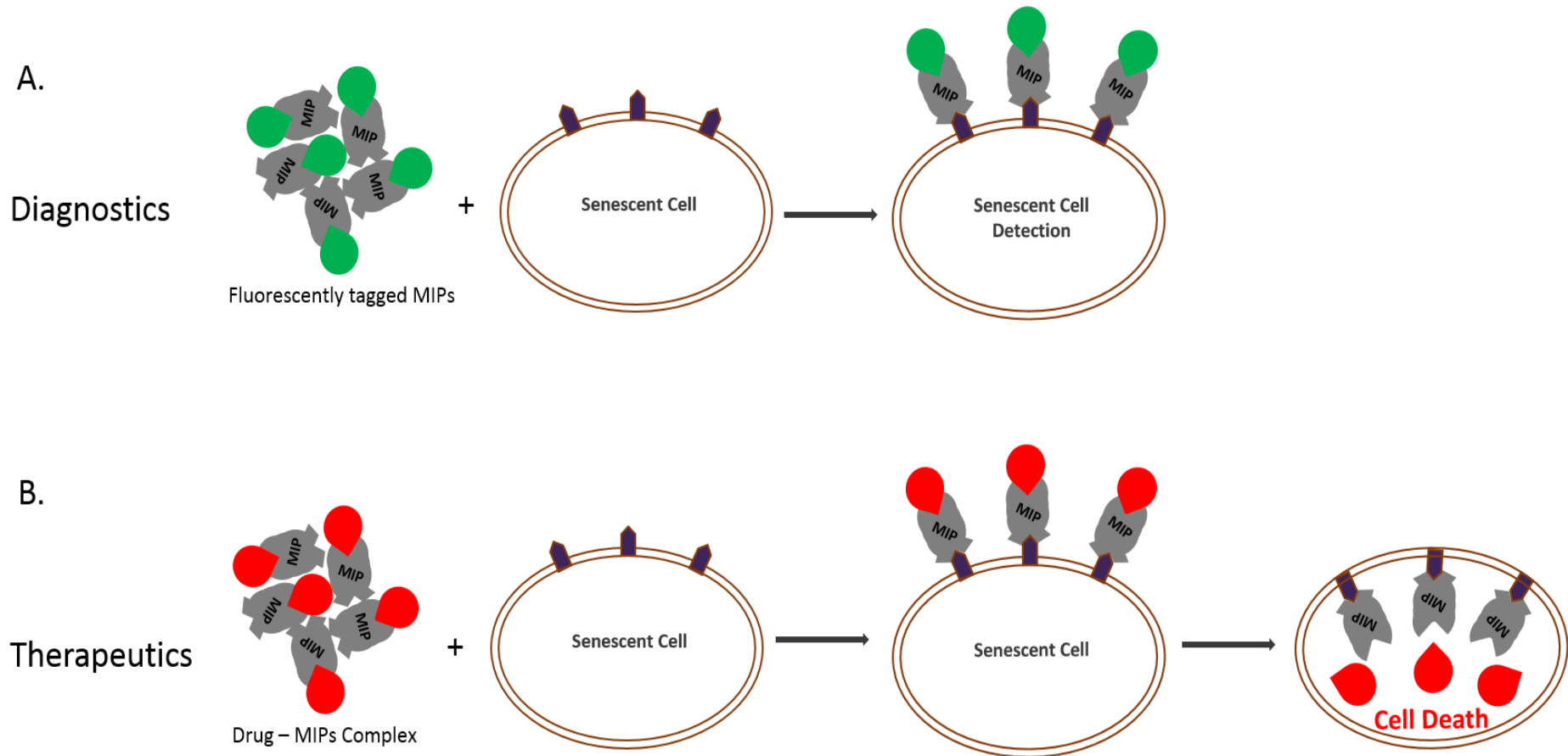


Figure 4-5 A schematic representation of senescent cell targeting by molecularly imprinted polymers (MIPs). Fluorescently-tagged MIPs can be used to identify protein markers on the surface of senescent cells for diagnostic purposes (A). Toxic drug compounds can also be conjugated to MIPs and be delivered into senescent cells (B), to kill these cells after binding to cell surface markers and being internalized in the senescent cells.

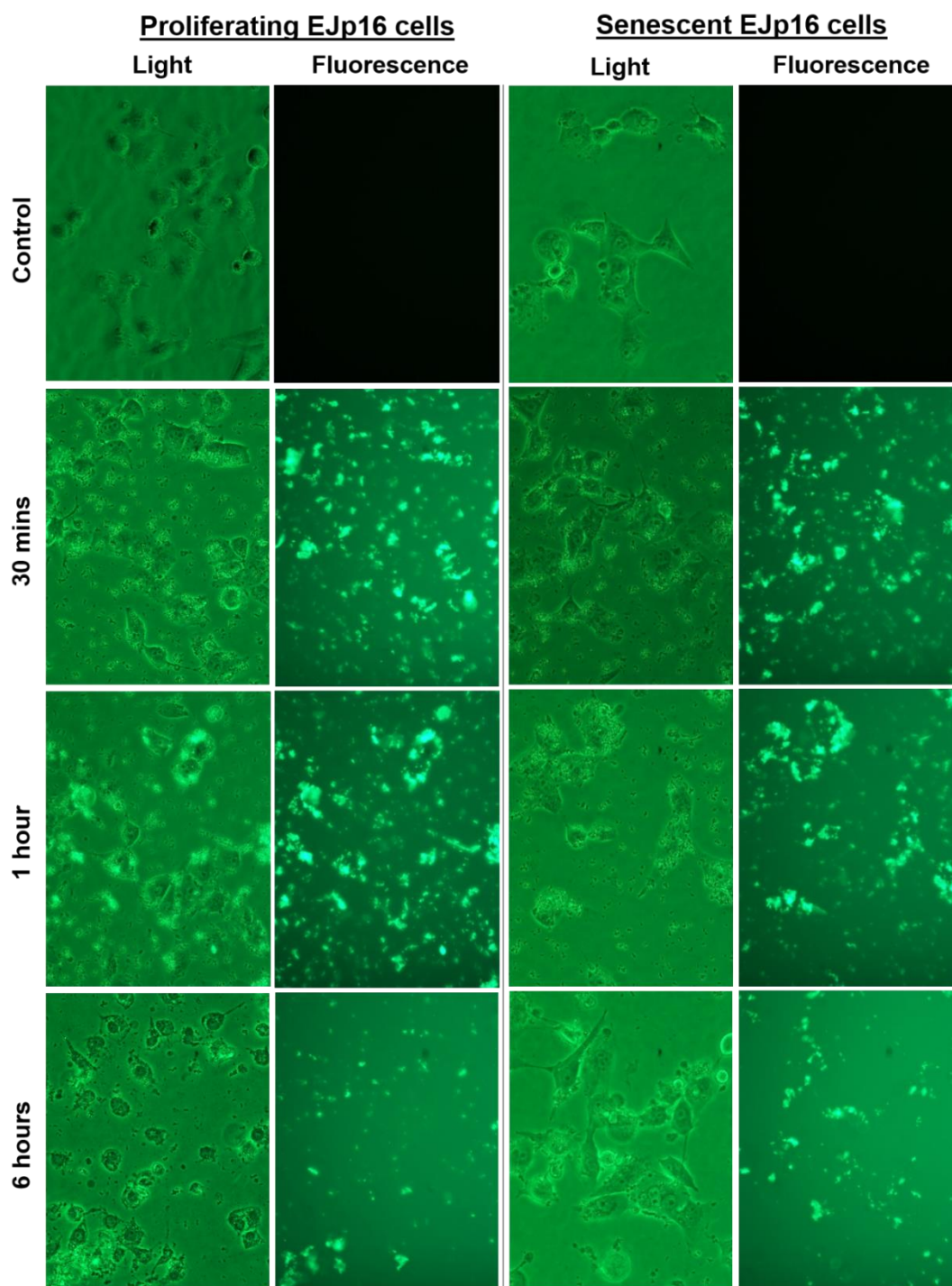


Figure 4-6 Fluorescence microscope images of 20% B2MG MIPs in EJp16 cells. Fluorescein-tagged B2MG MIPs diluted 1:5 (20%) in DMEM cell culture medium were added to EJp16 cells grown in 6-well plates. Fluorescence microscope images were taken after 30minutes, after 1 hour and after 6 hours. The above figure shows images taken using the green interference (GIF) filter, with the microscope light on (Light) and with the lights switched off (Fluorescence). Control samples had no MIPs.

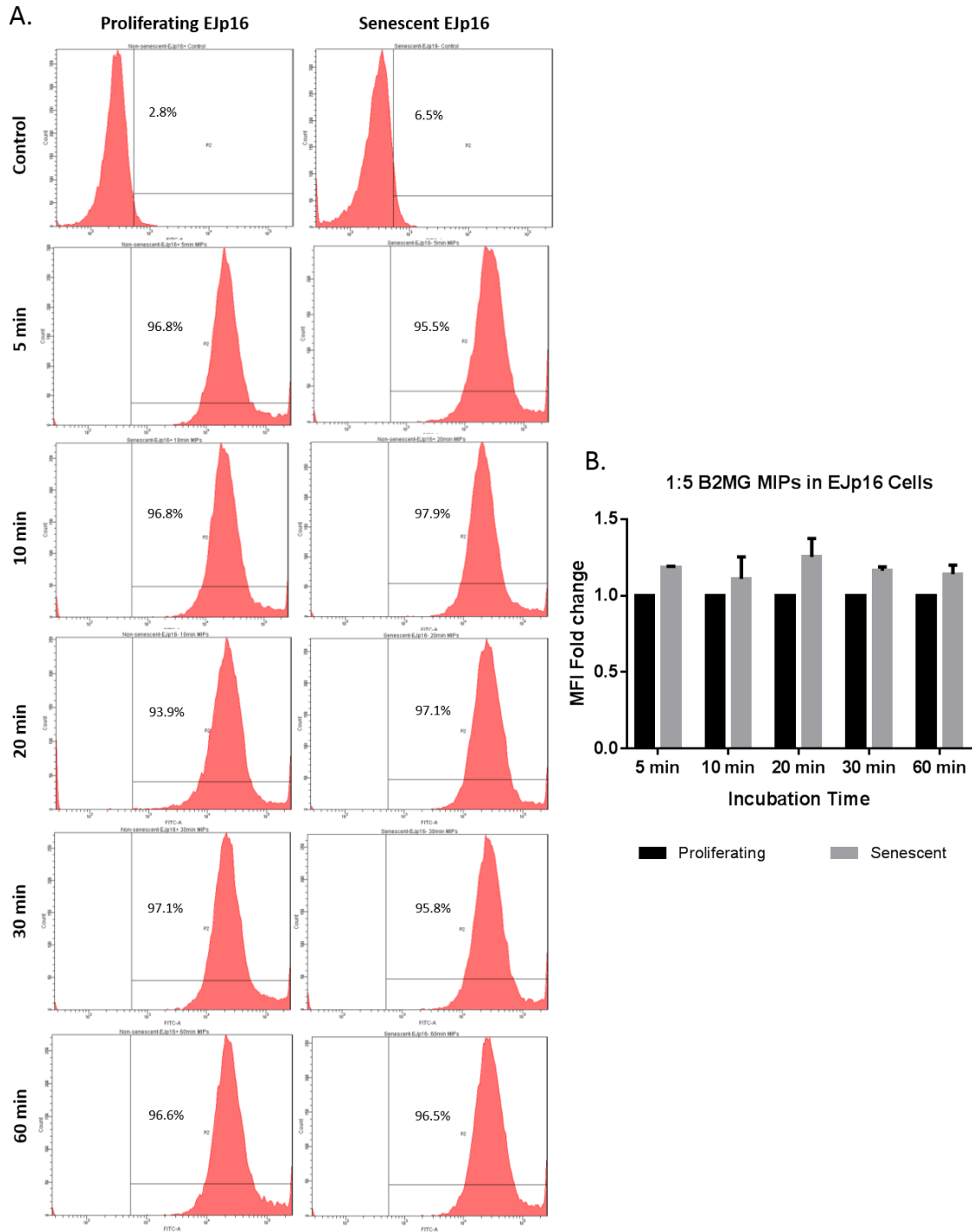


Figure 4-7 FACS binding assay with 20% B2MG MIPs in EJP16 cells. EJP16 cells were incubated (stained) with Fluorescein-tagged B2MG MIPs diluted 1:5 in FACS buffer, in polystyrene FACS tubes, on ice. The samples were read by flow cytometry after 5, 10, 20, 30 and 60 minutes. Unstained control samples were used to gate the histograms and the percentage of positive cells recorded (A). Fold changes of the mean fluorescence intensity (MFI) of senescent cells over proliferating cells were also calculated and graphs plotted using GraphPad Prism software (B). Results are from a single experiment in duplicates and are presented as mean \pm SD.

A modified antibody binding assay protocol was also used to detect the binding of these fluorescein-tagged B2MG MIPs by Flow Cytometry and the samples were read using the FITC channel. In the initial experiment, proliferating and senescent EJp16 cells were collected and incubated with a 1:5 (20%) concentration of MIPs, diluted in FACS buffer (2% FBS in PBS) on ice. In this experiment, the MIPs were applied as a leave-on stain and samples were read after 5, 10, 20, 30 and 60 minutes. Similarly to what was observed using the fluorescence microscope, this concentration of MIPs was too high to be able to detect any significant difference between senescent and proliferating cells by FACS, as all cells stained very positive for FITC (see Figure 4-7).

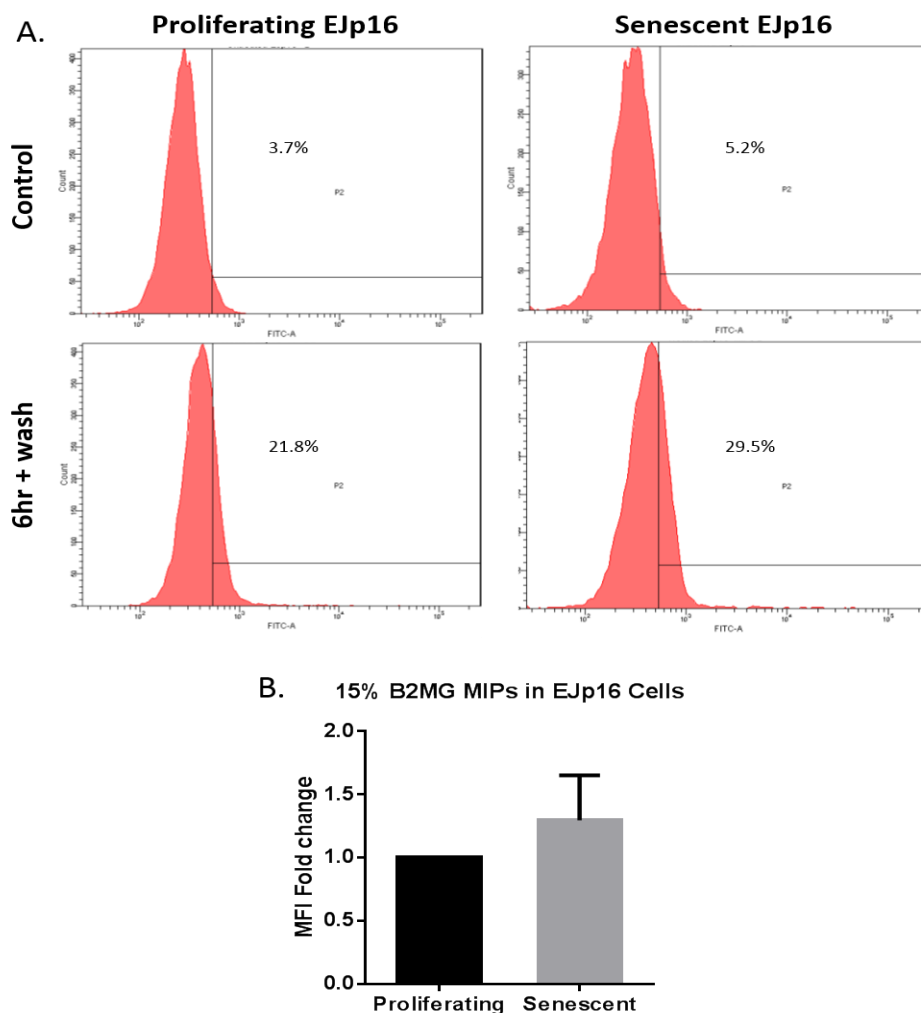


Figure 4-8 FACS binding assay for 15% B2MG MIPs in EJp16 cells.

EJp16 cells stained with MIPs for 6 hours were washed and their fluorescence measured by FACS. Unstained control samples were used to gate the histograms (A). Fold changes of the mean fluorescence intensity of senescent cells over proliferating cells were calculated (B). Results from a single experiment in duplicates are presented here as mean \pm SD. There was no statistical significance in the fold change at $p < 0.05$.

Next, proliferating and senescent EJp16 cells were incubated with 15% B2MG-targeted MIPs in a 6-well plate for 6 hours at 37°C. 300µl of the MIPs solution was added to cells in 1,700µl of culture media, bringing the final volume to 2ml. The control samples were incubated with 300µl of distilled water instead of MIPs, at 37°C for 6 hours. After 6hrs, all cells were collected using trypsin and washed with 2ml of PBS by centrifugation, to remove unbound MIPs (Figure 4-8). Cell pellets were re-suspended in FACS buffer before samples were read by FACS and the fluorescence measured.

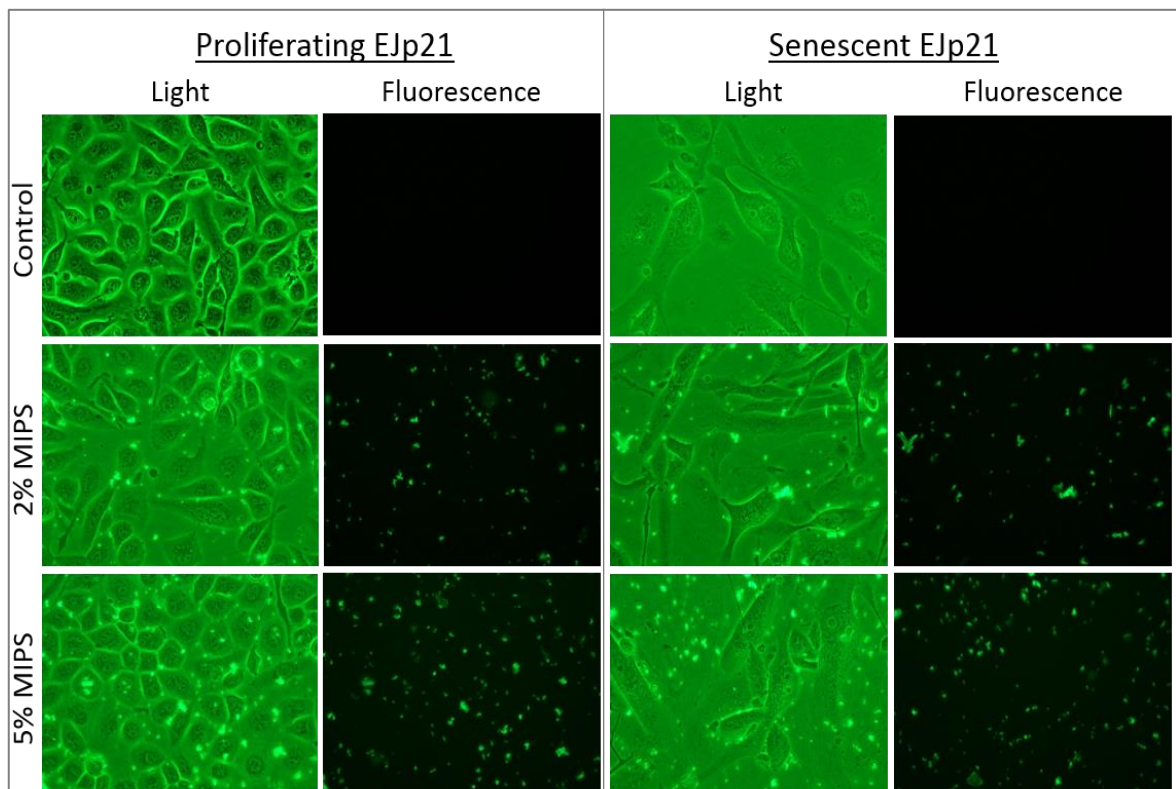


Figure 4-9 Fluorescence microscope images of 2% and 5% MIPs in EJp21 cells. Fluorescein-tagged B2MG MIPs were added to senescent and proliferating EJp21 cells in 6-well plates, in 2% and 5% concentrations. Cells were incubated at 37°C for 2 hours before being imaged. These lower concentrations provided a better view of the particles although still with no observable difference between senescent and proliferating cells due to the presence of unbound MIPs particles floating in the culture medium.

In order to obtain a more sensitive detection of B2MG-targeted MIPs by fluorescence microscopy or FACS, the concentration of MIPs used was further decreased to 5% and 2% (1:20 and 1:50 dilution). In the following experiments, EJp21 cells were used instead of EJp16 because they displayed a more

distinctive morphology when senescent. Proliferating and senescent EJp21 cells were incubated with the MIPs at 37°C for 2 hours before images were taken on the fluorescence microscope (see Figure 4-9).

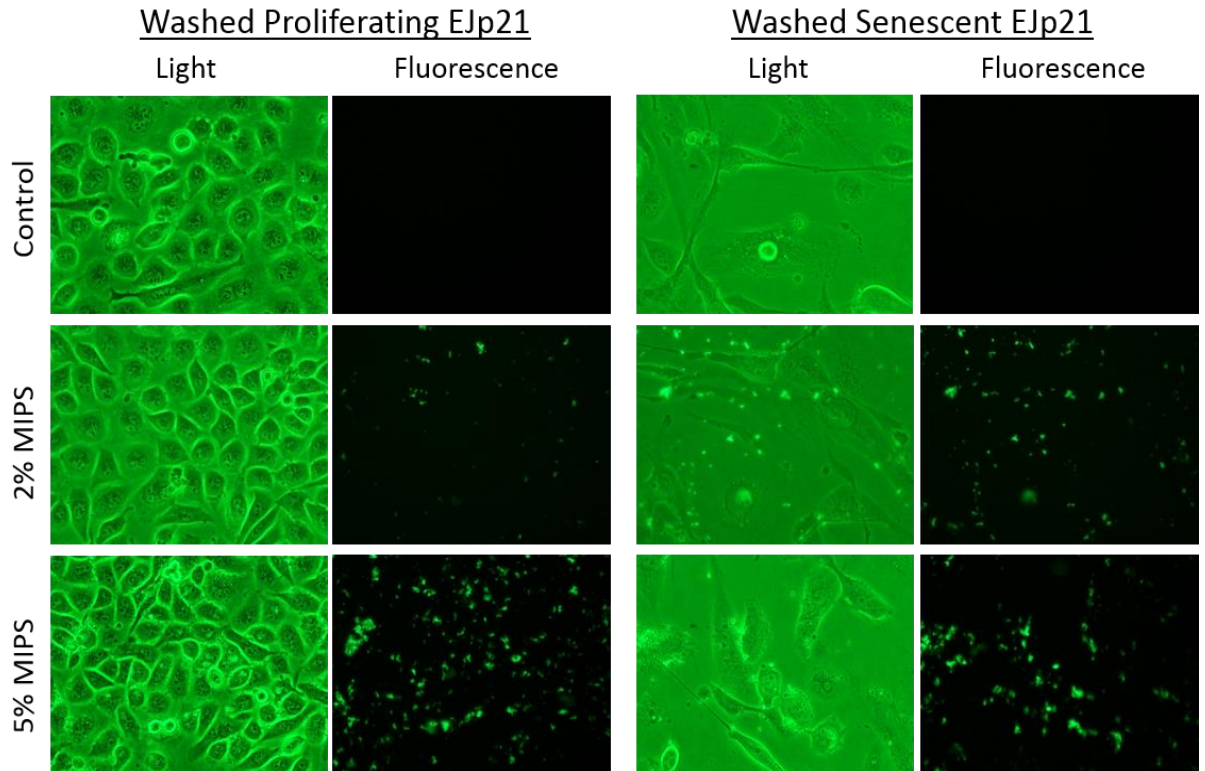


Figure 4-10 Fluorescence microscope images of MIPs in EJp21 cells after wash steps.

MIPs were washed off cells two hours after incubation and cells were re-incubated at 37°C for another 2 hours before images were taken. Washing off unbound MIPs gave clearer images and the 2% concentration was more sensitive than the 5% concentration of MIPs.

Although the culture media appeared clearer than in the 20% concentration, there was still no observable difference in MIPs binding between senescent and proliferating cells when viewed under the fluorescence microscope. To further address this problem, the culture media which contained MIPs was aspirated off and cells were gently washed with warm media to remove unbound MIPs before replacing the media. Samples were returned to the incubator and images re-taken after another two hours (4 hours incubation in total). The MIPs which remained after the wash step were bound to cells and could be seen distinctly around the membrane of the enlarged senescent cells (Figure 4-10). B2MG-targeted MIPs also showed greater affinity for the membrane of senescent cells

than that of proliferating cells, as images showed more particles surrounding the senescent cell membranes. Cells with the 2% MIPs concentration gave less non-specific binding when compared to the 5% concentration (see Figure 4-10), and this concentration was finally chosen for the experiments.

4.3 FLUORESCINE-TAGGED B2MG MIPs BIND TO SENESCENT CELLS *IN VITRO* AND ARE INTERNALIZED

4.3.1 FLUORESCENCE AND CONFOCAL MICROSCOPY OF MIPs

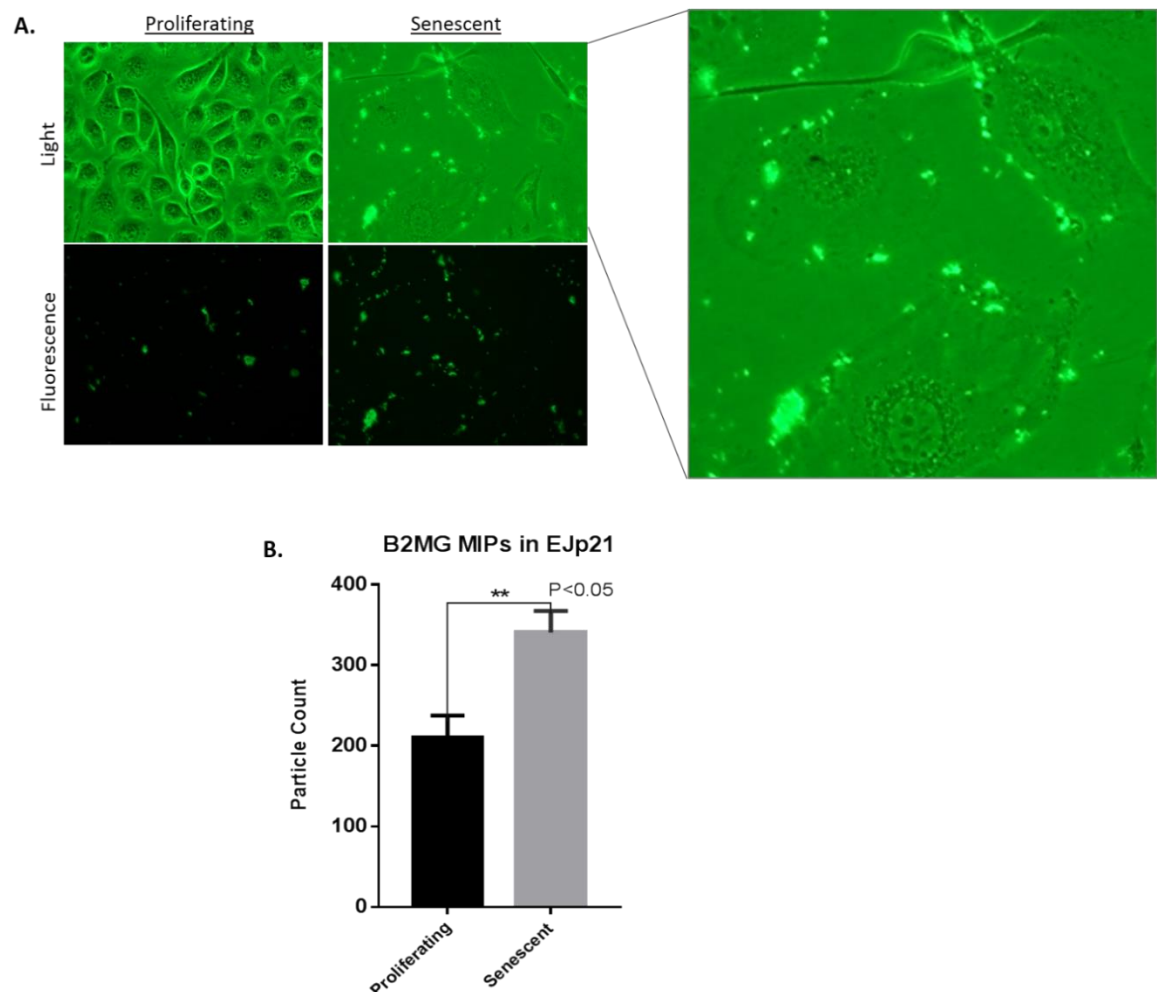


Figure 4-11 More B2MG MIPs bind to senescent EJp21 cells than proliferating cells

B2MG-targeted MIPs show a greater affinity for the membrane of senescent cells than that of non-senescent cells (A). Images were taken 4 hours after MIPs incubation and after a wash step. Fluorescent MIP particles were quantified using Image J software and the data plotted on a graph using GraphPad Prism software (B). Results are from three experimental replicates, presented as mean \pm SD. A two-tailed unpaired t test shows statistical significance at $p < 0.005$.

The introduction of a wash step to the protocol was found to improve the specificity of the MIPs and enhance visualization of the membrane-bound fluorescently-tagged MIPs. Also, the 2% concentration (1:50 dilution) was found to offer better sensitivity than higher ones, giving a better and more optimized detection method (see Figure 4-11). Hence this concentration of MIPs was used for subsequent experiments. More B2MG-targeted MIPs were bound to the membrane of senescent cells than the membrane of proliferating cells (Figure 4-11). The results show that B2MG can be targeted using fluorescent MIP particles, enabling the identification of senescent cells.

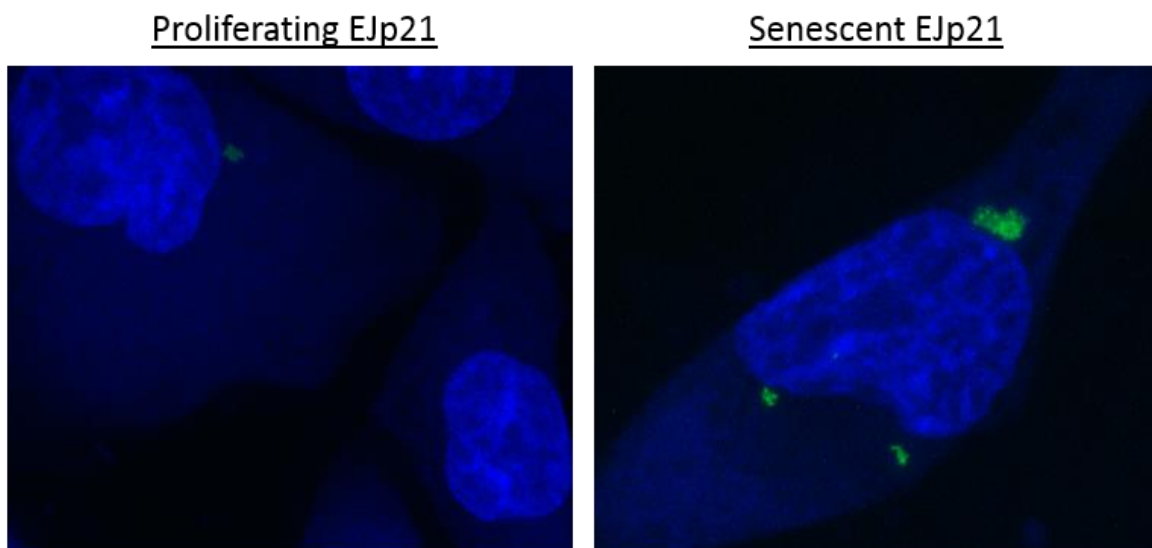


Figure 4-12 Confocal microscope images of B2MG-targeted MIPs in EJp21 cells. Proliferating and senescent EJp21 cells which had been incubated with B2MG MIPs and cultured for a total of 16 days were fixed and stained with DAPI. Fluorescein-tagged MIPs accumulate more within the senescent EJp21 cell and surround its nuclear membrane, compared to that of the proliferating cells.

These EJp21 cells with bound MIPs were further cultured for 16 more days before being fixed, stained with DAPI and imaged with the confocal microscope, in order to determine whether MIPs would remain in senescent cells for long periods of time. Confocal microscope images of these cells revealed an abundance of nanoMIPs internalised within the senescent cells compared to proliferating ones (Figure 4-12). The cells were fixed and stained with DAPI to visualise the nucleus,

using a modified immunofluorescence protocol, and more fluorescein-tagged nanoMIPs were seen accumulated within the cell and surrounding the nuclear membrane of the senescent EJp21 cell compared to proliferating cells. This showed that the MIPs were able to preferentially bind to and become internalized within senescent cells than in their proliferative counterparts. We concluded that these B2MG-targeted MIPs could therefore be used to detect the presence of senescent cells in culture.

B2MG-targeted MIPs were equally tested in the EJp16 senescent cell model in order to further assess the selectivity of the MIPs for different senescent cells. EJp16 cells were incubated with MIPs for 4 hours, after which the media was aspirated off, cells gently washed with warm media and fresh media replaced before imaging. MIP particles also showed a greater affinity for the membrane of senescent cells than that of the non-senescent EJp16 cells. Upon quantifying these images, senescent EJp16 cells had a higher particle count than the proliferating cells (see Figure 4-13).

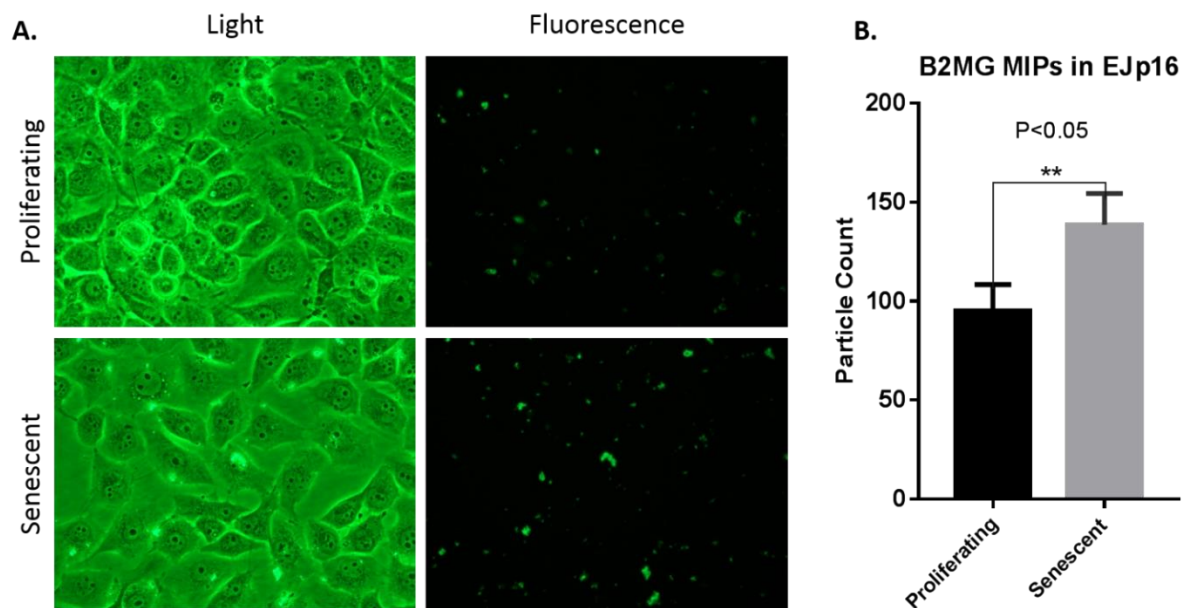


Figure 4-13 Fluorescence microscope images of 2% B2MG MIPs in EJp16 cells MIPs show a higher affinity for senescent EJp16 cells than proliferating cells as more fluorescent particles are seen retained in the senescent samples after the wash step (A). Particles in images from triplicate samples were quantified using Image J software and graphs plotted with GraphPad Prism software (B). Results are presented as mean \pm SD and a two-tailed unpaired t test shows statistical significance at $p < 0.005$.

Proliferating and 4 days senescent EJp16 cells were also seeded on coverslips and incubated with B2MG-targeted MIPs at 37°C for 24 hours. The cells were thereafter fixed with formalin and stained with DAPI to enable visualization of the nucleus with confocal microscopy. Confocal images of these EJp16 cells revealed the presence of MIPs in the cytoplasm of senescent cells whereas no particles were detected in the proliferating cell samples (see Figure 4-14).

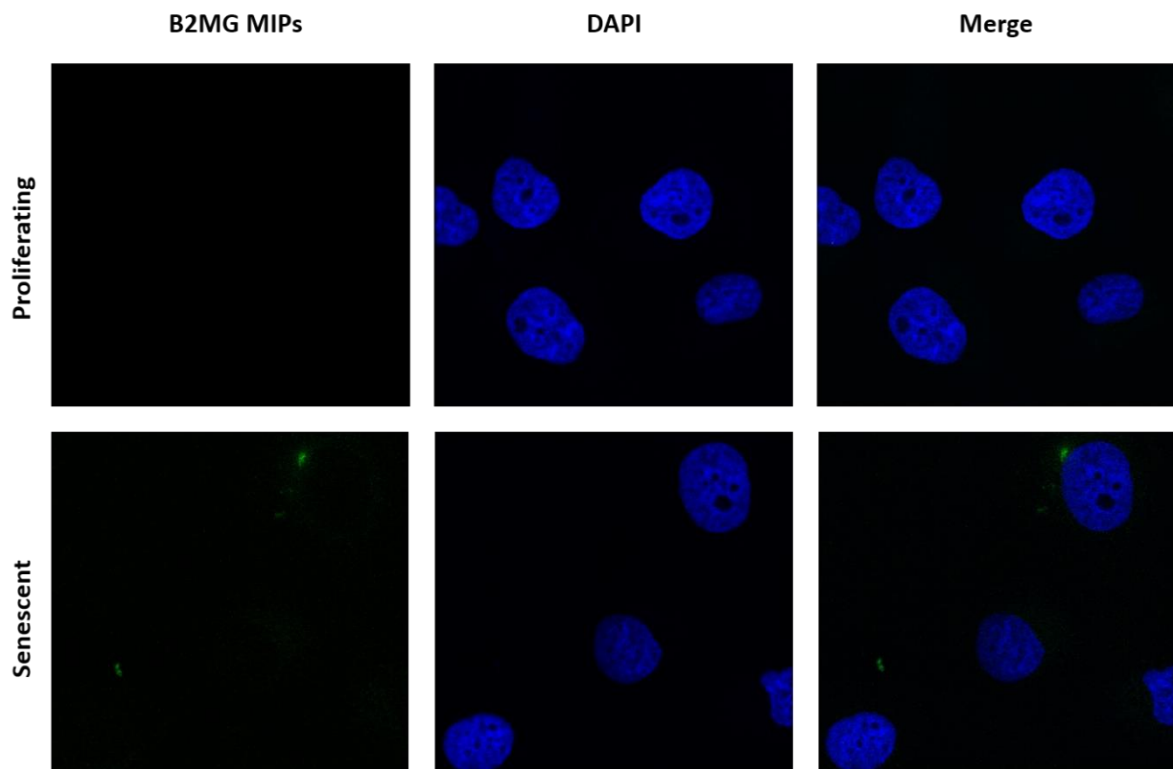
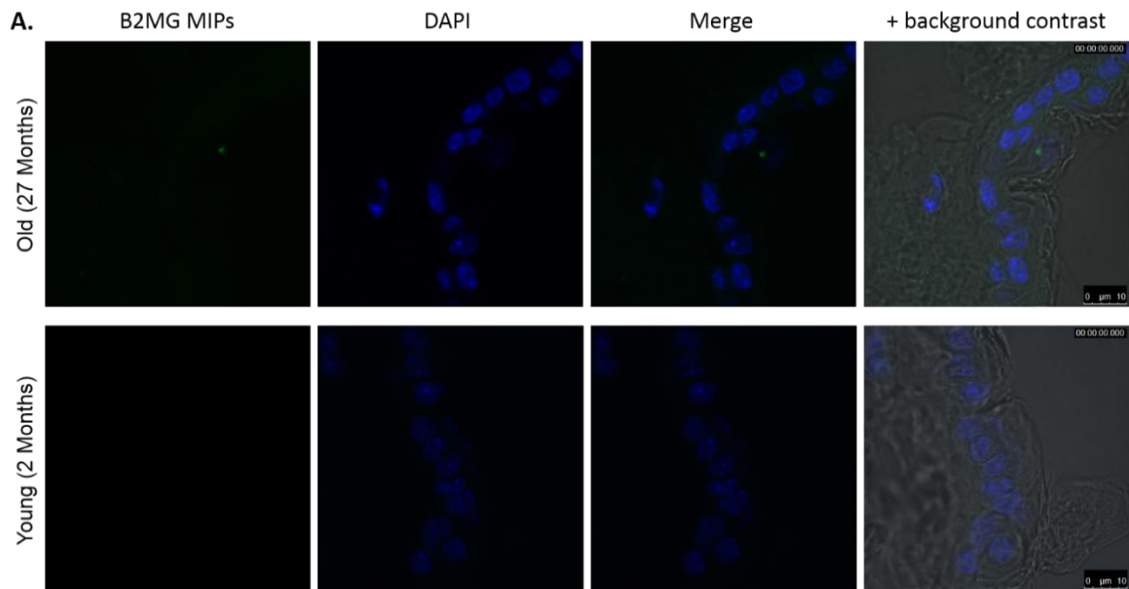


Figure 4-14 Confocal microscope images of B2MG-targeted MIPs in EJp16 cells
 Fluorescein-tagged MIPs are seen in the cytoplasm of senescent EJp16 cells and outside the nuclear membrane. No MIPs were detected in the proliferating EJp16 cells.

Old and young formalin fixed, paraffin embedded mice skin tissues obtained from the Shared Ageing Research Models (shARM) facility at the University of Sheffield were used for the detection of senescent cells in tissue by immunofluorescence using MIPs. A modified protocol of immunofluorescence revealed the presence of B2MG-targeted MIPs in old mice skin tissue while no

MIPs were detected in the skin tissue from the young control animal (see Figure 4-15). This further demonstrates the potential of these B2MG-targeted MIPs to detect the presence of senescent cells in tissue samples *in vitro*.



B. B2MG MIPs in Skin Tissue

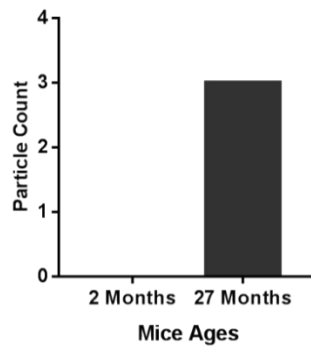


Figure 4-15 Confocal microscope images of B2MG-MIPs in mouse skin tissue
Formalin fixed paraffin embedded skin tissues from old (27 months old) and young (2 months old) mice were screened for the presence of senescent cells, by staining with fluorescein-tagged B2MG MIPs, using a modified immunofluorescence method. Confocal microscopy revealed the presence of fluorescent nanoMIPs in the older animal but not in the young one (A). Image J software was used to quantify the nanoMIPs particles (B).

4.3.2 B2MG-TARGETED MIPs BIND TO SENESCENT CELLS BY FLOW CYTOMETRY

Having found the 1:50 (2%) concentration of MIPs to be more sensitive for the detection of senescent cells by fluorescence and confocal microscopy, this concentration was also used for FACS binding assays in the EJ cells (see Figure 4-16). The B2MG MIPs had a greater binding affinity for senescent EJp16 cells than the other cell models used (Figure 4-16 B), consistent with the higher expression of the protein in these cells (see Figure 4-2). Histograms show 90.3% FITC positive senescent EJp16 cells, while EJp53 and EJp21 senescent cells were 27% and 12.5% FITC positive respectively. Calculation of their mean fluorescence intensities (MFI) showed more than a two-fold, significant increase in MIPs binding to senescent EJp16 cells compared to the other two models, which had very little fold increase in their MFI and were not statistically significant. This further backs the results previously obtained from fluorescence and confocal microscopy and suggests that FACS may not be sensitive enough to detect differences in senescent cells with low B2MG expression, such as EJp21 and EJp53.

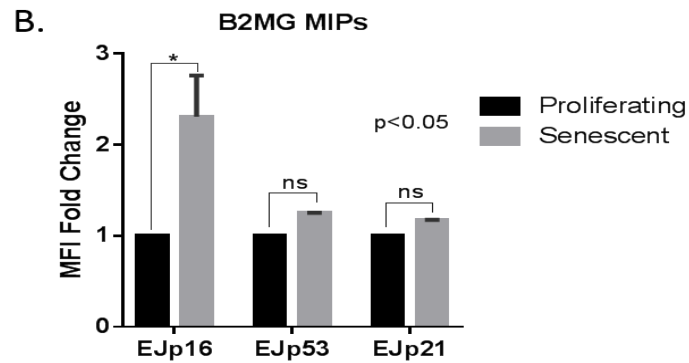
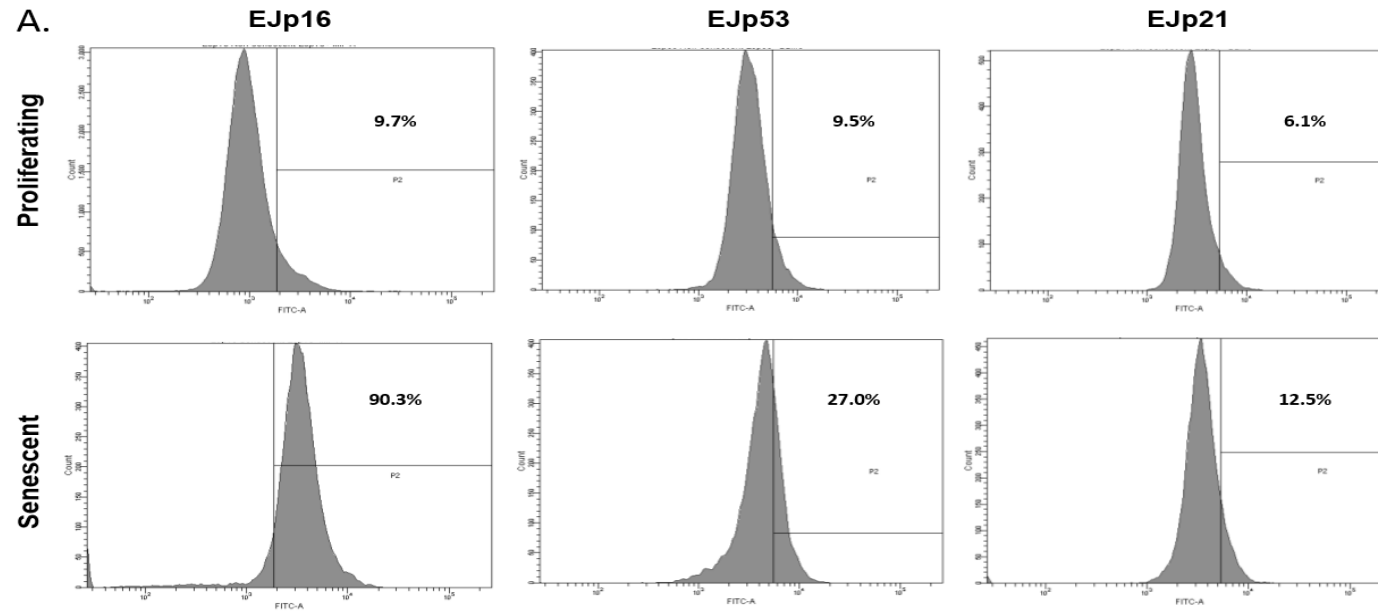


Figure 4-16 FACS binding of 2% B2MG-targeted MIPs in EJ cells

Fluorescein-tagged MIPs bind preferentially to senescent cells as shown by the percentage of positive cells on the histogram (A). Fold changes of the mean fluorescence intensities (MFI) of samples are plotted using GraphPad Prism software (B). Results are from three independent experiments and are presented as mean \pm SD. A two-tailed unpaired t test shows statistical significance in the EJp16 model at $p < 0.05$.

4.4 FLUORESCINE-TAGGED DEP1 MIPs BIND TO SENESCENT CELLS *IN VITRO*

Following the success with the B2MG-targeted MIPs, MIPs were also generated against the external epitope of mammalian density enhanced phosphatase 1 (DEP1) or PTPRJ. DEP1 MIPs bound preferentially to senescent cells as shown by the percentage of FITC-positive cells on the histogram. Additionally, upon calculating their mean fluorescence intensities (MFI), all senescent cells showed a significant fold increase in MFI than proliferating cells (see Figure 4-17).

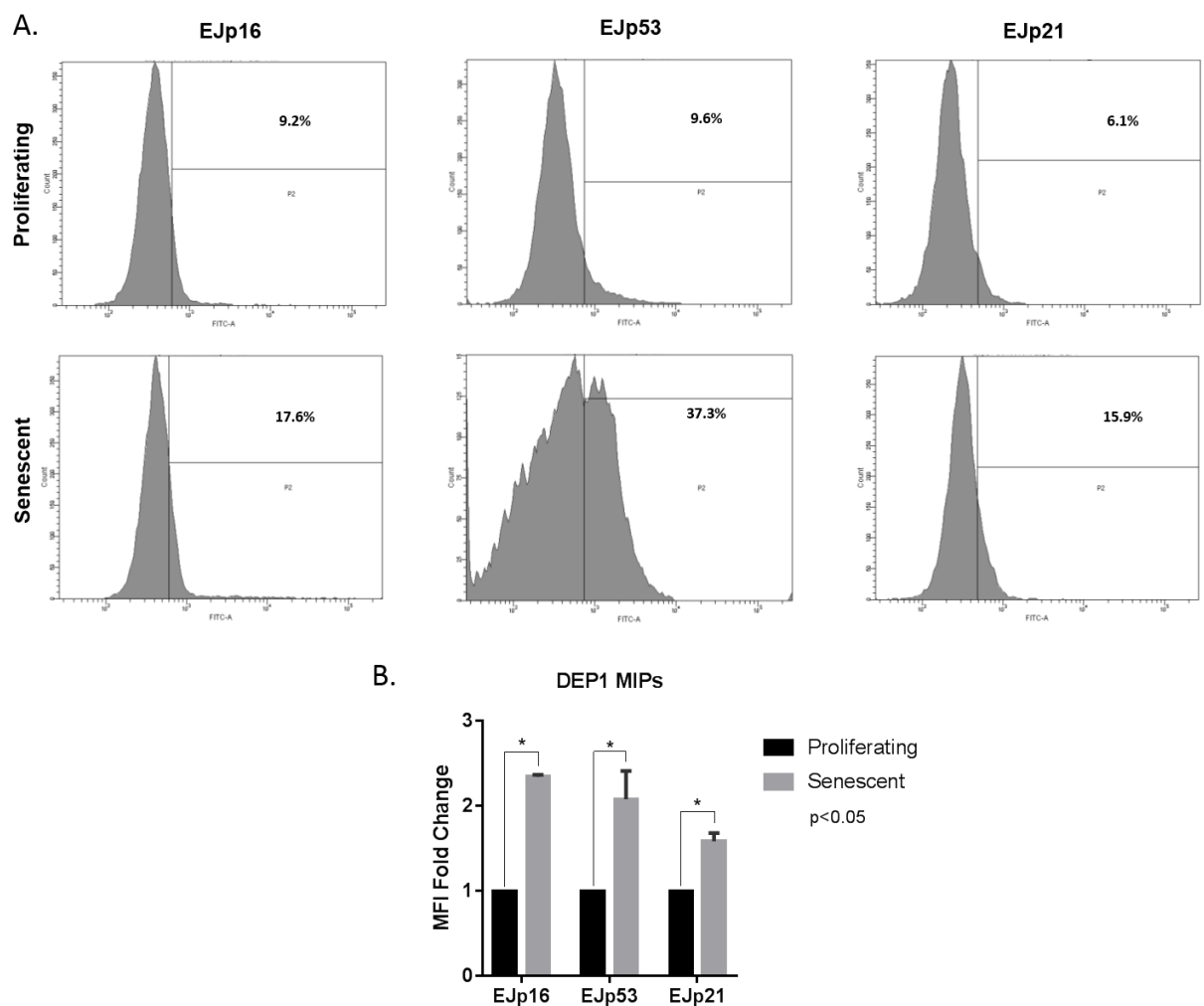


Figure 4-17 FACS binding of 2% DEP1-targeted MIPs in EJ cells
 DEP1 MIPs bind more to senescent cells than proliferating cells as seen by the percentage of FITC-positive cells on the histogram (A). Fold changes of the mean fluorescence intensities (MFI) of samples are also presented (B). The results are from three independent experiments and are represented as mean \pm SD. A two-tailed unpaired t test shows statistical significance at $p < 0.05$.

4.5 MIPS ARE BIOCOMPATIBLE AND NON-CYTOTOXIC

In order to ascertain whether MIPS are safe and non-toxic, the biocompatibility and cytotoxicity of nanoMIPs was evaluated by Propidium Iodide (PI) staining. The effect of these MIPS on the cell cycle and on cell death was assessed using the EJ senescent cell models. 10% and 1% dilutions of nanoMIPs were added to cells and incubated at 37°C for 12 hours and for 24 hours.

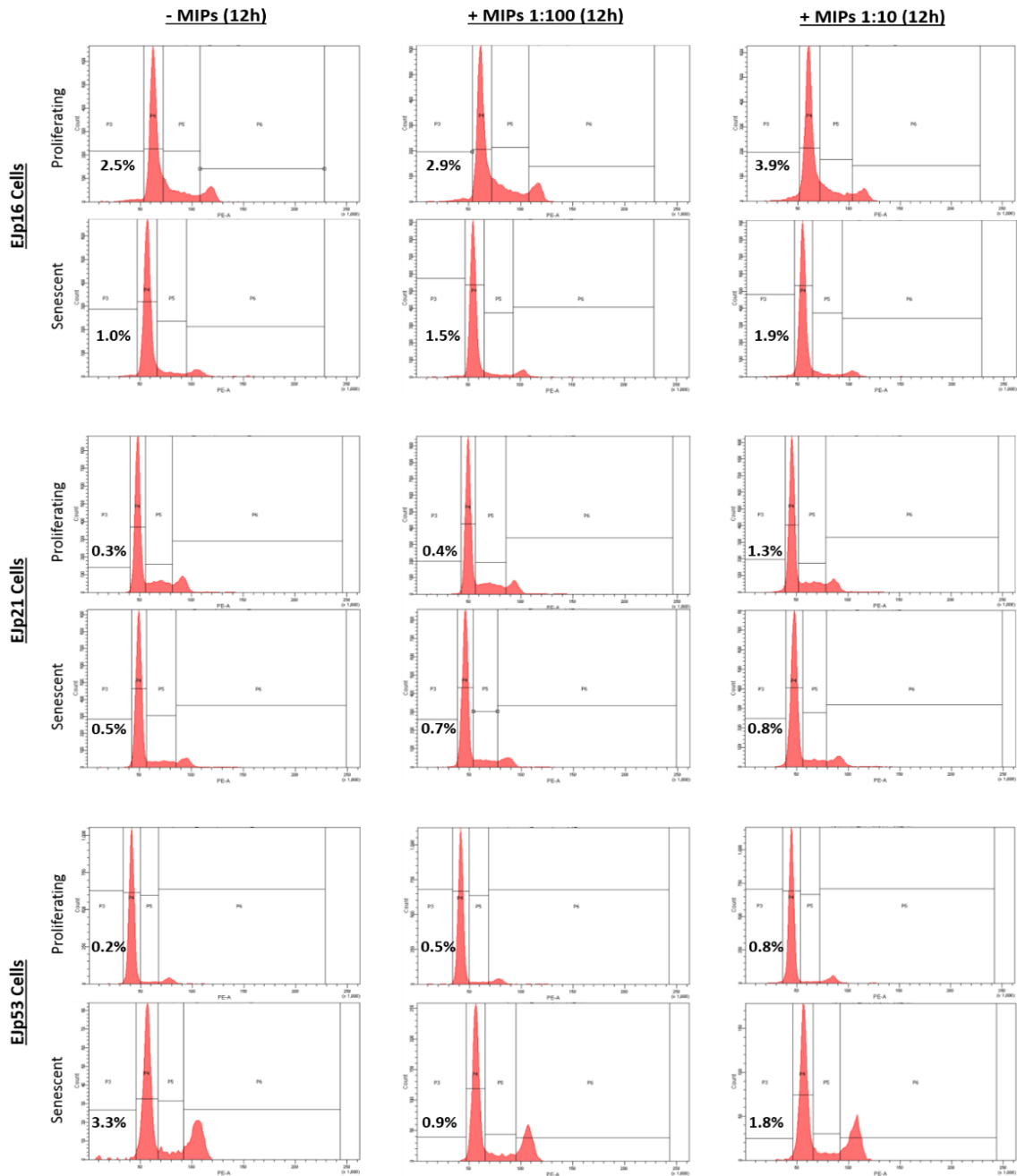


Figure 4-18 Cell cycle analysis of EJ cells incubated with MIPS for 12 hours. Cell cycle analysis of EJ cells incubated with nanoMIPs for 12 hours. MIPS were not toxic to these cells. Images show percentage cell death by the sub G1 population.

The results from flow cytometry indicate that the nanoMIPs on their own are not toxic to cells and do not have any effect on the cell cycle or DNA content (see Figure 4-18 and Figure 4-19).

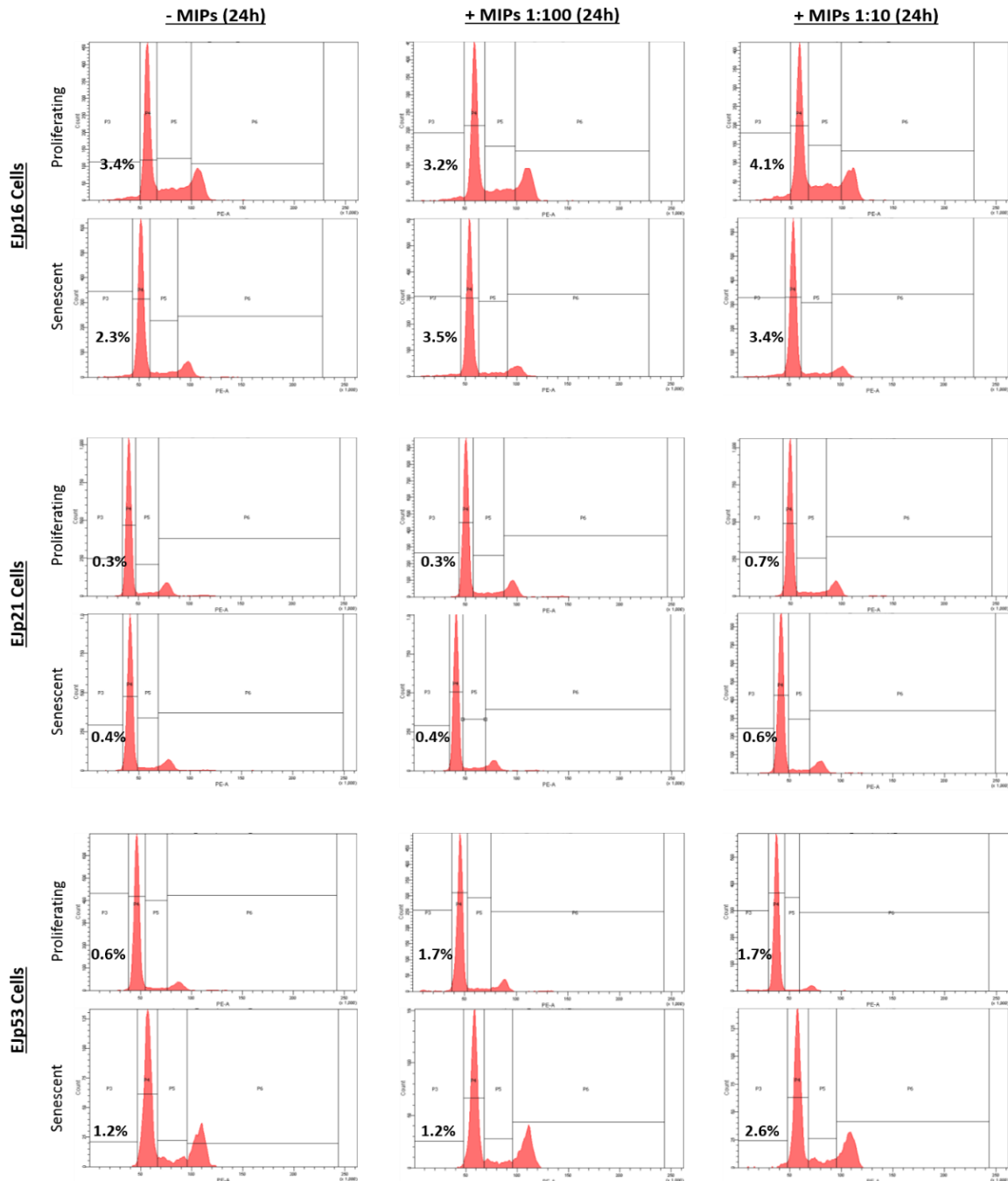


Figure 4-19 Cell cycle analysis of EJ cells incubated with MIPs for 24 hours
 Cell cycle analysis of EJ cells incubated with nanoMIPs for 24 hours. Percentage cell death in the sub G1 population are indicated. MIPs were not found to be cytotoxic.

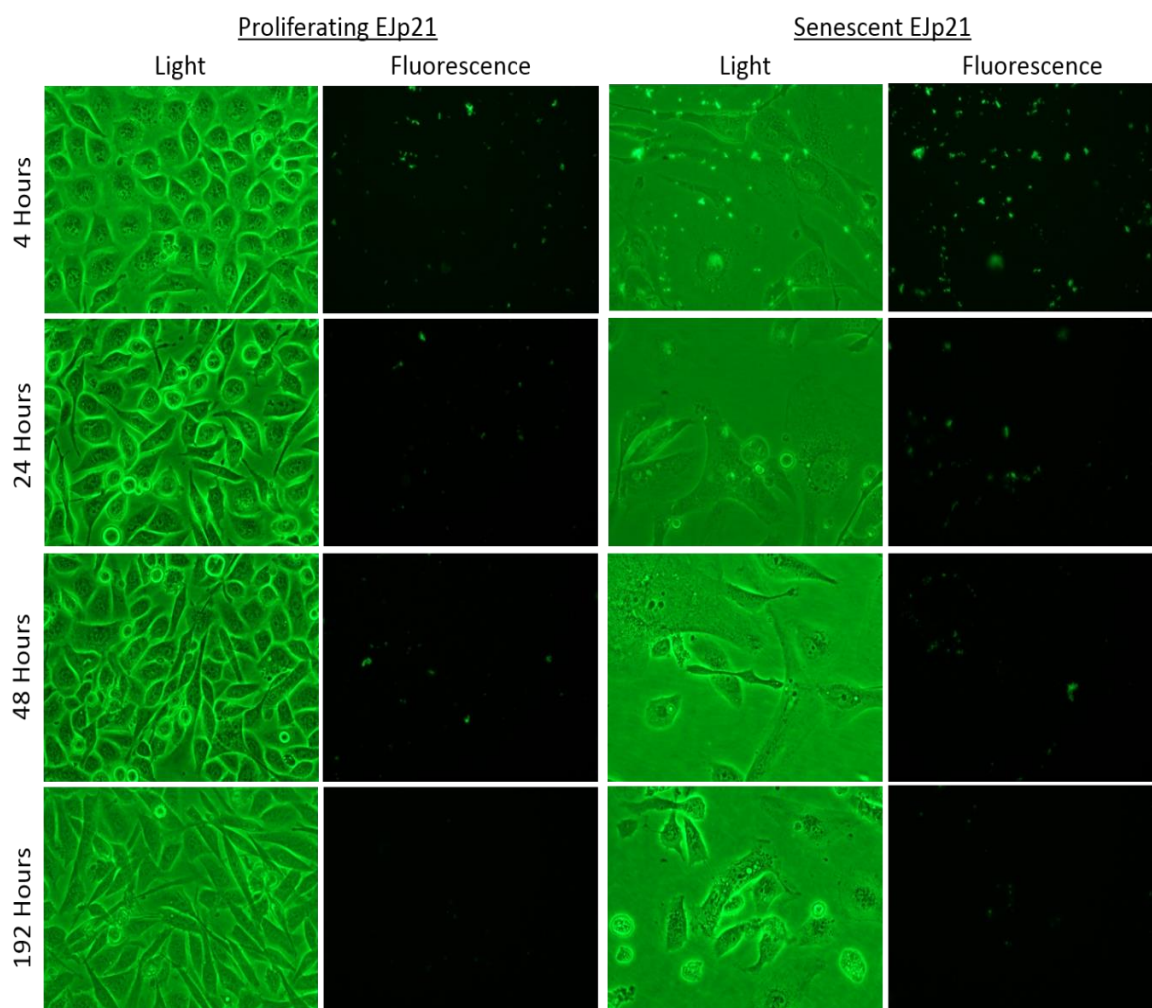


Figure 4-20 EJp21 cells incubated with 2% MIPs remain viable after several days
MIPs show biocompatibility and had no effect on cell viability or proliferation when imaged up to 8 days after incubation.

EJp21 cells incubated with 2% B2MG MIPs remained viable for several days and images were taken up to 8 days later (see Figure 4-20). The proliferating cells continued replicating as normal and were passaged every 3 days, while the senescent cells remained growth arrested but still viable. The fluorescence intensity of the fluorescein-tagged B2MG MIPs was found to decrease with time. Cell samples imaged after four hours had greater fluorescence than images taken after 24 hours, 48 hours and 192 hours. Cell samples imaged at 192 hours had the least visible MIPs fluorescence signal (see Figure 4-20). This suggests that the incubation time should also be taken into consideration when using fluorescent-tagged MIPs for detection *in vitro*, since the fluorescence of these MIPs decreased as the hours passed.

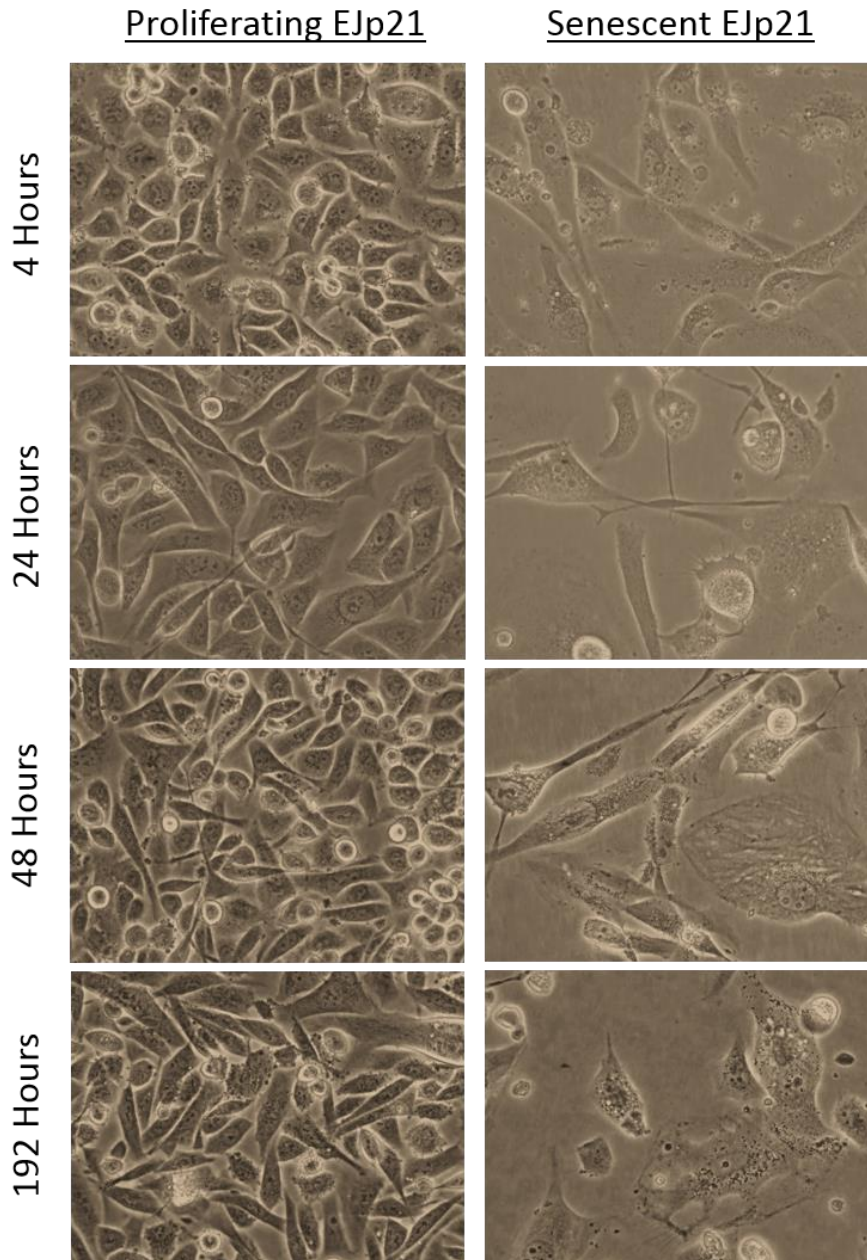


Figure 4-21 EJP21 cells incubated with 5% MIPs are still viable after 8 days
 EJP21 cells incubated with 5% MIPs remained viable after 8 days and continued proliferating. The MIPs were found to be biocompatible and non-toxic to the cells.

Proliferating and senescent EJP21 cells which had been incubated with a 5% (1:20) dilution of B2MG MIPs were similarly cultured for several days to assess the biocompatibility and toxicity of the MIPs. Images taken up to 8 days after incubation show that the cells remained viable and the presence of the MIPs had no toxic effect on the cells (see Figure 4-21).

Colony formation assays were also carried out in both EJp16 and EJp21 cells that were incubated with B2MG MIPs, in order to further assess the toxicity of the MIPs. For the assay, 500 cells were seeded in 6cm² plates and incubated with 2% MIPs for 14 days. Cells carrying MIPs showed no difference in their ability to form colonies when compared to control cells without MIPs. Cells with MIPs and control cells without MIPs both proliferated and formed colonies in a similar manner (see Figure 4-22), indicating that the MIPs did not affect the ability of single cells to form colonies. Also, cells were frozen down and stored in -80°C. Weeks later, these same cells were resuscitated and cultured as normal and the MIPs did not affect their recovery rate (data not shown).

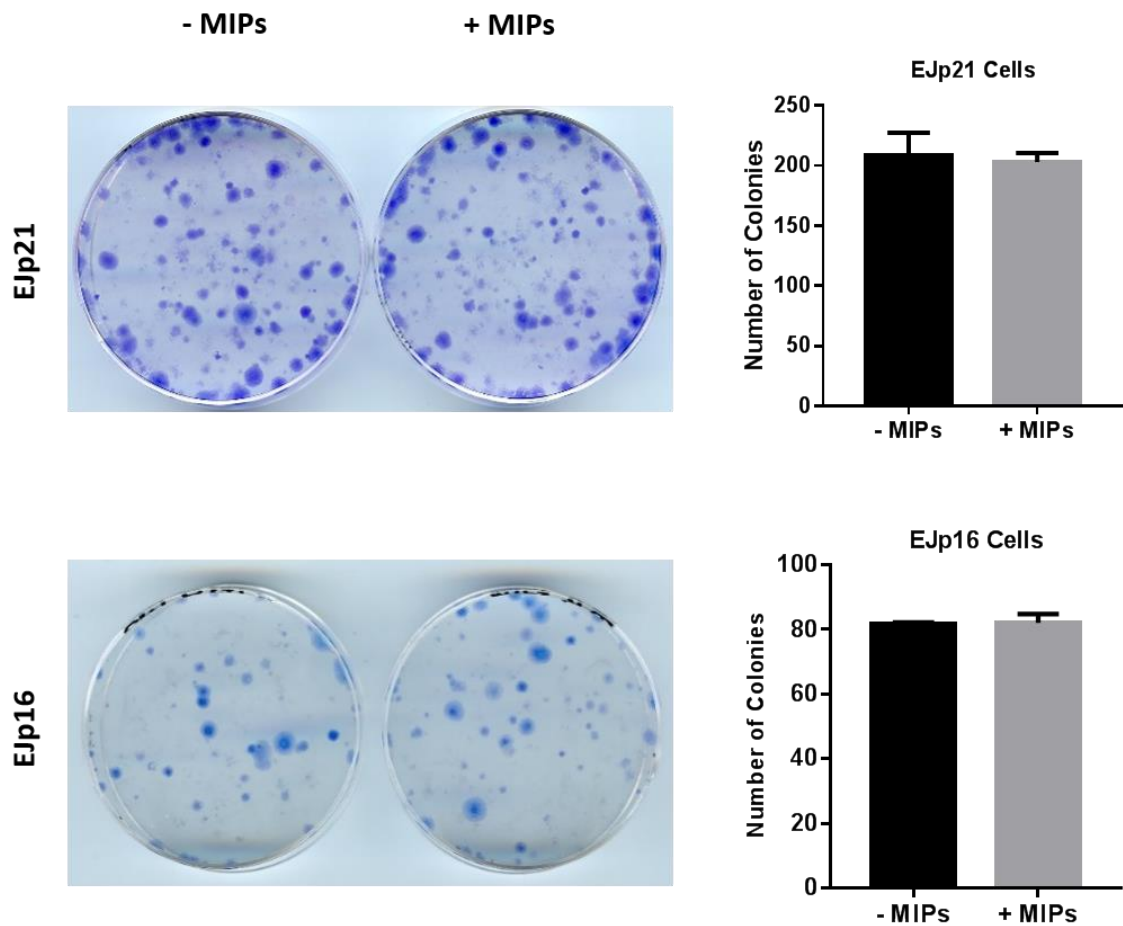


Figure 4-22 Colony Formation assays in EJ cells incubated with MIPs
 The presence of 2% B2MG-targeted MIPs did not impair the ability of single proliferating EJp21 or EJp16 cells to form colonies. Results here are from two independent experiments in duplicates and are shown as mean \pm SD.

4.6 FLUORESCENTLY TAGGED B2MG MIPS DETECT SENESCENT CELLS *IN VIVO*

Having seen the potential for senescent cell detection by B2MG-targeted MIPS *in vitro*, the MIPS were also employed to try to detect senescent cells *in vivo*, using old mice as a model of senescence and ageing. Old and middle aged wild type C57/BL6J mice ranging in age from 24 months to 11 months were used for the study, along with 2 months old wild type C57/BL6J mice as their young controls. B2MG-targeted nanoMIPs tagged with fluorescent molecules were either applied topically to an area of shaved skin on the mice due to the high B2MG expression observed in mouse skin tissues by Western blotting, or were administered intravenously after which the mice were imaged using the IVIS Spectrum imaging system (PerkinElmer Inc.).

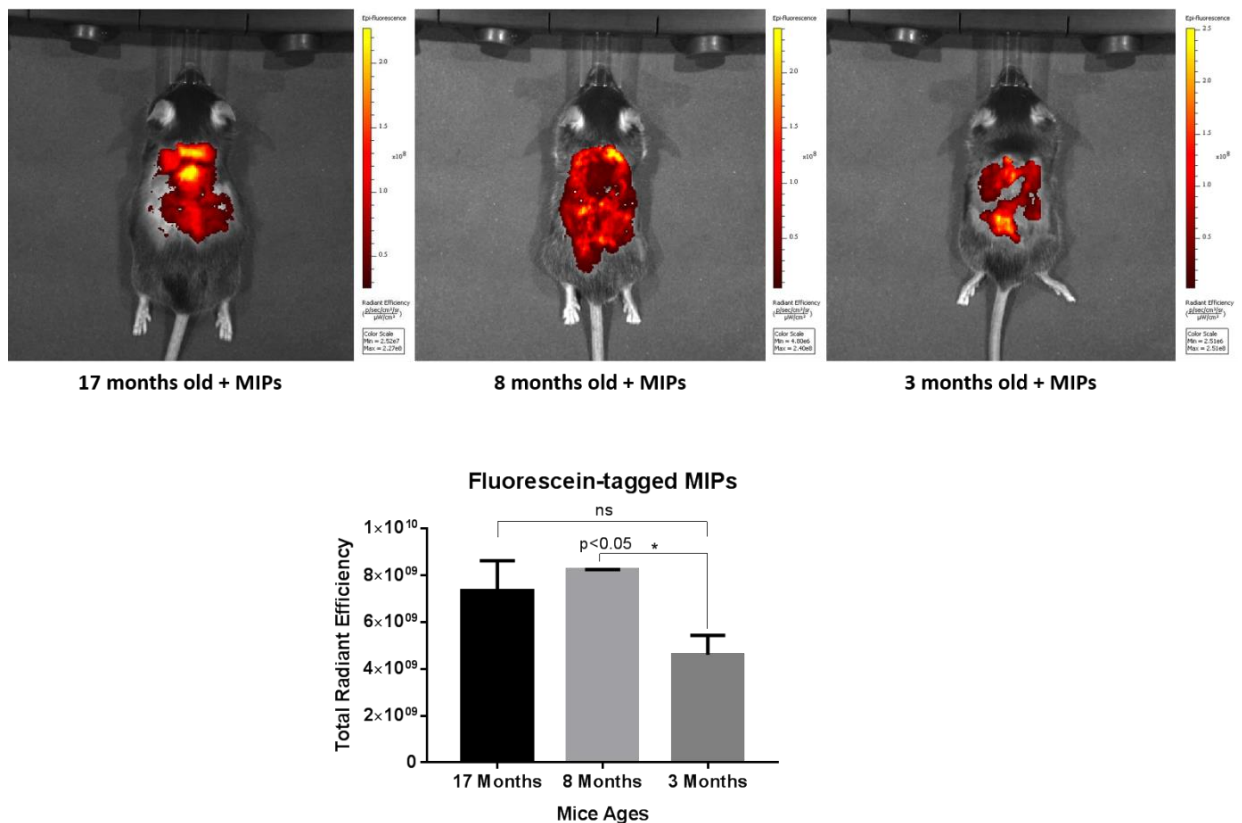


Figure 4-23 Detection of senescent cells by topically applied fluorescein-MIPs B2MG-targeted MIPS were applied topically to an area of shaved skin on the back of mice and animals were imaged 24 hours later. Results show higher fluorescence intensity in the 17 months and 8 months old animals than in the young 3 month old animals. Two mice were used per group and results are from a single study, presented as mean \pm SD. A two-tailed unpaired t test shows statistical significance in total radiant efficiency between the 8 month old mice and the young mice at $p < 0.05$.

In the course of this study, different fluorophores were tested for use as fluorescent tags for the B2MG nanoMIPs, to enable imaging and to optimize the technique for the detection of senescent cells *in vivo*. Total fluorescence signals were quantified in units of radiant efficiency by measuring similar whole abdomen regions of interest on the 2D epi-fluorescence images acquired from mice. Analyses were carried out using the Living Image software (version 4.5.2, PerkinElmer Inc.). Fluorescein-tagged nanoMIPs (see Figure 4-23) were initially employed to identify B2MG expressing senescent cells in aged mice. However, due to the low wavelength (Excitation 492nm, Emission 512nm) of this fluorophore and the interference of background tissue autofluorescence, the signal obtained from the images were indistinct and noisy (Figure 4-23), making it difficult to tell the actual signal from background autofluorescence. Thus, a higher wavelength fluorophore was sought for use as the fluorescent tag for these nanoMIPs in order to obtain a more distinct signal from *in vivo* imaging. Alexa Fluor 647 was selected as a fluorescent tag since it had a much higher wavelength than the previously used fluorescein. Fluorescence signals obtained were more distinct than that obtained from fluorescein-tagged MIPs. Aged, old and young mice aged 24 months, 13 months and 2 months were used for this study.

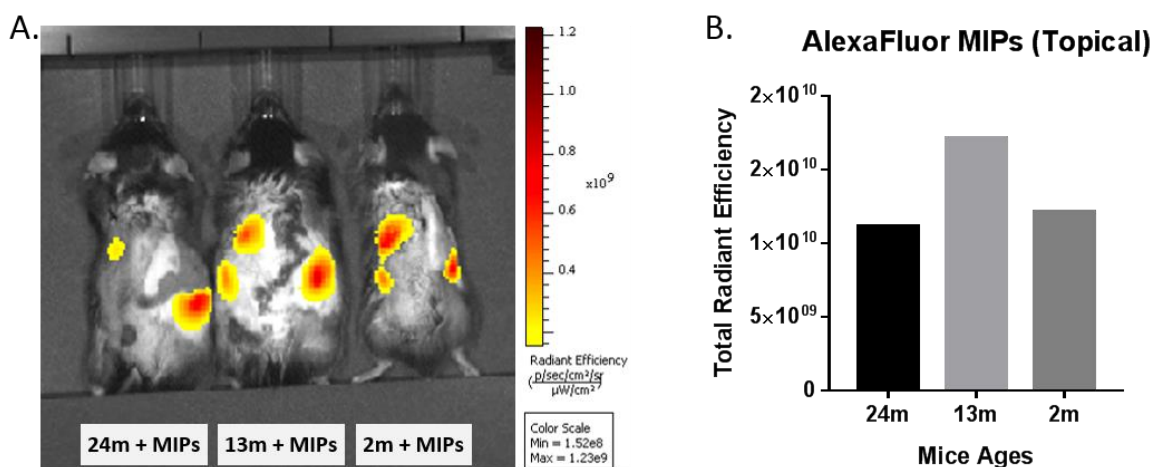


Figure 4-24 Detection of senescent cells by topically applied Alexa Fluor-MIPs
 Alexa Fluor647-tagged B2MG MIPs were applied to an area of shaved skin on the back of aged, old and young mice. 2D epi-fluorescence images were captured (A) using the IVIS Spectrum imaging system and total fluorescence signals were quantified in units of radiant efficiency (B). Result presented is from a single experiment using one animal per age group.

The MIPs were first applied topically to an area of shaved skin on the back of mice and images were taken after 24 hours (see Figure 4-24) using the IVIS Spectrum imaging system. The results did not show a consistent difference in total radiant efficiency between the older animals and the young control animal as the signals from the 24 month old mouse was less than the others. This suggested that the topical application of MIPs did not differentiate between young and aged skin. In order to check for non-specific binding of non-targeted MIPs, another control experiment was set up using Alexa Fluor-tagged control MIPs imprinted with a different molecule, targeting trypsin rather than B2MG (Figure 4-25). In this experiment, three 13 months old mice were used. One of the mice was painted topically with a solution of Alexa Fluor-tagged B2MG MIPs, another was painted with a solution of Alexa Fluor647-tagged control MIPs, while the third mouse was imaged without any MIPs being applied.

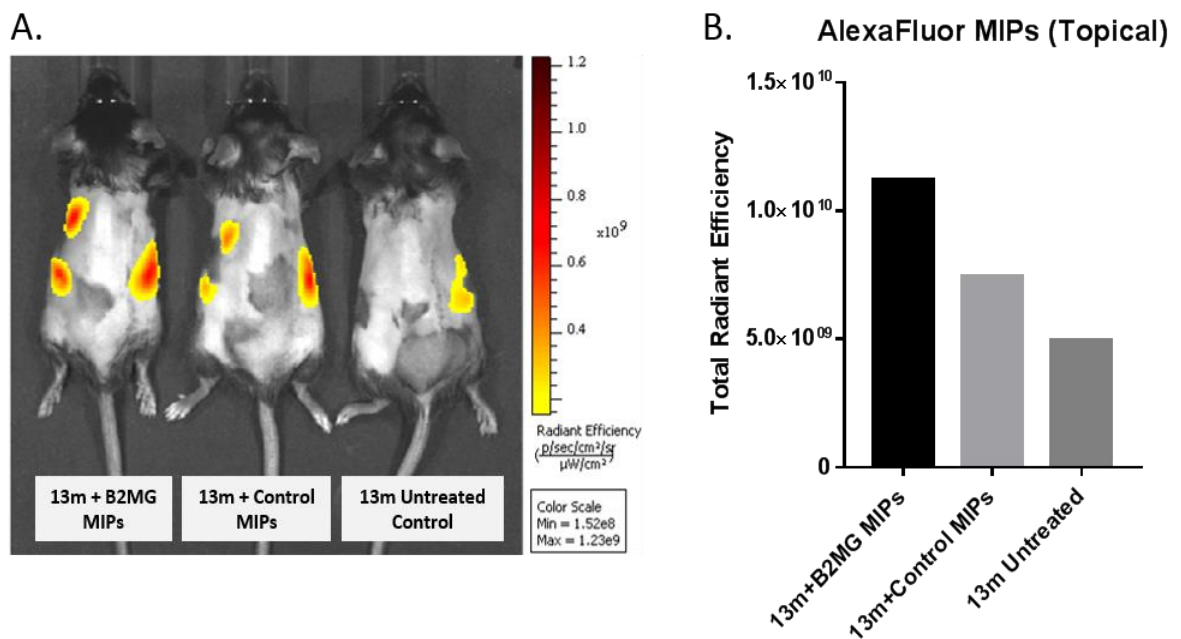


Figure 4-25 *In vivo* imaging of mice after topical application of MIPs

B2MG and non-targeted control MIPs were applied topically to an area of shaved skin on the back of mice and the animals were imaged after 24 hours. The untreated control animal was imaged without having any MIPs applied (A). Fluorescence signals were quantified and plotted in units of radiant efficiency (B).

The mouse treated with B2MG MIPs gave off higher fluorescence signals than the mouse treated with control MIPs as well as the untreated control animal. Contrary to what was expected, the trypsin imprinted MIPs also gave off high

fluorescence signals although at a lower intensity than the B2MG-targeted MIPs. This indicated that trypsin was not a good choice of control MIPs. Trypsin is generally considered a digestive enzyme but it is also active in various cellular processes including development and fibrocyte differentiation (White *et al.*, 2013). Also, trypsin gene expression has been reported in the spleen, liver, kidney, and brain of normal mice (Koshikawa *et al.*, 1998), making it a poor template molecule for control MIPs *in vivo*. The fluorescence signals were quantified and presented in units of radiant efficiency (Figure 4-25 B).

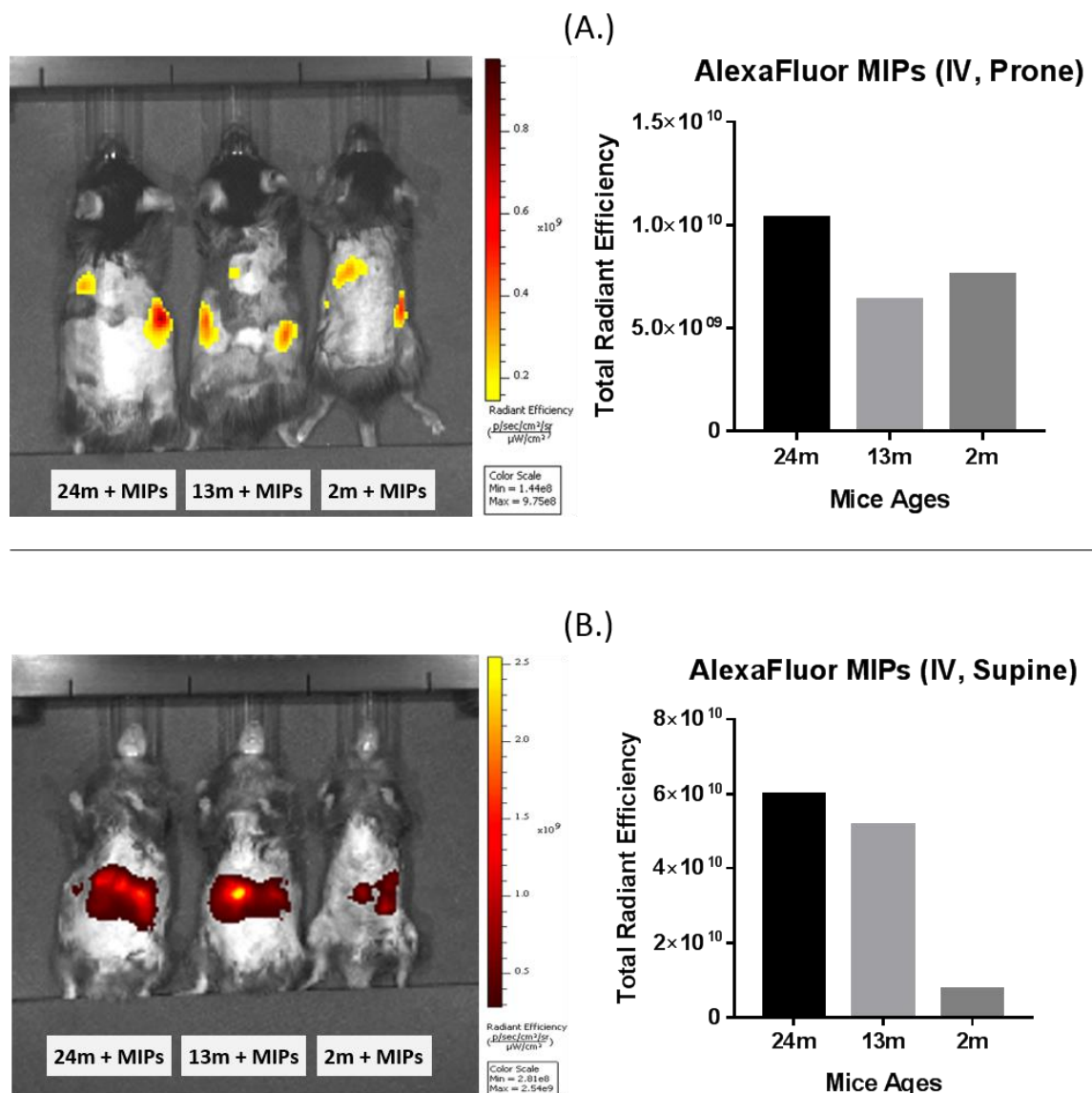


Figure 4-26 Detecting senescent cells with intravenous Alexa Fluor647-MIPs
 A solution of Alexa Fluor647-tagged nanoMIPs was administered intravenously, 5ml/kg body weight, to aged, old and young mice. Animals were imaged after 2 hours, in the prone (A) and supine (B) positions and their fluorescence signals quantified and presented as total radiant efficiency. Images are from a single experiment with one animal per age group.

The MIPs were next administered via intravenous route by tail vein injection, in an effort to see if they could detect systemic differences in the expression of senescent cells between young and old mice. 2D epi-fluorescence images of the animals were taken both in the prone and supine positions (see Figure 4-26). In both images, the 24 month old mouse had a higher total radiant efficiency than the 13month and 2month old mice, with the fluorescence signal increasing distinctly with age in the supine position compared to the prone position.

To rule out what could be background tissue autofluorescence in these images, an untreated control animal was introduced into the next study. Three animals, one aged 15 months and two aged 2 months, were used for this experiment. The 15 month old animal and one 2 month old young control animal were given intravenous Alexa Fluor-tagged B2MG nanoMIPs and imaged after two hours. The second 2 month old animal was imaged without being administered any MIPs (see Figure 4-27).

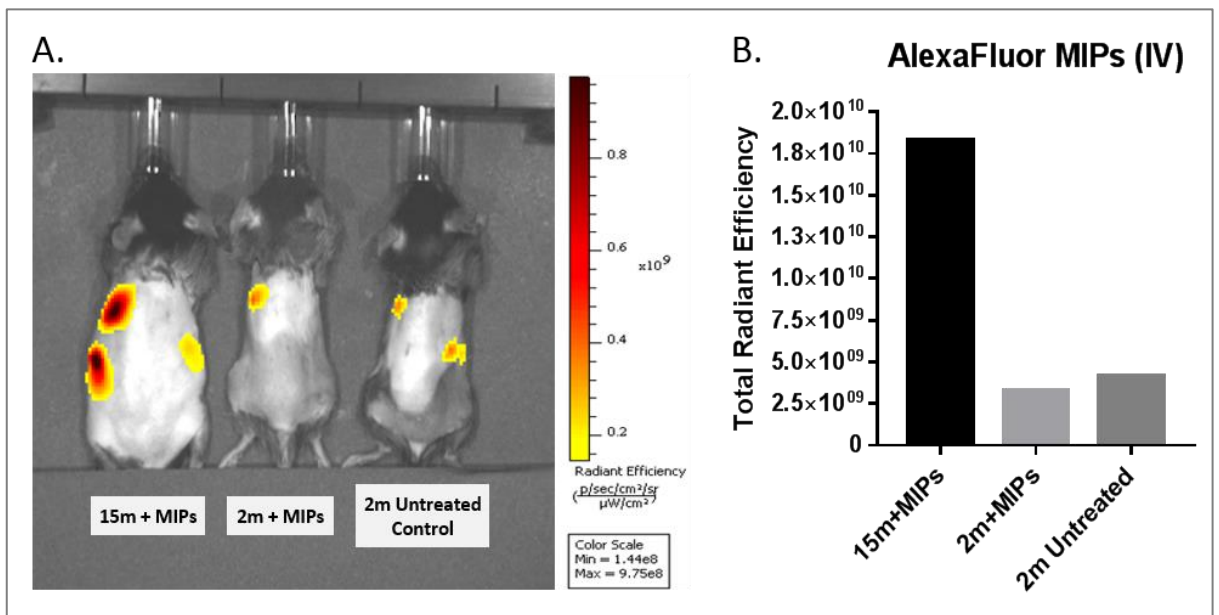


Figure 4-27 Fluorescent B2MG MIPs detect senescent cells in old but not young mice

Intravenously administered Alexa Fluor647-tagged B2MG MIPs were preferentially retained by senescent cells in the old animal and not in the young controls, both treated and untreated (A). Total fluorescence signals were quantified and are shown in units of radiant efficiency (B). The result is from a single experiment with one animal in each age group.

The 2 month old treated animal emitted a fluorescence signal that was comparable to the background signal from the untreated control 2 month old animal. This result indicated that there were no senescent cells in the young animal as both control animals of the same age emitted minimal fluorescence signals. The 15 month old animal, on the other hand, emitted signals that were more than four times that of the two young animals (Figure 4-27).

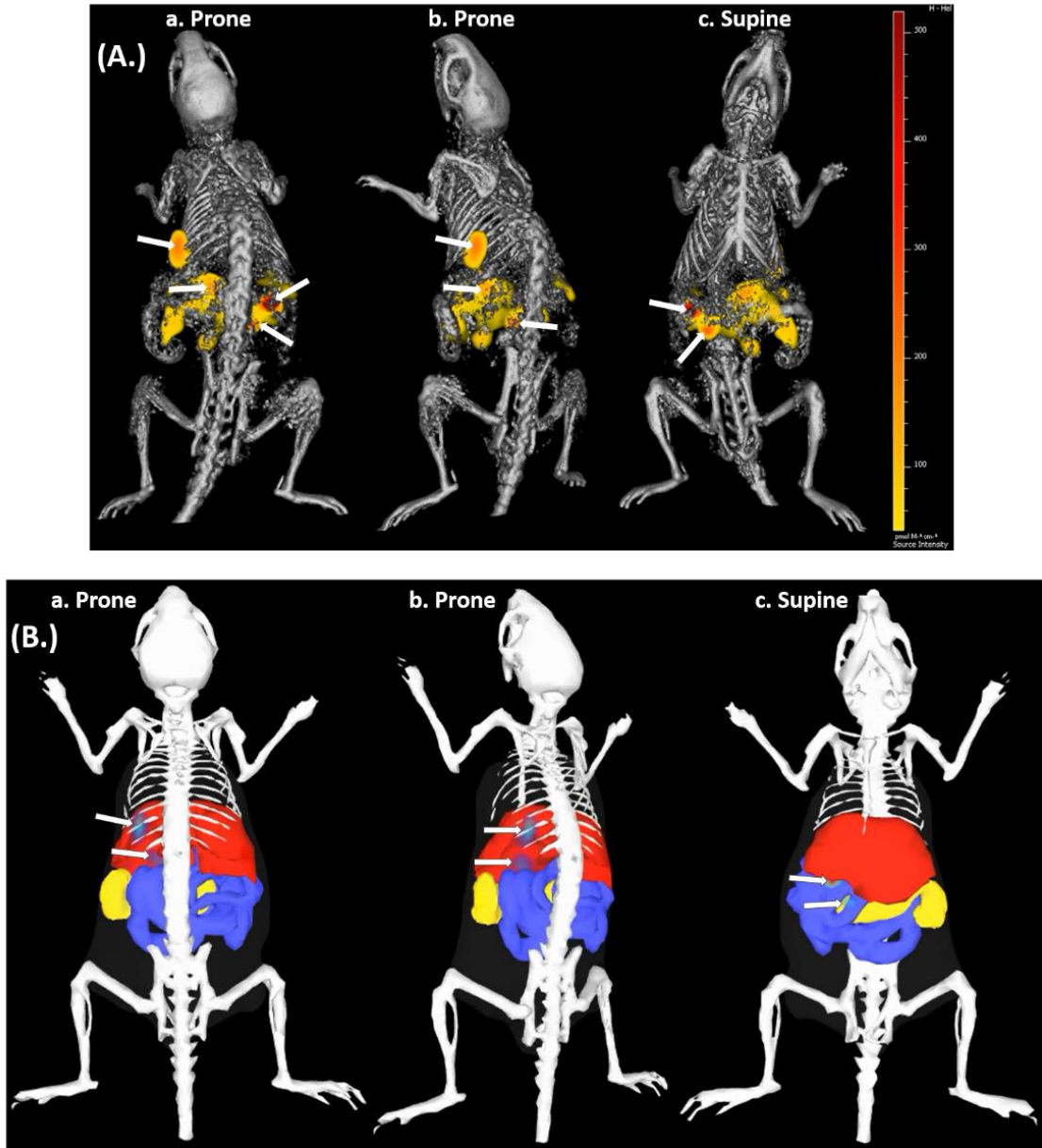


Figure 4-28 Mouse whole-body micro-CT and fluorescence imaging tomography
 Representative 3D whole-body micro-CT (A) and fluorescence imaging tomography (FLIT) (B) images showing the localization of fluorescent signals (arrows) obtained from the 15 month old mouse treated with intravenous Alexa Fluor647-tagged B2MG nanoMIPs. Signals appear to be coming from the right lung, right kidney and jejunum areas.

Representative 3D whole-body micro computed tomography (micro-CT) as well as fluorescence imaging tomography (FLIT) (see Figure 4-28 A and B) images of the 15 month old animal were acquired using the QuantumFX and IVIS Spectrum micro-CT scanner (PerkinElmer Inc.) respectively, in order to localize the signal source. The signals appeared to be from the right lung and right kidneys as well as the jejunum.

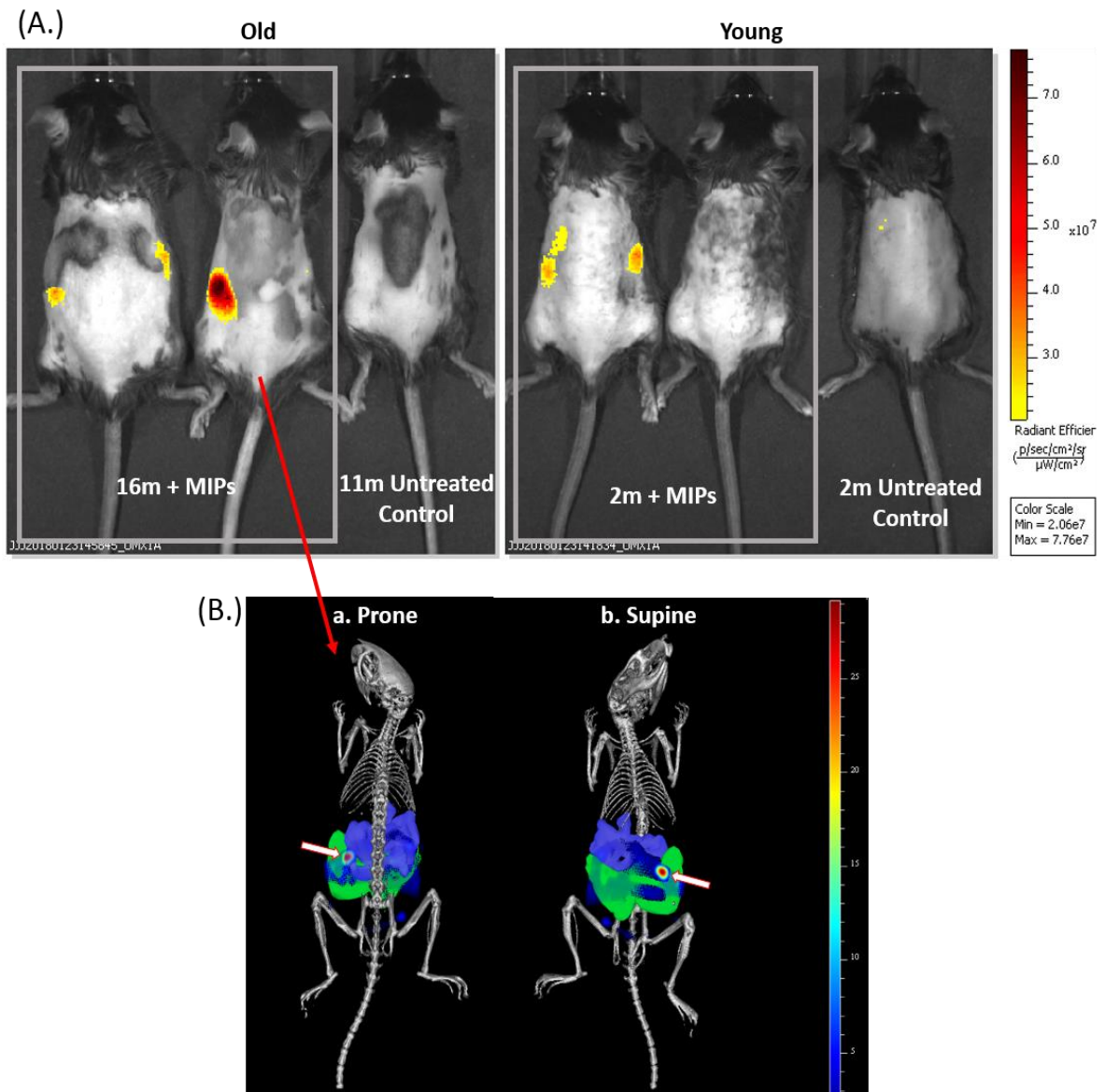


Figure 4-29 In vivo imaging of senescent cells using DyLight™ 800-labelled MIPs

2D epi-fluorescence images of old and young mice with IV injected DyLight™ 800-labelled MIPs along with their untreated controls from same age group (A). The pair of treated 16 months old animals gave off higher signals while the untreated 11 month old control mice had no fluorescence signal. One of the young treated animals emitted fluorescence signal while the other along with its untreated control emitted no signal. A 3D registration and signal localization of DyLight™ 800-labelled B2MG MIPs in a 16 month old mouse is shown (B).

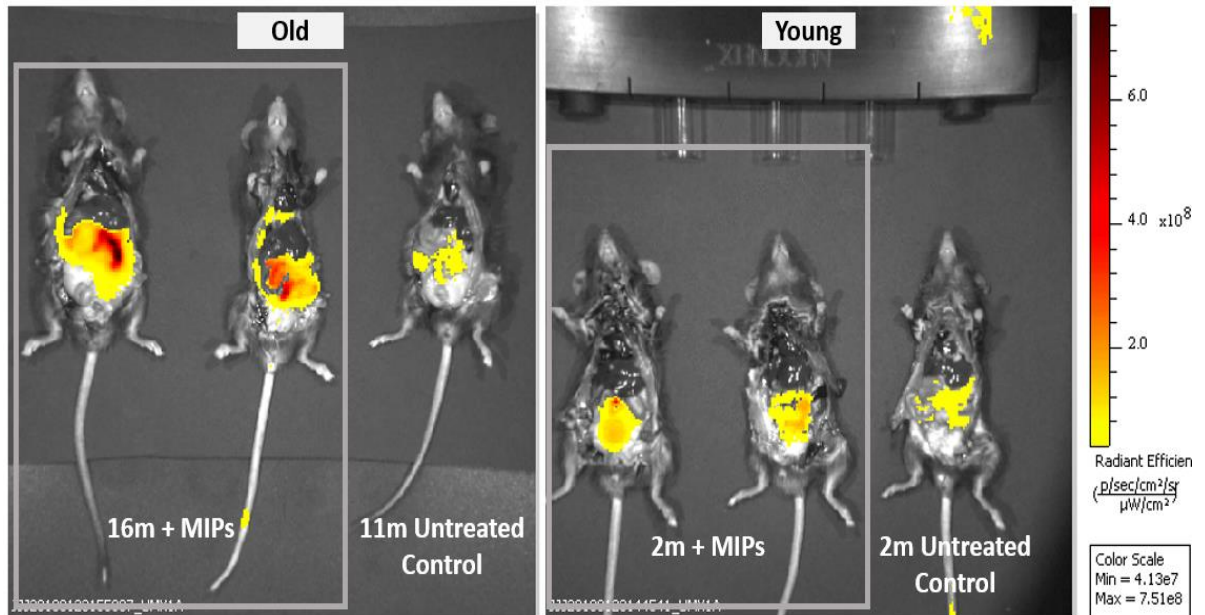
The Alexa Fluor-tagged MIPs offered more clear and distinct fluorescence signals compared to the previously used fluorescein-labelled MIPs. However, upon imaging the untreated control animal, there was still some background tissue autofluorescence observed at this wavelength (Figure 4-27). As a result of this, a much higher wavelength of fluorophore was sought, in order to completely eliminate background noise. The DyLight™ 800 NHS Ester was next used to label the B2MG nanoMIPs.

This near-infrared fluorophore allowed for better imaging and image analysis, with little or no background autofluorescence detected. A pair each of 16 months old mice and 2 months old mice were used for this experiment along with old and young untreated control mice (see Figure 4-29). The old treated group of animals emitted higher fluorescent signals than the young treated groups. The old and young untreated control animals on the other hand, gave off no fluorescence signals, as did one of the young treated animals (Figure 4-29), suggesting the absence of senescent cells in this young mouse. A 3D best-case registration to micro-CT and organ atlas was performed for the 16 month old mice with the highest fluorescence signal. The signal here appeared to come from the left abdominal cavity, as can be seen from 3D registration for both the prone and supine positions (Figure 4-29 B). Organ atlas analysis suggested this to be coming from the jejunum.

After imaging in the prone position, mice were humanely culled and quickly dissected open, to reveal the internal organs. Ex vivo imaging was done in the supine position and the total fluorescence signal from animals were quantified and presented as total radiant efficiency (see Figure 4-30). Animals in the old and young treated groups were in duplicates while single animals were used for each of the untreated controls. The older treated animals had total radiant efficiency that was more than three times that of the younger animals (Figure 4-30), consistent with the MIPs being able to bind to B2MG-expressing senescent cells *in vivo*.

All image analyses and 3D reconstruction of images using Alexa Fluor and DyLight™ 800-labelled MIPs were obtained with the help of Dr. Michael Kelly and Justyna Janus, of the Preclinical Imaging Unit, Centre for Core Biotechnological

Services (CBS), University of Leicester. One of the limitations of this study was the small sample size. More animals could be added to increase the study power and give better statistical significance to the experimental data. Due to time constraints, it was not possible to repeat these *in vivo* imaging experiments using DEP1 MIPs.



DyLight 800 MIPs (IV, Supine)

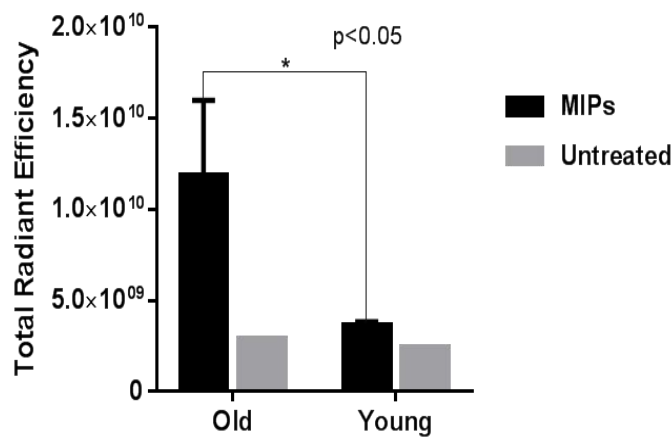


Figure 4-30 Mice *ex vivo* imaging in supine position using DyLight™ 800 MIPs
 Mice were dissected and their *ex vivo* organs imaged in the supine position. Total radiant efficiency of fluorescence signals is shown. Results for the treatment groups are presented as mean \pm SD. The old and young untreated controls only had a single animal each. Unpaired t test shows statistical significance in total radiant efficiency between the 16 months old treatment group and the 2 months old treated group at $p < 0.05$.

4.7 MIPs TARGETED DRUG DELIVERY INTO SENESCENT CELLS

We have shown that MIPs can detect senescent cells *in vitro* and possibly also *in vivo*. This could be exploited to design anti-senescent therapies. In order to investigate the potential ability of B2MG-targeted MIPs to selectively bind to and deliver drugs into target cells as hypothesized, several drug compounds were tested for their toxic effect on senescent cells (see Figure 4-31). Propidium Iodide staining was used to assess cell viability and the percentage of dead cells were recorded. This was done in order to identify the best candidate to use as a toxic payload inside the MIPs. After screening drug compounds, the antimicrobial peptide Gramicidin (Liou *et al.*, 2015), as well as the reported senolytic compounds ABT-263 (Navitoclax) (Chang *et al.*, 2016; Zhu *et al.*, 2016) and Dasatinib (Zhu *et al.*, 2015) were selected as a potential candidates for drug delivery into senescent cells using MIPs.

The EJp16 senescence model was used for the drug delivery assays because this model had a higher expression of B2MG by western blot (see Figure 4-2) and by FACS (see Figure 4-16) when compared to the other models of cellular senescence previously used. Also, the drugs selected were chosen because of their toxic effect on EJp16 cells (see Figure 4-31) and the potential to be slowly released from MIPs into these cells, enhancing their toxic effect. In future studies, other cell models of senescence besides the EJ Cells, such as models of replicative senescence, radiation-induced senescence, oxidative stress-induced senescence and other chemically-induced senescent cells could also be used to confirm the robustness of our therapeutic tools.

In order to test the targeted delivery of toxic drugs, 5 μ M of MIP-Drug conjugates for ABT-263, Dasatinib and Gramicidin were screened on EJp16 cells in 24-well plates and samples were assayed using the MTS cell viability assay. The 48 hour MIP-Dasatinib treatment was found to kill more senescent cells compared to other drugs and incubation times tested (see Figure 4-32). The 5 μ M MIP-Dasatinib conjugates killed 18.5% proliferating cells and 50.7% senescent cells, while the free drug killed 37% proliferating cells and 9.2% senescent cells (see Figure 4-32 and Figure 4-33 A).

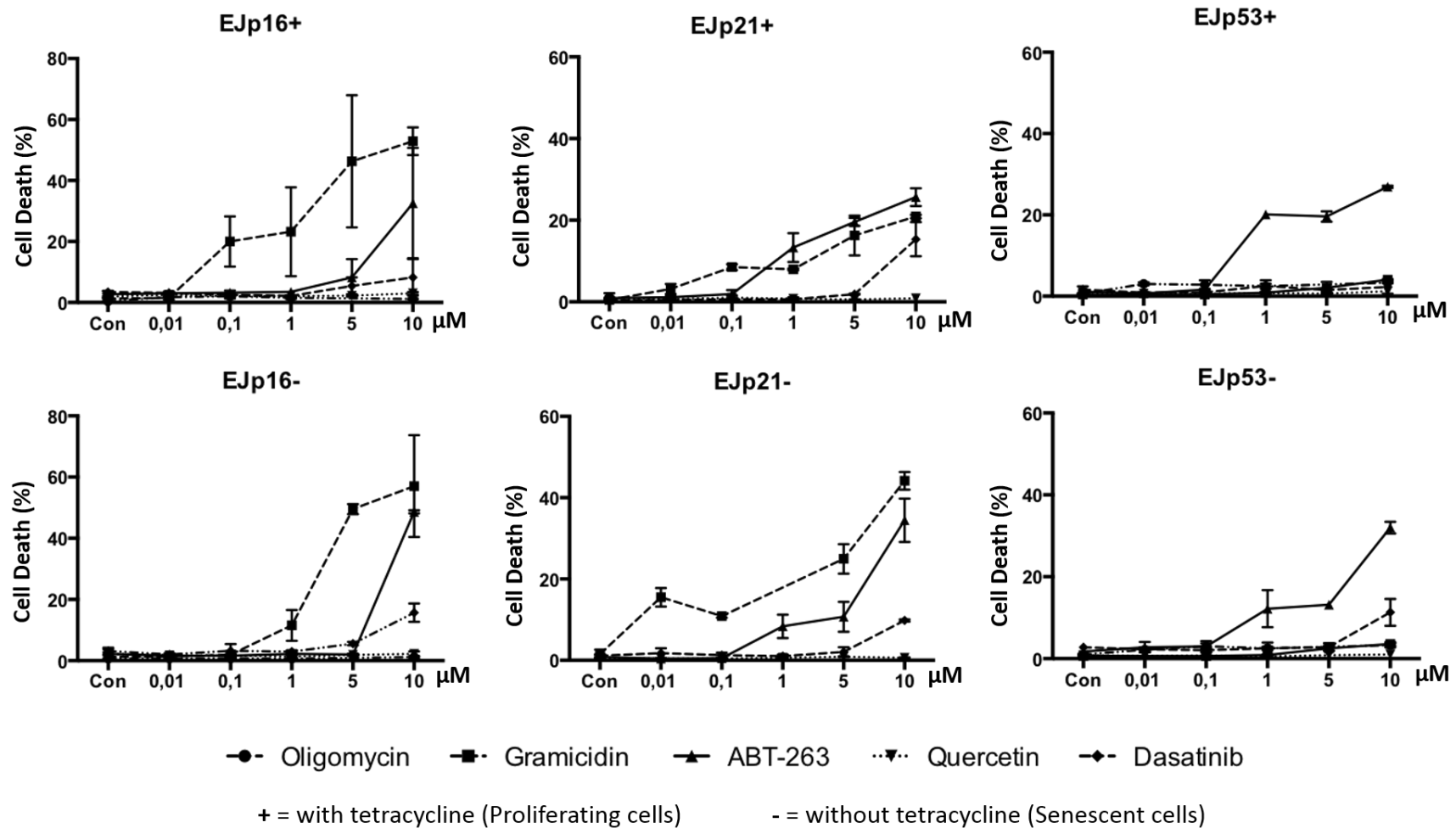


Figure 4-31 Screening of drug compounds for targeted delivery into cells using MIPs

Drug compounds were tested by Propidium Iodide staining using the BD FACSCanto™ II, for their toxicity in senescent cells in order to pick the most potent toxic payload for targeted drug delivery into senescent cells. These results are from a single experiment done in duplicates, and are represented as mean ± SD.

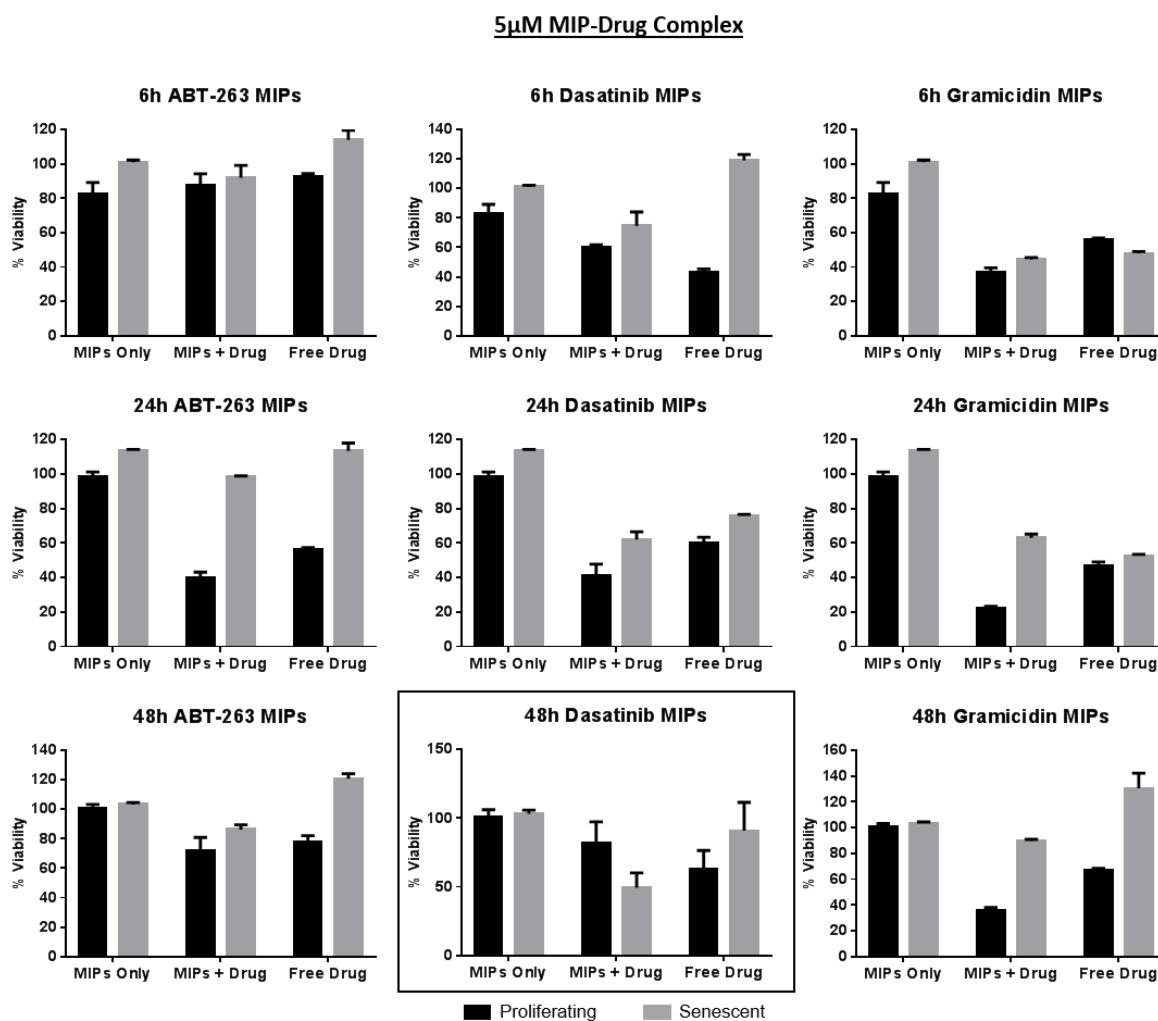


Figure 4-32 MTS cell viability assay for 5 μ M MIP-Drug complexes in EJp16 cells
Proliferating and senescent EJp16 cells were treated with 5 μ M of Drugs conjugated with B2MG-targeted MIPs in 24-well plates. Some samples had MIP-drug complexes, some had free drug and others received MIPs only. Some sample wells had distilled water and were used as a control to normalize all other treatment groups. Samples were incubated at 37 $^{\circ}$ C for 6 hours, 24 hours and 48 hours, after which MTS reagent was added, incubated for 1 hour and plates were read on the Hidex Sense Plate Reader. These results are from a single experiment done in four replicates, and are represented as mean \pm SD.

Next, based on this promising data, Dasatinib was selected for further screening and the incubation time was reduced from 48 hours to 24 hours, while the drug concentration was increased to 10 μ M and 20 μ M (Figure 4-33 B and C). This was done in order to assess the maximum dose of the free drug that would exert a selective toxic effect on senescent EJp16 cells. 10 μ M of MIP-Dasatinib conjugates killed 33.6% of proliferating cells and 84.6% of senescent cells, while 10 μ M free Dasatinib killed 19.8% proliferating cells and 21.6% senescent cells.

The 20 μ M concentration of MIP-Dasatinib conjugates on the other hand was found to kill 11.4% proliferating cells and 83% senescent cells, while the 20 μ M free drug killed 55.5% of senescent cells but did not appear to be toxic to the proliferating cells. These results indicate the potential of B2MG-targeted MIPs to enhance drug delivery into senescent cells and selectively kill them. However, these experiments will need to be further optimized.

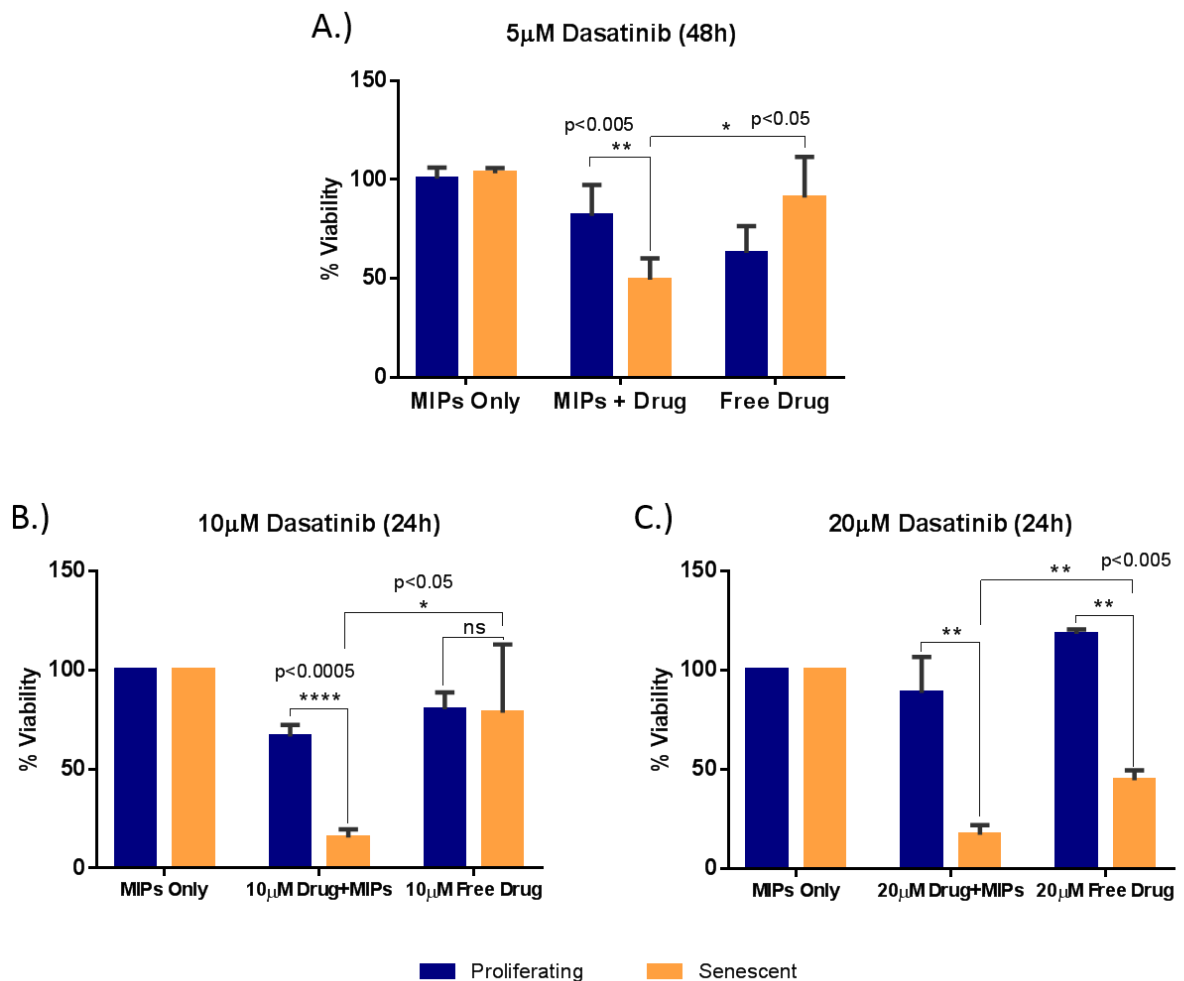


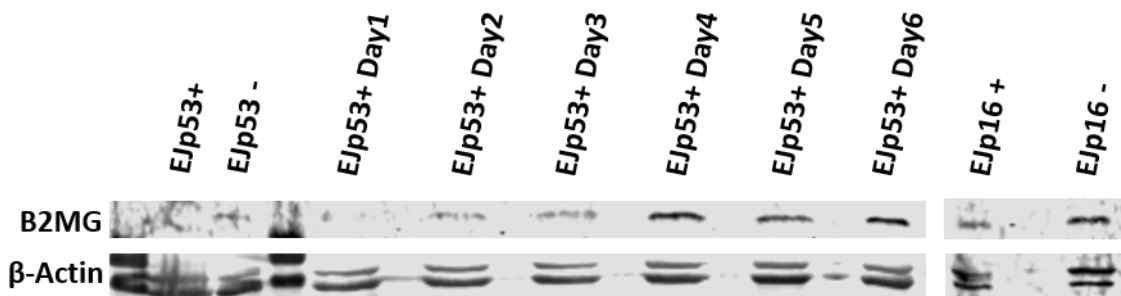
Figure 4-33 Drug delivery into senescent cells using 5 μ M, 10 μ M and 20 μ M MIP-Dasatinib Complex

Proliferating and senescent EJp16 cells were treated with 5 μ M MIP-Dasatinib conjugates in 24-well plates for 48 hours (A) (see Figure 4-32). The drug concentration was afterwards increased for subsequent experiments to 10 μ M (B) and 20 μ M (C) and samples were incubated at 37 $^{\circ}$ C for 24 hours. Results presented are from a single experiment in four replicates and are represented as mean \pm SD. A two-tailed paired t test shows statistical significance at $p < 0.05$, $p < 0.005$ and $p < 0.0005$ as indicated.

4.8 ANTIBODY-DRUG CONJUGATES (ADCs) SELECTIVELY KILL SENESCENT CELLS

In an effort to further validate our novel markers of senescence and to ascertain their usefulness in targeted therapy for senescent cells, antibody-drug conjugates (ADCs) were produced to target B2MG on the surface of senescent cells. ADCs are renowned for their potency and selectivity for intended targets, due to the specificity of the monoclonal antibodies used as well as the cytotoxicity of the drug compounds they carry (Perez *et al.*, 2014). With the help of our collaborators, ABZENA and Leicester Drug Discovery and Diagnostics (LD3), B2MG ADCs coupled with the cytotoxic drug Duocarmycin were manufactured for the targeted clearance of senescent cells *in vitro*.

The EJp16 senescence model was used to test the ADCs because they overexpressed B2MG better than the other models of senescence used (see Figure 4-2 and Figure 4-16). Cell samples used for the assays included senescent and proliferating EJp16. EJp53 cells were transfected with B2MG cDNA for overexpression of the protein and used as a positive control sample for the protein expression. EJp16 cells could not be used for transfection because they are grown in the selection antibiotic needed for the cDNA plasmid and are therefore resistant. The expression of exogenous B2MG can be comparable to that expressed by senescent EJp16 cells used (see Figure 4-34).



+ = with tetracycline (Proliferating cells) - = without tetracycline (Senescent cells)

Figure 4-34 Western Blot analysis of EJp53 cells transfected with B2MG cDNA
B2MG was overexpressed in EJp53 cells and samples were collected over 6 days to check for protein expression levels by western blot. Non-transfected proliferating and senescent EJp53 as well as EJp16 cells were also assessed.

The cell viability assays after treatment with ADCs were carried out in 96-well plates, using the CellTiter-Glo® Luminescent Cell Viability Assay reagent. Three types of B2MG ADCs were supplied and screened in order to pick the best conjugate (Figure 4-35). The B2MG monoclonal antibody alone was also used as a negative control (Figure 4-35 D). B2MG ADC 2 was found to be the most potent against senescent cells. This result suggests that targeting B2MG with ADCs could be a novel therapeutic strategy for the clearance of senescent cells *in vivo*. The ADC cell viability assays and data analyses were performed by Dr. Ana Sousa Manso of the Leicester Drug Discovery and Diagnostics (LD3).

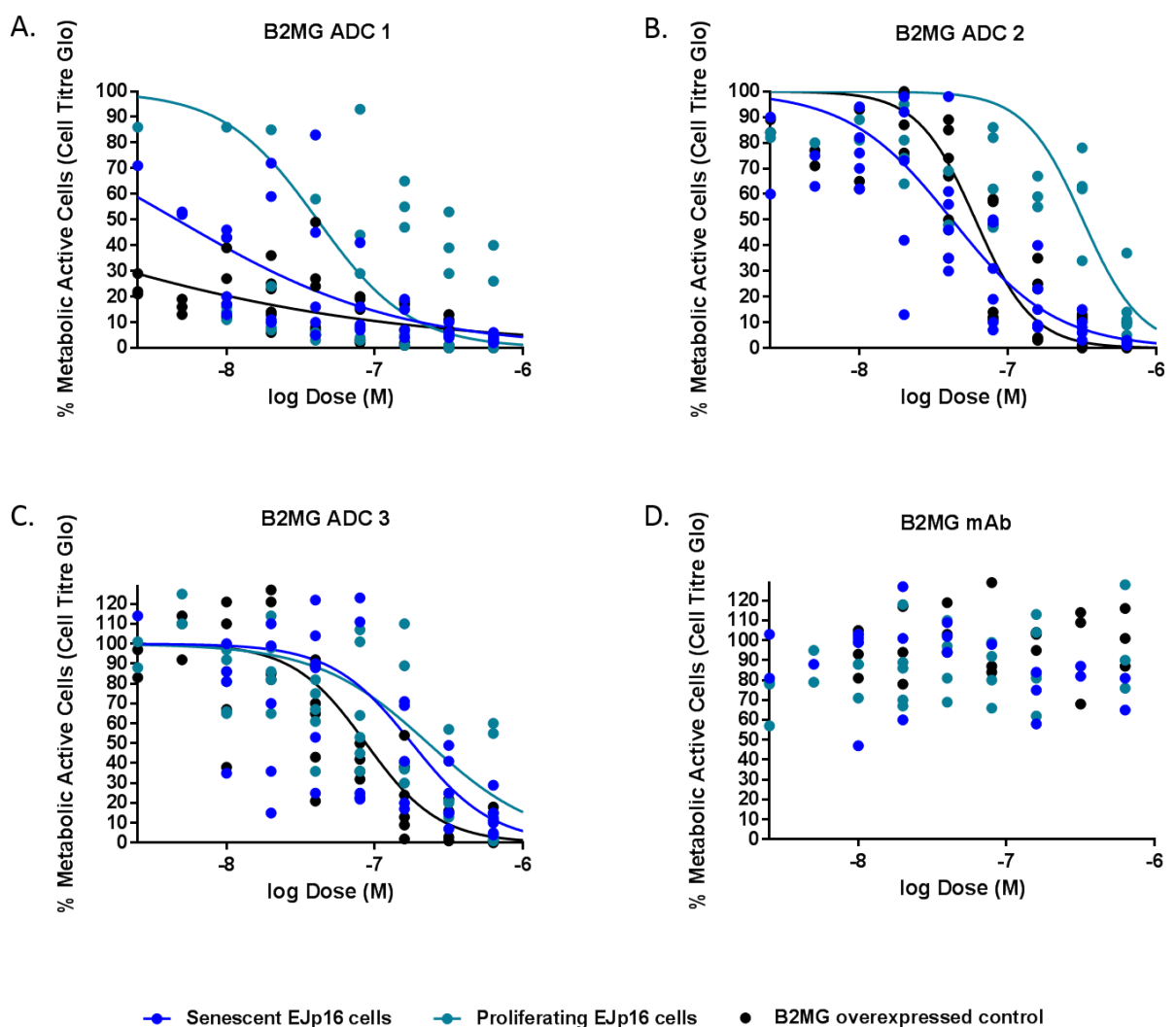


Figure 4-35 Antibody-drug conjugates targeting B2MG kill senescent cells
 ADCs against B2MG target and selectively kill senescent cells over proliferating cells. Three different B2MG ADCs were designed and tested (A, B, C), while the B2MG monoclonal antibody only was used as a negative control (D). B2MG ADC 2 (B) was found to be the most potent against senescent cells, also killing the B2MG overexpressed control cells more than proliferating cells.

4.9 DISCUSSION

The ability to identify or visualize specific biological markers and targets for diseases and to design therapeutics for them has been invaluable to the management of many ailments. Targeted therapies have been used for the treatment of cancer and several other diseases because of their specificity and their high efficacy. Cellular senescence is implicated in the pathology of many diseases due to the deleterious effects of accumulated senescent cells and their secretome in tissues of the body. Senescent cells have therefore been targeted in numerous interventions aimed at lifespan and healthspan improvement, mostly through genetic manipulations (Baker *et al.*, 2011; Kirkland & Tchkonja, 2015; Moreno-Blas *et al.*, 2018) and more recently by the use of senolytic drug compounds (Zhu *et al.*, 2015; Zhu *et al.*, 2016; Chang *et al.*, 2016; Zhu *et al.*, 2017; Lehmann *et al.*, 2017; Pan *et al.*, 2017). However, despite these efforts and progress made so far, senescent cells still prove difficult to target in humans due to the fact that there isn't a specific bio-marker for the identification of senescent cells. Common markers used to identify senescent cells are not exclusive to the senescent state and could therefore lead to false positives if used as sole determinants of cellular senescence. It has therefore been necessary to discover novel bio-markers of senescence which could be used either alone or in combination with other markers to accurately identify senescent cells *in vivo* and *in vitro*.

4.9.1 BETA-2 MICROGLOBULIN AS A MARKER OF SENESCENCE

Here we present Beta-2 Microglobulin (β 2Microglobulin, β 2M, B2M or B2MG) as a novel marker of senescence, which can potentially be used for imaging as well as for the therapeutic targeting and clearance of senescent cells. We also establish for the first time the use of molecularly imprinted polymer nanoparticles (nanoMIPs) and antibody-drug conjugates (ADCs) as proof-of-concept for the targeted clearance of senescent cells through the targeting of B2MG. Our results show that B2MG-targeted MIPs can be used to identify senescent cells both in culture and *in vivo*, and that B2MG MIPs or antibody-drug conjugates can potentially be used therapeutically for the targeted clearance of senescent cells.

4.9.2 BIO-DISTRIBUTION, CYTOTOXICITY AND BIOCOMPATIBILITY OF MIPs

Not much is currently known about the bio-distribution and clearance of MIPs from the body when applied *in vivo*. A study by Hoshino and colleagues has shown that MIP nanoparticles did not produce toxicity in liver, lung or kidneys of mice 2 weeks after intravenous administration (Hoshino *et al.*, 2010). They also found upon analysis of each organ that the MIPs accumulated more in the liver. They postulated that these MIPs were cleared from the animal's blood by the liver's mononuclear phagocytes. In the *in vivo* images presented in our study, the high fluorescent signals appear to come from the lungs, kidneys and jejunum areas, some of which are clearance routes. We can postulate here that more B2MG targeted MIPs bind to senescent cells in older animals, where they accumulate and are retained in their organs compared to the younger animals, which have less MIPs bound and readily clear out unbound MIPs, hence giving less signals. In the Hoshino group study, a high concentration of MIPs (30mg/kg) was used in order to achieve efficient capturing of a toxic peptide in the blood stream. In our study, we used 1.9mg of B2MG-targeted nanoMIPs per kg body weight of mice to achieve *in vivo* imaging of accumulated senescent cells, further reducing any potential toxicity that could have arisen from the use of higher concentrations of these MIPs.

In addition to the B2MG nanoMIPs being non-cytotoxic *in vitro*, no immunogenic response was observed in mice 2 hours after intravenous administration or 24 hours after topical application of B2MG-targeted MIPs and control MIPs. Research by Gagliardi and colleagues has also shown that MIP nanoparticles are biodegradable, displaying a decrease in mean diameter over time. They demonstrated in their study that about 50% - 54% residual diameter of the MIP nanoparticles they used remained after 30 days (Gagliardi *et al.*, 2017). It would be useful to follow up on our study and establish how biodegradable these B2MG nanoMIPs are. It is also acknowledged that long term toxicity studies need to be carried out to ascertain the long-term toxic effect of *in vivo* usage of these B2MG nanoMIPs and to also understand their bio-clearance from the body.

MIPs are a stable and inexpensive tool for the detection and targeting of cellular markers. MIPs could be a more robust alternative to antibodies due to their ease of production and adaptation, cost effectiveness, high stability – eliminating cold chain logistics, as well as their long shelf life. We have found these MIPs to be biocompatible, non-toxic to cells in the long-term and non-toxic to animals in the short-term. It is possible that MIPs could find applications in the nearest future in disease diagnosis, for assessing or measuring ageing, or even to predict which patients would respond to senolytic therapy for a specific disease.

4.9.3 TARGETED SENOLYTIC THERAPY USING MIPs AND ADCs

MIPs have the potential to be used as selective carriers for drug delivery into cells by binding to target molecules on the cell's surface once more data is obtained about their safety and efficacy *in vivo*. Our results show that B2MG nanoMIPs enhance drug delivery into target senescent cells, killing these cells significantly more than their proliferating counterparts. The MIP-Drug complex was found to be ≥ 4 times more effective than the free senolytic drug alone (see Figure 4-33). In the future, this could be a useful novel approach to the clearance of senescent cells and consequently, treatment of many diseases of ageing, but it currently provides proof-of-principle data for targeted clearance of senescent cells using B2MG as the target.

Also, antibody-drug conjugates (ADCs) designed to target B2MG on the surface of senescent cells significantly killed more senescent cells than proliferating cells. Several ADCs are already being used in clinical trials and some have already been approved for the treatment of various diseases (Gébleux & Casi, 2016; Sau *et al.*, 2017). Thus, clinical trials of a senolytic ADC might not be out of reach.

These data together not only demonstrate the suitability of B2MG as a marker of senescence, but also establish the ability of MIPs and ADCs to target and eliminate senescent cells by releasing a toxic payload into these B2MG overexpressing cells. It is worthy of note also that in a study by Zhang and colleagues, they used an antibody-dependent cell-mediated cytotoxicity (ADCC) approach to target $\beta 2$ Microglobulin for the treatment of multiple myeloma (Zhang *et al.*, 2016). Their study presented $\beta 2$ M as a potential target for multiple

myeloma (MM) treatment and also suggested combining the anti- β 2M antibodies with existing MM treatment regimes.

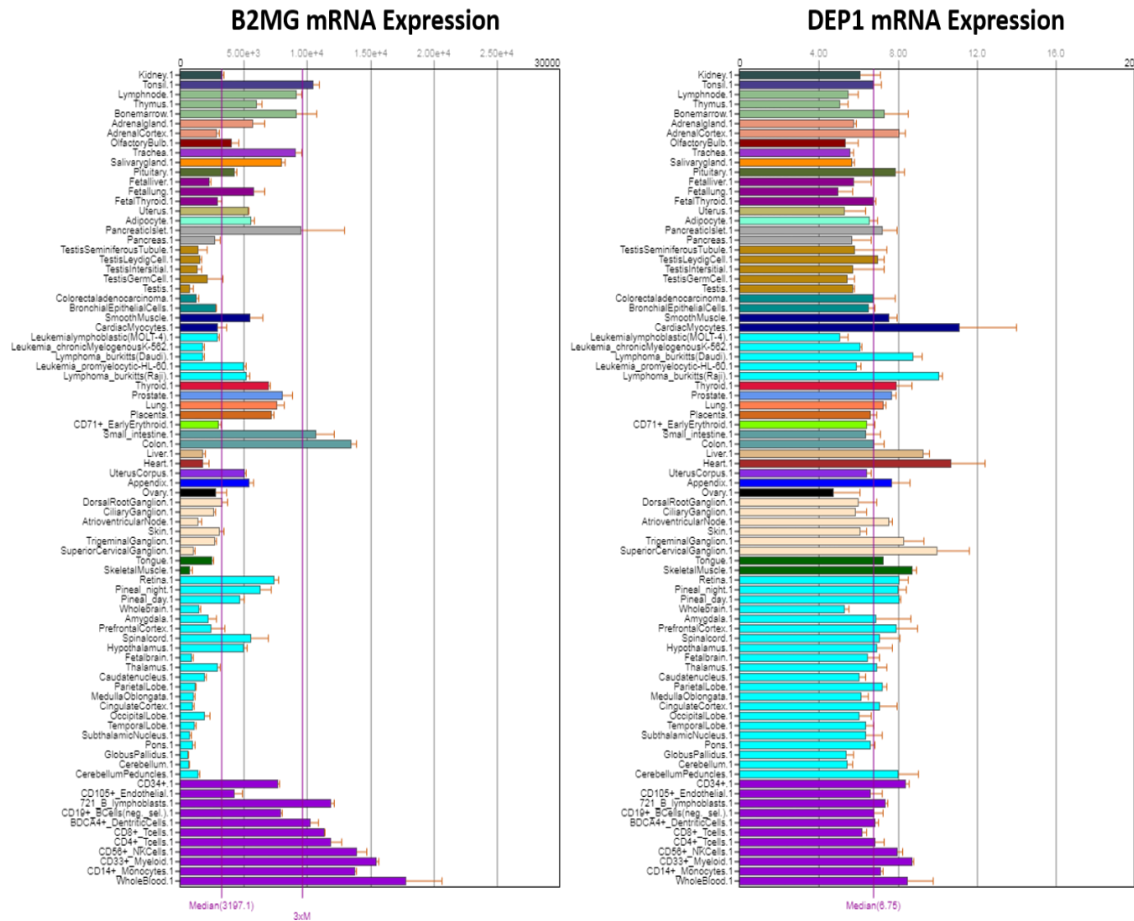


Figure 4-36 Basal mRNA expression of B2MG and DEP1 in human tissues

The basal expression levels of B2MG and DEP1 mRNA in human tissues are shown here. The basal expression of B2MG in tissues is much higher compared to DEP1, as the B2MG protein is expressed in all nucleated cells, except red blood cells.

Data obtained from BioGPS, a publicly available free gene annotation portal

(<http://ds.bioGPS.org/?dataset=GSE1133&gene=567>) and

(<http://ds.bioGPS.org/?dataset=GSE1133&gene=5795>).

We propose the use of B2MG-targeted MIPs and ADCs for the therapeutic clearance of senescent cells. We also propose that they could potentially be used in combination with other existing therapeutic strategies to combat age-related diseases, including cancers. Due to the high basal expression of B2MG in several tissues (see Figure 4-36), its usage as a therapeutic target should be limited to conditions showing a high overexpression of the protein to avoid off target effects.

DEP1 could be a more suitable senescence marker and therapeutic target for age-related diseases and cancers due to its low basal expression in tissues. The DEP1 protein needs to be further researched into for this purpose.

In future studies, it would be worthwhile to carry out additional validation of the selectivity and specificity of these MIPs *in vitro* and *in vivo*. Additional experiments could include using commercially available antibodies alongside the MIPs in flow cytometry. Western blot could also be carried out to compare the binding of MIPs onto a nitrocellulose membrane with antibodies targeting similar protein epitopes. Additionally, control MIPs which do not target any senescence or ageing associated proteins, or empty non-targeting MIPs, could be used alongside the B2MG and DEP1 MIPs in both *in vivo* and *in vitro* experiments.

CHAPTER 5 THE EFFECT OF BTK INHIBITION ON AGEING

Elimination of senescent cells has been shown, in several recent studies, to reduce symptoms associated with ageing and also to extend lifespan and healthspan (Baker *et al.*, 2011; Baker *et al.*, 2016; Chang *et al.*, 2016; Demaria *et al.*, 2017; Baar *et al.*, 2017). Previous studies carried out in our laboratory identified the Bruton's tyrosine kinase (BTK) as one of the proteins overexpressed in senescent cells (Althubiti *et al.*, 2014). This finding led to further studies which demonstrated that Ibrutinib, a BTK inhibitor, was able to ameliorate symptoms associated with ageing (improved physical activity) (Althubiti, 2015) and extend lifespan in *Drosophila melanogaster* (unpublished data). These results were in line with the first report by Honigberg and colleagues using mouse models of autoimmune disease, which showed that Ibrutinib suppressed collagen-induced arthritis and reduced the levels of circulating autoantibodies in arthritic mice, and also reduced renal disease as well as the production of autoantibodies in a mouse lupus model (Honigberg *et al.*, 2010). *In vitro* studies in our laboratory further showed that BTK phosphorylates p53 and modulates its apoptotic and senescence related activities, as inhibition of BTK reduced p53 expression and also blocked p53-induced senescence (Althubiti *et al.*, 2016), while reducing the activity of MDM2 (Rada *et al.*, 2017).

The above mentioned findings about BTK prompted us to carry out *in vivo* studies to assess the effect of Ibrutinib on ageing using the Zinc Metalloproteinase STE24 deficient (*Zmpste24^{-/-}*) mouse model of Hutchinson-Gilford progeria syndrome (Leung *et al.*, 2001; Bergo *et al.*, 2002; Pendás *et al.*, 2002; Gonzalo *et al.*, 2017). These fast-ageing mice were chosen for convenience, since they display signs of ageing within only a few months. Mice were treated with the BTK inhibitor Ibrutinib, administered bi-weekly by oral gavage, in doses of 20mg/kg body weight in the pilot study and 10/mg/kg body weight in the main study. Ibrutinib or PCI-32765 is an irreversible small-molecule inhibitor of BTK which binds covalently to BTK at the cysteine-481 residue, inhibiting its kinase activity (Honigberg *et al.*, 2010; Hendriks *et al.*, 2014; Davids & Brown, 2014; Aw & Brown, 2017). It is a clinically available drug that has been approved for the

treatment of chronic lymphocytic leukaemia (CLL) and mantle cell lymphoma (MCL) (Hendriks *et al.*, 2014; Hutchinson & Dyer, 2014).

The animals were dosed and assessed for clinical signs of frailty, which were scored using a Mouse Frailty Assessment Form (Whitehead *et al.*, 2014). Muscle strength, anxiety levels and cognitive function were also assessed using the Kondziela's inverted screen test, weights lifting tests, the Elevated Plus maze and the Barnes maze as previously described in the methods section. Animals were allowed to reach their humane end-point and survival analysis was carried out between the Ibrutinib treated and the control animals. The data collected allowed us to assess changes in lifespan or healthspan in these mice due to inhibition of BTK.

5.1 CONFIRMING THE GENOTYPE OF ZMPSTE24^{-/-} MICE

Ear punches obtained from mouse identification were collected and used for genotyping, in order to accurately select mice that had the *ZMPSTE24* gene completely knocked out (*Zmpste24*^{-/-}) for use in our study.

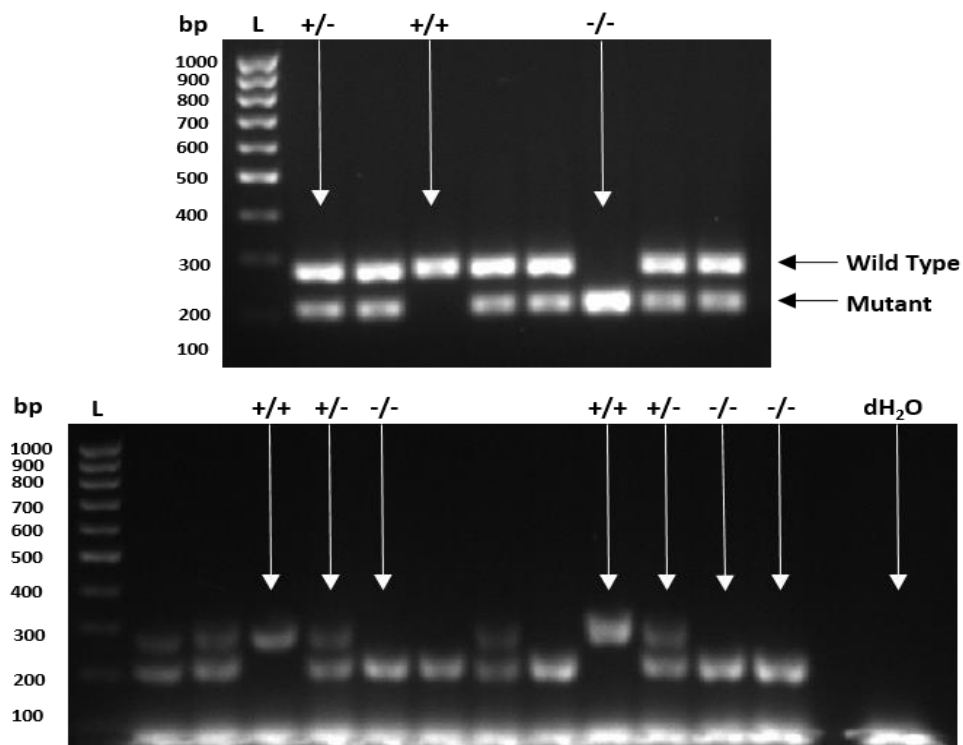


Figure 5-1: Sample genotyping results for ZMPSTE24 deficient mice

Gel images show mouse samples having either wild type (^{+/+}), heterozygous (^{+/-}), or homozygous (^{-/-}) *ZMPSTE24* gene. Ethidium bromide was added to the gels to enable visualisation. PCR Ranger 100bp DNA Ladder was used as a marker to identify the size of the PCR products and distilled water (dH₂O) was run as a blank.

The mice were bred as previously described in the materials and methods, and the offsprings genotyped to determine whether they had a homozygous ($^{-/-}$) or heterozygous ($^{+/-}$) deletion of *ZMPSTE24* or if they had the wild type ($^{+/+}$) gene. Figure 5-1 shows an example of our mouse genotyping results on agarose gel scanned using a Gel Doc. The bands display either the wild type gene at 300 base pairs (bp), the mutant gene at 220 bp, or both genes. Only homozygous offsprings were included in the BTK inhibition study.

5.2 PILOT STUDY ON THE EFFECT OF BTK INHIBITION ON AGEING IN *ZMPSTE24*^{-/-} MICE

To enable us study the effect of BTK inhibition on senescence and ageing *in vivo*, a pilot study was first carried out using nine (9) homozygous *Zmpste24* knock out (KO) mice (*Zmpste24*^{-/-}). Five of the mice (3 females, 2 males) were administered 20mg/kg dose of Ibrutinib twice a week, while four (3 females, 1 male) were given vehicle (distilled water with appropriate volume of DMSO) twice weekly.

5.2.1 ASSESSMENT OF MUSCLE STRENGTH IN THE PILOT STUDY

During the pilot study, animals were assessed for muscle strength using weight lifting tests (Figure 5-2) and the Kondziela's inverted screen test (Figure 5-3). Animals were assessed by the weight lifting tests on the first day of Ibrutinib treatment (Day 0) and afterwards every week for five weeks (i.e. Days 0, 7, 14, 21 and 28). Results from the weight lifting tests indicate that Ibrutinib treated mice showed better muscle strength than the vehicle group although this was not statistically significant (Figure 5-2 A). *Zmpste24*^{-/-} study animals that reached the humane endpoint before the end of the muscle tests were withdrawn from the study and culled humanely. The wild type (WT) cage mates of the study animals were included in the muscle strength tests for comparison but they did not receive drugs or any form of treatment. The weights lifting tests proved difficult to carry out due to the amount of stress it placed on the mice. It was observed that mice from all groups, including the wild-type, were struggling to hold on to the weights, thus generating very variable results. This raised concerns about how much the weight lifting test could be depended on as a measure of strength. Therefore, the test was discontinued after 28 days, to avoid generating unreliable data due to excessive stress on the animals.

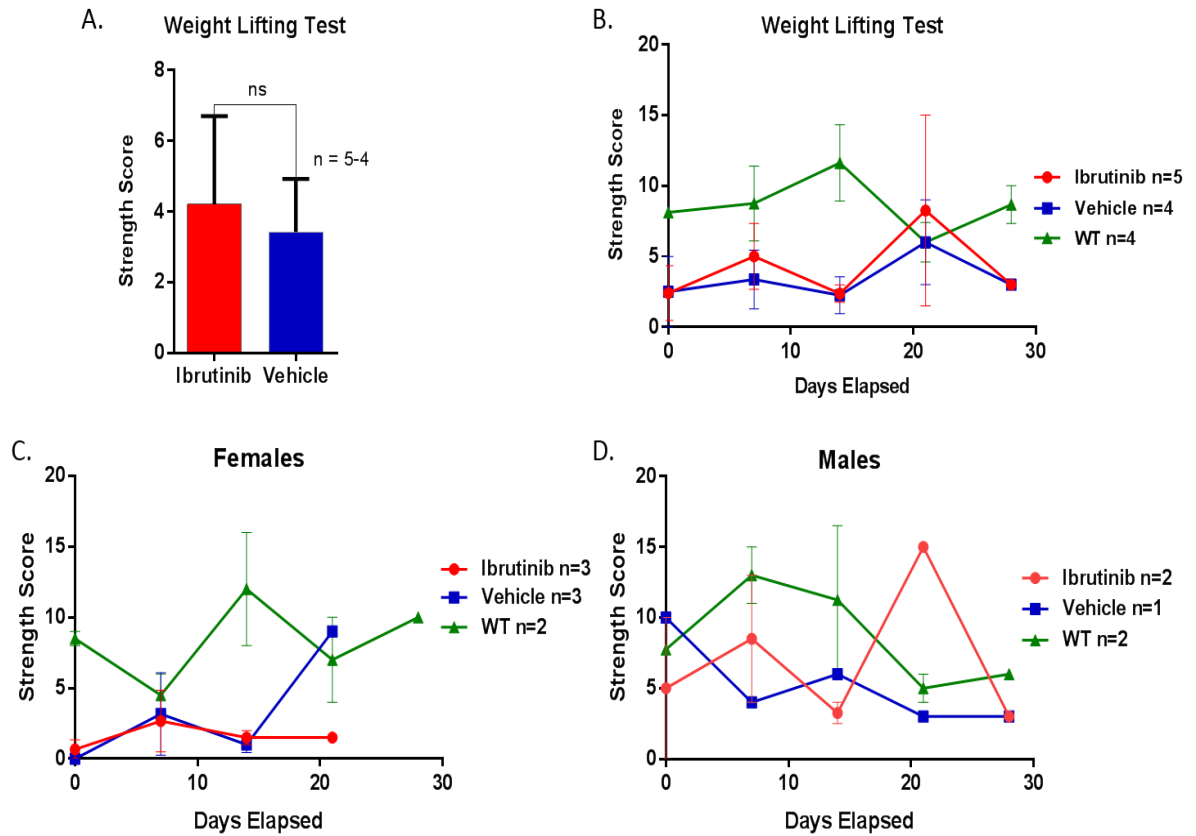


Figure 5-2: Strength score from mouse weight lifting tests

Weights lifting tests were conducted weekly, over five weeks (Days 0 – 28) and results were scored. The average strength score for both Ibrutinib and vehicle treated animals were plotted on a graph (A). This was not significant when analysed by an unpaired *t* test. The weekly performance of each treatment group as well as the wild type animals (WT) is presented (B) and results are also presented for both female (C) and male (D) groups. The results are presented as mean \pm SEM.

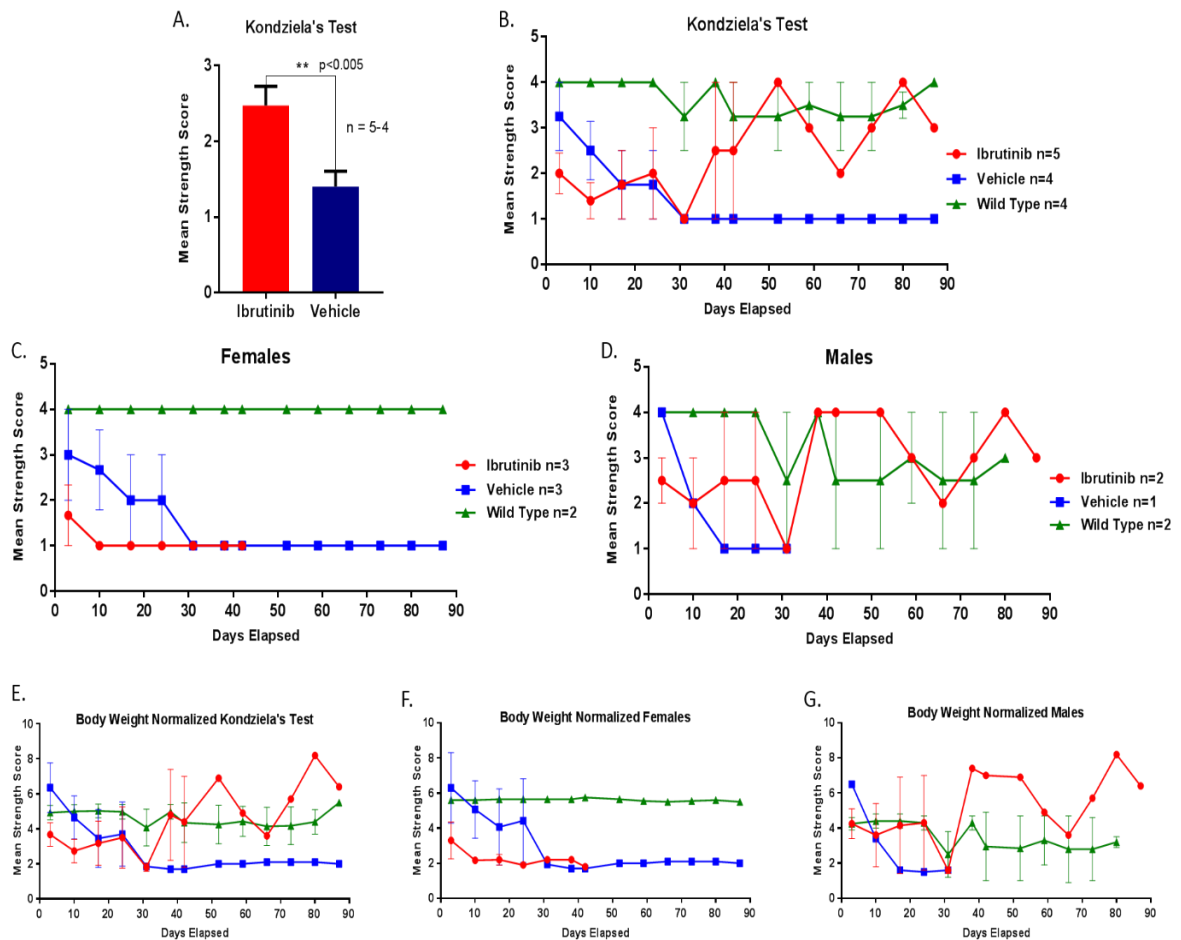


Figure 5-3: Strength scores from the Kondziela's inverted screen test

Measurement of muscle strength in mice was done using the Kondziela's test. Animals were tested weekly from Day 3 to Day 87 of Ibrutinib treatment and their strength scores recorded. Ibrutinib treated mice showed significantly higher muscle strength compared to the vehicle group as analysed by a two-tailed unpaired *t* test (A). Weekly performance of the mice were recorded (B) and results shown by sex (C and D) along with their body weight normalized scores (E-G). Data is shown as mean \pm SEM.

Results from the Kondziela's test showed that Ibrutinib significantly improved muscle strength in fast ageing mice (Figure 5-3 A and B), specifically in males (Figure 5-3 C and D). When the strength scores were normalized by the animals' body weights, the performance of the Ibrutinib treated progeroid mice was found to be better than that of the wild type mice (Figure 5-3 E-G). In general, results from the pilot study suggest an improvement in muscle grip and strength in Ibrutinib treated mice over mice that were administered the vehicle.

5.2.2 PILOT STUDY SURVIVAL ANALYSIS

The animals continued to receive treatment and remained in the study until they reached a humane endpoint (HEP) as indicated on the Project Licence, after which they were culled humanely. The pilot study lasted for 90 days when the last set of animals reached their HEP. In order to determine the effect of BTK inhibition on lifespan in *Zmpste24^{-/-}* mice, survival analysis was done and Kaplan Meier survival curves were generated for both the treatment and the vehicle control groups, using GraphPad Prism software version 7.0. Ibrutinib was however not found to improve survival or extend lifespan in these mice by the end of the 90 days pilot study.

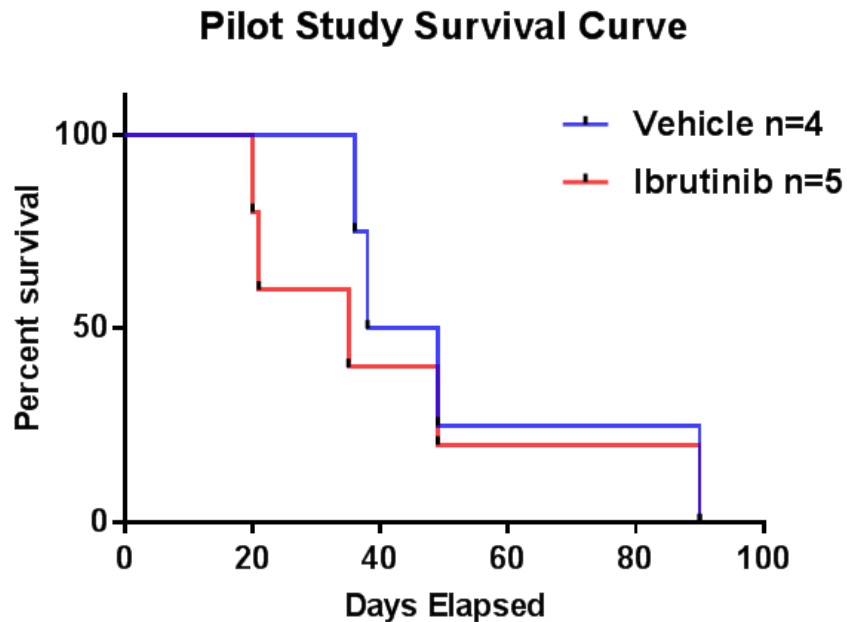


Figure 5-4: Kaplan Meier survival curve for the pilot *Zmpste24^{-/-}* mice study

Survival curves were generated for Ibrutinib treated and vehicle control group animals from the pilot study. Ibrutinib treatment was not found to improve survival of *Zmpste24^{-/-}* Mice. Mean and median survival for Ibrutinib group was 43 days and 39 days respectively, while that for the vehicle group was 53.3 days and 43.5 days respectively. This was not statistically significant by the Log-rank (Mantel-Cox) test which gave a P value of 0.5280.

5.3 FULL STUDY ON THE EFFECT OF BTK INHIBITION ON AGEING IN ZMPSTE24^{-/-} MICE

A total of 38 homozygous *Zmpste24* KO mice were recruited into the main study in order to assess the effect of BTK inhibition on senescence and ageing *in vivo*. The dose of Ibrutinib was reduced from 20mg/kg used in the pilot study, to 10mg/kg to reduce potential side effects. Also, we wanted to observe the effect that a lower dose of Ibrutinib would have when taken over a longer period of time.

20 of these mice were treated with 10mg/kg dose of Ibrutinib twice weekly by oral gavage, while 18 received the vehicle. Animals were added onto the study only after they reached 8 weeks of age, as instructed in the Project Licence. As a result of this, rather than starting drug treatment on all animals at the same time, the study was designed to be staggered and was carried out over a period of 8 months. Consequently, the mice behavioural and cognitive function assessments were carried out in four different groups by age, depending on availability of homozygous litters. The results were then collated into one at the end of the study.

The Project Licence only allowed these *Zmpste24^{-/-}* mice to be kept for a maximum of 8 months of age since they easily developed health disorders, fragile phenotypes and aged faster than their wild type littermates which usually live up to 2½ years of age. Therefore, an animal could only be on the study for a maximum of 6 months if it started treatment at 8 weeks of age. In the course of this study, mice were assessed for muscle strength, signs of clinical frailty, anxiety-like behaviour, cognitive function (spatial memory) as well as survival.

5.3.1 ASSESSMENT OF MUSCLE STRENGTH

The Kondziela's inverted screen test was used to assess the effect of long term Ibrutinib administration on muscle strength in mice, having observed an improvement in muscle strength in the pilot study. The results show no significant differences between the two groups (Figure 5-5 A). There was a similar decrease in muscle strength of the *Zmpste24^{-/-}* mice over time as the animals aged, irrespective of the type of treatment given (Figure 5-5) and when normalized by their body weights (Figure 5-5 C).

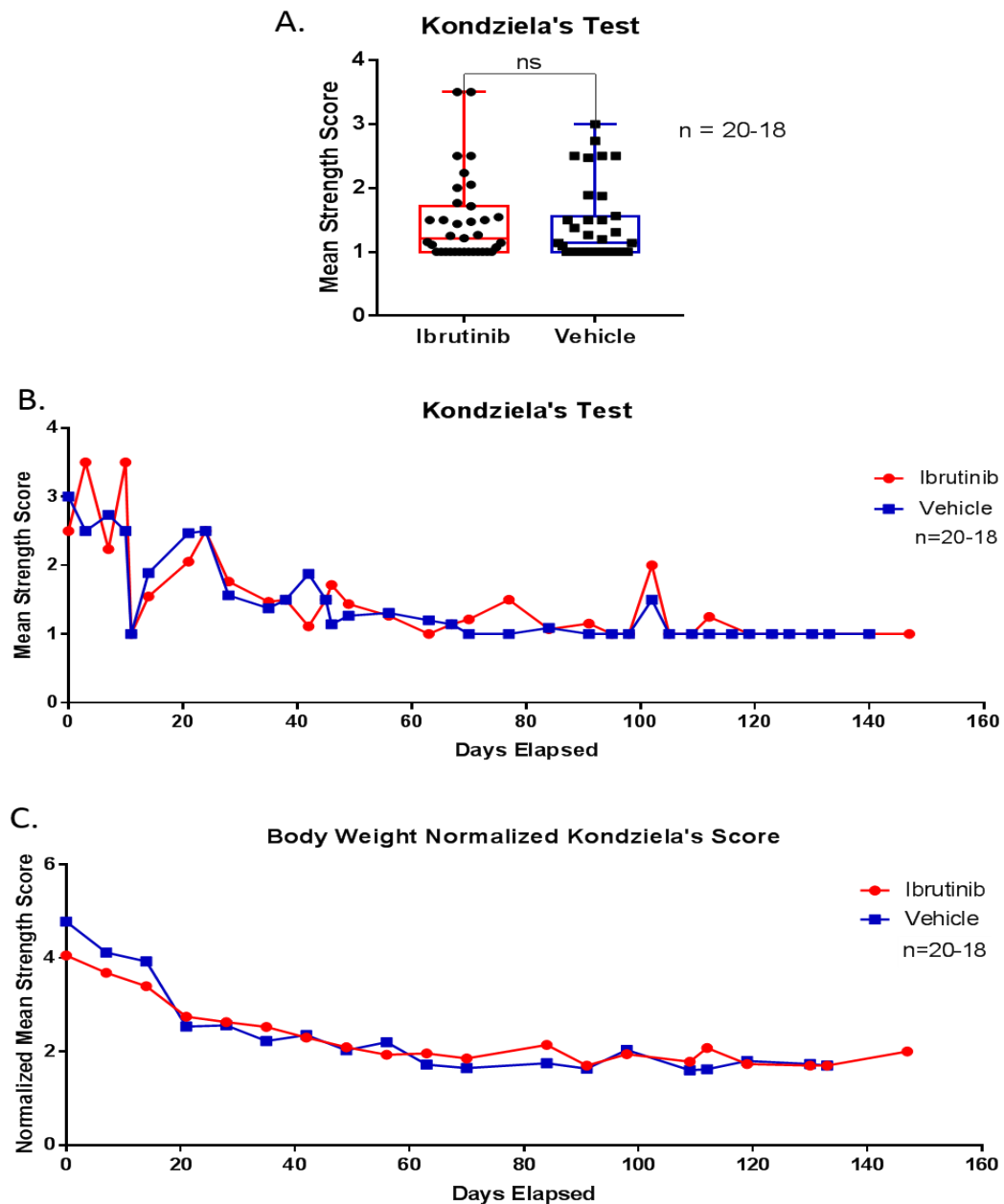


Figure 5-5 Main study Kondziela's strength scores

Strength scores from the Kondziela's inverted screen test for the main study were recorded and analysed using GraphPad Prism. There was no statistical significance in total strength score between Ibrutinib treatment and vehicle control groups using student's *t* tests (A). The strength scores for mice from both groups was seen to decrease as they aged (B) and this was not different when normalized by their body weights (C). Results are presented as mean \pm SEM.

5.3.2 ASSESSMENT OF CLINICAL FRAILTY IN MICE

In order to accurately assess clinical frailty in the study animals, 30 of the 31 health-related variables previously described by Jocelyne Whitehead and colleagues (Whitehead *et al.*, 2014) were measured. These clinical frailty measurements included assessment of the integument, the

physical/musculoskeletal systems, the vestibulocochlear/auditory system, the oculo-nasal system, the digestive system, the urogenital system, the respiratory system, signs of discomfort as well as the body weight (see Figure 2-4). Body surface temperature was not part of the parameters measured in these animals.

The vehicle treated mice had significantly higher frailty index scores towards the end of their lifespan (Day 133 – Day 150) compared to the Ibrutinib treated mice (Figure 5-6 B & C). This suggests that long-term administration of Ibrutinib prevented late-life clinical frailty and ameliorated signs of ageing. When the total clinical frailty scores were calculated, there was no statistically significant difference between the two groups (Figure 5-6 A). However, the frailty scores was similar between both groups from the start of the experiment until the last 3 weeks of the animals' life-span (day 133 onwards) when the vehicle group deteriorated but the Ibrutinib group did not.

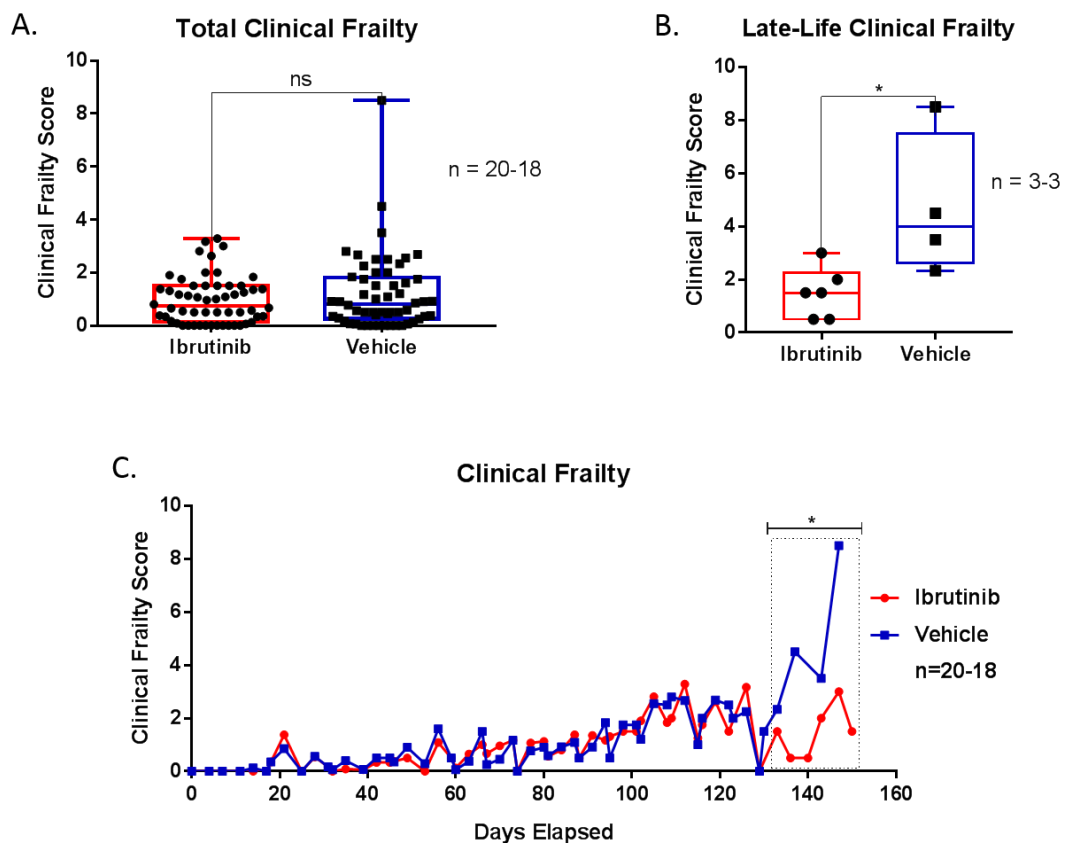


Figure 5-6 Clinical Frailty Scoring in *Zmpste24*^{-/-} mice

Results from clinical frailty assessments of Ibrutinib treated and vehicle control *Zmpste24*^{-/-} mice showing a significant amelioration of late-life frailty in the treated animals (B & C). Total clinical frailty scores were however not statistically significant.

Data was presented as the mean \pm SEM and statistical analysis done using an unpaired *t* test.

Table 5.1 Variables used to measure clinical frailty in mice. Number of cases and % of cases are shown.

| PARAMETERS | NUMBER OF ANIMALS WITH INCIDENTS | | | | | | PERCENTAGE OF CASES RECORDED (%) | | | | | |
|---|----------------------------------|-----------|------------|----------------|-----------|------------|----------------------------------|------------|------------|----------------|------------|------------|
| | IBRUTINIB (n=20) | | | VEHICLE (n=18) | | | IBRUTINIB (n=20) | | | VEHICLE (n=18) | | |
| | Mild | Severe | Total | Mild | Severe | Total | Mild | Severe | Total | Mild | Severe | Total |
| Alopecia | 6 | - | 6 | 8 | - | 8 | 30 | - | 30 | 44 | - | 44 |
| Loss of fur colour | 10 | - | 10 | 6 | - | 6 | 50 | - | 50 | 33 | - | 33 |
| Dermatitis | 2 | - | 2 | - | - | - | 10 | - | 10 | - | - | - |
| Loss of whiskers | 1 | - | 1 | - | 1 | 1 | 5 | - | 5 | - | 6 | 6 |
| Coat condition | 7 | 5 | 12 | 7 | 5 | 12 | 35 | 25 | 60 | 39 | 28 | 67 |
| Kyphosis | 14 | - | 14 | 13 | - | 13 | 70 | - | 70 | 72 | - | 72 |
| Tail stiffening | 1 | - | 1 | - | - | - | 5 | - | 5 | - | - | - |
| Gait disorders | 4 | - | 4 | 3 | - | 3 | 20 | - | 20 | 17 | - | 17 |
| Tremor | 12 | - | 12 | 11 | 1 | 12 | 60 | - | 60 | 61 | 6 | 67 |
| Forelimb grip strength | 17 | 2 | 19 | 14 | 1 | 15 | 85 | 10 | 95 | 78 | 6 | 84 |
| Body condition score | 8 | 3 | 11 | 4 | 5 | 9 | 40 | 15 | 55 | 22 | 28 | 50 |
| Hearing loss | 7 | 1 | 8 | 8 | 1 | 9 | 35 | 5 | 40 | 44 | 6 | 50 |
| Corneal Opacity | 3 | - | 3 | - | 1 | 1 | 15 | - | 15 | - | 6 | 6 |
| Eye discharge/swelling | 6 | 2 | 8 | 5 | 3 | 8 | 30 | 10 | 40 | 28 | 17 | 45 |
| Malocclusions | 2 | 7 | 9 | 6 | 4 | 10 | 10 | 35 | 45 | 33 | 22 | 56 |
| Vaginal/uterine/penile prolapse | 4 | 2 | 6 | 7 | 1 | 8 | 20 | 10 | 30 | 39 | 6 | 45 |
| Diarrhoea | - | - | - | 1 | - | 1 | - | - | - | 6 | - | 6 |
| Breathing rate/depth | - | - | - | 1 | - | 1 | - | - | - | 6 | - | 6 |
| Piloerection | 7 | 4 | 11 | 9 | 4 | 13 | 35 | 20 | 55 | 50 | 22 | 72 |
| Body weight loss (20% threshold) | 8 | 11 | 19 | 8 | 10 | 18 | 40 | 55 | 95 | 44 | 56 | 100 |
| TOTAL SUM | 119 | 37 | 156 | 111 | 37 | 148 | 595 | 185 | 780 | 616 | 209 | 826 |

Out of the 30 variables assessed, the *Zmpste24*^{-/-} mice showed signs for 20 of them, where there was an incidence recorded at least once during the study. The results are presented in Table 5.1 as number of cases recorded and as the percentage of mice that presented with an incidence.

5.3.3 EFFECT OF BTK INHIBITION ON ANXIETY-LIKE BEHAVIOUR IN ZMPSTE24^{-/-} MICE

Anxiety disorders have been shown to increase in ageing (Perna *et al.*, 2015) hence, our study animals were tested on the elevated plus maze (EPM) in order to assess the effect of the BTK inhibitor Ibrutinib on anxiety-like behaviour in aged mice. In the EPM test, the number of times a mouse entered into each arm of the maze (entries made), as well as the amount of time spent there were recorded. The number of times the mice peeked into the open arms without actually entering in was also recorded. This information was analysed on GraphPad Prism (Figure 5-7) and used to characterize augmented anxiety-like behaviour in these mice. Again, this maze test was done in a staggered manner due to the different start dates of the study animals, and results were collated at the end of the study.

A total of 34 fast-ageing mice from the study were tested on the EPM. 18 of them were on Ibrutinib treatment while 16 were given the vehicle. A total of 19 wild-type and heterozygous cage-mates (buddies) which were not given any treatment were also included in the EPM tests for comparison. In the basal EPM tests, there were 7 mice in the Ibrutinib group, 7 mice in the vehicle group and also 7 buddies. In the EPM test done 4 weeks after treatment, there were 10 mice in each group, while the EPM done after 12 weeks had 15 mice in the Ibrutinib group, 10 mice in the vehicle group and 16 buddies. The results are summarised in Figure 5-7 and indicate a reduced anxiety-like behaviour in the Ibrutinib treated animals, consistent with the prolonged healthspan suggested by the clinical frailty assessment. In all parameters measured, the pattern of exploration of the maze did not change for the buddy group from baseline to 4 weeks and after 12 weeks. Ibrutinib treated mice showed significant reduction in the number of peeks made into the open arms after 4 weeks and 12 weeks of treatment. For unknown reasons, the vehicle treated mice made no entries into the open arm when tested

at 4 weeks, nevertheless, they spent more time in the open arms when tested 3 months (12 weeks) after treatment.

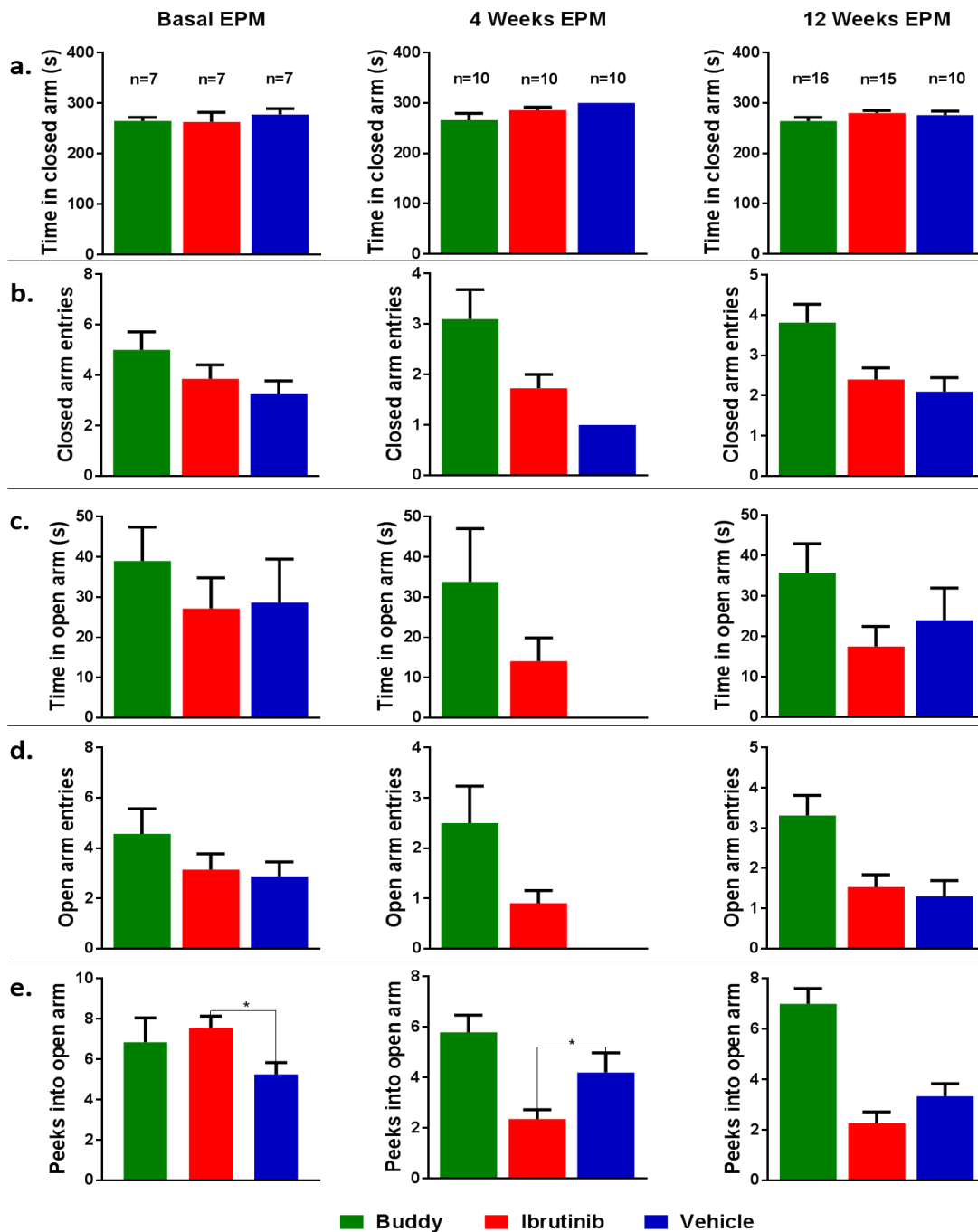


Figure 5-7 Behavioural effects of Ibrutinib treatment in mice using the EPM

Anxiety-like behaviour was assessed in mice using the elevated plus maze (EPM). There was no significant change in mice entry into the closed arms for both Ibrutinib and vehicle groups (a & b). Ibrutinib treated mice were found to spend more time in the open arms after 4 weeks of treatment (c), and they made more entries into the open arm than vehicle treated mice (d). There was also a significant reduction in the number of peeks made by the Ibrutinib treated mice into the open arm of the maze (e). Overall, the results indicate increased anxiety-like behaviour in the vehicle group compared to the Ibrutinib group. Statistical analyses were done using paired *t* tests and results are presented as mean \pm SEM.

5.3.4 EFFECT OF BTK INHIBITION ON SPATIAL MEMORY IN ZMPSTE24^{-/-} MICE

Memory loss, cognitive dysfunction and dementia are some of the symptoms associated with ageing and are manifest in conditions such as Alzheimer's disease (Esiri, 2007; Attar *et al.*, 2013; Yang *et al.*, 2017). Barnes maze experiments were carried out in order to test the effect of Ibrutinib therapy on spatial memory in Zmpste24^{-/-} mice. Wild-type and heterozygous cage mates (buddies) of the study animals were also included in the tests for comparison.

5.3.4.1 ACQUISITION TRIALS

All mice demonstrated good learning progress during the acquisition or training phase, as can be seen by the steady reduction in their primary latency time (Figure 5-8 A) and the time taken to enter inside the escape box or secondary latency (Figure 5-8 B).

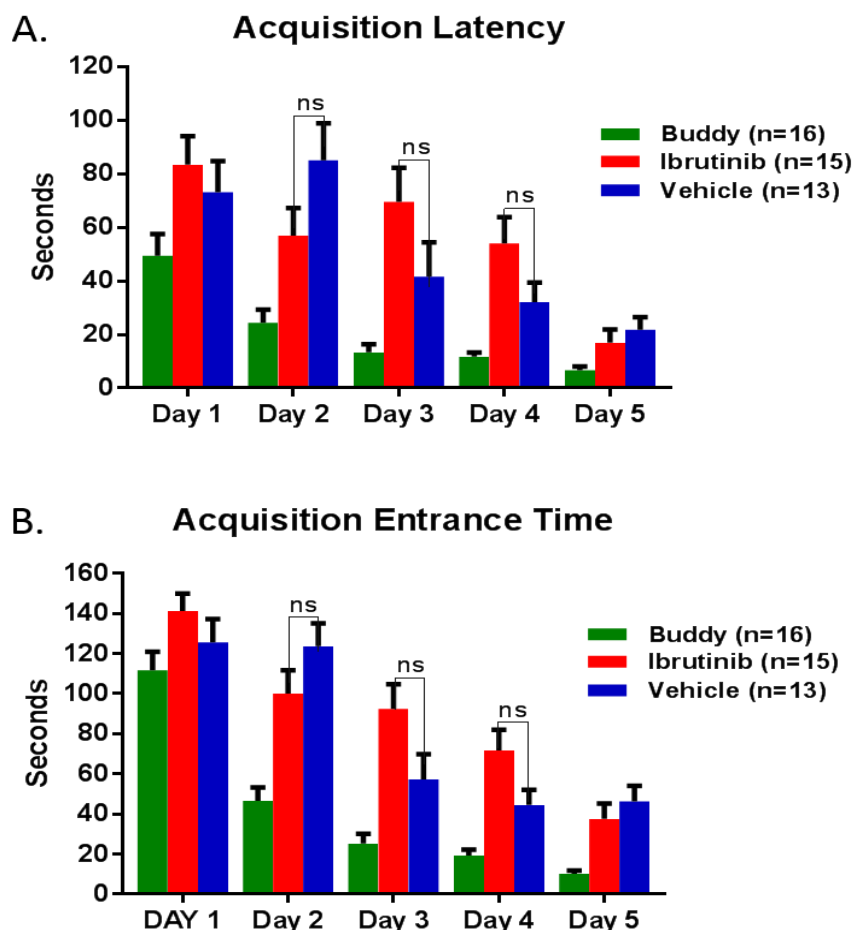


Figure 5-8 Latency and entrance time of mice into target hole during acquisition

All mice demonstrated learning by the progressive decrease in their latency (A) and time taken to enter the escape box (B). The Ibrutinib treated mice took longer to reach and enter into the target hole except on days 2 and 5, although these differences were not significant at $p < 0.05$. The data is presented as mean \pm SEM.

All groups of animals also had a higher frequency of nose pokes into the target hole than into other holes on the first two days of acquisition, as shown by the bell shaped graphs (Figure 5-9), but this pattern was lost by the third day.

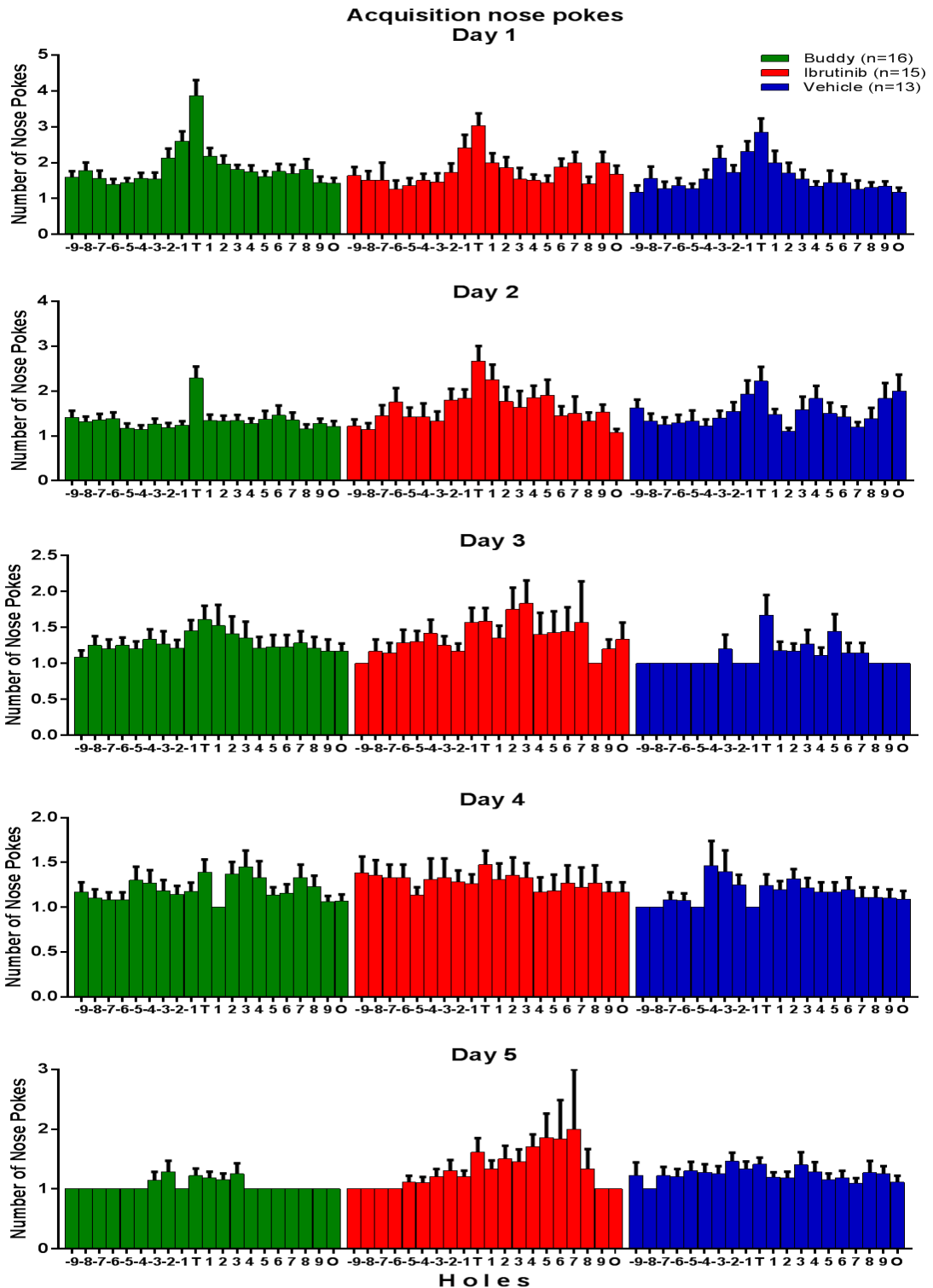


Figure 5-9 Mice nose pokes into maze holes during acquisition stage
 Number of nose pokes into the Barnes maze holes show a higher frequency of target holes pokes in the first two days. Data is presented as mean \pm SEM.

The percentage of nose pokes into the target hole (Figure 5-10) was calculated from the total number of nose pokes recorded (Figure 5-9). This gave information about the frequency and accuracy with which the mice were able to identify the target hole during the learning period as the acquisition training days went by. Mice from both treatment groups as well as the buddies showed gradual daily improvement in their accuracy for the target hole. For unknown reasons, Ibrutinib treated mice were found to have an increased accuracy for the target hole than the vehicle group on days 2 and 5, while their data for the other three days were comparable (Figure 5-10).

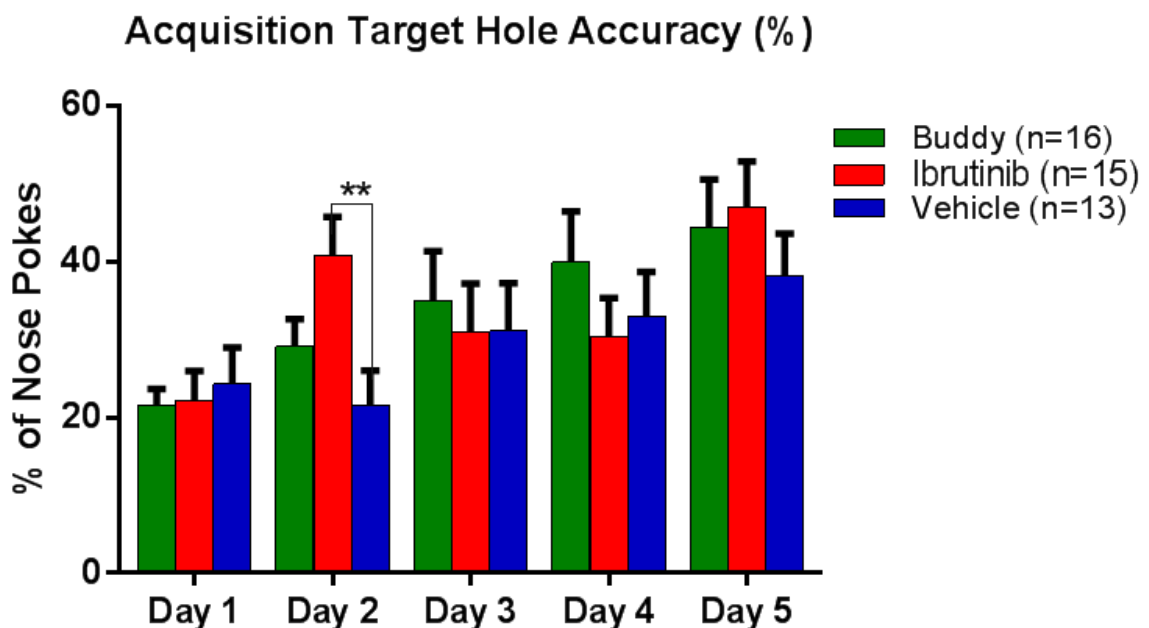


Figure 5-10 Accuracy of Target Hole Identification during Acquisition

Mice from all three groups progressively learned to identify the target hole with the Ibrutinib group identifying the hole at a higher percentage accuracy than the vehicle group on days 2 and 5. Results are presented as mean \pm SEM and a paired *t* test was used to determine statistical significance at $p < 0.05$.

5.3.4.2 PROBE TRIAL

On the day of the probe trial, when the escape box was taken away from the maze, the vehicle group exhibited reduced latency in reaching the target hole compared to the Ibrutinib treated group (Figure 5-11 A). The result was similar for both female and male animals (Figure 5-11 B & C). Although this was not statistically significant, it was contrary to the observed accuracy or percentage of nose pokes they made into the target hole during the acquisition stage (Figure

5-10). As expected, the buddies also reached the target hole in significantly less amount of time than either of the fast-ageing mice groups. The latency during the probe trial is used as a measure of short-term spatial memory in mice. This result (Figure 5-11) on its own suggests that BTK inhibition could have a negative effect on short-term memory.

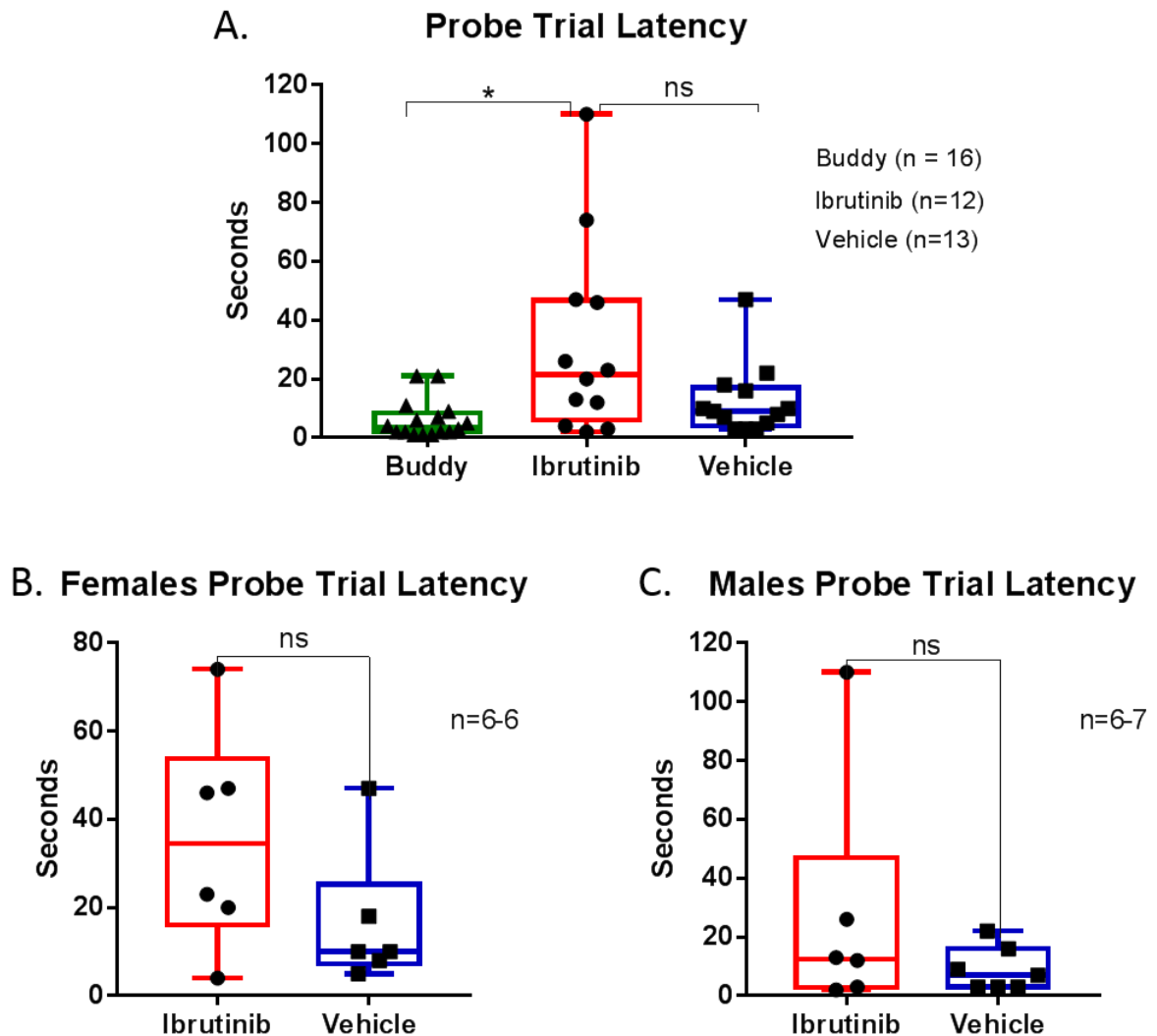


Figure 5-11 Latency during Barnes Maze Probe Trial

During the probe trial, the vehicle treated mice reached the target hole in less time than the Ibrutinib treated mice (A). The pattern was similar for both females (B) and males (C) but there was no statistical significance at $p < 0.05$ using paired t tests. The buddies also had significantly less latency than the fast-ageing mice. Results are presented as mean \pm SEM.

In agreement with the latency results, the vehicle treated mice also had a higher number of nose pokes into the target hole during the probe trial compared to the

Ibrutinib treated group (Figure 5-12 A). They also demonstrated a higher percentage of nose pokes into the target hole than the Ibrutinib treated mice (Figure 5-12 B), although this was not statistically significant at $p < 0.05$.

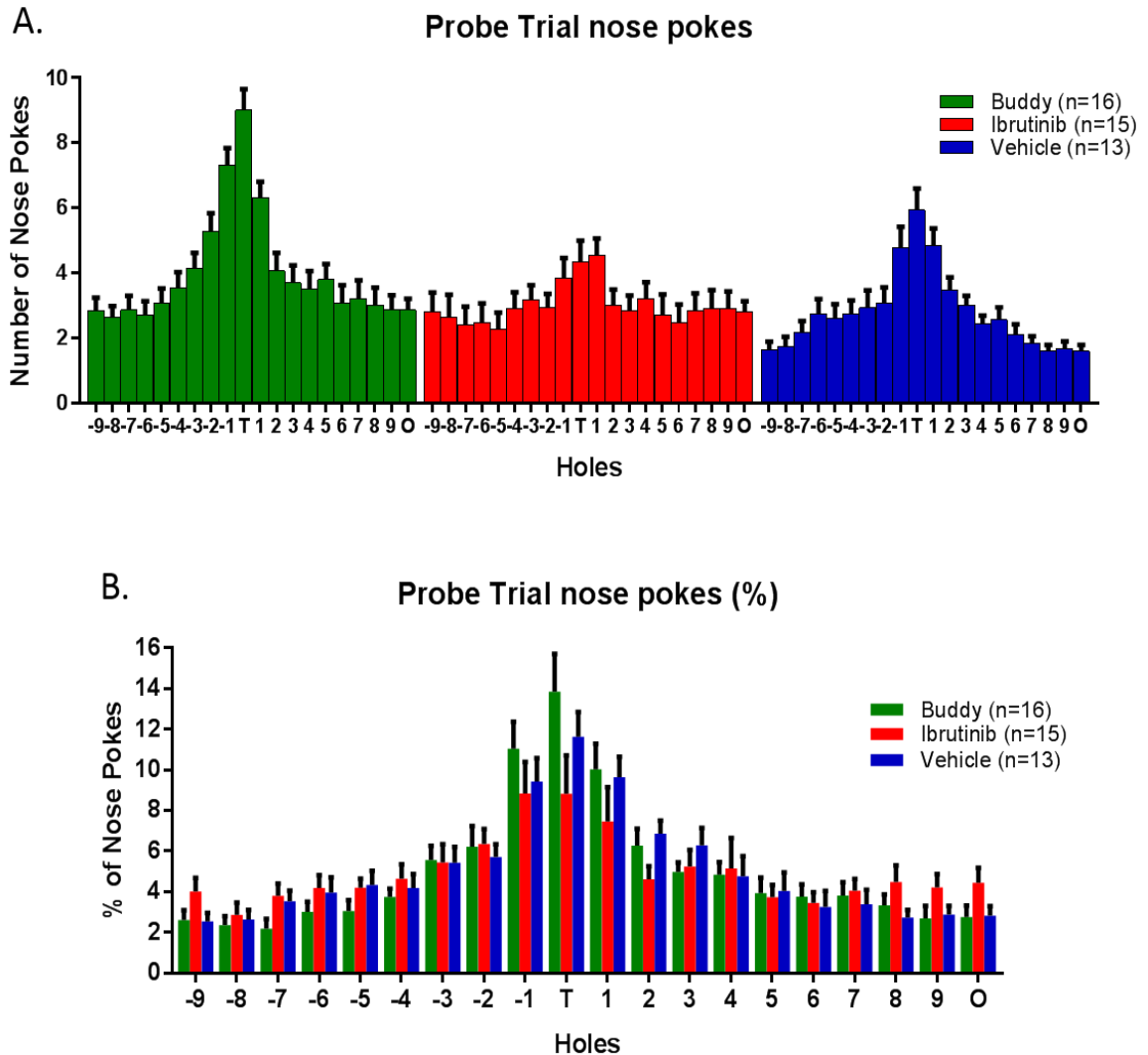


Figure 5-12 Mice Nose Pokes into holes during the Probe Trial

Number of nose pokes into maze holes (A) and the percentage of nose pokes (B) are shown. Results are presented as mean \pm SEM.

5.3.4.3 RECALL

The recall latency, which is the time it takes for a mouse to reach the target hole 7 days after the probe trial, was recorded. This recall latency is used as a measure of long-term memory in mice and is thought to be a true test of memory compared to the probe trial. Although the Ibrutinib treated mice had a mean recall latency that was comparable to the buddy group and lower than that of the vehicle

group, this was not statistically significant at $p < 0.05$ (Figure 5-13 A). Interestingly, the male Ibrutinib treated mice showed a significant reduction in their recall latency, indicating more than a two-fold improvement in long-term memory compared to the vehicle treated male mice (Figure 5-13 C). The reverse was the case for the female mice (Figure 5-13 B).

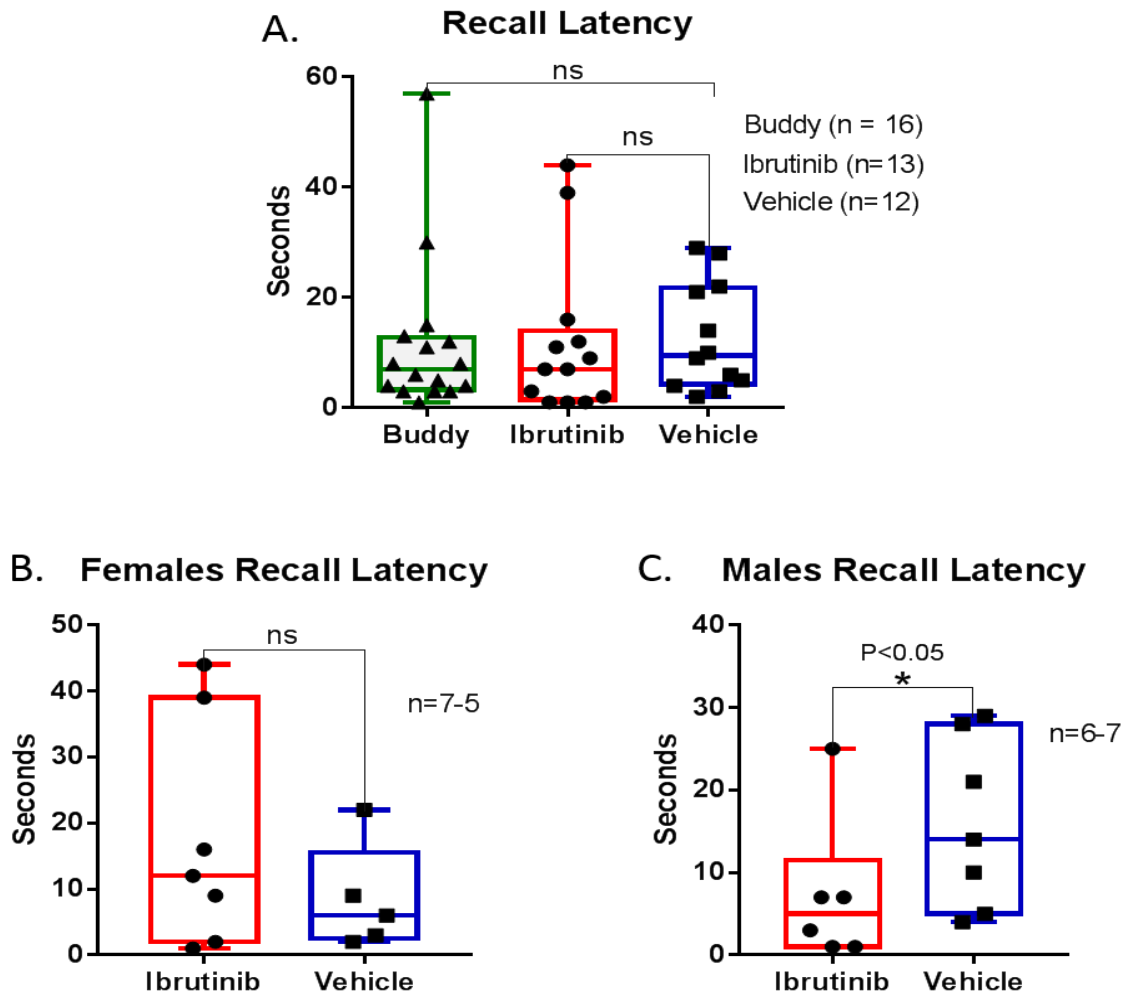


Figure 5-13 Latency during the Barnes Maze Recall tests

Total recall latency for all animal groups are presented (A). Male Ibrutinib treated mice have a significantly lower latency than their vehicle treated counterparts (C). The opposite was the case for female group (B). Statistical significance was determined using paired t tests and all results are presented as mean \pm SEM.

On the day of the recall test, all three animal groups had more nose pokes into the target hole and its nearby holes than the more distant holes on the maze (Figure 5-14 A). However, the Ibrutinib treated mice demonstrated a higher accuracy in remembering the target hole after 7 days, with 16.4% of their nose pokes being into the target hole while the vehicle group made 13.2% nose pokes

into the target hole (Figure 5-14 B). The recall data indicates that Ibrutinib treatment improved long-term memory in these fast-ageing mice, specifically in the males.

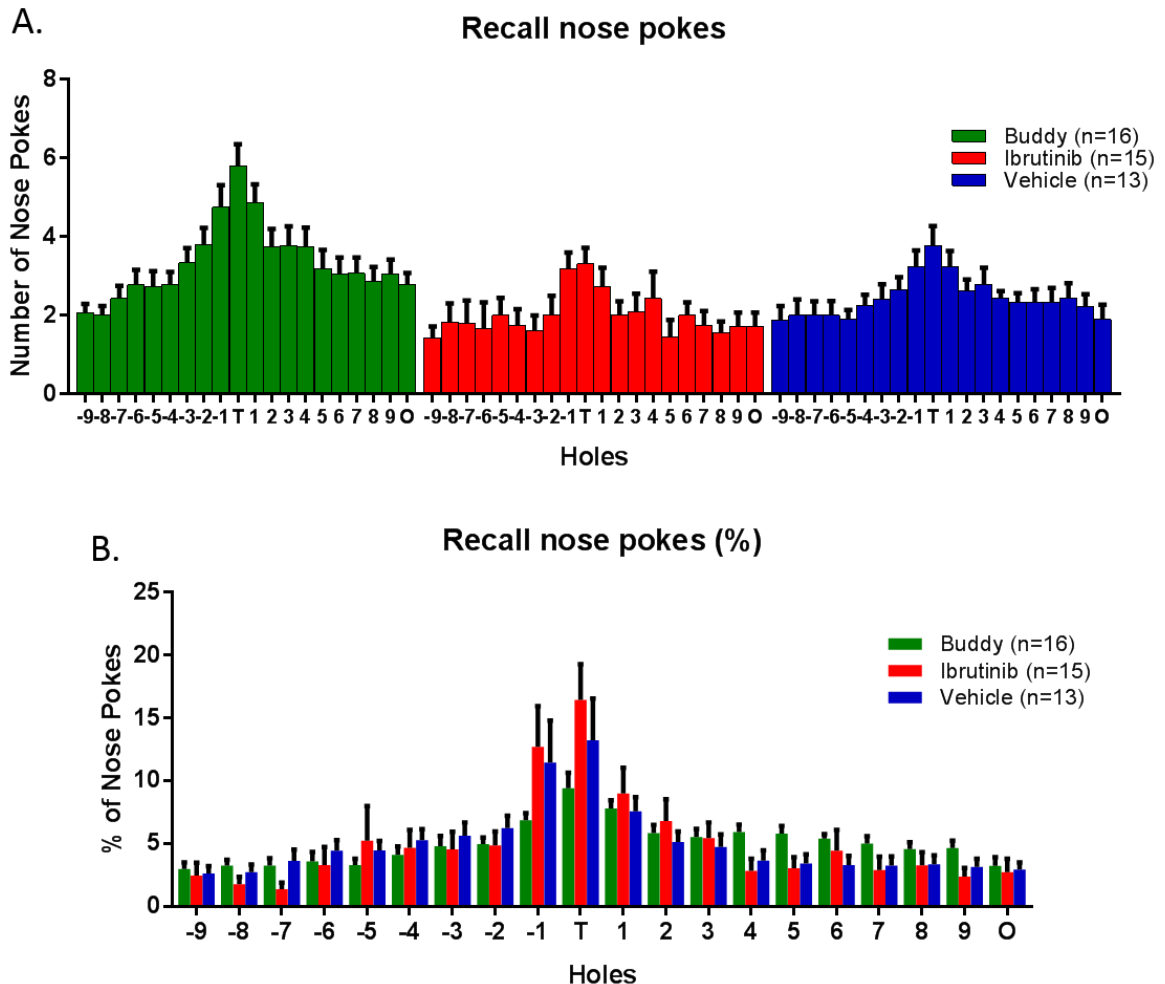


Figure 5-14 Mice nose pokes into Barnes maze holes during Recall tests
 Recall tests done 7 days after the Probe Trial showing mice nose pokes into the maze holes (A). The Ibrutinib treated group had a higher accuracy (%) of identifying the target hole than other groups (B). The difference in number of nose pokes at the target hole between both groups was not statistically significant at $p < 0.05$ using paired t test. Data is presented as mean \pm SEM.

5.3.5 SURVIVAL ANALYSIS

Kaplan Meier survival curves were plotted for all animals as well as for female and male animals separately. Ibrutinib was found to improve the maximum lifespan of *Zmpste24^{-/-}* mice. Similar results were also observed in both female and male animals and the female Ibrutinib treated mice had better survival than their male counterparts (Figure 5-15).

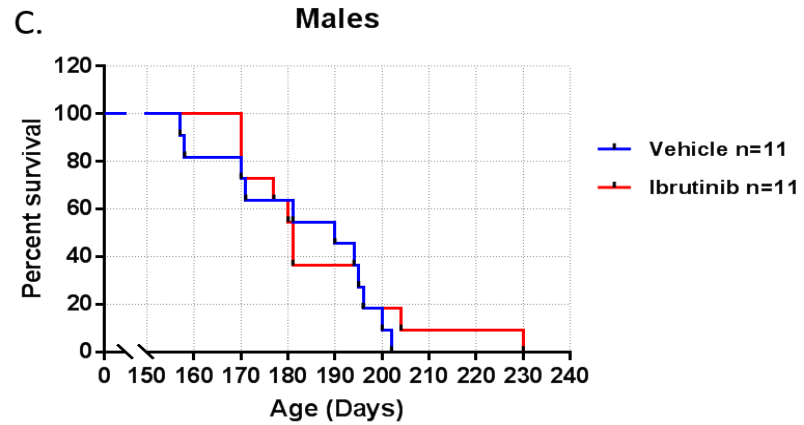
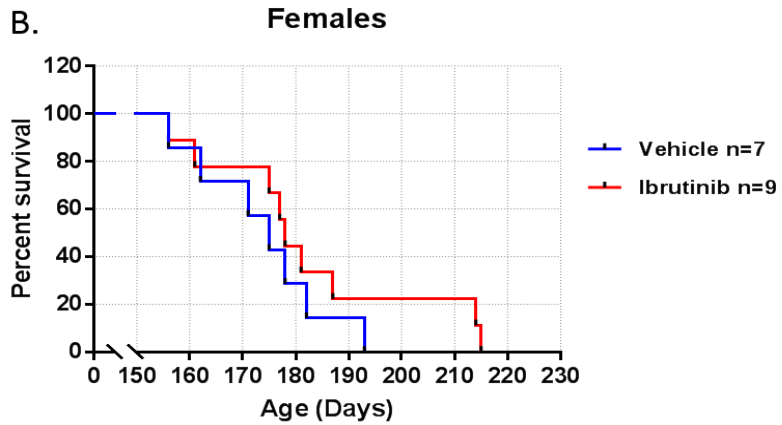
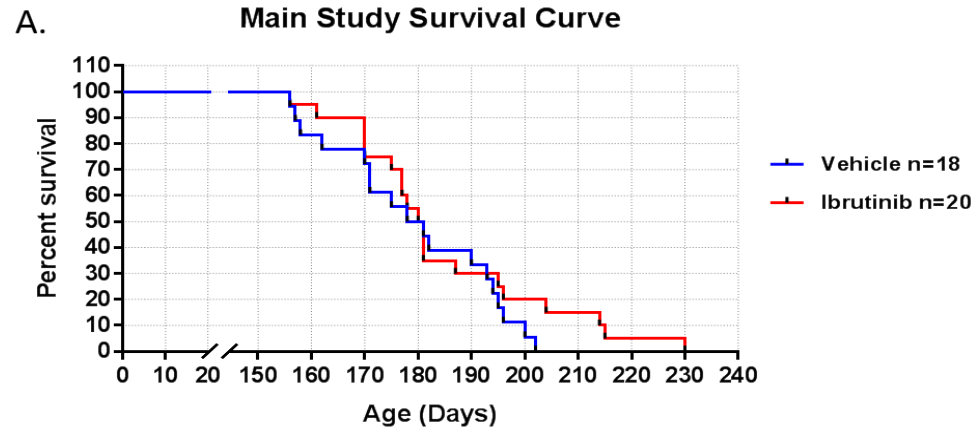


Figure 5-15 Kaplan Meier survival curves for the *Zmpste24*^{-/-} mice main study

Survival curves were generated for all animals at the end of the main study (A) and survival was also presented by gender (B and C). Ibrutinib treatment improved the survival of *Zmpste24*^{-/-} mice, more in females than in males. Mean and median survival for Ibrutinib treated animals was 184.9 and 180.5 days respectively, and that of the vehicle group was 179.5 days each. The data was however not statistically significant ($P=0.2813$) by the Log-rank (Mantel-Cox) test. Mean and median survival for female treated animals was 182.7 and 178 days respectively, and that for the female vehicle group was 173.8 and 175 days respectively. Whereas the mean and median survival for male treated mice was 186.7 and 181 days, that of the vehicle group was 183 and 190 days respectively. These were also not statistically significant.

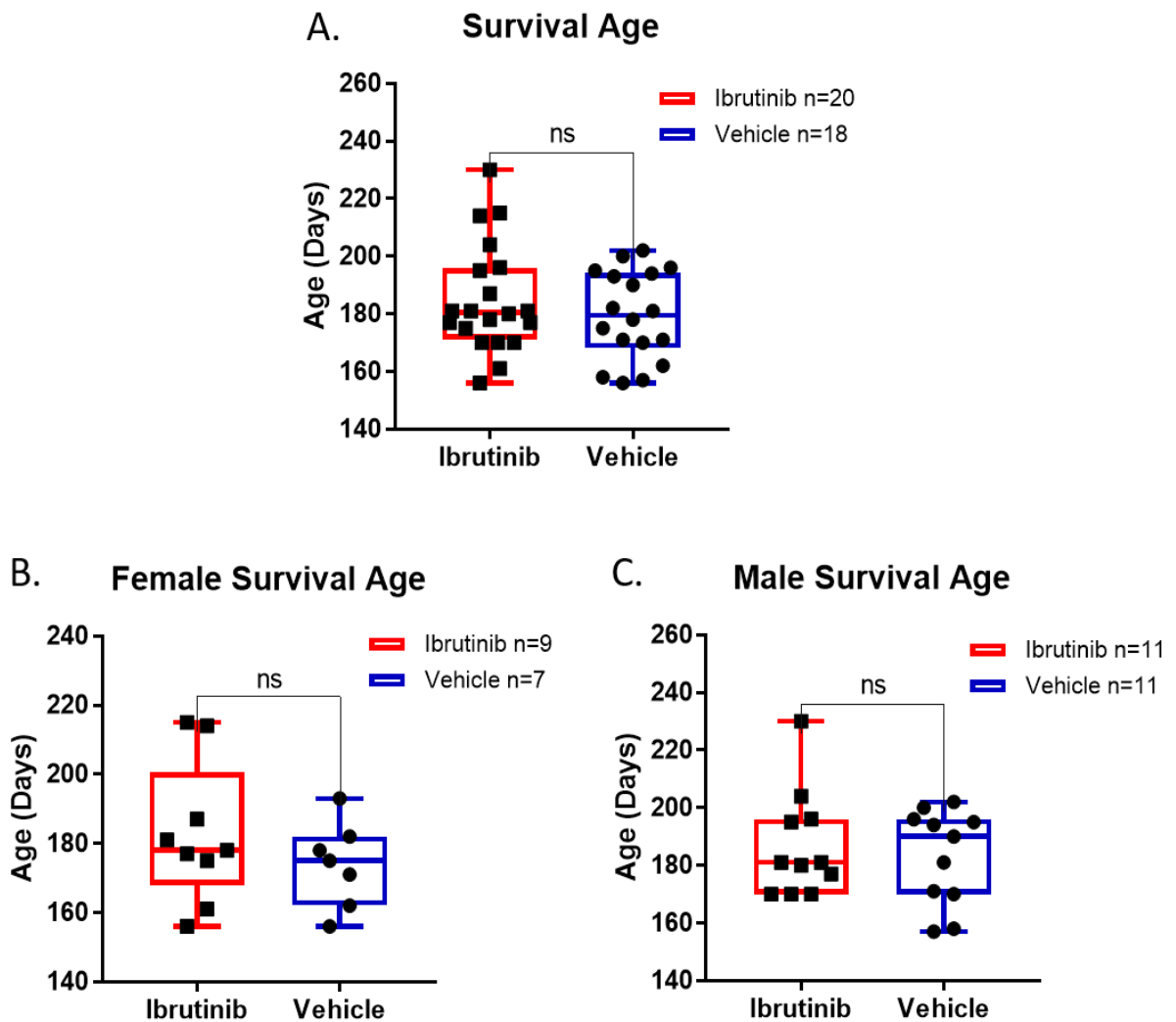


Figure 5-16 Average lifespan for male and female study animals

Box & whiskers plots showing the average age of survival (lifespan) for all (A) female (B) and male (C) study animals. Paired *t* tests were used to determine statistical significance at $p < 0.05$.

A box and whiskers plot of the average lifespan of study animals was presented according to their gender (Figure 5-16) and female Ibrutinib treated mice showed a higher average lifespan than the vehicle group (Figure 5-16 A). However, there were no statistically significant differences in average lifespan between Ibrutinib treated and vehicle control groups for both male and female animals.

5.4 DISCUSSION

Ageing is a major risk factor for the development of many debilitating diseases, including sarcopenia, cardiac dysfunction, Parkinson's disease, Alzheimer's disease as well as overall clinical frailty (Rando & Chang, 2012; Howlett & Rockwood, 2013; Whitehead *et al.*, 2014; Cosgrove *et al.*, 2014; Ocampo *et al.*, 2016; McHugh & Gil, 2018). Several anti-ageing interventions have been explored to date with the aim of ameliorating the symptoms associated with ageing (de Cabo *et al.*, 2014; Kane *et al.*, 2016; Soto-Gamez & Demaria, 2017), although none have yet been shown to work in humans. Results from our study show that inhibition of the Bruton's tyrosine kinase (BTK), is able to ameliorate symptoms of ageing and prolong both health-span and life-span in mice, and suggest that it could be used clinically to achieve these effects.

5.4.1 IMPROVEMENT OF MUSCLE STRENGTH

Pilot study results for the Kondziela's test showed a significant improvement in the muscle strength of Ibrutinib treated mice over the vehicle control group. Although variable, the results from the weights lifting tests also suggested a considerable improvement in muscle strength in the Ibrutinib treated mice over the control group. The main study's Kondziela's test results however showed no difference in muscle strength between the treatment group and control group over time. This may have been as a result of the simultaneous running of several behavioural tests on these mice, which caused them to lose the motivation and perhaps strength to perform on the inverted screen. There was also a soft bedding underneath the screen, onto which the mice could comfortably fall on if they lost grip on the Kondziela's inverted screen. This also might have had an effect on the animals' motivation to perform in this test. A more reliable test for the assessment of muscle strength could be the use of an apparatus which minimizes or completely eliminates all elements of emotion and behaviour, such as the commercially available Grip Strength Meters.

5.4.2 PREVENTION OF LATE-LIFE CLINICAL FRAILITY

Signs of clinical frailty, which often manifest in old age, were measured in our main study. The results obtained show that Ibrutinib therapy prevented late-life frailty in mice and reduced the overall percentage cases of clinical frailty recorded (Figure 5-6 and Table 5.1). This suggests that Ibrutinib is able to improve the

healthspan of aged mice. It was however noticed that two animals which were treated with Ibrutinib had mild cases of dermatitis while there were no such cases in the vehicle group. This is not surprising, as development of rashes have been reported as one of the adverse effects of Ibrutinib therapy (Akinleye *et al.*, 2013; Akinleye *et al.*, 2014; Novero *et al.*, 2014). There was also one mild case of tail stiffening in the Ibrutinib treated group but this may have been an isolated case unrelated to the treatment. Although diarrhoea has been reported as a common adverse effect of Ibrutinib therapy (Akinleye *et al.*, 2013; Akinleye *et al.*, 2014; Novero *et al.*, 2014), none of our Ibrutinib treated study animals presented with a case of diarrhoea. Instead, there was one case of mild diarrhoea and one mild case of laboured breathing recorded for the vehicle group of animals. Also, there were no spontaneous or secondary tumour formation as a result of Ibrutinib treatment in our study.

5.4.3 REDUCED ANXIETY-LIKE BEHAVIOUR

Results from our study showed that Ibrutinib treated mice significantly reduced the number of peeks they made into the open arm of the Elevated Plus Maze (EPM). Instead, they were found to make more actual entries into the open arm than the vehicle treated group, which although not statistically significant, is suggestive of a lower anxiety-like behaviour. This is contrary to a report that anxiety is one of the adverse effects of Ibrutinib therapy (Akinleye *et al.*, 2014). The relationship between anxiety and ageing has been debated for many years. A study conducted by French researchers reported a high incidence of anxiety and depression in older French individuals (Ritchie *et al.*, 2004). In the UK also, studies have reported a prevalence of anxiety and depression symptoms in the elderly (Silveira & Allebeck, 2001; Gale *et al.*, 2011). However, there has been controversy around the directionality of this relationship, bordering on whether anxiety causes ageing or ageing leads to anxiety (Kananen *et al.*, 2010; Verhoeven *et al.*, 2015; Perna *et al.*, 2015). Molecular signs of brain aging such as short telomere length, oxidative/nitrosative stress, immune-inflammatory stress, and $A\beta$ accumulation were highly expressed in anxious subjects and patients with panic disorders (Kananen *et al.*, 2010; Perna *et al.*, 2015). Also, anxiety disorders such as generalized anxiety disorder (GAD) and social phobia or agoraphobia (AG) have been found to be predominant in old age (Perna *et al.*,

2015; Verhoeven *et al.*, 2015). Regardless of the debate, Ibrutinib was found to reduce anxiety-like behaviour in mice in our study, indicating an improved healthspan which could be related to improved neurological functions.

5.4.4 IMPROVEMENT IN COGNITIVE FUNCTION

Using the *Zmpste24^{-/-}* mouse model of ageing, we show that Ibrutinib therapy improved long-term memory and cognitive function in these mice, specifically in the males. Ibrutinib has been reported to cross the blood brain barrier, thus explaining the possibility of its effect on the brain and hippocampus (Bernard *et al.*, 2015; Mason *et al.*, 2017). There was an observed increase in latency for the Ibrutinib treated group during the probe trial, suggesting that the drug could have a temporary adverse effect on short-term memory. However, this was not statistically significant. Although Ibrutinib appeared to have a deleterious effect on short-term spatial memory in these animals, data from the recall tests show a marked improvement in long-term spatial memory and cognitive function in Ibrutinib treated mice, suggesting the temporary nature and reversibility of the adverse effect. It could also be that the mice were physically worn out from the daily acquisition trials in addition to any adverse effects of the drug that they were not in the best shape to reach the target hole quickly during the probe trial. The Barnes maze was our choice maze for cognitive tests because it relies on extra-maze visual cues and does not use strong aversive stimuli, thereby inducing less stress in the animals than other mazes used for cognitive assessment, such as the Radial Arm maze and the water mazes (Harrison *et al.*, 2006; Sunyer *et al.*, 2007; Hernandez-Rabaza *et al.*, 2010; O'Leary & Brown, 2013; Rosenfeld & Ferguson, 2014; Loxton & Canales, 2017).

5.4.5 INCREASED SURVIVAL

Kaplan-Meier survival curves revealed that Ibrutinib treated mice had better average survival than the control mice, although this was not statistically significant. Also, the female Ibrutinib-treated animals were found to have better survival than the males. It was interesting to see that male mice treated with Ibrutinib performed better in muscle strength and cognitive function, while the female mice had better survival instead. Hormonal differences could have a part to play in these occurrences and it would be worthwhile to research further into this.

Several adverse effects of Ibrutinib therapy have been reported during clinical trials (Akinleye *et al.*, 2013; Novero *et al.*, 2014). Our study animals did not seem to have many measurable adverse effects other than two cases of mild dermatitis. It is therefore not certain whether the drug's adverse effects may have affected the performance of the mice during the study. Ibrutinib delivers off-target inhibition of epidermal growth factor receptor, interleukin-2-inducible kinase (ITK) and TEC family proteins besides BTK, partly explaining the adverse effects and toxicities resulting from its use. Novel BTK inhibitors that aim to improve the adverse effect profile without reducing efficacy are currently under development (Aw & Brown, 2017).

CHAPTER 6 DISCUSSION AND CONCLUSION

6.1 DETECTION AND CLEARANCE OF SENESCENT CELLS USING TARGETED APPROACHES AGAINST SPECIFIC MEMBRANE MARKERS

Novel markers of senescence overexpressed on the surface of senescent cells were identified in our laboratory, as previously described (Althubiti *et al.*, 2014). Results from our study indicate that seven of these markers, namely B2MG, STX4, DEP1, NTAL, EBP50, ARMCX3 and BTK, are highly present in aged or diseased mouse or human tissues. Their expression has, however, been observed to not be universal but both tissue and disease specific. B2MG, STX4, DEP1 and BTK were expressed in fibrotic lesions and could be useful as prognostic markers or therapeutic targets for fibrotic disease. The observed overexpression of B2MG in fibrotic mouse liver is in line with a previous study which showed that B2MG deficient mice, which have greatly reduced CD8⁺ and NKT cells, were protected from liver fibrosis and damage when placed on a choline-deficient high-fat diet (CD-HFD), alongside wild type C57BL/6 mice (Wolf *et al.*, 2014). This suggests that B2MG aggravates liver fibrosis possibly via direct induction of the senescence pro-inflammatory secretome, including IL6, IL1, CD8⁺ and NKT cells, and could be a promising therapeutic target for inflammatory diseases and fibrosis. The abundance of B2MG in older mice compared to the young controls, as detected by fluorescent B2MG-labelled MIPs, also goes to indicate the accumulation of senescent cells in tissues of aged animals.

Our results bring B2MG to light as a marker of cellular senescence, in addition to some of its pro-ageing and disease biomarker functions hitherto reported in other studies. B2MG has previously been found to be elevated in the blood of aged humans and mice and has been recognised as a circulating factor that negatively regulates cognitive and regenerative function in the adult hippocampus in an age-dependent manner (Smith *et al.*, 2015). The cerebrospinal fluid (CSF) of Alzheimer's disease patients (Carrette *et al.*, 2003) and patients with HIV-associated dementia was found to have increased levels of soluble B2MG (McArthur *et al.*, 1992). B2MG can also reportedly regulate synaptic plasticity,

normal brain development as well as behaviour (Shatz, 2009; Lee *et al.*, 2014). In addition, B2MG is constantly shed into the serum from the surface of cells exhibiting HLA class 1 molecules, from where it is transported to the kidneys for excretion. In the event of renal failure, its concentration in the serum rises up to sixty-fold. Hence, increased serum B2MG levels has also been used as an indicator of impaired renal function (Bernier, 1980; Trinh *et al.*, 2002).

We show for the first time that fluorescent-labelled B2MG-targeted nanoMIPs can be used to detect senescent cells both *in vitro* and *in vivo*, signifying that this could find application as a disease detection or diagnostic tool. We furthermore show that these B2MG nanoMIPs as well as B2MG antibody-drug conjugates (ADCs) can be used to targeted and kill senescent cells *in vitro*. The results from our study also demonstrate that nanoMIPs are biocompatible and non-cytotoxic *in vitro* and *in vivo*. We propose that B2MG and some of our other novel senescence markers could be used first to identify and then to eliminate senescent cells from the body using tools such as molecularly imprinted polymers (MIPs) and antibody-drug conjugates (ADCs), which could prove valuable therapeutics for age-related diseases, including cancers. Identifying specific targets is key to the selectivity of targeted therapy using MIPs or ADCs. Since none of the currently used markers of senescence are exclusively specific to the senescent state, there is the need for a more reliable senescence marker or a combination of markers. Our identified markers could therefore be used either alone or alongside others as tissue specific and disease specific markers of senescence and ageing. Given that the cellular events and molecular pathways that lead to senescence vary, it would be necessary to define clearly the pharmacodynamics of each potential anti-senescence therapeutic candidate not only to minimise off-target effects, ensure sensitivity and specificity, but to also identify potential synergistic effects or even contraindications when they are used in combination with other medications.

6.2 BTK INHIBITION IMPROVES HEALTHSPAN AND LIFESPAN *IN VIVO*

Using the *Zmpste24*^{-/-} mouse model of Hutchinson-Guilford's progeria syndrome (HGPS), we demonstrate here that inhibition of the Bruton's tyrosine kinase (BTK) by its clinically approved small molecule inhibitor Ibrutinib, prolongs lifespan and healthspan *in vivo*. Progeroid mice treated with Ibrutinib showed an increase in maximum lifespan and a reduction in age-related fitness decline. Specifically, these mice displayed increased physical strength, improved long-term memory and a reduction in anxiety-like behaviour. We showed that BTK inhibition prevented late-life clinical frailty in our mouse models, signifying a slowing down of the ageing process, while the control mice deteriorated significantly later in life. BTK is one of the novel senescence markers identified in our lab through mass spectrometry screening (Althubiti *et al.*, 2014). It is crucial for B-cell maturation and is already a target for the treatment of B-cell malignancies such as chronic lymphocytic leukaemia (CLL). It has previously been shown that BTK binds to and phosphorylates p53 and MDM2, resulting in increased p53 activity, while inhibition of BTK impaired p53-induced senescence (Althubiti *et al.*, 2016; Rada *et al.*, 2017). It is worthy of note that our study animals did not present with any spontaneous or secondary tumour formation that could have resulted from the interruption of the tumour suppressor functions of p53.

In our study, male Ibrutinib-treated mice were found to do better in cognitive function and muscle strength assessment than the female treated mice, while the female Ibrutinib treated mice survived longer. Sex biased genetic differences in brain development and neurodevelopmental disorders have been reported previously (Shi *et al.*, 2016). More recently, gender differences have also been reported during senescence related *in vivo* reprogramming, and this was thought to be due to the anti-inflammatory effect of oestrogens (Mosteiro *et al.*, 2018). The liver oestrogen receptor alpha is also reported to mediate sex differences in energy metabolism and response to diseases (Della Torre *et al.*, 2018). Moreover, inhibition of the insulin-like growth factor-1 receptor (IGF-1R) in late-life preferentially improved lifespan and healthspan in female mice over male mice (Mao *et al.*, 2018). It would therefore be worthwhile to investigate the relationship between BTK inhibition and the oestrogen receptor as well as the

insulin-like growth factor-1 receptor in future studies, especially relating to the prolongation of lifespan and healthspan *in vivo*. A recent study has shown that mice undergo normal programmed senescence in their skeleton at late puberty (Li *et al.*, 2017). During the screening of our markers in mouse tissues, there was an observed increase in senescence markers in tissues from mice that were aged around late puberty, notably an increase in p16, STX4 and B2MG was seen in muscle, brain and skin tissues as observed by Western blot.

6.3 CONCLUDING REMARKS

Targeting senescent cells has become necessary because of the implication of cellular senescence in the pathogenesis of several age-related ailments, including cancer. This research validates novel markers of senescence and brings to light the diagnostic and therapeutic potential of molecularly imprinted polymer nanoparticles as well as antibody-drug conjugates designed to target these novel senescence markers. In future experiments, it would be worthwhile to also validate the expression of these markers in a wider range of senescence models and disease conditions in order to further characterise their function and activities. It would also be useful to test the applications of these MIPs and ADCs in other senescence-related disease models.

Several anti-ageing interventions have been proposed but none has been shown to work in humans yet. Here we show that blocking BTK has an effect on ageing, increasing both lifespan and healthspan, and propose that specific inhibitors could be used in humans to treat progeroid syndromes and to prevent the age-related degeneration and tissue dysfunction. This research could also be followed up by further biochemical analyses of the tissues obtained from Ibrutinib treated *Zmpste24^{-/-}* mice, to better understand the various pathways responsible for the observed effects of BTK inhibition on lifespan and healthspan.

REFERENCES

- Abbas, T. & Dutta, A., 2009. p21 in cancer: intricate networks and multiple activities. *Nature Reviews.Cancer*. **9**, 400-414.
- Acosta, J.C., O'Loughlen, A., Banito, A., Guijarro, M.V., Augert, A., Raguz, S., Fumagalli, M., Da Costa, M., Brown, C., Popov, N., Takatsu, Y., Melamed, J., d'Adda di Fagagna, F., Bernard, D., Hernando, E., Gil, J., 2008. Chemokine signaling via the CXCR2 receptor reinforces senescence. *Cell*. **133**, 1006-1018.
- Acosta, J.C. & Gil, J., 2009. A Role for CXCR2 in Senescence, but What about in Cancer? *Cancer Res*. **69**, 2167.
- Acosta, J.C., Banito, A., Wuestefeld, T., Georgilis, A., Janich, P., Morton, J.P., Athineos, D., Kang, T., Lasitschka, F., Andrulis, M., Pascual, G., Morris, K.J., Khan, S., Jin, H., Dharmalingam, G., Snijders, A.P., Carroll, T., Capper, D., Pritchard, C., Inman, G.J., Longerich, T., Sansom, O.J., Benitah, S.A., Zender, L., Gil, J., 2013. A complex secretory program orchestrated by the inflammasome controls paracrine senescence. *Nature Cell Biology*. **15**, 978.
- Adams, P.D., 2007. Remodeling of chromatin structure in senescent cells and its potential impact on tumor suppression and aging.
- Agostini, A., Mondragon, L., Bernardos, A., Martinez-Manez, R., Marcos, M.D., Sancenon, F., Soto, J., Costero, A., Manguan-Garcia, C., Perona, R., Moreno-Torres, M., Aparicio-Sanchis, R., Murguia, J.R., 2012. Targeted cargo delivery in senescent cells using capped mesoporous silica nanoparticles. *Angewandte Chemie (International Ed.in English)*. **51**, 10556-10560.
- Agostini, M., Annicchiarico-Petruzzelli, M., Melino, G., Rufini, A., 2016. Metabolic pathways regulated by TAp73 in response to oxidative stress. *Oncotarget*. **7**, 29881-29900.
- Agostini, M., Niklison-Chirou, M.V., Annicchiarico-Petruzzelli, M.M., Grelli, S., Di Daniele, N., Pestlikis, I., Knight, R.A., Melino, G., Rufini, A., 2018. p73 Regulates Primary Cortical Neuron Metabolism: a Global Metabolic Profile. *Molecular Neurobiology*. **55**, 3237-3250.
- Akinleye, A., Chen, Y., Mukhi, N., Song, Y., Liu, D., 2013. Ibrutinib and novel BTK inhibitors in clinical development. *Journal of Hematology & Oncology*. **6**, 59.
- Akinleye, A., Furqan, M. and Adekunle, O., 2014. Ibrutinib and Indolent B-Cell Lymphomas.
- Alder, J.K., Chen, J.J., Lancaster, L., Danoff, S., Su, S.C., Cogan, J.D., Vulto, I., Xie, M., Qi, X., Tuder, R.M., Phillips, J.A., Lansdorp, P.M., Loyd, J.E., Armanios, M.Y., 2008. Short telomeres are a risk factor for idiopathic pulmonary fibrosis. *Proceedings of the National Academy of Sciences of the United States of America*. **105**, 13051-13056.

Alexandraki, K.I., Munayem Khan, M., Chahal, H.S., Dalantaeva, N.S., Trivellin, G., Berney, D.M., Caron, P., Popovic, V., Pfeifer, M., Jordan, S., Korbonits, M., Grossman, A.B., 2012. Oncogene-induced senescence in pituitary adenomas and carcinomas. *Hormones (Athens, Greece)*. **11**, 297.

Althubiti, M., Lezina, L., Carrera, S., Jukes-Jones, R., Giblett, S.M., Antonov, A., Barlev, N., Saldanha, G.S., Pritchard, C.A., Cain, K., Macip, S., 2014. Characterization of novel markers of senescence and their prognostic potential in cancer. *Cell Death & Disease*. **5**, e1528.

Althubiti, M., Rada, M., Samuel, J., Escorsa, J.M., Najeeb, H., Lee, K.G., Lam, K.P., Jones, G.D., Barlev, N.A., Macip, S., 2016. BTK Modulates p53 Activity to Enhance Apoptotic and Senescent Responses. *Cancer Research*. **76**, 5405-5414.

Althubiti, M.A.M., 2015. *Characterisation of novel markers and effectors of senescence and their role in cancer and ageing*. Ph. D. University of Leicester.

Alwahaibi, N.Y., Budin, S.B., Mohamed, J.H., 2011. Absence of p53 gene expression in selenium molecular prevention of chemically induced hepatocarcinogenesis in rats. *Saudi Journal of Gastroenterology : Official Journal of the Saudi Gastroenterology Association*. **17**, 328-334.

Amsellem, V., Gary-Bobo, G., Marcos, E., Maitre, B., Chaar, V., Validire, P., Stern, J.B., Nouredine, H., Sapin, E., Rideau, D., Hue, S., Le Corvoisier, P., Le Gouvello, S., Dubois-Rande, J.L., Boczkowski, J., Adnot, S., 2011. Telomere dysfunction causes sustained inflammation in chronic obstructive pulmonary disease. *American Journal of Respiratory and Critical Care Medicine*. **184**, 1358-1366.

Anisimov, V.N., Zabezhinski, M.A., Popovich, I.G., Piskunova, T.S., Semenchenko, A.V., Tyndyk, M.L., Yurova, M.N., Rosenfeld, S.V., Blagosklonny, M.V., 2011. Rapamycin increases lifespan and inhibits spontaneous tumorigenesis in inbred female mice. *Cell Cycle (Georgetown, Tex.)*. **10**, 4230-4236.

Aoshiha, K., Zhou, F., Tsuji, T., Nagai, A., 2012. DNA damage as a molecular link in the pathogenesis of COPD in smokers. *The European Respiratory Journal*. **39**, 1368-1376.

Arai, Y., *et al*, 2015. Inflammation, But Not Telomere Length, Predicts Successful Ageing at Extreme Old Age: A Longitudinal Study of Semi-supercentenarians.

Aravinthan, A., 2015. Cellular senescence: a hitchhiker's guide. *Human Cell*. **28**, 51-64.

Aravinthan, A.D. and Alexander, G.J.M., 2016. Senescence in chronic liver disease: Is the future in aging? .

Arbulo-Echevarria, M.M., Munoz-Miranda, J.P., Caballero-Garcia, A., Poveda-Diaz, J.L., Fernandez-Ponce, C., Duran-Ruiz, M.C., Miazek, A., Garcia-Cozar, F., Aguado, E., 2016. Non-T cell activation linker (NTAL) proteolytic cleavage as a terminator of activatory intracellular signals. *Journal of Leukocyte Biology*. **100**, 351-360.

Astle, M.V., Hannan, K.M., Ng, P.Y., Lee, R.S., George, A.J., Hsu, A.K., Haupt, Y., Hannan, R.D., Pearson, R.B., 2011. AKT induces senescence in human cells via mTORC1 and p53 in the absence of DNA damage: implications for targeting mTOR during malignancy. *Oncogene*. **31**, 1949.

Attar, A., Liu, T., Chan, W.T., Hayes, J., Nejad, M., Lei, K., Bitan, G., 2013. A shortened Barnes maze protocol reveals memory deficits at 4-months of age in the triple-transgenic mouse model of Alzheimer's disease. *PloS One*. **8**, e80355.

Austad, S.N. & Kirkwood, T.B.L., 2000. Why do we age? *Nature*. **408**, 233-238.

Aw, A. & Brown, J.R., 2017. Current Status of Bruton's Tyrosine Kinase Inhibitor Development and Use in B-Cell Malignancies. *Drugs & Aging*. **34**, 509-527.

Aya-Bonilla, C., Green, M.R., Camilleri, E., Benton, M., Keane, C., Marlton, P., Lea, R., Gandhi, M.K., Griffiths, L.R., 2013. High-resolution loss of heterozygosity screening implicates PTPRJ as a potential tumor suppressor gene that affects susceptibility to Non-Hodgkin's lymphoma. *Genes, Chromosomes & Cancer*. **52**, 467-479.

Baar, M.P., Brandt, R.M., Putavet, D.A., Klein, J.D., Derks, K.W., Bourgeois, B.R., Stryeck, S., Rijksen, Y., van Willigenburg, H., Feijtel, D.A., van der Pluijm, I., Essers, J., van Cappellen, W.A., van IJcken, W.F., Houtsmuller, A.B., Pothof, J., de Bruin, R.W., Madl, T., Hoeijmakers, J.H., Campisi, J., de Keizer, P.L., 2017. Targeted Apoptosis of Senescent Cells Restores Tissue Homeostasis in Response to Chemotoxicity and Aging. *Cell*. **169**, 147.e16.

Badiola, I., Santaolalla, F., Garcia-Gallastegui, P., Ana, S.D., Unda, F., Ibarretxe, G., 2015. Biomolecular bases of the senescence process and cancer. A new approach to oncological treatment linked to ageing. *Ageing Research Reviews*. **23**, 125-138.

Baird, D.M., Rowson, J., Wynford-Thomas, D., Kipling, D., 2003. Extensive allelic variation and ultrashort telomeres in senescent human cells. *Nature Genetics*. **33**, 203-207.

Baker, D.J., Childs, B.G., Durik, M., Wijers, M.E., Sieben, C.J., Zhong, J., Saltness, R.A., Jeganathan, K.B., Verzosa, G.C., Pezeshki, A., Khazaie, K., Miller, J.D., van Deursen, J.M., 2016. Naturally occurring p16(Ink4a)-positive cells shorten healthy lifespan. *Nature*. **530**, 184-189.

Baker, D.J., Perez-Terzic, C., Jin, F., Pitel, K.S., Niederlander, N.J., Jeganathan, K., Yamada, S., Reyes, S., Rowe, L., Hiddinga, H.J., Eberhardt, N.L., Terzic, A.,

van Deursen, J.M., 2008. Opposing roles for p16Ink4a and p19Arf in senescence and ageing caused by BubR1 insufficiency. *Nature Cell Biology*. **10**, 825-836.

Baker, D., Weaver, R. and van Deursen, J., 2013. p21 Both Attenuates and Drives Senescence and Aging in BubR1 Progeroid Mice.

Baker, D.J., Wijshake, T., Tchkonia, T., LeBrasseur, N.K., Childs, B.G., van de Sluis, B., Kirkland, J.L., van Deursen, J.M., 2011. Clearance of [p16.sup.Ink4a]-positive senescent cells delays ageing-associated disorders. *Nature*. **479**, 232.

Banchio, C., Lingrell, S., Vance, D.E., 2007. Sp-1 binds promoter elements that are regulated by retinoblastoma and regulate CTP:phosphocholine cytidyltransferase- α transcription. *The Journal of Biological Chemistry*. **282**, 14827-14835.

Bannister, A.J., Zegerman, P., Partridge, J.F., Miska, E.A., Thomas, J.O., Allshire, R.C., Kouzarides, T., 2001. Selective recognition of methylated lysine 9 on histone H3 by the HP1 chromo domain. *Nature*. **410**, 120.

Barardo, D., Thornton, D., Thoppil, H., Walsh, M., Sharifi, S., Ferreira, S., Anzic, A., Fernandes, M., Monteiro, P., Grum, T., Cordeiro, R., De-Souza, E.A., Budovsky, A., Araujo, N., Gruber, J., Petrascheck, M., Fraifeld, V.E., Zhavoronkov, A., Moskalev, A., de Magalhaes, J.P., 2017. The DrugAge database of aging-related drugs. *Aging Cell*. **16**, 594-597.

Barger, J.L., Vann, J.M., Cray, N.L., Pugh, T.D., Mastaloudis, A., Hester, S.N., Wood, S.M., Newton, M.A., Weindruch, R., Prolla, T.A., 2017. Identification of tissue-specific transcriptional markers of caloric restriction in the mouse and their use to evaluate caloric restriction mimetics. *Aging Cell*. **16**, 750-760.

Barnes, C.A., 1979. Memory deficits associated with senescence: a neurophysiological and behavioral study in the rat. *Journal of Comparative and Physiological Psychology*. **93**, 74-104.

Barnes, C.A., Nadel, L., Honig, W.K., 1980. Spatial memory deficit in senescent rats. *Canadian Journal of Psychology*. **34**, 29-39.

Barnes, P.J., 2017. Senescence in COPD and Its Comorbidities. *Annual Review of Physiology*. **79**, 517-539.

Barr, A.J., Ugochukwu, E., Lee, W.H., King, O.N., Filippakopoulos, P., Alfano, I., Savitsky, P., Burgess-Brown, N.A., Muller, S., Knapp, S., 2009. Large-scale structural analysis of the classical human protein tyrosine phosphatome. *Cell*. **136**, 352-363.

Barradas, M., Anderton, E., Acosta, J.C., Li, S., Banito, A., Rodriguez-Niedenfuhr, M., Maertens, G., Banck, M., Zhou, M.M., Walsh, M.J., Peters, G., Gil, J., 2009. Histone demethylase JMJD3 contributes to epigenetic control of INK4a/ARF by oncogenic RAS. *Genes & Development*. **23**, 1177-1182.

Beausejour, C.M., Krtolica, A., Galimi, F., Narita, M., Lowe, S.W., Yaswen, P., Campisi, J., 2003. Reversal of human cellular senescence: roles of the p53 and p16 pathways. *The EMBO Journal*. **22**, 4212-4222.

Bergo, M.O., Gavino, B., Ross, J., Schmidt, W.K., Hong, C., Kendall, L.V., Mohr, A., Meta, M., Genant, H., Jiang, Y., Wisner, E.R., Van Bruggen, N., Carano, R.A., Michaelis, S., Griffey, S.M., Young, S.G., 2002. Zmpste24 deficiency in mice causes spontaneous bone fractures, muscle weakness, and a prelamin A processing defect. *Proceedings of the National Academy of Sciences of the United States of America*. **99**, 13049-13054.

Bernard, S., Goldwirt, L., Amorim, S., Brice, P., Brière, J., de Kerviler, E., Mourah, S., Sauvageon, H., Thieblemont, C., 2015. Activity of ibrutinib in mantle cell lymphoma patients with central nervous system relapse. *Blood*. **126**, 1695.

Bernardes de Jesus, B., Schneeberger, K., Vera, E., Tejera, A., Harley, C.B., Blasco, M.A., 2011. The telomerase activator TA-65 elongates short telomeres and increases health span of adult/old mice without increasing cancer incidence. *Aging Cell*. **10**, 604-621.

Bernardes, d.J., Vera, E., Schneeberger, K., Tejera, A.M., Ayuso, E., Bosch, F., Blasco, M.A., 2012. Telomerase gene therapy in adult and old mice delays aging and increases longevity without increasing cancer. *EMBO Mol Med*. **4**, 691.

Bernier, G.M., 1980. beta 2-Microglobulin: structure, function and significance. *Vox Sanguinis*. **38**, 323-327.

Bhat, R., Crowe, E.P., Bitto, A., Moh, M., Katsetos, C.D., Garcia, F.U., Johnson, F.B., Trojanowski, J.Q., Sell, C., Torres, C., 2012. Astrocyte senescence as a component of Alzheimer's disease. *PLoS One*. **7**, e45069.

Bianchi-Smiraglia, A. & Nikiforov, M.A., 2012. Controversial aspects of oncogene-induced senescence. *Cell Cycle*. **11**, 4147-4151.

Biegging, K.T., Mello, S.S., Attardi, L.D., 2014. Unravelling mechanisms of p53-mediated tumour suppression. **14**, 359.

Biran, A., Perelmutter, M., Gal, H., Burton, D.G.A., Ovadya, Y., Vadai, E., Geiger, T., Krizhanovskiy, V., 2015. Senescent cells communicate via intercellular protein transfer. *Genes & Development*. **29**, 791.

Birch, J., Anderson, R.K., Correia-Melo, C., Jurk, D., Hewitt, G., Marques, F.M., Green, N.J., Moisey, E., Birrell, M.A., Belvisi, M.G., Black, F., Taylor, J.J., Fisher, A.J., De Soyza, A., Passos, J.F., 2015. DNA damage response at telomeres contributes to lung aging and chronic obstructive pulmonary disease. *American Journal of Physiology. Lung Cellular and Molecular Physiology*. **309**, 1124.

Birch, J., Victorelli, S., Rahmatika, D., Anderson, R.K., Jiwa, K., Moisey, E., Ward, C., Fisher, A.J., De Soyza, A., Passos, J.F., 2016. Telomere Dysfunction

and Senescence-associated Pathways in Bronchiectasis. *American Journal of Respiratory and Critical Care Medicine*. **193**, 929-932.

Birch, J., Barnes, P.J. and Passos, J.F., 2017. Mitochondria, telomeres and cell senescence: Implications for lung ageing and disease.

Bitto, A., *et al*, 2010. Stress-induced senescence in human and rodent astrocytes.

Bjedov, I., *et al*, 2010. Mechanisms of Life Span Extension by Rapamycin in the Fruit Fly *Drosophila melanogaster*.

Bjorkman, P.J., Saper, M.A., Samraoui, B., Bennett, W.S., Strominger, J.L., Wiley, D.C., 1987. Structure of the human class I histocompatibility antigen, HLA-A2. *Nature*. **329**, 506-512.

Blagosklonny, M.V., 2017. From rapalogs to anti-aging formula. *Oncotarget*. **8**, 35492-35507.

Blagosklonny, M.V., 2014. Geroconversion: irreversible step to cellular senescence. *Cell Cycle (Georgetown, Tex.)*. **13**, 3628-3635.

Blagosklonny, M.V., 2013. Selective anti-cancer agents as anti-aging drugs. *Cancer Biology & Therapy*. **14**, 1092-1097.

Blagosklonny, M.V., 2008. Aging: ROS or TOR. *Cell Cycle (Georgetown, Tex.)*. **7**, 3344-3354.

Blagosklonny, M.V., 2012. Rapalogs in cancer prevention. *Cancer Biology & Therapy*. **13**, 1349-1354.

Bodnar, A.G., Ouellette, M., Frolkis, M., Holt, S.E., Chiu, C.P., Morin, G.B., Harley, C.B., Shay, J.W., Lichtsteiner, S., Wright, W.E., 1998. Extension of life-span by introduction of telomerase into normal human cells. *Science (New York, N.Y.)*. **279**, 349-352.

Brasher, M.I., Martynowicz, D.M., Grafinger, O.R., Hucik, A., Shanks-Skinner, E., Uniacke, J., Coppolino, M.G., 2017. Interaction of Munc18c and syntaxin4 facilitates invadopodium formation and extracellular matrix invasion of tumor cells. *The Journal of Biological Chemistry*. **292**, 16199-16210.

Brugarolas, J., Chandrasekaran, C., Gordon, J.I., Beach, D., Jacks, T., Hannon, G.J., 1995. Radiation-induced cell cycle arrest compromised by p21 deficiency. *Nature*. **377**, 552-557.

BRUTON, O.C., 1952. Agammaglobulinemia. *Pediatrics*. **9**, 722-728.

Burton, D.G.A. & Krizhanovsky, V., 2014. Physiological and pathological consequences of cellular senescence. *Cellular and Molecular Life Sciences*. **71**, 4373-4386.

Caceres, C., Canfarotta, F., Chianella, I., Pereira, E., Moczko, E., Esen, C., Guerreiro, A., Piletska, E., Whitcombe, M.J., Piletsky, S.A., 2016. Does size matter? Study of performance of pseudo-ELISAs based on molecularly imprinted polymer nanoparticles prepared for analytes of different sizes. *The Analyst*. **141**, 1405-1412.

Cai, D., *et al*, 2004. IKK β /NF- κ B Activation Causes Severe Muscle Wasting in Mice.

Calado, R.T., 2014. Telomeres in lung diseases. *Progress in Molecular Biology and Translational Science*. **125**, 173-183.

Campisi, J., 2013. Aging, cellular senescence, and cancer. *Annual Review of Physiology*. **75**, 685-705.

Campisi, J., 1997. The biology of replicative senescence.

Campisi, J., 2011. Cellular senescence: putting the paradoxes in perspective. *Current Opinion in Genetics & Development*. **21**, 107-112.

Campisi, J., 2005. Senescent Cells, Tumor Suppression, and Organismal Aging: Good Citizens, Bad Neighbors. *Cell*. **120**, 513-522.

Campisi, J., 2003. Cellular senescence and apoptosis: how cellular responses might influence aging phenotypes. *Experimental Gerontology*. **38**, 5-11.

Campisi, J., 2001. Cellular senescence as a tumor-suppressor mechanism.

Campisi, J., Andersen, J.K., Kapahi, P., Melov, S., 2011. Cellular senescence: a link between cancer and age-related degenerative disease? *Seminars in Cancer Biology*. **21**, 354-359.

Campisi, J., Debacq-Chainiaux, F., Erusalimsky, J.D., Toussaint, O., 2009. Protocols to detect senescence-associated beta-galactosidase (SA- β gal) activity, a biomarker of senescent cells in culture and in vivo. *Nature Protocols*. **4**, 1798-1806.

Cancer Research UK, Cancer Incidence by age, <http://www.cancerresearchuk.org/health-professional/cancer-statistics/incidence/age#heading-Zero>, Accessed June, 2015.

Canfarotta, F., Poma, A., Guerreiro, A., Piletsky, S., 2016a. Solid-phase synthesis of molecularly imprinted nanoparticles. *Nature Protocols*. **11**, 443-455.

Canfarotta, F., Waters, A., Sadler, R., McGill, P., Guerreiro, A., Papkovsky, D., Haupt, K., Piletsky, S., 2016b. Biocompatibility and internalization of molecularly imprinted nanoparticles. *Nano Research*. **9**, 3463-3477.

Capilla-Gonzalez, V., Gil-Perotin, S., Ferragud, A., Bonet-Ponce, L., Canales, J.J., Garcia-Verdugo, J.M., 2012. Exposure to N-ethyl-N-nitrosourea in adult

mice alters structural and functional integrity of neurogenic sites. *PLoS One*. **7**, e29891.

Carrera, S., Senra, J., Acosta, M.I., Althubiti, M., Hammond, E.M., de Verdier, P.J., Macip, S., 2014. The role of the HIF-1alpha transcription factor in increased cell division at physiological oxygen tensions. *PLoS One*. **9**, e97938.

Carrette, O., Demalte, I., Scherl, A., Yalkinoglu, O., Corthals, G., Burkhard, P., Hochstrasser, D.F., Sanchez, J.C., 2003. A panel of cerebrospinal fluid potential biomarkers for the diagnosis of Alzheimer's disease. *Proteomics*. **3**, 1486-1494.

Casi, G. and Neri, D., 2012. Antibody–drug conjugates: Basic concepts, examples and future perspectives.

Cecchini, A., Raffa, V., Canfarotta, F., Signore, G., Piletsky, S., MacDonald, M.P., Cuschieri, A., 2017. In Vivo Recognition of Human Vascular Endothelial Growth Factor by Molecularly Imprinted Polymers. *Nano Letters*.

Centre for Disease Control and Prevention; The State of Aging and Health in America 2013, <http://www.cdc.gov/aging/pdf/state-aging-health-in-america-2013.pdf>, Accessed June, 2015.

Chabot, C., Spring, K., Gratton, J.P., Elchebly, M., Royal, I., 2009. New role for the protein tyrosine phosphatase DEP-1 in Akt activation and endothelial cell survival. *Molecular and Cellular Biology*. **29**, 241-253.

Chang, B.D., Broude, E.V., Dokmanovic, M., Zhu, H., Ruth, A., Xuan, Y., Kandel, E.S., Lausch, E., Christov, K., Roninson, I.B., 1999a. A senescence-like phenotype distinguishes tumor cells that undergo terminal proliferation arrest after exposure to anticancer agents. *Cancer Research*. **59**, 3761-3767.

Chang, B.D., Xuan, Y., Broude, E.V., Zhu, H., Schott, B., Fang, J., Roninson, I.B., 1999b. Role of p53 and p21waf1/cip1 in senescence-like terminal proliferation arrest induced in human tumor cells by chemotherapeutic drugs. *Oncogene*. **18**, 4808-4818.

Chang, B.Y., Francesco, M., De Rooij, M.F., Magadala, P., Steggerda, S.M., Huang, M.M., Kuil, A., Herman, S.E., Chang, S., Pals, S.T., Wilson, W., Wiestner, A., Spaargaren, M., Buggy, J.J., Elias, L., 2013. Egress of CD19(+)CD5(+) cells into peripheral blood following treatment with the Bruton tyrosine kinase inhibitor ibrutinib in mantle cell lymphoma patients. *Blood*. **122**, 2412-2424.

Chang, J., Wang, Y., Shao, L., Laberge, R.M., Demaria, M., Campisi, J., Janakiraman, K., Sharpless, N.E., Ding, S., Feng, W., Luo, Y., Wang, X., Aykin-Burns, N., Krager, K., Ponnappan, U., Hauer-Jensen, M., Meng, A., Zhou, D., 2016. Clearance of senescent cells by ABT263 rejuvenates aged hematopoietic stem cells in mice. *Nature Medicine*. **22**, 78-83.

- Chen, J.H., Hales, C.N., Ozanne, S.E., 2007. DNA damage, cellular senescence and organismal ageing: causal or correlative? *Nucleic Acids Research*. **35**, 7417-7428.
- Chen, J., Huang, X., Halicka, D., Brodsky, S., Avram, A., Eskander, J., Bloomgarden, N.A., Darzynkiewicz, Z., Goligorsky, M.S., 2006. Contribution of p16INK4a and p21CIP1 pathways to induction of premature senescence of human endothelial cells: permissive role of p53. *American Journal of Physiology. Heart and Circulatory Physiology*. **290**, 1575.
- Chen, Q., Liu, K., Robinson, A.R., Clauson, C.L., Blair, H.C., Robbins, P.D., Niedernhofer, L.J., Ouyang, H., 2013. DNA damage drives accelerated bone aging via an NF-kappaB-dependent mechanism. *Journal of Bone and Mineral Research : The Official Journal of the American Society for Bone and Mineral Research*. **28**, 1214-1228.
- Chen, Z., Trotman, L.C., Shaffer, D., Lin, H.K., Dotan, Z.A., Niki, M., Koutcher, J.A., Scher, H.I., Ludwig, T., Gerald, W., Cordon-Cardo, C., Pandolfi, P.P., 2005. Crucial role of p53-dependent cellular senescence in suppression of Pten-deficient tumorigenesis. *Nature*. **436**, 725-730.
- Chianella, I., Guerreiro, A., Moczko, E., Caygill, J.S., Piletska, E.V., De Vargas Sansalvador, I M, Whitcombe, M.J., Piletsky, S.A., 2013. Direct replacement of antibodies with molecularly imprinted polymer nanoparticles in ELISA--development of a novel assay for vancomycin. *Analytical Chemistry*. **85**, 8462-8468.
- Chiche, A., Le Roux, I., von Joest, M., Sakai, H., Aguin, S.B., Cazin, C., Salam, R., Fiette, L., Alegria, O., Flamant, P., Tajbakhsh, S., Li, H., 2017. Injury-Induced Senescence Enables In Vivo Reprogramming in Skeletal Muscle. *Cell Stem Cell*. **20**, 414.e4.
- Childs, B.G., Baker, D.J., Kirkland, J.L., Campisi, J., van Deursen, J.M., 2014. Senescence and apoptosis: dueling or complementary cell fates? *EMBO Reports*. **15**, 1139-1153.
- Childs, B.G., Baker, D.J., Wijshake, T., Conover, C.A., Campisi, J., van Deursen, J.M., 2016. Senescent intimal foam cells are deleterious at all stages of atherosclerosis. *Science (New York, N.Y.)*. **354**, 472-477.
- Childs, B.G., Durik, M., Baker, D.J., van Deursen, J.M., 2015. Cellular senescence in aging and age-related disease: from mechanisms to therapy. *Nature Medicine*. **21**, 1424-1435.
- Chilosi, M., Poletti, V., Rossi, A., 2012. The pathogenesis of COPD and IPF: Distinct horns of the same devil? *Respiratory Research*. **13**, 3.
- Chinta, S.J., Lieu, C.A., Demaria, M., Laberge, R.M., Campisi, J., Andersen, J.K., 2013. Environmental stress, ageing and glial cell senescence: a novel

mechanistic link to Parkinson's disease? *Journal of Internal Medicine*. **273**, 429-436.

Cichowski, K. and Hahn, W.C., 2008. Unexpected Pieces to the Senescence Puzzle.

Collado, M., Blasco, M.A., Serrano, M., 2007. Cellular Senescence in Cancer and Aging. *Cell*. **130**, 223-233.

Collado, M., Gil, J., Efeyan, A., Guerra, C., 2005. Senescence in premalignant tumours. *Nature*. **436**, 642.

Collado, M. & Serrano, M., 2010. Senescence in tumours: evidence from mice and humans. *Nature Reviews.Cancer*. **10**, 51-57.

Cooke, H.J. & Smith, B.A., 1986. Variability at the telomeres of the human X/Y pseudoautosomal region. *Cold Spring Harbor Symposia on Quantitative Biology*. **51 Pt 1**, 213-219.

Coppe, J.P., Desprez, P.Y., Krtolica, A., Campisi, J., 2010. The senescence-associated secretory phenotype: the dark side of tumor suppression. *Annual Review of Pathology*. **5**, 99-118.

Coppe, J.P., Patil, C.K., Rodier, F., Sun, Y., Munoz, D.P., Goldstein, J., Nelson, P.S., Desprez, P.Y., Campisi, J., 2008. Senescence-associated secretory phenotypes reveal cell-nonautonomous functions of oncogenic RAS and the p53 tumor suppressor. *PLoS Biology*. **6**, 2853-2868.

Coppe, J.P., Rodier, F., Patil, C.K., Freund, A., Desprez, P.Y., Campisi, J., 2011. Tumor suppressor and aging biomarker p16(INK4a) induces cellular senescence without the associated inflammatory secretory phenotype. *The Journal of Biological Chemistry*. **286**, 36396-36403.

Cosgrove, B.D., Gilbert, P.M., Porpiglia, E., Mourkioti, F., Lee, S.P., Corbel, S.Y., Llewellyn, M.E., Delp, S.L., Blau, H.M., 2014. Rejuvenation of the muscle stem cell population restores strength to injured aged muscles. *Nature Medicine*. **20**, 255-264.

Courtois-Cox, S., Jones, S.L., Cichowski, K., 2008. Many roads lead to oncogene-induced senescence. *Oncogene*. **27**, 2801.

Courtois-Cox, S., *et al*, 2006. A negative feedback signaling network underlies oncogene-induced senescence.

Cui, H., Kong, Y., Xu, M., Zhang, H., 2013. Notch3 Functions as a Tumor Suppressor by Controlling Cellular Senescence. *Cancer Res*. **73**, 3451.

Cunliffe, D., Kirby, A. and Alexander, C., 2005. Molecularly imprinted drug delivery systems.

d'Adda di Fagagna, F., Reaper, P.M., Clay-Farrace, L., Fiegler, H., Carr, P., Von Zglinicki, T., Saretzki, G., Carter, N.P., Jackson, S.P., 2003. A DNA damage checkpoint response in telomere-initiated senescence. *Nature*. **426**, 194-198.

d'Adda di Fagagna, F. & Campisi, J., 2007. Cellular senescence: when bad things happen to good cells. *Nature Reviews Molecular Cell Biology*. **8**, 729-740.

d'Adda, d.F., 2008. Living on a break: cellular senescence as a DNA-damage response. **8**, 512.

Dadparvar, M., *et al*, 2011. HI 6 human serum albumin nanoparticles—Development and transport over an in vitro blood–brain barrier model.

Dai, J., Cai, H., Li, H., Zhuang, Y., Min, H., Wen, Y., Yang, J., Gao, Q., Shi, Y., Yi, L., 2015. Association between telomere length and survival in patients with idiopathic pulmonary fibrosis. *Respirology (Carlton, Vic.)*. **20**, 947-952.

Danilov, A., Shaposhnikov, M., Plyusnina, E., Kogan, V., Fedichev, P., Moskalev, A., 2013. Selective anticancer agents suppress aging in *Drosophila*. *Oncotarget*. **4**, 1507-1526.

Daste, A., *et al*, 2016. Targeted therapy and elderly people: A review.

Davaapil, H., Brockes, J.P., Yun, M.H., 2017. Conserved and novel functions of programmed cellular senescence during vertebrate development. *Development (Cambridge, England)*. **144**, 106-114.

Davids, M.S. & Brown, J.R., 2014. Ibrutinib: a first in class covalent inhibitor of Bruton's tyrosine kinase. *Future Oncology (London, England)*. **10**, 957-967.

Davies, H., Bignell, G.R., Cox, C., Stephens, P., Edkins, S., Clegg, S., Teague, J., Woffendin, H., Garnett, M.J., Bottomley, W., Davis, N., Dicks, E., Ewing, R., Floyd, Y., Gray, K., Hall, S., Hawes, R., Hughes, J., Kosmidou, V., Menzies, A., Mould, C., Parker, A., Stevens, C., Watt, S., Hooper, S., Wilson, R., Jayatilake, H., Gusterson, B.A., Cooper, C., Shipley, J., Hargrave, D., Pritchard-Jones, K., Maitland, N., Chenevix-Trench, G., Riggins, G.J., Bigner, D.D., Palmieri, G., Cossu, A., Flanagan, A., Nicholson, A., Ho, J.W.C., Leung, S.Y., Yuen, S.T., Weber, B.L., Seigler, H.F., Darrow, T.L., Paterson, H., Marais, R., Marshall, C.J., Wooster, R., Stratton, M.R., Futreal, P.A., 2002. Mutations of the BRAF gene in human cancer. *Nature*. **417**, 949.

de Cabo, R., Carmona-Gutierrez, D., Bernier, M., Hall, M.N., Madeo, F., 2014. The search for antiaging interventions: from elixirs to fasting regimens. *Cell*. **157**, 1515-1526.

de Jesus, B.B. & Blasco, M.A., 2012. Assessing Cell and Organ Senescence Biomarkers. *Circulation Research*. **111**, 97-109.

de Keizer, P.L., 2016. The Fountain of Youth by Targeting Senescent Cells? *Trends in Molecular Medicine*.

de la Rosa, J., Freije, J.M., Cabanillas, R., Osorio, F.G., Fraga, M.F., Fernandez-Garcia, M.S., Rad, R., Fanjul, V., Ugalde, A.P., Liang, Q., Prosser, H.M., Bradley, A., Cadinanos, J., Lopez-Otin, C., 2013. Prelamin A causes progeria through cell-extrinsic mechanisms and prevents cancer invasion. *Nature Communications*. **4**, 2268.

de Magalhães, J.P. and Passos, J.F., 2017. Stress, cell senescence and organismal ageing.

Deacon, R.M., 2013. Measuring the strength of mice. *Journal of Visualized Experiments : JoVE*. **(76)**. doi, 10.3791/2610.

Debacq-Chainiaux, F., Ben Ameer, R., Bauwens, E., Dumortier, E., Touffaire, M. and Toussaint, O., 2016. Stress-Induced (Premature) Senescence. In Rattan, S. I. S. & Hayflick, L., eds, *Cellular Ageing and Replicative Senescence*. Cham: Springer International Publishing. 243-262.

Della Torre, S., *et al*, 2018. Short-Term Fasting Reveals Amino Acid Metabolism as a Major Sex-Discriminating Factor in the Liver.

Dellambra, E. & Dimri, G.P., 2009. Chapter 7 - Cellular Senescence and Skin Aging. In by, E. & Dayan, N., eds, *Skin Aging Handbook*. Norwich, NY: William Andrew Publishing. 129-148.

Demaria, M., 2017. Senescent cells: New target for an old treatment? *Molecular & Cellular Oncology*. **4**, e1299666.

Demaria, M., O'Leary, M.N., Chang, J., Shao, L., Liu, S., Alimirah, F., Koenig, K., Le, C., Mitin, N., Deal, A.M., Alston, S., Academia, E.C., Kilmarx, S., Valdovinos, A., Wang, B., de Bruin, A., Kennedy, B.K., Melov, S., Zhou, D., Sharpless, N.E., Muss, H., Campisi, J., 2017. Cellular Senescence Promotes Adverse Effects of Chemotherapy and Cancer Relapse. *Cancer Discovery*. **7**, 165-176.

Demidenko, Z.N. & Blagosklonny, M.V., 2008. Growth stimulation leads to cellular senescence when the cell cycle is blocked. *Cell Cycle (Georgetown, Tex.)*. **7**, 3355-3361.

Demidenko, Z.N., Korotchkina, L.G., Gudkov, A.V., Blagosklonny, M.V., 2010. Paradoxical suppression of cellular senescence by p53. *Proceedings of the National Academy of Sciences of the United States of America*. **107**, 9660-9664.

Demidenko, Z.N., Zubova, S.G., Bukreeva, E.I., Pospelov, V.A., Pospelova, T.V., Blagosklonny, M.V., 2009. Rapamycin decelerates cellular senescence. *Cell Cycle (Georgetown, Tex.)*. **8**, 1888-1895.

Deng, C., Zhang, P., Harper, J.W., Elledge, S.J., Leder, P., 1995. Mice lacking p21CIP1/WAF1 undergo normal development, but are defective in G1 checkpoint control. *Cell*. **82**, 675-684.

- Deng, Q., Liao, R., Wu, B.L., Sun, P., 2004. High intensity ras signaling induces premature senescence by activating p38 pathway in primary human fibroblasts. *The Journal of Biological Chemistry*. **279**, 1050-1059.
- Deursen, J M A van, 2014. The role of senescent cells in ageing. *Volume=509;Startpage=439;Endpage=446*. **509**, 439-446.
- Dhillon, V., Bull, C. and Fenech, M., 2016. Chapter 10 - Telomeres, Aging, and Nutrition. In Malavolta, M. & Mocchegiani, E., eds, *Molecular Basis of Nutrition and Aging*. San Diego: Academic Press. 129-140.
- Di Leonardo, A., Linke, S.P., Clarkin, K., Wahl, G.M., 1994. DNA damage triggers a prolonged p53-dependent G1 arrest and long-term induction of Cip1 in normal human fibroblasts. *Genes & Development*. **8**, 2540-2551.
- Di Micco, R., Fumagalli, M., Cicalese, A., Piccinin, S., Gasparini, P., Luise, C., Schurra, C., Garre', M., Nuciforo, P.G., Bensimon, A., Maestro, R., Pelicci, P.G., d'Adda di Fagagna, F., 2006. Oncogene-induced senescence is a DNA damage response triggered by DNA hyper-replication. *Nature*. **444**, 638-642.
- Di Micco, R., Sulli, G., Dobрева, M., Lontos, M., Botrugno, O.A., Gargiulo, G., dal Zuffo, R., Matti, V., d'Ario, G., Montani, E., Mercurio, C., Hahn, W.C., Gorgoulis, V., Minucci, S., d'Adda di Fagagna, F., 2011. Interplay between oncogene-induced DNA damage response and heterochromatin in senescence and cancer. *Nature Cell Biology*. **13**, 292-302.
- Dimri, G.P., Lee, X., Basile, G., Acosta, M., Scott, G., Roskelley, C., Medrano, E.E., Linskens, M., Rubelj, I., Pereira-Smith, O., 1995. A biomarker that identifies senescent human cells in culture and in aging skin in vivo. *Proceedings of the National Academy of Sciences of the United States of America*. **92**, 9363-9367.
- Donath, M.Y., Dalmas, E., Sauter, N.S., Boni-Schnetzler, M., 2013. Inflammation in obesity and diabetes: islet dysfunction and therapeutic opportunity. *Cell Metabolism*. **17**, 860-872.
- Dong, Q., *et al*, 2017. HCSGD: An integrated database of human cellular senescence genes.
- Donnell, A.F., *et al*, 2017. Macrocyclic pyrrolobenzodiazepine dimers as antibody-drug conjugate payloads.
- Downward, J., 2003. Targeting RAS signalling pathways in cancer therapy. **3**, 11.
- Drayton, S. and Peters, G., 2002. Immortalisation and transformation revisited.
- Drayton, S., *et al*, 2003. Tumor suppressor p16INK4a determines sensitivity of human cells to transformation by cooperating cellular oncogenes.
- Dumont, P., *et al*, 2000. Induction of replicative senescence biomarkers by sublethal oxidative stresses in normal human fibroblast.

Edwards, M.G., Anderson, R.M., Yuan, M., Kendzierski, C.M., Weindruch, R., Prolla, T.A., 2007. Gene expression profiling of aging reveals activation of a p53-mediated transcriptional program. *BMC Genomics*. **8**, 80.

Ehrlich, P., 1906. The relationship existing between chemical constitution, distribution and pharmacological action. *Collected Studies on Immunity*. 441-450.

el-Deiry, W.S., Tokino, T., Velculescu, V.E., Levy, D.B., Parsons, R., Trent, J.M., Lin, D., Mercer, W.E., Kinzler, K.W., Vogelstein, B., 1993. WAF1, a potential mediator of p53 tumor suppression. *Cell*. **75**, 817-825.

Erusalimsky, J.D. and Kurz, D.J., 2005. Cellular senescence in vivo: Its relevance in ageing and cardiovascular disease.

Esiri, M.M., 2007. Ageing and the brain. *The Journal of Pathology*. **211**, 181-187.

Evan, G.I. & d'Adda di Fagagna, F., 2009. Cellular senescence: hot or what? *Current Opinion in Genetics & Development*. **19**, 25-31.

Evangelou, K., Lougiakis, N., Rizou, S.V., Kotsinas, A., Kletsas, D., Munoz-Espin, D., Kastrinakis, N.G., Pouli, N., Marakos, P., Townsend, P., Serrano, M., Bartek, J., Gorgoulis, V.G., 2017. Robust, universal biomarker assay to detect senescent cells in biological specimens. *Aging Cell*. **16**, 192-197.

Faner, R., Rojas, M., Macnee, W., Agusti, A., 2012. Abnormal lung aging in chronic obstructive pulmonary disease and idiopathic pulmonary fibrosis. *American Journal of Respiratory and Critical Care Medicine*. **186**, 306-313.

Fang, L., Igarashi, M., Leung, J., Sugrue, M.M., Lee, S.W., Aaronson, S.A., 1999. p21Waf1/Cip1/Sdi1 induces permanent growth arrest with markers of replicative senescence in human tumor cells lacking functional p53. *Oncogene*. **18**, 2789-2797.

Faragher, R.G., Jones, C.J., Kipling, D., 1998. Telomerase and cellular lifespan: ending the debate? *Nature Biotechnology*. **16**, 701-702.

Farr, J.N., Xu, M., Weivoda, M.M., Monroe, D.G., Fraser, D.G., Onken, J.L., Negley, B.A., Sfeir, J.G., Ogrodnik, M.B., Hachfeld, C.M., LeBrasseur, N.K., Drake, M.T., Pignolo, R.J., Pirtskhalava, T., Tchkonja, T., Oursler, M.J., Kirkland, J.L., Khosla, S., 2017. Targeting cellular senescence prevents age-related bone loss in mice. *Nature Medicine*. **23**, 1072-1079.

Feng, D., Xiong, Y., Peng, Z., Ma, Q., Tao, T., Liu, H., Liang, J., Wei, Z., Zheng, J., Wang, L., Zhang, H., 2017. Reduced EBP50 expression levels are correlated with unfavorable clinicopathological features of extrahepatic bile duct carcinoma and promote the proliferation and migration of QBC939 cells. *Oncology Letters*. **13**, 2758-2764.

Filiano, A.J. & Kipnis, J., 2015. Breaking bad blood: beta2-microglobulin as a pro-aging factor in blood. *Nature Medicine*. **21**, 844-845.

Florence, A.T. and Lee, V.H.L., 2011. Personalised medicines: More tailored drugs, more tailored delivery.

Fong, L.G., Ng, J.K., Meta, M., Cote, N., Yang, S.H., Stewart, C.L., Sullivan, T., Burghardt, A., Majumdar, S., Reue, K., Bergo, M.O., Young, S.G., 2004. Heterozygosity for Lmna deficiency eliminates the progeria-like phenotypes in Zmpste24-deficient mice. *Proceedings of the National Academy of Sciences of the United States of America*. **101**, 18111-18116.

Fontana, L., Partridge, L., Longo, V.D., 2010. Extending healthy life span--from yeast to humans. *Science (New York, N.Y.)*. **328**, 321-326.

Franceschi, C., Bonafe, M., Valensin, S., Olivieri, F., De Luca, M., Ottaviani, E., De Benedictis, G., 2000. Inflamm-aging. An evolutionary perspective on immunosenescence. *Annals of the New York Academy of Sciences*. **908**, 244-254.

Franceschi, C. & Campisi, J., 2014. Chronic Inflammation (Inflammaging) and Its Potential Contribution to Age-Associated Diseases. *The Journals of Gerontology: Series A*. **69**, S9.

Franken, N.A.P., Rodermond, H.M., Stap, J., Haveman, J., van Bree, C., 2006. Clonogenic assay of cells in vitro. *Nature Protocols*. **1**, 2315.

Freije, J.M. and López-Otín, C., 2012. Reprogramming aging and progeria.

Fuhrmann-Stroissnigg, H., Ling, Y.Y., Zhao, J., McGowan, S.J., Zhu, Y., Brooks, R.W., Grassi, D., Gregg, S.Q., Stripay, J.L., Dorronsoro, A., Corbo, L., Tang, P., Bukata, C., Ring, N., Giacca, M., Li, X., Tchkonja, T., Kirkland, J.L., Niedernhofer, L.J., Robbins, P.D., 2017. Identification of HSP90 inhibitors as a novel class of senolytics. *Nature Communications*. **8**, z.

Gagliardi, M., Bertero, A., Bifone, A., 2017. Molecularly Imprinted Biodegradable Nanoparticles. *Scientific Reports*. **7**, 40046.

Galanos, P., Vougas, K., Walter, D., Polyzos, A., Maya-Mendoza, A., Haagensen, E.J., Kokkalis, A., Roumelioti, F., Gagos, S., Tzetis, M., Canovas, B., Igea, A., Ahuja, A.K., Zellweger, R., Havaki, S., Kanavakis, E., Kletsas, D., Roninson, I.B., Garbis, S.D., Lopes, M., Nebreda, A., Thanos, D., Blow, J. ., Townsend, P., Sørensen, C.S., Bartek, J., Gorgoulis, V.G., 2016. Chronic p53-independent p21 expression causes genomic instability by deregulating replication licensing. *Nature Cell Biology*. **18**, 777.

Gale, C.R., Sayer, A.A., Cooper, C., Dennison, E.M., Starr, J.M., Whalley, L.J., Gallacher, J.E., Ben-Shlomo, Y., Kuh, D., Hardy, R., Craig, L., Deary, I.J., 2011. Factors associated with symptoms of anxiety and depression in five cohorts of community-based older people: the HALCyon (Healthy Ageing across the Life Course) Programme. *Psychological Medicine*. **41**, 2057-2073.

Gallage, S. & Gil, J., 2016. Mitochondrial Dysfunction Meets Senescence. *Trends in Biochemical Sciences*. **41**, 207-209.

Gazzeri, S., Gouyer, V., Vour'ch, C., Brambilla, C., Brambilla, E., 1998. Mechanisms of p16INK4A inactivation in non small-cell lung cancers. *Oncogene*. **16**, 497.

Gébleux, R. and Casi, G., 2016. Antibody-drug conjugates: Current status and future perspectives.

Georgakilas, A.G., Martin, O.A. and Bonner, W.M., 2017. p21: A Two-Faced Genome Guardian.

Georgakopoulou, E.A., Tsimaratou, K., Evangelou, K., Fernandez Marcos, P.J., Zoumpourlis, V., Trougakos, I.P., Kletsas, D., Bartek, J., Serrano, M., Gorgoulis, V.G., 2013. Specific lipofuscin staining as a novel biomarker to detect replicative and stress-induced senescence. A method applicable in cryo-preserved and archival tissues. *Aging*. **5**, 37-50.

Georgakopoulou, E., *et al*, 2016. Apoptosis or senescence? Which exit route do epithelial cells and fibroblasts preferentially follow? .

Gil, J., Kerai, P., Lleonart, M., Bernard, D., Cigudosa, J.C., Peters, G., Carnero, A., Beach, D., 2005. Immortalization of Primary Human Prostate Epithelial Cells by c-Myc. *Cancer Res*. **65**, 2179.

Gire, V. & Dulic, V., 2015. Senescence from G2 arrest, revisited. *Cell Cycle (Georgetown, Tex.)*. **14**, 297-304.

Gire, V., Roux, P., Wynford-Thomas, D., Brondello, J.M., Dulic, V., 2004. DNA damage checkpoint kinase Chk2 triggers replicative senescence. *The EMBO Journal*. **23**, 2554-2563.

Goldstein, S., 1990. Replicative senescence: the human fibroblast comes of age. *Science (New York, N.Y.)*. **249**, 1129-1133.

Gonzalez-Navarro, H., Abu Nabah, Y.N., Vinue, A., Andres-Manzano, M.J., Collado, M., Serrano, M., Andres, V., 2010. p19(ARF) deficiency reduces macrophage and vascular smooth muscle cell apoptosis and aggravates atherosclerosis. *Journal of the American College of Cardiology*. **55**, 2258-2268.

Gonzalo, S., Kreienkamp, R., Askjaer, P., 2017. Hutchinson-Gilford Progeria Syndrome: A premature aging disease caused by LMNA gene mutations. *Ageing Research Reviews*. **33**, 18-29.

Gorgoulis, V.G. and Halazonetis, T.D., 2010. Oncogene-induced senescence: the bright and dark side of the response.

Grandori, C., Wu, K.J., Fernandez, P., Ngouenet, C., Grim, J., Clurman, B.E., Moser, M.J., Oshima, J., Russell, D.W., Swisshelm, K., Frank, S., Amati, B.,

Dalla-Favera, R., Monnat, R.J., 2003. Werner syndrome protein limits MYC-induced cellular senescence. *Genes & Development*. **17**, 1569-1574.

Groeger, A.M., Caputi, M., Esposito, V., De Luca, A., Bagella, L., Pacilio, C., Klepetko, W., Giordano, G.G., Baldi, F., Kaiser, H.E., Wolner, E., Giordano, A., 1999. Independent prognostic role of p16 expression in lung cancer. *The Journal of Thoracic and Cardiovascular Surgery*. **118**, 529-535.

Guarente, L. & Kenyon, C., 2000. Genetic pathways that regulate ageing in model organisms. *Nature*. **408**, 255-262.

Guney, I. & Sedivy, J.M., 2006. Cellular senescence, epigenetic switches and c-Myc. *Cell Cycle (Georgetown, Tex.)*. **5**, 2319-2323.

Gustafsson, M.O., Hussain, A., Mohammad, D.K., Mohamed, A.J., Nguyen, V., Metalnikov, P., Colwill, K., Pawson, T., Smith, C.I., Nore, B.F., 2012. Regulation of nucleocytoplasmic shuttling of Bruton's tyrosine kinase (Btk) through a novel SH3-dependent interaction with ankyrin repeat domain 54 (ANKRD54). *Molecular and Cellular Biology*. **32**, 2440-2453.

Hackbusch, D., Dulsner, A., Gatzke, N., Kruger, J., Hillmeister, P., Nagorka, S., Blaschke, F., Ritter, Z., Thone-Reineke, C., Bohmer, F.D., Buschmann, I., Kappert, K., 2013. Knockout of Density-Enhanced Phosphatase-1 impairs cerebrovascular reserve capacity in an arteriogenesis model in mice. *BioMed Research International*. **2013**, 802149.

Haferkamp, S., *et al*, 2009. Oncogene-Induced Senescence Does Not Require the p16INK4a or p14ARF Melanoma Tumor Suppressors.

Hanahan, D. and Weinberg, R., 2011. Hallmarks of Cancer: The Next Generation.

Hanahan, D. and Weinberg, R.A., 2000. The Hallmarks of Cancer.

Hardy, T., Oakley, F., Anstee, Q.M., Day, C.P., 2016. Nonalcoholic Fatty Liver Disease: Pathogenesis and Disease Spectrum. *Annual Review of Pathology*. **11**, 451-496.

Harley, C.B., Futcher, A.B., Greider, C.W., 1990. Telomeres shorten during ageing of human fibroblasts. *Nature*. **345**, 458.

Harrison, D.E., Strong, R., Sharp, Z.D., Nelson, J.F., Astle, C.M., Flurkey, K., Nadon, N.L., Wilkinson, J.E., Frenkel, K., Carter, C.S., Pahor, M., Javors, M.A., Fernandez, E., Miller, R.A., 2009. Rapamycin fed late in life extends lifespan in genetically heterogeneous mice. *Nature*. **460**, 392-395.

Harrison, F.E., Reiserer, R.S., Tomarken, A.J., McDonald, M.P., 2006. Spatial and nonspatial escape strategies in the Barnes maze. *Learning & Memory (Cold Spring Harbor, N.Y.)*. **13**, 809-819.

- Hashimoto, M., Asai, A., Kawagishi, H., Mikawa, R., Iwashita, Y., Kanayama, K., Sugimoto, K., Sato, T., Maruyama, M., Sugimoto, M., 2016. Elimination of p19(ARF)-expressing cells enhances pulmonary function in mice. *JCI Insight*. **1**, e87732.
- Hayflick, L., 1998. How and why we age. *Experimental Gerontology*. **33**, 639-653.
- Hayflick, L., 1997. Mortality and immortality at the cellular level. A review. *Biochemistry (Moscow)*. **62**, 1180-1190.
- Hayflick, L., 1965. The limited in vitro lifetime of human diploid cell strains. *Experimental Cell Research*. **37**, 614-636.
- Hayflick, L. & Moorhead, P.S., 1961. The serial cultivation of human diploid cell strains. *Experimental Cell Research*. **25**, 585-621.
- He, S. and Sharpless, N.E., 2017. Senescence in Health and Disease.
- Helman, A., Klochendler, A., Azazmeh, N., Gabai, Y., Horwitz, E., Anzi, S., Swisa, A., Condiotti, R., Granit, R.Z., Nevo, Y., Fixler, Y., Shreibman, D., Zamir, A., Tornovsky-Babeay, S., Dai, C., Glaser, B., Powers, A.C., Shapiro, A.M.J., Magnuson, M.A., Dor, Y., Ben-Porath, I., 2016. p16Ink4a-induced senescence of pancreatic beta cells enhances insulin secretion. *Nature Medicine*. **22**, 412.
- Hendriks, R.W., Yuvaraj, S., Kil, L.P., 2014. Targeting Bruton's tyrosine kinase in B cell malignancies. *Nature Reviews.Cancer*. **14**, 219-232.
- Hensler, P.J. & Pereira-Smith, O.M., 1995. Human replicative senescence. A molecular study. *The American Journal of Pathology*. **147**, 1-8.
- Herbig, U., Jobling, W.A., Chen, B.P., Chen, D.J., Sedivy, J.M., 2004. Telomere shortening triggers senescence of human cells through a pathway involving ATM, p53, and p21(CIP1), but not p16(INK4a). *Molecular Cell*. **14**, 501-513.
- Herbig, U. & Sedivy, J.M., 2006. Regulation of growth arrest in senescence: telomere damage is not the end of the story. *Mechanisms of Ageing and Development*. **127**, 16-24.
- Herfs, M., Hubert, P., Delvenne, P., 2009. Epithelial metaplasia: adult stem cell reprogramming and (pre)neoplastic transformation mediated by inflammation? *Trends in Molecular Medicine*. **15**, 245-253.
- Herman, S.E., Gordon, A.L., Hertlein, E., Ramanunni, A., Zhang, X., Jaglowski, S., Flynn, J., Jones, J., Blum, K.A., Buggy, J.J., Hamdy, A., Johnson, A.J., Byrd, J.C., 2011. Bruton tyrosine kinase represents a promising therapeutic target for treatment of chronic lymphocytic leukemia and is effectively targeted by PCI-32765. *Blood*. **117**, 6287-6296.

Hernandez-Rabaza, V., Navarro-Mora, G., Velazquez-Sanchez, C., Ferragud, A., Marin, M.P., Garcia-Verdugo, J.M., Renau-Piqueras, J., Canales, J.J., 2010. Neurotoxicity and persistent cognitive deficits induced by combined MDMA and alcohol exposure in adolescent rats. *Addiction Biology*. **15**, 413-423.

Hernandez-Segura, A., de Jong, T.V., Melov, S., Guryev, V., Campisi, J., Demaria, M., 2017. Unmasking Transcriptional Heterogeneity in Senescent Cells. *Current Biology : CB*.

Herranz, N., Gallage, S., Mellone, M., Wuestefeld, T., Klotz, S., Hanley, C.J., Raguz, S., Acosta, J.C., Innes, A., Banito, A., Georgilis, A., Montoya, A., Wolter, K., Dharmalingam, G., Faull, P., Carroll, T., Martínez-Barbera, J.P., Cutillas, P., Reisinger, F., Heikenwalder, M., Miller, R., Withers, D., Zender, L., Thomas, G.J., Gil, J., 2015. mTOR regulates MAPKAPK2 translation to control the senescence-associated secretory phenotype. *Nature Cell Biology*. **17**, 1205.

Herranz, N. & Gil, J., 2016. Mitochondria and senescence: new actors for an old play. *The EMBO Journal*. **35**, 701-702.

Hewitt, G., Jurk, D., Marques, F.D.M., Correia-Melo, C., Hardy, T., Gackowska, A., Anderson, R., Taschuk, M., Mann, J., Passos, J.F., 2012. Telomeres are favoured targets of a persistent DNA damage response in ageing and stress-induced senescence. **3**, 708.

Hirai, H., Roussel, M.F., Kato, J.Y., Ashmun, R.A., Sherr, C.J., 1995. Novel INK4 proteins, p19 and p18, are specific inhibitors of the cyclin D-dependent kinases CDK4 and CDK6. *Molecular and Cellular Biology*. **15**, 2672-2681.

Hoare, M., Das, T., Alexander, G., 2010. Ageing, telomeres, senescence, and liver injury. *Journal of Hepatology*. **53**, 950-961.

Hoare, M. & Narita, M., 2017. NOTCH and the 2 SASPs of senescence. *Cell Cycle*. **16**, 239-240.

Hoare, M. & Narita, M., 2013. Transmitting senescence to the cell neighbourhood. *Nature Cell Biology*. **15**, 887.

Holt, S.E. & Shay, J.W., 1999. Role of telomerase in cellular proliferation and cancer. *Journal of Cellular Physiology*. **180**, 10-18.

Holz, O., Zuhlke, I., Jaksztat, E., Muller, K.C., Welker, L., Nakashima, M., Diemel, K.D., Branscheid, D., Magnussen, H., Jorres, R.A., 2004. Lung fibroblasts from patients with emphysema show a reduced proliferation rate in culture. *The European Respiratory Journal*. **24**, 575-579.

Honigberg, L.A., Smith, A.M., Sirisawad, M., Verner, E., Louny, D., Chang, B., Li, S., Pan, Z., Thamm, D.H., Miller, R.A., Buggy, J.J., 2010. The Bruton tyrosine kinase inhibitor PCI-32765 blocks B-cell activation and is efficacious in models of autoimmune disease and B-cell malignancy. *Proc Natl Acad Sci USA*. **107**, 13075.

- Hoshino, Y., Koide, H., Urakami, T., Kanazawa, H., Kodama, T., Oku, N., Shea, K.J., 2010. Recognition, Neutralization, and Clearance of Target Peptides in the Bloodstream of Living Mice by Molecularly Imprinted Polymer Nanoparticles: A Plastic Antibody. *Journal of the American Chemical Society*. **132**, 6644-6645.
- Howlett, S.E. & Rockwood, K., 2013. New horizons in frailty: ageing and the deficit-scaling problem. *Age and Ageing*. **42**, 416-423.
- Huang, C., Taki, T., Higashiyama, M., Kohno, N., Miyake, M., 1999. p16 protein expression is associated with a poor prognosis in squamous cell carcinoma of the lung. *British Journal of Cancer*. **82**, 374.
- Hudson, M.M., Ness, K.K., Gurney, J.G., Mulrooney, D.A., Chemaitilly, W., Krull, K.R., Green, D.M., Armstrong, G.T., Nottage, K.A., Jones, K.E., Sklar, C.A., Srivastava, D.K., Robison, L.L., 2013. Clinical ascertainment of health outcomes among adults treated for childhood cancer. *Jama*. **309**, 2371-2381.
- Huhne, R., Thalheim, T., Suhnel, J., 2014. AgeFactDB--the JenAge Ageing Factor Database--towards data integration in ageing research. *Nucleic Acids Research*. **42**, 892.
- Hutchinson, C.V. & Dyer, M.J., 2014. Breaking good: the inexorable rise of BTK inhibitors in the treatment of chronic lymphocytic leukaemia. *British Journal of Haematology*. **166**, 12-22.
- Itahana, K., Campisi, J., Dimri, G.P., 2007. Methods to detect biomarkers of cellular senescence: the senescence-associated beta-galactosidase assay. *Methods in Molecular Biology (Clifton, N.J.)*. **371**, 21.
- Itahana, K. & Dimri, G.P., 2017. Cancer and Senescence. In Quah, S. R., ed, *International Encyclopedia of Public Health (Second Edition)*. Oxford: Academic Press. 328-331.
- Ito, K. and Barnes, P.J., 2009. COPD as a Disease of Accelerated Lung Aging.
- Ito, Y., Hoare, M. and Narita, M., 2017. Spatial and Temporal Control of Senescence.
- Iuliano, R., Le Pera, I., Cristofaro, C., Baudi, F., Arturi, F., Pallante, P., Martelli, M.L., Trapasso, F., Chiariotti, L., Fusco, A., 2004. The tyrosine phosphatase PTPRJ/DEP-1 genotype affects thyroid carcinogenesis. *Oncogene*. **23**, 8432-8438.
- Iwaki, S., Jensen, B.M., Gilfillan, A.M., 2007. Ntal/Lab/Lat2. *The International Journal of Biochemistry & Cell Biology*. **39**, 868-873.
- Jacobs, J.J., 2013. Senescence: back to telomeres. *Nature Reviews.Molecular Cell Biology*. **14**, 196.

Jenny, N.S., French, B., Arnold, A.M., Strotmeyer, E.S., Cushman, M., Chaves, P.H., Ding, J., Fried, L.P., Kritchevsky, S.B., Rifkin, D.E., Sarnak, M.J., Newman, A.B., 2012. Long-term assessment of inflammation and healthy aging in late life: the Cardiovascular Health Study All Stars. *The Journals of Gerontology. Series A, Biological Sciences and Medical Sciences*. **67**, 970-976.

Jeon, O.H., Kim, C., Laberge, R.M., Demaria, M., Rathod, S., Vasserot, A.P., Chung, J.W., Kim, D.H., Poon, Y., David, N., Baker, D.J., van Deursen, J.M., Campisi, J., Elisseeff, J.H., 2017. Local clearance of senescent cells attenuates the development of post-traumatic osteoarthritis and creates a pro-regenerative environment. *Nature Medicine*. **23**, 775-781.

Jeyapalan, J.C., Ferreira, M., Sedivy, J.M., Herbig, U., 2007. Accumulation of senescent cells in mitotic tissue of aging primates. *Mechanisms of Ageing and Development*. **128**, 36-44.

Jeyapalan, J.C. and Sedivy, J.M., 2008. Cellular senescence and organismal aging.

Ji, M., Yuan, L., Lv, X., Dong, W., Peng, X., 2014. EBP50 regulates the apoptosis of pancreatic cancer cells by decreasing the expression levels of Bcl-2. *Experimental and Therapeutic Medicine*. **8**, 919-924.

Jiang, J., *et al*, 2016. HER2-targeted antibody drug conjugates for ovarian cancer therapy.

Jimenez, R., *et al*, 2005. Replicative senescence in patients with chronic kidney failure.

Jurk, D., Wilson, C., Passos, J.F., Oakley, F., Correia-Melo, C., Greaves, L., Saretzki, G., Fox, C., Lawless, C., Anderson, R., Hewitt, G., Pender, S.L., Fullard, N., Nelson, G., Mann, J., van de Sluis, B., Mann, D.A., von Zglinicki, T., 2014. Chronic inflammation induces telomere dysfunction and accelerates ageing in mice. *Nature Communications*. **2**, 4172.

Kadono, N., Miyazaki, T., Okugawa, Y., Nakajima, K., Hirai, Y., 2012. The impact of extracellular syntaxin4 on HaCaT keratinocyte behavior. *Biochemical and Biophysical Research Communications*. **417**, 1200-1205.

Kamijo, T., *et al*, 1997. Tumor Suppression at the Mouse INK4a Locus Mediated by the Alternative Reading Frame Product p19 ARF.

Kananen, L., Surakka, I., Pirkola, S., Suvisaari, J., Lonqvist, J., Peltonen, L., Ripatti, S., Hovatta, I., 2010. Childhood adversities are associated with shorter telomere length at adult age both in individuals with an anxiety disorder and controls. *PloS One*. **5**, e10826.

Kane, A.E., Hilmer, S.N., Boyer, D., Gavin, K., Nines, D., Howlett, S.E., de Cabo, R., Mitchell, S.J., 2016. Impact of Longevity Interventions on a Validated Mouse

Clinical Frailty Index. *The Journals of Gerontology. Series A, Biological Sciences and Medical Sciences*. **71**, 333-339.

Karimian, A., Ahmadi, Y. and Yousefi, B., 2016. Multiple functions of p21 in cell cycle, apoptosis and transcriptional regulation after DNA damage.

Kastan, M.B., Onyekwere, O., Sidransky, D., Vogelstein, B., Craig, R.W., 1991. Participation of p53 protein in the cellular response to DNA damage. *Cancer Research*. **51**, 6304-6311.

Ke, X. and Shen, L., 2017. Molecular targeted therapy of cancer: The progress and future prospect.

Kempe, H., Parareda Pujolràs, A., Kempe, M., 2015. Molecularly Imprinted Polymer Nanocarriers for Sustained Release of Erythromycin. *Pharmaceutical Research*. **32**, 375-388.

Kim, K.H., Chen, C.C., Monzon, R.I., Lau, L.F., 2013. Matricellular protein CCN1 promotes regression of liver fibrosis through induction of cellular senescence in hepatic myofibroblasts. *Molecular and Cellular Biology*. **33**, 2078-2090.

Kim, K.M., Noh, J.H., Bodogai, M., Martindale, J.L., Yang, X., Indig, F.E., Basu, S.K., Ohnuma, K., Morimoto, C., Johnson, P.F., Biragyn, A., Abdelmohsen, K., Gorospe, M., 2017. Identification of senescent cell surface targetable protein DPP4. *Genes & Development*.

Kimball, A.B., *et al*, 2018. Age-induced and photoinduced changes in gene expression profiles in facial skin of Caucasian females across 6 decades of age.

Kirkland, J.L. & Tchkonja, T., 2017. Cellular Senescence: A Translational Perspective. *EBioMedicine*. **21**, 21-28.

Kirkland, J.L. & Tchkonja, T., 2015. Clinical strategies and animal models for developing senolytic agents. *Experimental Gerontology*. **68**, 19-25.

Kiyono, T., Foster, S.A., Koop, J.I., McDougall, J.K., Galloway, D.A., Klingelutz, A.J., 1998. Both Rb/p16INK4a inactivation and telomerase activity are required to immortalize human epithelial cells. *Nature*. **396**, 84-88.

Knudsen, E.S. & Jean Y. J. Wang, 2010. Targeting the RB-pathway in Cancer Therapy. *Clinical Cancer Research*. **16**, 1094-1099.

Kolesnichenko, M., Hong, L., Liao, R., Vogt, P.K., Sun, P., 2012. Attenuation of TORC1 signaling delays replicative and oncogenic RAS-induced senescence. *Cell Cycle*. **11**, 2391-2401.

Kolodych, S., *et al*, 2017. Development and evaluation of β -galactosidase-sensitive antibody-drug conjugates.

Komada, M., Takao, K., Miyakawa, T., 2008. Elevated Plus Maze for Mice. *Journal of Visualized Experiments : JoVE*. 1088.

KONDZIELLA, W., 1964. A New Method for the Measurement of Muscle Relaxation in White Mice. *Archives Internationales De Pharmacodynamie Et De Therapie*. **152**, 277-284.

Koshikawa, N., Hasegawa, S., Nagashima, Y., Mitsuhashi, K., Tsubota, Y., Miyata, S., Miyagi, Y., Yasumitsu, H., Miyazaki, K., 1998. Expression of trypsin by epithelial cells of various tissues, leukocytes, and neurons in human and mouse. *The American Journal of Pathology*. **153**, 937-944.

Krishnamurthy, J., Torrice, C., Ramsey, M.R., Kovalev, G.I., Al-Regaiey, K., Su, L., Sharpless, N.E., 2004. Ink4a/Arf expression is a biomarker of aging. *The Journal of Clinical Investigation*. **114**, 1299-1307.

Kuehl, W.M. & Bergsagel, P.L., 2012. Molecular pathogenesis of multiple myeloma and its premalignant precursor. *The Journal of Clinical Investigation*. **122**, 3456-3463.

Kuilman, T., Michaloglou, C., Vredeveld, L.C., Douma, S., van Doorn, R., Desmet, C.J., Aarden, L.A., Mooi, W.J., Peeper, D.S., 2008. Oncogene-induced senescence relayed by an interleukin-dependent inflammatory network. *Cell*. **133**, 1019-1031.

Kuilman, T. & Peeper, D.S., 2009. Senescence-messaging secretome: SMS-ing cellular stress. *Nature Reviews.Cancer*. **9**, 81-94.

Kuilman, T., Michaloglou, C., Mooi, W.J., Peeper, D.S., 2010. The essence of senescence. *Genes & Development*. **24**, 2463-2479.

Kumar, A., *et al*, 2017. Chapter Twelve - Antibody-Drug Conjugates. Academic Press.

Kurz, D.J., Decary, S., Hong, Y., Erusalimsky, J.D., 2000. Senescence-associated (beta)-galactosidase reflects an increase in lysosomal mass during replicative ageing of human endothelial cells. *Journal of Cell Science*. **113 (Pt 20)**, 3613-3622.

Kuwano, K., *et al*, 2016. Cellular senescence and autophagy in the pathogenesis of chronic obstructive pulmonary disease (COPD) and idiopathic pulmonary fibrosis (IPF).

Laberge, R., Sun, Y., Orjalo, A.V., Patil, C.K., Freund, A., Zhou, L., Curran, S., Davalos, A.R., Wilson-Edell, K., Liu, S., Limbad, C., Demaria, M., Li, P., Hubbard, G.B., Ikeno, Y., Javors, M., Desprez, P., Benz, C.C., Kapahi, P., Nelson, P.S., Campisi, J., 2015. MTOR regulates the pro-tumorigenic senescence-associated secretory phenotype by promoting IL1A translation. *Nature Cell Biology*. **17**, 1049.

- Lachner, M., O'Carroll, D., Rea, S., Mechtler, K., Jenuwein, T., 2001. Methylation of histone H3 lysine 9 creates a binding site for HP1 proteins. *Nature*. **410**, 116.
- Lane, D.P., 1992. p53, guardian of the genome. *Nature*. **358**, 15.
- Lasry, A. & Ben-Neriah, Y., 2015. Senescence-associated inflammatory responses: aging and cancer perspectives. *Trends in Immunology*. **36**, 217-228.
- Lawless, C., *et al*, 2010. Quantitative assessment of markers for cell senescence.
- Lee, A.C., Fenster, B.E., Ito, H., Takeda, K., Bae, N.S., Hirai, T., Yu, Z.X., Ferrans, V.J., Howard, B.H., Finkel, T., 1999. Ras proteins induce senescence by altering the intracellular levels of reactive oxygen species. *The Journal of Biological Chemistry*. **274**, 7936-7940.
- Lee, H., Brott, B.K., Kirkby, L.A., Adelson, J.D., Cheng, S., Feller, M.B., Datwani, A., Shatz, C.J., 2014. Synapse elimination and learning rules co-regulated by MHC class I H2-Db. *Nature*. **509**, 195-200.
- Lee, S.W., Fang, L., Igarashi, M., Ouchi, T., Lu, K.P., Aaronson, S.A., 2000. Sustained activation of Ras/Raf/mitogen-activated protein kinase cascade by the tumor suppressor p53. *Proceedings of the National Academy of Sciences of the United States of America*. **97**, 8302-8305.
- Lehmann, M., Korfei, M., Mutze, K., Klee, S., Skronska-Wasek, W., Alsafadi, H.N., Ota, C., Costa, R., Schiller, H.B., Lindner, M., Wagner, D.E., Gunther, A., Konigshoff, M., 2017. Senolytic drugs target alveolar epithelial cell function and attenuate experimental lung fibrosis ex vivo. *The European Respiratory Journal*. **50**, 2016. Print 2017 Aug.
- Lemons, J.M.S., Feng, X., Bennett, B.D., Legesse-Miller, A., Johnson, E.L., Raitman, I., Pollina, E.A., Rabitz, H.A., Rabinowitz, J.D., Collier, H.A., 2010. Quiescent Fibroblasts Exhibit High Metabolic Activity. *PLoS Biology*. **8**, e1000514.
- Leontieva, O.V. & Blagosklonny, M.V., 2017. While reinforcing cell cycle arrest, rapamycin and Torins suppress senescence in UVA-irradiated fibroblasts. *Oncotarget*. **8**, 109848-109856.
- Leontieva, O.V. & Blagosklonny, M.V., 2016. Gerosuppression by pan-mTOR inhibitors. *Aging*. **8**, 3535-3551.
- Leslie, K.L., Song, G.J., Barrick, S., Wehbi, V.L., Vildardaga, J.P., Bauer, P.M., Bisello, A., 2013. Ezrin-radixin-moesin-binding phosphoprotein 50 (EBP50) and nuclear factor-kappaB (NF-kappaB): a feed-forward loop for systemic and vascular inflammation. *The Journal of Biological Chemistry*. **288**, 36426-36436.
- Leung, G.K., Schmidt, W.K., Bergo, M.O., Gavino, B., Wong, D.H., Tam, A., Ashby, M.N., Michaelis, S., Young, S.G., 2001. Biochemical studies of Zmpste24-deficient mice. *The Journal of Biological Chemistry*. **276**, 29051-29058.

Leung, T.H., Zhang, L.F., Wang, J., Ning, S., Knox, S.J., Kim, S.K., 2013. Topical hypochlorite ameliorates NF-kappaB-mediated skin diseases in mice. *The Journal of Clinical Investigation*. **123**, 5361-5370.

Levine, A.J., 1997. p53, the Cellular Gatekeeper for Growth and Division.

Levine, B. and Kroemer, G., 2008. Autophagy in the Pathogenesis of Disease.

Li, C., Chai, Y., Wang, L., Gao, B., Chen, H., Gao, P., Zhou, F.Q., Luo, X., Crane, J.L., Yu, B., Cao, X., Wan, M., 2017. Programmed cell senescence in skeleton during late puberty. *Nature Communications*. **8**, 0.

Li, P., *et al*, 2012. Telomere dysfunction induced by chemotherapeutic agents and radiation in normal human cells.

Lin, A.W., Barradas, M., Stone, J.C., van Aelst, L., Serrano, M., Lowe, S.W., 1998. Premature senescence involving p53 and p16 is activated in response to constitutive MEK/MAPK mitogenic signaling. *Genes & Development*. **12**, 3008-3019.

Liou, J.W., Hung, Y.J., Yang, C.H., Chen, Y.C., 2015. The antimicrobial activity of gramicidin A is associated with hydroxyl radical formation. *PloS One*. **10**, e0117065.

Lister, R.G., 1987. The use of a plus-maze to measure anxiety in the mouse. *Psychopharmacology*. **92**, 180-185.

Liu, H., Zhao, W.L., Wang, J.P., Xin, B.M., Shao, R.G., 2017. EBP50 suppresses the proliferation of MCF-7 human breast cancer cells via promoting Beclin-1/p62-mediated lysosomal degradation of c-Myc. *Acta Pharmacologica Sinica*.

Liu, S., Nugroho, A.E., Shudou, M., Maeyama, K., 2012. Regulation of mucosal mast cell activation by short interfering RNAs targeting syntaxin4. *Immunology and Cell Biology*. **90**, 337-345.

Loaiza, N. & Demaria, M., 2016. Cellular senescence and tumor promotion: Is aging the key? *Biochimica Et Biophysica Acta*. **1865**, 155-167.

Longo, V.D., Antebi, A., Bartke, A., Barzilai, N., Brown-Borg, H.M., Caruso, C., Curiel, T.J., de Cabo, R., Franceschi, C., Gems, D., Ingram, D.K., Johnson, T.E., Kennedy, B.K., Kenyon, C., Klein, S., Kopchick, J.J., Lepperdinger, G., Madeo, F., Mirisola, M.G., Mitchell, J.R., Passarino, G., Rudolph, K.L., Sedivy, J.M., Shadel, G.S., Sinclair, D.A., Spindler, S.R., Suh, Y., Vijg, J., Vinciguerra, M., Fontana, L., 2015. Interventions to Slow Aging in Humans: Are We Ready? *Aging Cell*. **14**, 497-510.

Lopez-Domenech, G., Serrat, R., Mirra, S., D'Aniello, S., Somorjai, I., Abad, A., Vituriera, N., Garcia-Arumi, E., Alonso, M.T., Rodriguez-Prados, M., Burgaya, F., Andreu, A.L., Garcia-Sancho, J., Trullas, R., Garcia-Fernandez, J., Soriano, E.,

2012. The Eutherian Armcx genes regulate mitochondrial trafficking in neurons and interact with Miro and Trak2. *Nature Communications*. **3**, 814.
- López-Otín, C., Blasco, M.A., Partridge, L., Serrano, M., Kroemer, G., 2013. The hallmarks of aging. *Cell*. **153**, 1194-1217.
- López-Otín, C., *et al*, 2016. Metabolic Control of Longevity.
- Lowe, S.W. and Sherr, C.J., 2003. Tumor suppression by Ink4a–Arf: progress and puzzles.
- Loxton, D. & Canales, J.J., 2017. Long-term cognitive, emotional and neurogenic alterations induced by alcohol and methamphetamine exposure in adolescent rats. *Progress in Neuro-Psychopharmacology & Biological Psychiatry*. **74**, 1-8.
- Lozano-Torres, B., Galiana, I., Rovira, M., Garrido, E., Chaib, S., Bernardos, A., Muñoz-Espin, D., Serrano, M., Martínez-Manez, R., Sancenon, F., 2017. An OFF-ON Two-Photon Fluorescent Probe for Tracking Cell Senescence in Vivo. *Journal of the American Chemical Society*. **139**, 8808-8811.
- Luh, F.Y., Archer, S.J., Domaille, P.J., Smith, B.O., Owen, D., Brotherton, D.H., Raine, A.R.C., Xu, X., Brizuela, L., Brenner, S.L., Laue, E.D., 1997. Structure of the cyclin-dependent kinase inhibitor p19Ink4d. *Nature*. **389**, 999.
- Luliński, P., 2017. Molecularly imprinted polymers based drug delivery devices: a way to application in modern pharmacotherapy. A review.
- Lundberg, A.S., *et al*, 2000. Genes involved in senescence and immortalization.
- Maciel-Barón, L.A., Morales-Rosales, S., Aquino-Cruz, A., Triana-Martínez, F., Galván-Arzate, S., Luna-López, A., González-Puertos, V.Y., López-Díazguerrero, N.E., Torres, C., Königsberg, M., 2016. Senescence associated secretory phenotype profile from primary lung mice fibroblasts depends on the senescence induction stimuli. *Age*. **38**, 26.
- Macip, S., Igarashi, M., Berggren, P., Yu, J., Lee, S.W., Aaronson, S.A., 2003. Influence of induced reactive oxygen species in p53-mediated cell fate decisions. *Molecular and Cellular Biology*. **23**, 8576-8585.
- Macip, S., Igarashi, M., Fang, L., Chen, A., Pan, Z.Q., Lee, S.W., Aaronson, S.A., 2002. Inhibition of p21-mediated ROS accumulation can rescue p21-induced senescence. *The EMBO Journal*. **21**, 2180-2188.
- Maddox, P.H. & Jenkins, D., 1987. 3-Aminopropyltriethoxysilane (APES): a new advance in section adhesion. *Journal of Clinical Pathology*. **40**, 1256-1257.
- Madeo, F., Zimmermann, A., Maiuri, M.C., Kroemer, G., 2015. Essential role for autophagy in life span extension. *The Journal of Clinical Investigation*. **125**, 85-93.

Malaquin, N., Martinez, A. and Rodier, F., 2016. Keeping the senescence secretome under control: Molecular reins on the senescence-associated secretory phenotype.

Mannino, D.M. and Buist, A.S., 2007. Global burden of COPD: risk factors, prevalence, and future trends.

Mao, K., Quipildor, G.F., Tabrizian, T., Novaj, A., Guan, F., Walters, R.O., Delahaye, F., Hubbard, G.B., Ikeno, Y., Ejima, K., Li, P., Allison, D.B., Salimi-Moosavi, H., Beltran, P.J., Cohen, P., Barzilai, N., Huffman, D.M., 2018. Late-life targeting of the IGF-1 receptor improves healthspan and lifespan in female mice. *Nature Communications*. **9**, 5.

Martin-Ruiz, C.M., Gussekloo, J., van Heemst, D., von Zglinicki, T., Westendorp, R.G., 2005. Telomere length in white blood cells is not associated with morbidity or mortality in the oldest old: a population-based study. *Aging Cell*. **4**, 287-290.

Masgras, I., Carrera, S., de Verdier, P.J., Brennan, P., Majid, A., Makhtar, W., Tulchinsky, E., Jones, G.D., Roninson, I.B., Macip, S., 2012. Reactive oxygen species and mitochondrial sensitivity to oxidative stress determine induction of cancer cell death by p21. *The Journal of Biological Chemistry*. **287**, 9845-9854.

Mason, C., Savona, S., Rini, J.N., Castillo, J.J., Xu, L., Hunter, Z.R., Treon, S.P., Allen, S.L., 2017. Ibrutinib penetrates the blood brain barrier and shows efficacy in the therapy of Bing Neel syndrome. *British Journal of Haematology*. **179**, 339-341.

Masso-Valles, D., Jauset, T., Serrano, E., Sodik, N.M., Pedersen, K., Affara, N.I., Whitfield, J.R., Beaulieu, M.E., Evan, G.I., Elias, L., Arribas, J., Soucek, L., 2015. Ibrutinib exerts potent antifibrotic and antitumor activities in mouse models of pancreatic adenocarcinoma. *Cancer Research*. **75**, 1675-1681.

Matjusaitis, M., *et al*, 2016. Biomarkers to identify and isolate senescent cells.

Mattison, J.A., Colman, R.J., Beasley, T.M., Allison, D.B., Kemnitz, J.W., Roth, G.S., Ingram, D.K., Weindruch, R., de Cabo, R., Anderson, R.M., 2017. Caloric restriction improves health and survival of rhesus monkeys. *Nature Communications*. **8**, 14063.

McArthur, J.C., Nance-Sproson, T.E., Griffin, D.E., Hoover, D., Selnes, O.A., Miller, E.N., Margolick, J.B., Cohen, B.A., Farzadegan, H., Saah, A., 1992. The diagnostic utility of elevation in cerebrospinal fluid beta 2-microglobulin in HIV-1 dementia. Multicenter AIDS Cohort Study. *Neurology*. **42**, 1707-1712.

McHugh, D. & Gil, J., 2018. Senescence and aging: Causes, consequences, and therapeutic avenues. *J Cell Biol*. **217**, 65.

MDuff, F.K.E. and Turner, S.D., 2011. Jailbreak: Oncogene-induced senescence and its evasion.

Michaloglou, C., Vredeveld, L.C., Soengas, M.S., Denoyelle, C., Kuilman, T., van der Horst, C M, Majoor, D.M., Shay, J.W., Mooi, W.J., Peeper, D.S., 2005. BRAFE600-associated senescence-like cell cycle arrest of human naevi. *Nature*. **436**, 720-724.

Milanovic, M., Fan, D.N.Y., Belenki, D., Däbritz, J.H.M., Zhao, Z., Yu, Y., Dörr, J.R., Dimitrova, L., Lenze, D., Monteiro Barbosa, I.A., Mendoza-Parra, M., Kanashova, T., Metzner, M., Pardon, K., Reimann, M., Trumpp, A., Dörken, B., Zuber, J., Gronemeyer, H., Hummel, M., Dittmar, G., Lee, S., Schmitt, C.A., 2017. Senescence-associated reprogramming promotes cancer stemness. *Nature*. **553**, 96.

Miller, K.N., Burhans, M.S., Clark, J.P., Howell, P.R., Polewski, M.A., DeMuth, T.M., Eliceiri, K.W., Lindstrom, M.J., Ntambi, J.M., Anderson, R.M., 2017. Aging and caloric restriction impact adipose tissue, adiponectin, and circulating lipids. *Aging Cell*. **16**, 497-507.

Minagawa, S., Araya, J., Numata, T., Nojiri, S., Hara, H., Yumino, Y., Kawaishi, M., Odaka, M., Morikawa, T., Nishimura, S.L., Nakayama, K., Kuwano, K., 2011. Accelerated epithelial cell senescence in IPF and the inhibitory role of SIRT6 in TGF-beta-induced senescence of human bronchial epithelial cells. *American Journal of Physiology.Lung Cellular and Molecular Physiology*. **300**, 391.

Mirra, S., Ulloa, F., Gutierrez-Vallejo, I., Marti, E., Soriano, E., 2016. Function of Armcx3 and Armc10/SVH Genes in the Regulation of Progenitor Proliferation and Neural Differentiation in the Chicken Spinal Cord. *Frontiers in Cellular Neuroscience*. **10**, 47.

Mohamed, A.J., Yu, L., Backesjo, C.M., Vargas, L., Faryal, R., Aints, A., Christensson, B., Berglof, A., Vihinen, M., Nore, B.F., Smith, C.I., 2009. Bruton's tyrosine kinase (Btk): function, regulation, and transformation with special emphasis on the PH domain. *Immunological Reviews*. **228**, 58-73.

Moiseeva, O., Bourdeau, V., Roux, A., Deschênes-Simard, X., Ferbeyre, G., 2009. Mitochondrial Dysfunction Contributes to Oncogene-Induced Senescence. *Molecular and Cellular Biology*. **29**, 4495-4507.

Moreno-Blas, D., Gorostieta-Salas, E. and Castro-Obregón, S., 2018. Connecting chaperone-mediated autophagy dysfunction to cellular senescence.

Moskalev, A., Chernyagina, E., Tsvetkov, V., Fedintsev, A., Shaposhnikov, M., Krut'ko, V., Zhavoronkov, A., Kennedy, B.K., 2016. Developing criteria for evaluation of geroprotectors as a key stage toward translation to the clinic. *Aging Cell*. **15**, 407-415.

Mosteiro, L., Pantoja, C., Alcazar, N., Marion, R.M., Chondronasiou, D., Rovira, M., Fernandez-Marcos, P.J., Munoz-Martin, M., Blanco-Aparicio, C., Pastor, J., Gomez-Lopez, G., De Martino, A., Blasco, M.A., Abad, M., Serrano, M., 2016. Tissue damage and senescence provide critical signals for cellular

reprogramming in vivo. *Science (New York, N.Y.)*. **354**, 10.1126/science.aaf4445.

Mosteiro, L., Pantoja, C., Martino, A., Serrano, M., 2018. Senescence promotes in vivo reprogramming through p16INK4a and IL-6. *Aging Cell*. **17**, n/a.

Mou, Z., Tapper, A.R., Gardner, P.D., 2009. The armadillo repeat-containing protein, ARMCX3, physically and functionally interacts with the developmental regulatory factor Sox10. *The Journal of Biological Chemistry*. **284**, 13629-13640.

Muller, K.C., Welker, L., Paasch, K., Feindt, B., Erpenbeck, V.J., Hohlfeld, J.M., Krug, N., Nakashima, M., Branscheid, D., Magnussen, H., Jorres, R.A., Holz, O., 2006. Lung fibroblasts from patients with emphysema show markers of senescence in vitro. *Respiratory Research*. **7**, 32.

Muniz, L., *et al*, 2017. Control of Gene Expression in Senescence through Transcriptional Read-Through of Convergent Protein-Coding Genes.

Muñoz-Espín, D., Rovira, M., Galiana, I., Giménez, C., Lozano-Torres, B., Paez-Ribes, M., Llanos, S., Chaib, S., Muñoz-Martín, M., Uceró, A.C., Garaulet, G., Mulero, F., Dann, S.G., VanArsdale, T., Shields, D.J., Bernardos, A., Murguía, J.R., Martínez-Máñez, R., Serrano, M., 2018. A versatile drug delivery system targeting senescent cells. *EMBO Mol Med*.

Munoz-Espin, D., Canamero, M., Maraver, A., Gomez-Lopez, G., Contreras, J., Murillo-Cuesta, S., Rodriguez-Baeza, A., Varela-Nieto, I., Ruberte, J., Collado, M., Serrano, M., 2013. Programmed cell senescence during mammalian embryonic development. *Cell*. **155**, 1104-1118.

Muñoz-Espín, D. & Serrano, M., 2014. Cellular senescence: from physiology to pathology. *Nature Reviews.Molecular Cell Biology*. **15**, 482.

Narita, M. & Lowe, S.W., 2005. Senescence comes of age. *Nature Medicine*. **11**, 920-922.

Narita, M., Nunez, S., Heard, E., Narita, M., Lin, A.W., Hearn, S.A., Spector, D.L., Hannon, G.J., Lowe, S.W., 2003. Rb-mediated heterochromatin formation and silencing of E2F target genes during cellular senescence. *Cell*. **113**, 703-716.

Naylor, R.M., Deursen, J M A van, Baker, D.J., 2013. Senescent cells: a novel therapeutic target for aging and age-related diseases. **93**, 105-116.

Neves, J., Demaria, M., Campisi, J., Jasper, H., 2015. Of flies, mice, and men: evolutionarily conserved tissue damage responses and aging. *Developmental Cell*. **32**, 9-18.

Noureddine, H., Gary-Bobo, G., Alifano, M., Marcos, E., Saker, M., Vienney, N., Amsellem, V., Maitre, B., Chaouat, A., Chouaid, C., Dubois-Rande, J.L., Damotte, D., Adnot, S., 2011. Pulmonary artery smooth muscle cell senescence

is a pathogenic mechanism for pulmonary hypertension in chronic lung disease. *Circulation Research*. **109**, 543-553.

Novero, A., Ravella, P.M., Chen, Y., Dous, G., Liu, D., 2014. Ibrutinib for B cell malignancies. *Experimental Hematology & Oncology*. **3**, 4.

Ocampo, A., Reddy, P., Martinez-Redondo, P., Platero-Luengo, A., Hatanaka, F., Hishida, T., Li, M., Lam, D., Kurita, M., Beyret, E., Araoka, T., Vazquez-Ferrer, E., Donoso, D., Roman, J.L., Xu, J., Rodriguez Esteban, C., Nunez, G., Nunez Delicado, E., Campistol, J.M., Guillen, I., Guillen, P., Izpisua Belmonte, J.C., 2016. In Vivo Amelioration of Age-Associated Hallmarks by Partial Reprogramming. *Cell*. **167**, 1733.e12.

Ogrodnik, M., Miwa, S., Tchkonja, T., Tiniakos, D., Wilson, C.L., Lahat, A., Day, C.P., Burt, A., Palmer, A., Anstee, Q.M., Grellescheid, S.N., Hoeijmakers, J.H.J., Barnhoorn, S., Mann, D.A., Bird, T.G., Vermeij, W.P., Kirkland, J.L., Passos, J.F., von Zglinicki, T., Jurk, D., 2017. Cellular senescence drives age-dependent hepatic steatosis. **8**, 15691.

Oh, Y., Heo, K., Kim, E., Jang, J., Bae, S.S., Park, J.B., Kim, Y.H., Song, M., Kim, S.R., Ryu, S.H., Kim, I., Suh, P., 2017. Dynamic relocalization of NHERF1 mediates chemotactic migration of ovarian cancer cells toward lysophosphatidic acid stimulation. *Experimental & Molecular Medicine*. **49**, e351.

O'Leary, T.P. & Brown, R.E., 2013. Optimization of apparatus design and behavioral measures for the assessment of visuo-spatial learning and memory of mice on the Barnes maze. *Learning & Memory (Cold Spring Harbor, N. Y.)*. **20**, 85-96.

Osorio, F.G., *et al*, 2016. Chapter Four - NF- κ B signaling as a driver of ageing. Academic Press.

Ostman, A., Yang, Q., Tonks, N.K., 1994. Expression of DEP-1, a receptor-like protein-tyrosine-phosphatase, is enhanced with increasing cell density. *Proceedings of the National Academy of Sciences of the United States of America*. **91**, 9680-9684.

Östman, A., Hellberg, C., Böhmer, F.D., 2006. Protein-tyrosine phosphatases and cancer. *Nature Reviews Cancer*. **6**, 307.

Pan, J., *et al*, 2017. Inhibition of Bcl-2/xl With ABT-263 Selectively Kills Senescent Type II Pneumocytes and Reverses Persistent Pulmonary Fibrosis Induced by Ionizing Radiation in Mice.

Park, H.Y. & Sin, D.D., 2014. Chapter 16 - Stress-Induced Premature Senescence: Another Mechanism Involved in the Process of Accelerated Aging in Chronic Obstructive Pulmonary Disease. In Rahman, I. & Bagchi, D., eds, *Inflammation, Advancing Age and Nutrition*. San Diego: Academic Press. 193-202.

Parkes, T.L., Hilliker, A.J. and Phillips, J.P., 1999. Motorneurons, reactive oxygen, and life span in *Drosophila*☆.

Parrinello, S., Coppe, J.P., Krtolica, A., Campisi, J., 2005. Stromal-epithelial interactions in aging and cancer: senescent fibroblasts alter epithelial cell differentiation. *Journal of Cell Science*. **118**, 485-496.

Parrinello, S., Samper, E., Krtolica, A., Goldstein, J., Melov, S., Campisi, J., 2003. Oxygen sensitivity severely limits the replicative lifespan of murine fibroblasts. *Nature Cell Biology*. **5**, 741.

Pauliah, M., *et al*, 2018. Chapter 10 - Tumor-Targeted Therapy. Elsevier.

Pellow, S., *et al*, 1985. Validation of open : closed arm entries in an elevated plus-maze as a measure of anxiety in the rat.

Pendás, A.M., Zhou, Z., Cadiñanos, J., Freije, J.M.P., Wang, J., Hultenby, K., Astudillo, A., Wernerson, A., Rodríguez, F., Tryggvason, K., López-Otín, C., 2002. Defective prelamin A processing and muscular and adipocyte alterations in *Zmpste24* metalloproteinase-deficient mice. *Nature Genetics*. **31**, 94.

Pereira, C., Gimenez-Xavier, P., Pros, E., Pajares, M.J., Moro, M., Gomez, A., Navarro, A., Condom, E., Moran, S., Gomez-Lopez, G., Grana, O., Rubio-Camarillo, M., Martinez-Marti, A., Yokota, J., Carretero, J., Galbis, J.M., Nadal, E., Pisano, D., Sozzi, G., Felip, E., Montuenga, L.M., Roz, L., Villanueva, A., Sanchez-Cespedes, M., 2017. Genomic Profiling of Patient-Derived Xenografts for Lung Cancer Identifies B2M Inactivation Impairing Immunorecognition. *Clinical Cancer Research : An Official Journal of the American Association for Cancer Research*. **23**, 3203-3213.

Perez, H.L., *et al*, 2014. Antibody–drug conjugates: current status and future directions.

Pérez-Mancera, P.A., Young, A.R.J., Narita, M., 2014. Inside and out: the activities of senescence in cancer. *Nature Reviews.Cancer*. **14**, 547.

Perna, G., Iannone, G., Alciati, A., Caldirola, D., 2015. Are Anxiety Disorders Associated with Accelerated Aging? A Focus on Neuroprogression. *Neural Plasticity*. **2016**, 8457612.

Petermann, A., Stampnik, Y., Cui, Y., Morrison, H., Pachow, D., Kliese, N., Mawrin, C., Bohmer, F.D., 2015. Deficiency of the protein-tyrosine phosphatase DEP-1/PTPRJ promotes matrix metalloproteinase-9 expression in meningioma cells. *Journal of Neuro-Oncology*. **122**, 451-459.

Piletska, E.V., Piletsky, S.S., Whitcombe, M.J., Chianella, I., Piletsky, S.A., 2012. Development of a New Microtiter Plate Format for Clinically Relevant Assays. *Analytical Chemistry*. **84**, 2038-2043.

Piletska, E., Yawer, H., Canfarotta, F., Moczko, E., Smolinska-Kempisty, K., Piletsky, S.S., Guerreiro, A., Whitcombe, M.J., Piletsky, S.A., 2017. Biomimetic Silica Nanoparticles Prepared by a Combination of Solid-Phase Imprinting and Ostwald Ripening. *Scientific Reports*. **7**, 11537.

Piletsky, S.A., Turner, N.W., Laitenberger, P., 2006. Molecularly imprinted polymers in clinical diagnostics--future potential and existing problems. *Medical Engineering & Physics*. **28**, 971-977.

Piletsky, S.S., Rabinowicz, S., Yang, Z., Zagar, C., Piletska, E.V., Guerreiro, A., Piletsky, S.A., 2017. Development of molecularly imprinted polymers specific for blood antigens for application in antibody-free blood typing. *Chemical Communications (Cambridge, England)*. **53**, 1793-1796.

Pinkston, J.M., Garigan, D., Hansen, M., Kenyon, C., 2006. Mutations that increase the life span of *C. elegans* inhibit tumor growth. *Science (New York, N.Y.)*. **313**, 971-975.

Pollock, P.M., Harper, U.L., Hansen, K.S., Yudt, L.M., Stark, M., Robbins, C.M., Moses, T.Y., Hostetter, G., Wagner, U., Kakareka, J., Salem, G., Pohida, T., Heenan, P., Duray, P., Kallioniemi, O., Hayward, N.K., Trent, J.M., Meltzer, P.S., 2002. High frequency of BRAF mutations in nevi. *Nature Genetics*. **33**, 19.

Poma, A., Turner, A.P.F. and Piletsky, S.A., 2010. Advances in the manufacture of MIP nanoparticles.

Povedano, J., *et al*, 2015. Mice with Pulmonary Fibrosis Driven by Telomere Dysfunction.

Powers, R.W., Kaeberlein, M., Caldwell, S.D., Kennedy, B.K., Fields, S., 2005. Extension of chronological life span in yeast by decreased TOR pathway signaling. *Genes & Development*. **20**, 174-184.

Prizment, A.E., Linabery, A.M., Lutsey, P.L., Selvin, E., Nelson, H.H., Folsom, A.R., Church, T.R., Drake, C.G., Platz, E.A., Joshi, C., 2016. Circulating Beta-2 Microglobulin and Risk of Cancer: The Atherosclerosis Risk in Communities Study (ARIC). *Cancer Epidemiology, Biomarkers & Prevention : A Publication of the American Association for Cancer Research, Cosponsored by the American Society of Preventive Oncology*. **25**, 657-664.

Provinciali, M., Pierpaoli, E., Piacenza, F., Giacconi, R., Costarelli, L., Basso, A., Recchioni, R., Marcheselli, F., Bray, D., Benlhassan, K. and Malavolta, M., 2016. Chapter 22 - Nutritional Modulators of Cellular Senescence In Vitro. In Malavolta, M. & Mocchegiani, E., eds, *Molecular Basis of Nutrition and Aging*. San Diego: Academic Press. 293-312.

Puoci, F., Cirillo, G., Curcio, M., Parisi, O.I., Iemma, F., Picci, N., 2011. Molecularly imprinted polymers in drug delivery: state of art and future perspectives. *Expert Opinion on Drug Delivery*. **8**, 1379-1393.

Qudrat, A., Wong, J., Truong, K., 2017. Engineering mammalian cells to seek senescence associated secretory phenotypes. *Journal of Cell Science*.

Rada, M., Althubiti, M., Ekpenyong-Akiba, A.E., Lee, K.G., Lam, K.P., Fedorova, O., Barlev, N.A., Macip, S., 2017. BTK blocks the inhibitory effects of MDM2 on p53 activity. *Oncotarget*. **8**, 106639-106647.

Rando, T. and Chang, H., 2012. Aging, Rejuvenation, and Epigenetic Reprogramming: Resetting the Aging Clock.

Rawlings, D.J., Scharenberg, A.M., Park, H., Wahl, M.I., Lin, S., Kato, R.M., Fluckiger, A.C., Witte, O.N., Kinet, J.P., 1996. Activation of BTK by a phosphorylation mechanism initiated by SRC family kinases. *Science (New York, N. Y.)*. **271**, 822-825.

Relaix, F. & Zammit, P.S., 2012. Satellite cells are essential for skeletal muscle regeneration: the cell on the edge returns centre stage. *Development (Cambridge, England)*. **139**, 2845-2856.

Ressler, S., Bartkova, J., Niederegger, H., Bartek, J., Scharffetter-Kochanek, K., Jansen-Durr, P., Wlaschek, M., 2006. p16INK4A is a robust in vivo biomarker of cellular aging in human skin. *Aging Cell*. **5**, 379-389.

Ritchie, K., Artero, S., Beluche, I., Ancelin, M.L., Mann, A., Dupuy, A.M., Malafosse, A., Boulenger, J.P., 2004. Prevalence of DSM-IV psychiatric disorder in the French elderly population. *The British Journal of Psychiatry : The Journal of Mental Science*. **184**, 147-152.

Ritschka, B., Storer, M., Mas, A., Heinzmann, F., Ortells, M.C., Morton, J.P., Sansom, O.J., Zender, L., Keyes, W.M., 2017. The senescence-associated secretory phenotype induces cellular plasticity and tissue regeneration. *Genes & Development*. **31**, 172-183.

Robida-Stubbs, S., Glover-Cutter, K., Lamming, D.W., Mizunuma, M., Narasimhan, S.D., Neumann-Haefelin, E., Sabatini, D.M., Blackwell, T.K., 2012. TOR signaling and rapamycin influence longevity by regulating SKN-1/Nrf and DAF-16/FoxO. *Cell Metabolism*. **15**, 713-724.

Rodier, F., Munoz, D.P., Teachenor, R., Chu, V., Le, O., Bhaumik, D., Coppe, J.P., Campeau, E., Beausejour, C.M., Kim, S.H., Davalos, A.R., Campisi, J., 2011. DNA-SCARS: distinct nuclear structures that sustain damage-induced senescence growth arrest and inflammatory cytokine secretion. *Journal of Cell Science*. **124**, 68-81.

Rodier, F. & Campisi, J., 2011. Four faces of cellular senescence. *The Journal of Cell Biology*. **192**, 547-556.

Rodier, F., Coppé, J., Patil, C.K., Hoeijmakers, W.A.M., Muñoz, D.P., Raza, S.R., Freund, A., Campeau, E., Davalos, A.R., Campisi, J., 2009. Persistent DNA

damage signalling triggers senescence-associated inflammatory cytokine secretion. *Nature Cell Biology*. **11**, 973.

Romagosa, C., Simonetti, S., López-Vicente, L., Mazo, A., Leonart, M.E., Castellvi, J., Ramon y Cajal, S., 2011. p16Ink4a overexpression in cancer: a tumor suppressor gene associated with senescence and high-grade tumors. *Oncogene*. **30**, 2087-2097.

Romanov, V.S. & Rudolph, K.L., 2016. p21 shapes cancer evolution. *Nature Cell Biology*. **18**, 722.

Rosenfeld, C.S. & Ferguson, S.A., 2014. Barnes maze testing strategies with small and large rodent models. *Journal of Visualized Experiments : JoVE*. **(84):e51194**. doi, e51194.

Rothwell, P.M., Fowkes, F.G., Belch, J.F., Ogawa, H., Warlow, C.P., Meade, T.W., 2011. Effect of daily aspirin on long-term risk of death due to cancer: analysis of individual patient data from randomised trials. *Lancet (London, England)*. **377**, 31-41.

Rubin, H., 1998. Telomerase and cellular lifespan: ending the debate? *Nature Biotechnology*. **16**, 396-397.

Rufini, A., Tucci, P., Celardo, I., Melino, G., 2013. Senescence and aging: the critical roles of p53. *Oncogene*. **32**, 5129.

Ruhland, M.K., Coussens, L.M., Stewart, S.A., 2016. Senescence and cancer: An evolving inflammatory paradox. *Biochimica Et Biophysica Acta*. **1865**, 14-22.

Ruivenkamp, C., Hermsen, M., Postma, C., Klous, A., Baak, J., Meijer, G., Demant, P., 2003. LOH of PTPRJ occurs early in colorectal cancer and is associated with chromosomal loss of 18q12-21. *Oncogene*. **22**, 3472-3474.

Salama, R., Sadaie, M., Hoare, M., Narita, M., 2014. Cellular senescence and its effector programs. *Genes & Development*. **28**, 99-114.

Salminen, A., Kauppinen, A. and Kaarniranta, K., 2012. Emerging role of NF- κ B signaling in the induction of senescence-associated secretory phenotype (SASP).

Sau, S., *et al*, 2017. Advances in antibody–drug conjugates: A new era of targeted cancer therapy.

Schafer, M.J., White, T.A., Iijima, K., Haak, A.J., Ligresti, G., Atkinson, E.J., Oberg, A.L., Birch, J., Salmonowicz, H., Zhu, Y., Mazula, D.L., Brooks, R.W., Fuhrmann-Stroissnigg, H., Pirtskhalava, T., Prakash, Y.S., Tchkonja, T., Robbins, P.D., Aubry, M.C., Passos, J.F., Kirkland, J.L., Tschumperlin, D.J., Kita, H., LeBrasseur, N.K., 2017. Cellular senescence mediates fibrotic pulmonary disease. *Nature Communications*. **8**, 14532.

- Scott, L.M., Lawrence, H.R., Sebti, S.M., Lawrence, N.J., Wu, J., 2010. Targeting Protein Tyrosine Phosphatases for Anticancer Drug Discovery. *Current Pharmaceutical Design*. **16**, 1843-1862.
- Sellergren, B. & Allender, C.J., 2005. Molecularly imprinted polymers: A bridge to advanced drug delivery. *Advanced Drug Delivery Reviews*. **57**, 1733-1741.
- Sengupta, S. & Sasisekharan, R., 2007. Exploiting nanotechnology to target cancer. *British Journal of Cancer*. **96**, 1315-1319.
- Senís, E., Mosteiro, L., Wilkening, S., Wiedtke, E., Nowrouzi, A., Afzal, S., Fronza, R., Landerer, H., Abad, M., Niopek, D., Schmidt, M., Serrano, M., Grimm, D., 2018. AAV vector-mediated in vivo reprogramming into pluripotency. *Nature Communications*. **9**, 2651.
- Serrano, M. and Blasco, M.A., 2001. Putting the stress on senescence.
- Serrano, M., *et al*, 1997. Oncogenic ras Provokes Premature Cell Senescence Associated with Accumulation of p53 and p16INK4a.
- Sharpless, N.E. & DePinho, R.A., 2007. How stem cells age and why this makes us grow old. *Nature Reviews.Molecular Cell Biology*. **8**, 703-713.
- Sharpless, N.E. & Sherr, C.J., 2015. Forging a signature of in vivo senescence. *Nature Reviews.Cancer*. **15**, 397-408.
- Sharpless, N.E. & DePinho, R.A., 1999. The INK4A/ ARF locus and its two gene products. *Current Opinion in Genetics & Development*. **9**, 22-30.
- Shatz, C.J., 2009. MHC class I: an unexpected role in neuronal plasticity. *Neuron*. **64**, 40-45.
- Shawi, M. and Autexier, C., 2008. Telomerase, senescence and ageing.
- Shay, J.W., 1997. Telomerase in human development and cancer. *Journal of Cellular Physiology*. **173**, 266-270.
- Shay, J.W. & Wright, W.E., 2005. Senescence and immortalization: role of telomeres and telomerase. *Carcinogenesis*. **26**, 867-874.
- Shay, J.W. & Roninson, I.B., 2004. Hallmarks of senescence in carcinogenesis and cancer therapy. *Oncogene*. **23**, 2919-2933.
- Sherr, C.J., 2012. Ink4-Arf locus in cancer and aging. *Wiley Interdisciplinary Reviews.Developmental Biology*. **1**, 731-741.
- Shi, L., Zhang, Z., Su, B., 2016. Sex Biased Gene Expression Profiling of Human Brains at Major Developmental Stages. *Scientific Reports*. **6**, 21181.

Shiohara, M., el-Deiry, W.S., Wada, M., Nakamaki, T., Takeuchi, S., Yang, R., Chen, D.L., Vogelstein, B., Koeffler, H.P., 1994. Absence of WAF1 mutations in a variety of human malignancies. *Blood*. **84**, 3781.

Sievers, E.L. & Senter, P.D., 2013. Antibody-drug conjugates in cancer therapy. *Annual Review of Medicine*. **64**, 15-29.

Sikora, E., Bielak-Zmijewska, A., Mosieniak, G., 2014. Cellular senescence in ageing, age-related disease and longevity. *Current Vascular Pharmacology*. **12**, 698-706.

Sikora, E., *et al*, 2011. Impact of cellular senescence signature on ageing research.

Silveira, E. & Allebeck, P., 2001. Migration, ageing and mental health: an ethnographic study on perceptions of life satisfaction, anxiety and depression in older Somali men in east London. *International Journal of Social Welfare*. **10**, 309-320.

Simboeck, E. & Di Croce, L., 2013. p16INK4a in cellular senescence. *Aging*. **5**, 590.

Sionov, R.V. & Haupt, Y., 1999. The cellular response to p53: the decision between life and death. *Oncogene*. **18**, 6145-6157.

Smith, L.K., He, Y., Park, J., Bieri, G., Snethlage, C.E., Lin, K., Gontier, G., Wabl, R., Plambeck, K.E., Udeochu, J., Wheatley, E.G., Bouchard, J., Eggel, A., Narasimha, R., Grant, J.L., Luo, J., Wyss-Coray, T., Villeda, S.A., 2015. β 2-microglobulin is a systemic pro-aging factor that impairs cognitive function and neurogenesis. *Nature Medicine*. **21**, 932.

Smolinska-Kempisty, K., Guerreiro, A., Canfarotta, F., Caceres, C., Whitcombe, M.J., Piletsky, S., 2016. A comparison of the performance of molecularly imprinted polymer nanoparticles for small molecule targets and antibodies in the ELISA format. *Scientific Reports*. **6**, 37638.

Soper, S.A., *et al*, 2006. Point-of-care biosensor systems for cancer diagnostics/prognostics.

Soto-Gamez, A. and Demaria, M., 2017. Therapeutic interventions for aging: the case of cellular senescence.

Sousa-Victor, P., Gutarra, S., Garcia-Prat, L., Rodriguez-Ubreva, J., Ortet, L., Ruiz-Bonilla, V., Jardi, M., Ballestar, E., Gonzalez, S., Serrano, A.L., Perdiguero, E., Munoz-Canoves, P., 2014. Geriatric muscle stem cells switch reversible quiescence into senescence. *Nature*. **506**, 316-321.

Spring, K., Chabot, C., Langlois, S., Lapointe, L., Trinh, N.T., Caron, C., Hebda, J.K., Gavard, J., Elchebly, M., Royal, I., 2012. Tyrosine phosphorylation of DEP-

1/CD148 as a mechanism controlling Src kinase activation, endothelial cell permeability, invasion, and capillary formation. *Blood*. **120**, 2745-2756.

Spring, K., Fournier, P., Lapointe, L., Chabot, C., Roussy, J., Pommey, S., Stagg, J., Royal, I., 2015. The protein tyrosine phosphatase DEP-1/PTPRJ promotes breast cancer cell invasion and metastasis. *Oncogene*. **34**, 5536-5547.

Staats, K., Schonefeldt, S., Van Rillaer, M., Van Hoecke, A., Van Damme, P., Robberecht, W., Liston, A., Van, D.B., 2013. Beta-2 microglobulin is important for disease progression in a murine model for amyotrophic lateral sclerosis. *Frontiers in Cellular Neuroscience*. **7**, 249.

Storer, M., Mas, A., Robert-Moreno, A., Pecoraro, M., Ortells, M.C., Di Giacomo, V., Yosef, R., Pilpel, N., Krizhanovsky, V., Sharpe, J., Keyes, W.M., 2013. Senescence is a developmental mechanism that contributes to embryonic growth and patterning. *Cell*. **155**, 1119-1130.

Strohl, W.R. & Strohl, L.M., 2012. 15 - Antibody-drug conjugates. In Strohl, W. R. & Strohl, L. M., eds, *Therapeutic Antibody Engineering*. Woodhead Publishing. 345-595.

Studer, L., Vera, E. and Cornacchia, D., 2015. Programming and Reprogramming Cellular Age in the Era of Induced Pluripotency.

Sturmelechner, I., Durik, M., Sieben, C.J., Baker, D.J., van Deursen, J.M., 2017. Cellular senescence in renal ageing and disease. *Nature Reviews.Nephrology*. **13**, 77-89.

Sugrue, M.M., Shin, D.Y., Lee, S.W., Aaronson, S.A., 1997. Wild-type p53 triggers a rapid senescence program in human tumor cells lacking functional p53. *Proceedings of the National Academy of Sciences of the United States of America*. **94**, 9648-9653.

Sun, W., Gui, L., Zuo, X., Zhang, L., Zhou, D., Duan, X., Ren, W., Xu, G., 2016. Human epithelial-type ovarian tumour marker beta-2-microglobulin is regulated by the TGF- β signaling pathway. *Journal of Translational Medicine*. **14**, 75.

Sunyer, B., Patil, S., H \diamond ger, H., Lubec, G., 2007. Barnes maze, a useful task to assess spatial reference memory in the mice. *Nat Protoc*. **390**, 10-38.

Suram, A., Kaplunov, J., Patel, P.L., Ruan, H., Cerutti, A., Boccardi, V., Fumagalli, M., Di Micco, R., Mirani, N., Gurung, R.L., Hande, M.P., d'Adda, d.F., Herbig, U., 2012. Oncogene-induced telomere dysfunction enforces cellular senescence in human cancer precursor lesions. *Embo J*. **31**, 2839.

Swanson, E.C., Manning, B., Zhang, H., Lawrence, J.B., 2013. Higher-order unfolding of satellite heterochromatin is a consistent and early event in cell senescence. *The Journal of Cell Biology*. **203**, 929-942.

Tacutu, R., Craig, T., Budovsky, A., Wuttke, D., Lehmann, G., Taranukha, D., Costa, J., Fraifeld, V.E., de Magalhaes, J.P., 2013. Human Ageing Genomic Resources: integrated databases and tools for the biology and genetics of ageing. *Nucleic Acids Research*. **41**, 1027.

Takahashi, A., Ohtani, N., Hara, E., 2007. Irreversibility of cellular senescence: dual roles of p16INK4a/Rb-pathway in cell cycle control. *Cell Division*. **2**, 10.

Takahashi, K. & Yamanaka, S., 2006. Induction of pluripotent stem cells from mouse embryonic and adult fibroblast cultures by defined factors. *Cell*. **126**, 663-676.

Tam, K.W., *et al*, 2013. CDKN2A/p16 Inactivation Mechanisms and Their Relationship to Smoke Exposure and Molecular Features in Non-Small-Cell Lung Cancer.

Taniguchi, K., Kohsaka, H., Inoue, N., Terada, Y., Ito, H., Hirokawa, K., Miyasaka, N., 1999. Induction of the p16INK4a senescence gene as a new therapeutic strategy for the treatment of rheumatoid arthritis. *Nature Medicine*. **5**, 760.

Tchkonia, T., Zhu, Y., van Deursen, J., Campisi, J., Kirkland, J.L., 2013. Cellular senescence and the senescent secretory phenotype: therapeutic opportunities. *The Journal of Clinical Investigation*. **123**, 966-972.

Terman, A. and Brunk, U.T., 2004. Lipofuscin.

Thomas, A., Teicher, B.A. and Hassan, R., 2016. Antibody–drug conjugates for cancer therapy.

Tichy, E.D., *et al*, 2017. Single Stem Cell Imaging and Analysis Reveals Telomere Length Differences in Diseased Human and Mouse Skeletal Muscles.

Tieppo, A., *et al*, 2012. Sustained in vivo release from imprinted therapeutic contact lenses.

Tigges, J., *et al*, 2014. The hallmarks of fibroblast ageing.

Toussaint, O., Dumont, P., Remacle, J., Dierick, J.F., Pascal, T., Fripiat, C., Magalhaes, J.P., Zdanov, S., Chainiaux, F., 2002a. Stress-induced premature senescence or stress-induced senescence-like phenotype: one in vivo reality, two possible definitions? *TheScientificWorldJournal*. **2**, 230-247.

Toussaint, O., Medrano, E.E. and von Zglinicki, T., 2000. Cellular and molecular mechanisms of stress-induced premature senescence (SIPS) of human diploid fibroblasts and melanocytes.

Toussaint, O., *et al*, 2002b. From the Hayflick mosaic to the mosaics of ageing.: Role of stress-induced premature senescence in human ageing.

Toussaint, O., *et al*, 2002c. Stress-induced premature senescence and tissue ageing.

Toussaint, O., Salmon, M., Pascal, T., Magalhaes, J.P. and Chainiaux, F., 2001. Stress-induced Premature Senescence (SIPS). *eLS*. John Wiley & Sons, Ltd.

Toutfaire, M., Bauwens, E. and Debacq-Chainiaux, F., 2017. The impact of cellular senescence in skin ageing: A notion of mosaic and therapeutic strategies.

Trail, P.A., Willner, D., Lasch, S.J., Henderson, A.J., Hofstead, S., Casazza, A.M., Firestone, R.A., Hellstrom, I., Hellstrom, K.E., 1993. Cure of xenografted human carcinomas by BR96-doxorubicin immunoconjugates. *Science (New York, N.Y.)*. **261**, 212-215.

Trail, P.A., Dubowchik, G.M. and Lowinger, T.B., 2018. Antibody drug conjugates for treatment of breast cancer: Novel targets and diverse approaches in ADC design.

Trinh, C.H., Smith, D.P., Kalverda, A.P., Phillips, S.E., Radford, S.E., 2002. Crystal structure of monomeric human beta-2-microglobulin reveals clues to its amyloidogenic properties. *Proceedings of the National Academy of Sciences of the United States of America*. **99**, 9771-9776.

Tsuji, T., Aoshiba, K., Nagai, A., 2006. Alveolar cell senescence in patients with pulmonary emphysema. *American Journal of Respiratory and Critical Care Medicine*. **174**, 886-893.

Tyagi, N., Arora, S., Deshmukh, S.K., Singh, S., Marimuthu, S., Singh, A.P., 2016. Exploiting Nanotechnology for the Development of MicroRNA-Based Cancer Therapeutics. *Journal of Biomedical Nanotechnology*. **12**, 28-42.

Ullman-Cullere, M.H. & Foltz, C.J., 1999. Body condition scoring: a rapid and accurate method for assessing health status in mice. *Laboratory Animal Science*. **49**, 319-323.

Valentijn, F.A., Falke, L.L., Nguyen, T.Q., Goldschmeding, R., 2017. Cellular senescence in the aging and diseased kidney. *Journal of Cell Communication and Signaling*.

Vasapollo, G., Sole, R.D., Mergola, L., Lazzoi, M.R., Scardino, A., Scorrano, S., Mele, G., 2011. Molecularly imprinted polymers: present and future prospective. *International Journal of Molecular Sciences*. **12**, 5908-5945.

Verhoeven, J.E., Révész, D., van Oppen, P., Epel, E.S., Wolkowitz, O.M., Penninx, Brenda W. J. H., 2015. Anxiety disorders and accelerated cellular ageing. *British Journal of Psychiatry*. **206**, 371-378.

Vetrie, D., Vořechovský, I., Sideras, P., Holland, J., Davies, A., Flinter, F., Hammarström, L., Kinnon, C., Levinsky, R., Bobrow, M., Smith, C.I.E., Bentley,

D.R., 1993. The gene involved in X-linked agammaglobulinaemia is a member of the src family of protein-tyrosine kinases. *Nature*. **361**, 226.

Victorelli, S. and Passos, J.F., 2017. Telomeres and Cell Senescence - Size Matters Not.

Vizioli, M.G., Santos, J., Pilotti, S., Mazzoni, M., Anania, M.C., Miranda, C., Pagliardini, S., Pierotti, M.A., Gil, J., Greco, A., 2014. Oncogenic RAS-induced senescence in human primary thyrocytes: molecular effectors and inflammatory secretome involved. *Oncotarget*. **5**, 8270-8283.

Vogt, M., Haggblom, C., Yeargin, J., Christiansen-Weber, T., Haas, M., 1998. Independent induction of senescence by p16INK4a and p21CIP1 in spontaneously immortalized human fibroblasts. *Cell Growth & Differentiation : The Molecular Biology Journal of the American Association for Cancer Research*. **9**, 139-146.

Voigt, J., Christensen, J., Shastri, V.P., 2014. Differential uptake of nanoparticles by endothelial cells through polyelectrolytes with affinity for caveolae. *Proceedings of the National Academy of Sciences of the United States of America*. **111**, 2942-2947.

von Zglinicki, T. & Martin-Ruiz, C.M., 2005. Telomeres as biomarkers for ageing and age-related diseases. *Current Molecular Medicine*. **5**, 197-203.

Vos, S.D., Miller, C.W., Takeuchi, S., Gombart, A.F., Cho, S.K., Koeffler, H.P., 1995. Alterations of CDKN2 (p16) in non-small cell lung cancer. *Genes, Chromosomes and Cancer*. **14**, 164-170.

Vredeveld, L.C., Possik, P.A., Smit, M.A., Meissl, K., Michaloglou, C., Horlings, H.M., Ajouaou, A., Kortman, P.C., Dankort, D., McMahon, M., Mooi, W.J., Peeper, D.S., 2012. Abrogation of BRAFV600E-induced senescence by PI3K pathway activation contributes to melanomagenesis. *Genes & Development*. **26**, 1055-1069.

Waldman, T., Kinzler, K.W., Vogelstein, B., 1995. p21 is necessary for the p53-mediated G1 arrest in human cancer cells. *Cancer Research*. **55**, 5187-5190.

Walter, H.S. & Ahmed, S., 2017. Targeted therapies in cancer. *Surgery (Oxford)*.

Walther, D.M. & Mann, M., 2011. Accurate quantification of more than 4000 mouse tissue proteins reveals minimal proteome changes during aging. *Molecular & Cellular Proteomics : MCP*. **10**, M110.004523.

Wang, C., Jurk, D., Maddick, M., Nelson, G., Martin-Ruiz, C., von Zglinicki, T., 2009. DNA damage response and cellular senescence in tissues of aging mice. *Aging Cell*. **8**, 311-323.

Wang, J.C. & Bennett, M., 2012. Aging and Atherosclerosis: Mechanisms, Functional Consequences, and Potential Therapeutics for Cellular Senescence. *Circulation Research*. **111**, 245-259.

Wang, L., Du, Y.R., Ji, M.Y., Wang, W., Zhan, N., Zhou, Q.S., Dong, W.G., 2014. Reduced EBP50 expression or mis-localization of the EBP50 protein is associated with the malignant progression of esophageal squamous cell carcinoma. *European Review for Medical and Pharmacological Sciences*. **18**, 3854-3863.

Wang, L., Qi, Y., Xiong, Y., Peng, Z., Ma, Q., Zhang, Y., Song, J., Zheng, J., 2017a. Ezrin-Radixin-Moesin Binding Phosphoprotein 50 (EBP50) Suppresses the Metastasis of Breast Cancer and HeLa Cells by Inhibiting Matrix Metalloproteinase-2 Activity. *Anticancer Research*. **37**, 4353-4360.

Wang, R., Sunchu, B. and Perez, V.I., 2017b. Rapamycin and the inhibition of the secretory phenotype.

Wang, Y., Horvath, O., Hamm-Baarke, A., Richelme, M., Gregoire, C., Guinamard, R., Horejsi, V., Angelisova, P., Spicka, J., Schraven, B., Malissen, B., Malissen, M., 2005. Single and combined deletions of the NTAL/LAB and LAT adaptors minimally affect B-cell development and function. *Molecular and Cellular Biology*. **25**, 4455-4465.

Wei, M., Brandhorst, S., Shelehchi, M., Mirzaei, H., Cheng, C.W., Budniak, J., Groshen, S., Mack, W.J., Guen, E., Di Biase, S., Cohen, P., Morgan, T.E., Dorff, T., Hong, K., Michalsen, A., Laviano, A., Longo, V.D., 2017. Fasting-mimicking diet and markers/risk factors for aging, diabetes, cancer, and cardiovascular disease. *Science Translational Medicine*. **9**, 10.1126/scitranslmed.aai8700.

Wei, S., Wei, W., Sedivy, J.M., 1999. Expression of catalytically active telomerase does not prevent premature senescence caused by overexpression of oncogenic Ha-Ras in normal human fibroblasts. *Cancer Research*. **59**, 1539-1543.

Weismann & August, 1891. *Essays upon Heredity and kindred biological problems. Authorised translation, edited by E. B. Poulton, S. Schönland, and A. E. Shipley.* [e-book]. Second Edition ed. Oxford, England: Clarendon Press. Available from : http://gateway.proquest.com/openurl?url_ver=Z39.88-2004&res_dat=xri:c19index-us&rft_dat=xri:c19index:NSTC:0951326.

Whitcombe, M.J., Chianella, I., Larcombe, L., Piletsky, S.A., Noble, J., Porter, R., Horgan, A., 2011. The rational development of molecularly imprinted polymer-based sensors for protein detection. *Chemical Society Reviews*. **40**, 1547-1571.

White, M.J., Glenn, M., Gomer, R.H., 2013. Trypsin potentiates human fibrocyte differentiation. *PLoS One*. **8**, e70795.

Whitehead, J.C., Hildebrand, B.A., Sun, M., Rockwood, M.R., Rose, R.A., Rockwood, K., Howlett, S.E., 2014. A clinical frailty index in aging mice:

comparisons with frailty index data in humans. *The Journals of Gerontology. Series A, Biological Sciences and Medical Sciences*. **69**, 621-632.

Wiley, C.D. & Campisi, J., 2016. From Ancient Pathways to Aging Cells-Connecting Metabolism and Cellular Senescence. *Cell Metabolism*. **23**, 1013-1021.

Wiley, C.D., Schaum, N., Alimirah, F., Lopez-Dominguez, J.A., Orjalo, A.V., Scott, G., Desprez, P.Y., Benz, C., Davalos, A.R., Campisi, J., 2018. Small-molecule MDM2 antagonists attenuate the senescence-associated secretory phenotype. *Scientific Reports*. **8**, 4.

Wiley, C., *et al*, 2016. Mitochondrial Dysfunction Induces Senescence with a Distinct Secretory Phenotype.

Wolf, M.J., Adili, A., Piotrowitz, K., Abdullah, Z., Boege, Y., Stemmer, K., Ringelhan, M., Simonavicius, N., Egger, M., Wohlleber, D., Lorentzen, A., Einer, C., Schulz, S., Clavel, T., Protzer, U., Thiele, C., Zischka, H., Moch, H., Tschop, M., Tumanov, A.V., Haller, D., Unger, K., Karin, M., Kopf, M., Knolle, P., Weber, A., Heikenwalder, M., 2014. Metabolic activation of intrahepatic CD8+ T cells and NKT cells causes nonalcoholic steatohepatitis and liver cancer via cross-talk with hepatocytes. *Cancer Cell*. **26**, 549-564.

Wright, W.E. & Shay, J.W., 2000a. Telomere dynamics in cancer progression and prevention: fundamental differences in human and mouse telomere biology. *Nature Medicine*. **6**, 849.

Wright, W.E. & Shay, J.W., 2000b. Hayflick, his limit, and cellular ageing. *Nature Reviews Molecular Cell Biology*. **1**, 72-76.

Xiang, X., Deng, Z., Zhuang, X., Ju, S., Mu, J., Jiang, H., Zhang, L., Yan, J., Miller, D., Zhang, H.G., 2012. Grhl2 determines the epithelial phenotype of breast cancers and promotes tumor progression. *PloS One*. **7**, e50781.

Xiao, P., *et al*, 2017. G protein-coupled receptor kinase 4-induced cellular senescence and its senescence-associated gene expression profiling.

Xu, Y., *et al*, 2014. Emerging roles of the p38 MAPK and PI3K/AKT/mTOR pathways in oncogene-induced senescence.

Yanagi, S., Tsubouchi, H., Miura, A., Matsuo, A., Matsumoto, N., Nakazato, M., 2017. The Impacts of Cellular Senescence in Elderly Pneumonia and in Age-Related Lung Diseases That Increase the Risk of Respiratory Infections. *International Journal of Molecular Sciences*. **18**, 10.3390/ijms18030503.

Yanai, H., Shteinberg, A., Porat, Z., Budovsky, A., Braiman, A., Zeische, R., Fraifeld, V.E., 2015. Cellular senescence-like features of lung fibroblasts derived from idiopathic pulmonary fibrosis patients. *Aging (Albany NY)*. **7**, 664-672.

Yang, N. & Hu, M., 2005. The limitations and validities of senescence associated- β -galactosidase activity as an aging marker for human foreskin fibroblast Hs68 cells. *Experimental Gerontology*. **40**, 813-819.

Yang, Q., Xie, Y., Miao, L., 2016. Tumor Promoting Aspects of Senescence in Cancer Progression. *Cancer Investigation*. 1-7.

Yang, Z., Jun, H., Choi, C.I., Yoo, K.H., Cho, C.H., Hussaini, S.M.Q., Simmons, A.J., Kim, S., van Deursen, J.M., Baker, D.J., Jang, M.H., 2017. Age-related decline in BubR1 impairs adult hippocampal neurogenesis. *Aging Cell*. **16**, 598-601.

Young, A.R.J., Narita, M. and Narita, M., 2013. Cell Senescence as Both a Dynamic and a Static Phenotype. In Galluzzi, L., Vitale, I., Kepp, O. and Kroemer, G., eds, *Cell Senescence: Methods and Protocols*. Totowa, NJ: Humana Press. 1-13.

Zhang, M., He, J., Yang, J., 2016. Targeting Human beta-Microglobulin with Monoclonal Antibodies in Multiple Myeloma - A Potential in Treatment. *Chemotherapy*. **5**, 7700.1000190. Epub 2016 Feb 20.

Zhang, Z., Rosen, D.G., Yao, J.L., Huang, J., Liu, J., 2006. Expression of p14ARF, p15INK4b, p16INK4a, and DCR2 increases during prostate cancer progression. *Modern Pathology : An Official Journal of the United States and Canadian Academy of Pathology, Inc.* **19**, 1339-1343.

Zhu, J., Woods, D., McMahon, M., Bishop, J.M., 1998. Senescence of human fibroblasts induced by oncogenic Raf. *Genes & Development*. **12**, 2997-3007.

Zhu, Y., Armstrong, J.L., Tchkonja, T., Kirkland, J.L., 2014. Cellular senescence and the senescent secretory phenotype in age-related chronic diseases. *Current Opinion in Clinical Nutrition and Metabolic Care*. **17**, 324-328.

Zhu, Y., Doornebal, E.J., Pirtskhalava, T., Giorgadze, N., Wentworth, M., Fuhrmann-Stroissnigg, H., Niedernhofer, L.J., Robbins, P.D., Tchkonja, T., Kirkland, J.L., 2017. New agents that target senescent cells: the flavone, fisetin, and the BCL-XL inhibitors, A1331852 and A1155463. *Aging*. **9**, 955-963.

Zhu, Y., Tchkonja, T., Fuhrmann-Stroissnigg, H., Dai, H.M., Ling, Y.Y., Stout, M.B., Pirtskhalava, T., Giorgadze, N., Johnson, K.O., Giles, C.B., Wren, J.D., Niedernhofer, L.J., Robbins, P.D., Kirkland, J.L., 2016. Identification of a novel senolytic agent, navitoclax, targeting the Bcl-2 family of anti-apoptotic factors. *Aging Cell*. **15**, 428-435.

Zhu, Y., Tchkonja, T., Pirtskhalava, T., Gower, A.C., Ding, H., Giorgadze, N., Palmer, A.K., Ikeno, Y., Hubbard, G.B., Lenburg, M., O'Hara, S.P., LaRusso, N.F., Miller, J.D., Roos, C.M., Verzosa, G.C., LeBrasseur, N.K., Wren, J.D., Farr, J.N., Khosla, S., Stout, M.B., McGowan, S.J., Fuhrmann-Stroissnigg, H., Gurkar, A.U., Zhao, J., Colangelo, D., Dorransoro, A., Ling, Y.Y., Barghouthy, A.S., Navarro, D.C., Sano, T., Robbins, P.D., Niedernhofer, L.J., Kirkland, J.L., 2015.

The Achilles' heel of senescent cells: from transcriptome to senolytic drugs. *Aging Cell.* **14**, 644-658.